N° d'ordre : 41111

Université Lille I

Ecole Doctorale des Sciences de la Matière, du Rayonnement et de l'Environnement

Thèse

pour obtenir le grade de

Docteur

Mention : « Molécules et Matières Condensée »

Par

Wenhao FANG

Production d'hydrogène par transformation du bioéthanol sur catalyseurs à base de nickel

28 juin 2013

Pedro L. Arias	Professeur	Bilbao UPV / EHU	Rapporteur
Florence Epron-Cognet	Chargée de Recherches CNRS	Université de Poitiers	Rapporteur
Patricia De Rango	Chargée de Recherches CNRS	Institut Néel / CRETA	Examinateur
Louise Duhamel	Chargée de Recherches CNRS	Université Lille1	Examinateur
Sébastien Paul	Professeur	Ecole Centrale Lille	Examinateur
Franck Dumeignil	Professeur	Université Lille1	Président

Acknowledgements

I would like to sincerely acknowledge my grant from Erasmus Mundus Tandem to financially support my doctor studies in France. This work is performed in Unité de Catalyse et Chimie du Solide - CNRS UMR8181, and Université Lille 1. I thank Pr. L. Montagne and Pr. F. Dumeignil very much for offering me this thesis and providing me all the necessary resources for my research.

I would love to express my sincere and heartfelt gratitude to my supervisor, Dr. Louise Duhamel who helps me quite a lot in every aspect. I do appreciate her patience, encouragement and professional guidance during my three-year-long PhD studies, leading me to a right way to the independent scientific research. She involves every step during the writing of my thesis in her own way by showing me how to do instead of what to do. The times when we work together leave me very pleasant memories.

I deeply thank Pr. Sébastien Paul, Pr. Franck Dumeignil and Dr. Mickaël Capron for their warm concern and kind help in both my study and life. Their specialty and enthusiasm in the scientific research encourage me a lot. I love the atmospheres working with them.

I feel grateful to Dr. Hervé Jobic who kindly helped me in the INS experiment performed in Institut Laue Langevin (ILL), Grenoble. Many thanks to him for the technical support and valuable discussions. I express my sincere gratitude to ILL for the financial support for INS experiments.

I am in great honor to have Pr. Pedro L. Arias and Dr. Florence Epron-Cognet as the reporters for my thesis, thank you so much for your valuable review. I also would like to sincerely thank Dr. Patricia De Rango for her participation in my defense.

I would like to dedicate my acknowledgements to all those who helped me during my PhD studies, our professional technicians, nice secretaries and friendly colleagues. I am very grateful to Ms. L. Burylo, Ms. M. Trentesaux, Mr. O. Gardoll, Mr. J. C. Morin and Mr. A. Addad for their valuable technical helps and discussions in characterizations.

I also own a special debt of thanksgiving to my dear friends, Ms. Elise Berrier, Ms. Asma Tougerti, Ms. Kaew-arpha Thavornprasert (Pam), Mr. Fangli Jing, Mr. Yong Miao, Mr. Lei Zhang and Mr. Chang Liu. My life in France cannot be so fruitful and joyful without you.

I finally would love to express my gratitude to my beloved parents who have always been helping me out of difficulties and supporting me without a word of complaint. You are always there whenever I need you. I love you forever!

This thesis is dedicated to my most beloved.

Wenhao Fang

May, 2013

Table of contents

1 General introduction

Energy is an important material basis for human survival and development. Energy is the driving force behind human engaged in various economic activities.

There are generally three major changes in the human history of the use of energy. First, coal replaced wood and became a major energy. Second, energy structure migrated from coal to oil and natural gas, which was very important significance to the development of the social economy. The third great changes in the energy structure began with the oil crisis in 1970s; people came to realize the non-renewability of fossil energy, and the development of new energy sources became an essential issue.

As non-renewable energy sources, exploitation and utilization of fossil fuels have been causing a series of social and environmental issues, mainly reflected in:

i) Pollutants emission. The mining and combustion of fossil fuels have led to a large number of pollutants emissions, especially the emission of fine dusts and acid gases results in severe air pollution, causing a great threat to human health.

ii) Global climate change. The emission of the greenhouse gas (mainly CO_2, CH_4 and N_2O) has shown a significant impact on the global climate.

iii) Non renewability. It can be predicted that the existing fossil fuels are facing the serious crisis of deletion in the near future.

Therefore, developing renewable and clean energy sources to substitute the conventional energy resources has become the mainstream development strategy in the present world.

Hydrogen is regarded as one of the most energy-efficient fuel sources based on its high efficiency and cleanness. H_2 energy has caused widespread concern due to:

i) Hydrogen is the most common element existing in the nature. It is mainly stored in the form of water. It is estimated if all the hydrogen was extracted from seawater, the total calories generated would be as 9000 times as that released by all the fossil fuels in the world.

ii) Hydrogen has the highest combustion value among all the fossil fuels, chemical fuels and biofuels except nuclear fuels. The value of 1.4×10^5 kJ kg^{-1} is as three times as that of gasoline.

iii) The unique product of hydrogen combustion is water which is super clean and can be recycled to generate hydrogen, leading to no emission of greenhouse gases and pollutants.

iv) Hydrogen has diverse applications. It can be utilized directly as a fuel in internal combustion engines, or can indirectly supply electricity *via* fuel cells.

v) The flexible storage of hydrogen, *i.e.*, in the forms of gas, liquid or solid, makes hydrogen well adapted for transportation and requirements of various applications.

Today H_2 production is mainly produced from fossil fuels *via* the steam reforming of natural gas, which is usually questioned. In the point view of environmentally friendly and sustainable energy development strategy, H_2 production from transformation of renewable sources, such as biomass or biomass-derived materials, is proposed to be an alternatively desirable route.

Bio-ethanol is one of the most important platforms as chemical carrier of hydrogen among all the biomass-derived materials. It is currently produced by the fermentation of biomass or agriculture waste products with mature technology. Hence the steam reforming of bio-ethanol is a very ideal route to produce hydrogen, which can provide a carbon-free emission process in theory since the CO_2 produced can be recycled back during biomass growth. The crucial factor is to develop highly active, selective, stable and low-cost catalysts to achieve high yield to hydrogen *via* the steam reforming of bio-ethanol.

The present work focuses on the studies of H_2 production by catalytic transformation of ethanol over Ni-based catalysts. After a general introduction (Chapter 1), in Chapter 2, the bibliography on H_2 production from biomass, *e.g.*, ethanol is reviewed. The very recent literatures on the catalytic systems of steam reforming of ethanol and oxidative steam reforming of ethanol are synthesized. Then Chapter 3 presents the methodology of preparation and the results of the different characterizations of the Ni-based catalysts studied in the present thesis. Two types of Ni-based catalysts, $CeNi_XO_Y$ and $Ni_XMg_2AlO_Y$ catalysts are characterized by numerous physicochemical techniques. The textural properties (N_2 physisorption), phase and crystalline structures (XRD, Raman), surface properties (XPS), reducibility (TPR, *in situ* XRD) and storage capacity of H_2 are studied.

In the following Chapters 4 and 5, H_2 production from ethanol is studied over $CeNi_XO_Y$ and $Ni_XMg_2AlO_Y$ catalysts *via* steam reforming and oxidative steam reforming routes, respectively. Many different reaction parameters are analyzed. Finally in Chapter 6, a general discussion based on all the catalytic results and catalysts characterizations (before and after test) is made. The common and different features of $CeNi_XO_Y$ and $Ni_XMg_2AlO_Y$ catalysts are compared; the correlations between catalytic performances and catalyst properties are established, and the active phase and active sites are proposed and discussed. Chapter 7 summarizes the present work and draws a general conclusion.

2 Bibliography

2.1 Hydrogen: Energy for 21st century

2.1.1 Global utilization and demand of H_2 production

Hydrogen (H_2) has been widely utilized as an important chemical reagent in various fields. **Fig. 2-1** illustrates the global utilization of H_2 production. It is principally consumed for the production of ammonia and fertilizers (49%), followed by petroleum refining (37%); then for the manufacture of methanol (8%) and various applications (6%). In addition, since H_2 production has become an important and integral part of petroleum refining for the productions of gasoline and diesel, the integration of H_2 production is also expected to improve the overall process economy of the future bio-refining.[1] The emerging H_2 energy economy and the fast growing demand have led to new demands on H_2 production capacity.[2]

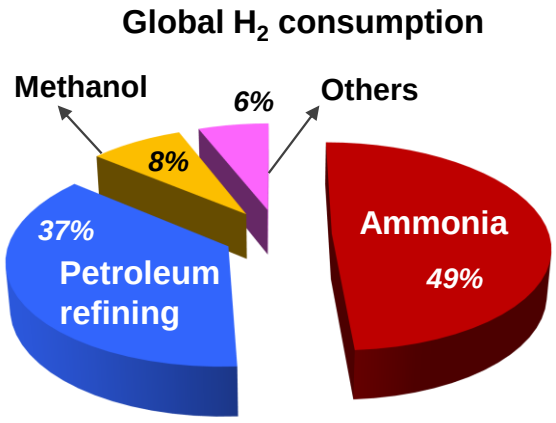

Fig. 2-1 The global utilization of H_2 production.[3]

As clearly shown in **Fig. 2-2**, the world H_2 demand undergoes a significant growth during the last ten years. It is predicted that the global H_2 demand would reach 475 billion m^3 in 2013. The newly gains will be mainly driven in refining low sulfur fuels. Meanwhile, the fast development of China, India and other Asia/Pacific countries is stimulating the strong growth of the demand of clean oil. The Asia/Pacific region will surpass North America as the global leader in H_2 consumption by 2013.

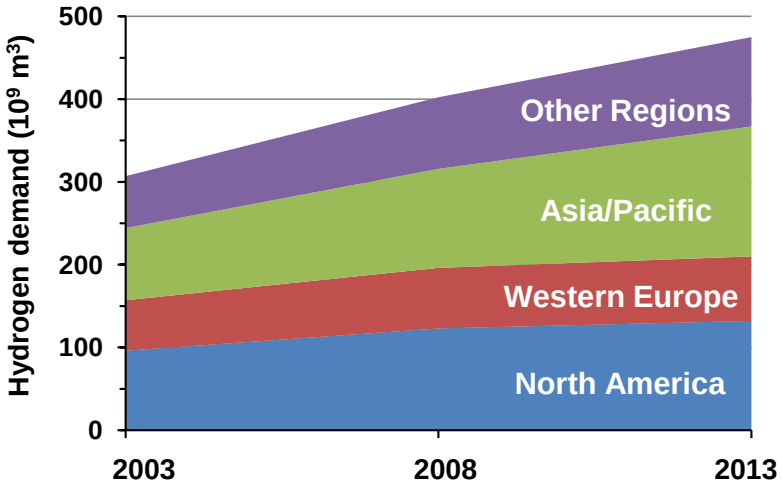

Fig. 2-2 World hydrogen demand during the past 10 years. Copyright 2010 by the research company Freedonia Group.

The world hydrogen market economy has been estimated to reach a record of $ 82.6 billion. It is predicted that petroleum refining, new energy vehicle and clean energy electricity generation would become the terminal consumption market. Meanwhile with the rapid growth of the global market demand for H_2 fuel cells and electricity generation by H_2 energy, the global H_2 production market growth rate is expected to remain around 5.6% from 2012-2016.

2.1.2 Global manufacture of H_2 production

Although hydrogen (H) is the most common element widely existing in the earth mainly stored in the form of water, the proportion of hydrogen molecule (H_2) is too low to exploit. Therefore, H_2 energy can be only obtained by the conversion of other energy sources. Producing H_2 in a large scale is not only a traditional chemical process, but also a cutting-edge research. At present, the global H_2 production in the industrial scale is almost produced *via* the steam reforming of hydrocarbon resources (**Fig. 2-3**), such as natural gas (48%), oil (30%) and coal (18%). Besides, a small part (4%) is derived from the electrolysis. As is clearly demonstrated in **Fig. 2-3**, the current manufacture routes for H_2 production still strongly rely on the conventional fossil fuel resources. Up to date, the exploitation and utilization of fossil fuels have caused a series of social and environmental issues.

Human beings have realized at the non-renewability of fossil fuels, and have started to pay close attention to the renewable energy sources. In the point view of the environmental benefit, future energy safety and sustainable energy development strategy, H_2 production from

transformation of renewable sources, such as biomass or biomass-derived materials, is proposed to be an alternatively desirable route.

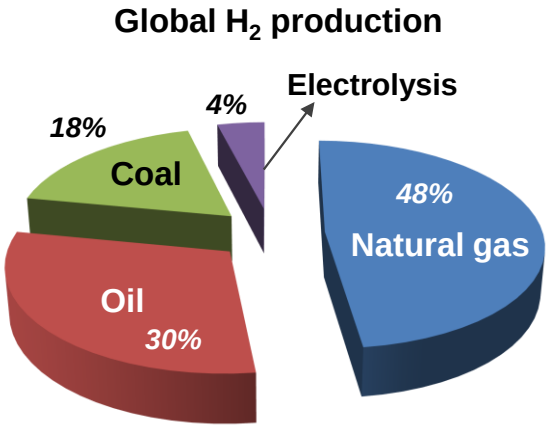

Fig. 2-3 The global manufacture routes for H_2 production.[4]

2.2 H_2 production from biomass

With the increasing global concern about the climate change and CO_2 emissions, it is urgent to produce H_2 in a CO_2 neutral route.[5] There are two major ways to obtain CO_2 neutral production of H_2. One is established on the existing technologies for H_2 production by means of steam reforming of non-renewable fossil fuels, combined with CO_2 sequestration. The other one is to produce H_2 from renewable resources, such as biomass (*e.g.* by catalytic conversion, **Fig. 2-4**) or water (*e.g.* by the action of sunlight).[6]

Biomass is a very important renewable energy source which widely exists in the nature mainly in the form of wood, plants, agriculture crop residues, municipal wastes, *etc*. Biomass can be largely generated by the photosynthesis reaction in plants. It is estimated that the biomass energy stored in plants each year is about 10 times equivalent to the global major fuel consumption, but its utilization as energy remain less than 1% of the total!

In all, biomass and biomass-derived materials have the advantages of renewability, availability, diversity and easy transportation (solid or liquid).[7-9] Moreover H_2 production from biomass could probably provide a CO_2-free emission process in theory since the CO_2 produced is recycled back during plants growth. Thereby, conversion of biomass to H_2 production has been the great interest of numerous studies in the context of the sustainable development (**Fig. 2-4**).

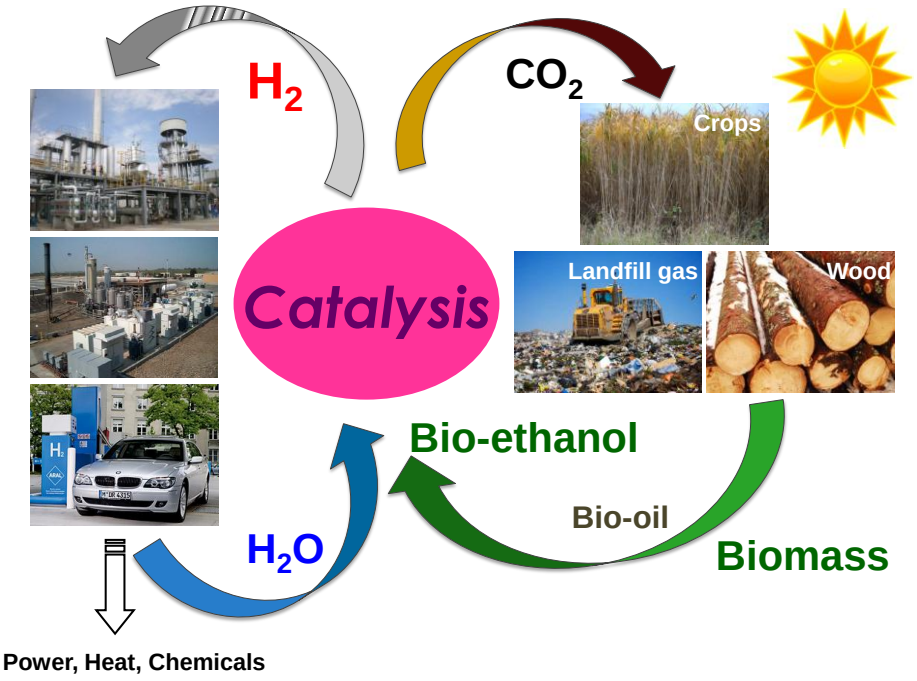

Fig. 2-4 Strategy for H_2 production from biomass.[6]

2.3 Thermo-chemical technologies for H_2 production from biomass

Conversion technologies from biomass to H_2 can be divided into two categories: i) direct production routes and ii) conversion of storable intermediates; both are established on thermo-chemical or biological means. The present work only focuses on the thermo-chemical process. **Fig. 2-5** shows the strategy for H_2 production from biomass by means of the thermo-chemical route. There are three platforms in the biomass conversion to H_2: gasification, pyrolysis and hydrolysis-sugar.[10-12] The starting feed is usually lignocellusic biomass, *e.g.*, grass, wood, crops and municipal wastes, *etc*.

The direct routes such as the gasification platform (**Fig. 2-5**) have the advantage of simplicity. However, lignocellusic biomass has low hydrogen content, leading to low H_2 yield in the direct route. The indirect routs such as the pyrolysis and hydrolysis-sugar platforms (**Fig. 2-5**) have additional steps, but they provide high H_2 yield. Besides there can be a distributed conversion of large volume biomass to the intermediates (bio-oil and sugars) for minimizing transportation cost. In the fast pyrolysis platform, lignocellusic biomass is liquefied to bio-oil that is a mixture containing a wide range of compounds.

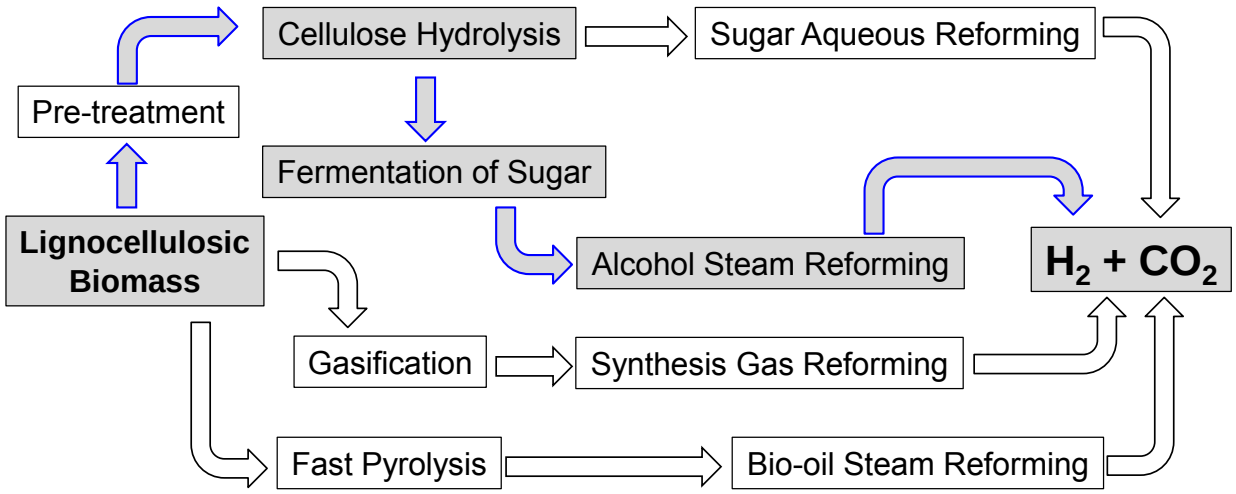

Fig. 2-5 Strategy for H_2 production from lignocellulosic biomass.[6]

Upon the addition of water, bio-oil is separated into: i) an aqueous phase containing mostly carbohydrate-derived compounds, and ii) a hydrophobic phase composed mainly of lignin-derived oligomers.[1] The aqueous part is often used for H_2 production by steam reforming. In the hydrolysis-sugar platform, H_2 can be produced either by directly reforming sugars or by the fermentation of the sugar to ethanol[13] and other polyols,[14] followed by steam reforming. The present work follows the route of ethanol steam reforming which is marked in grey in **Fig. 2-5**.

2.3.1 H_2 production from bio-oil by fast pyrolysis

Pyrolysis, including fast and low pyrolysis, converts biomass into liquid oil by heating biomass at a temperature range of 650-800 K at 0.1-0.5 MPa in the absence of air.[1,9,15,16] The slow pyrolysis mainly produces charcoal, which is not suitable for H_2 production. The products of the fast pyrolysis are distributed in all the gas, liquid and solid phases.[15] There have been intensive studies on the conversion of bio-oil aqueous fraction to synthesis gas or H_2 by steam reforming.

Currently, the predominant technology for H_2 production is still the steam reforming of fossil fuels, where Ni is the most commonly used catalyst.[17] Carbon formation is one of the main problems in the steam reforming process. The steam reforming of bio-oil is an extension of the steam reforming of fossil fuels, but it more severely suffers from the coke formation because some of the bio-oil components are thermally unstable and decompose upon heating.[18,19]

2.3.2 H_2 production from biomass gasification

Biomass gasification is a process to convert solid biomass or liquid biomass-derived compounds for the production of synthesis gas in the presence of air, steam or supercritical water. The gasification,[20,21] steam gasification,[22,23] and supercritical gasification[24,25] of biomass or sugars, followed by steam reforming (removing hydrocarbons and tar), water gas shift, and CO_2/H_2 separation steps, are the widely practiced routes for converting biomass to H_2 and CO_2.[6] In general, biomass gasification requires a lower temperature than coal gasification, which also involves complicated reaction pathways, including steam reforming, partial oxidation, pyrolysis and WGS, *etc*. The main product in gas phase is synthesis gas.

One of the major challenges in biomass gasification is to suppress tar formation. The current approaches for tar reduction can be classified into two categories: i) product gas cleaning after gasifier (secondary methods), and ii) treatment inside the gasifier (primary methods).[26] Another challenge for H_2 production by biomass gasification is the low yield of H_2 depending on the nature of biomass, such as the contents of cellulose, hemicelluloses and lignin, elemental composition, moisture content, inherent mineral content and physical properties, *etc*.

2.3.3 H_2 production from sugar and sugar-derived carbohydrates

The steam reforming of biomass-derived carbohydrates has been widely practiced for production of synthesis gas, with both the water gas shift reaction and pressure swing separation being typical follow-up steps for pure H_2 production. Among the carbohydrates, the steam reforming of bio-ethanol,[7,27,28] bio-glycerol,[29,30] and bio-butanol[31] has been extensively studied. Arias and his co-workers have also performed studies on steam reforming of bio-ethanol mixtures with addition of glycerol or glycerine.[32,33] The steam reforming of sugar, *e.g.*, glucose, xylose and sucrose, remains a great challenge, mainly due to that they are readily pyrolyzed upon injection and form charcoal in the reaction freeboard. The reforming of sugars apparently requires a very high steam-to-carbon ratio (> 14). The high content of water in the feed was found to reduce sugar decomposition by shortening the residence time of the sugar feed in the high-temperature freeboard above the catalyst bed.[34] One strategy for lowering the requirement of the steam-to-carbon ratio is to improve the contact between the non-volatile molecules and catalyst surfaces in a fluidized-bed reactor, which could largely improve the hydrogen yield and reduce the coke formation.[35] In the meantime, aqueous phase reforming,[36-39] gasification in supercritical water[40] and sorption enhanced reforming[11,41] are interesting alternatives for H_2

production from sugars and sugar-derived carbohydrates in terms of high H_2 yield and low coke formation.

2.4 Bio-ethanol production

Bio-ethanol is one of the most important platform molecules as chemical carrier for hydrogen. Compared with methanol and glycerol, bio-ethanol has advantages of high hydrogen content, low toxicity, low price, *etc*, which lead bio-ethanol very well to a distributed production strategy.[42-44] Besides, as a mixture of ethanol and water, bio-ethanol can involve water that is the most renewable, abundant and cleanest hydrogen carrier into the H_2 generation process.

2.4.1 Ethanol production from sugar and sugar-derived carbohydrates

Bio-ethanol is produced by fermentation of biomass materials. When oxygen is insufficient for normal cellular respiration, anaerobic respiration takes place by yeasts, converting glucose into ethanol and carbon dioxide (**Eq. 2-1**). Sugar cane, switchgrass, potatoes, corns, and other starch-rich materials can be efficiently converted to ethanol by fermentation (**Fig. 2-6**). This method is mature and easy to control. However, the cost of ethanol production is still high mainly due to the expensive feedstock plantation.

$$C_6H_{12}O_6 \rightarrow 2\ C_2H_5OH + CO_2 \qquad \textbf{Eq. 2-1}$$

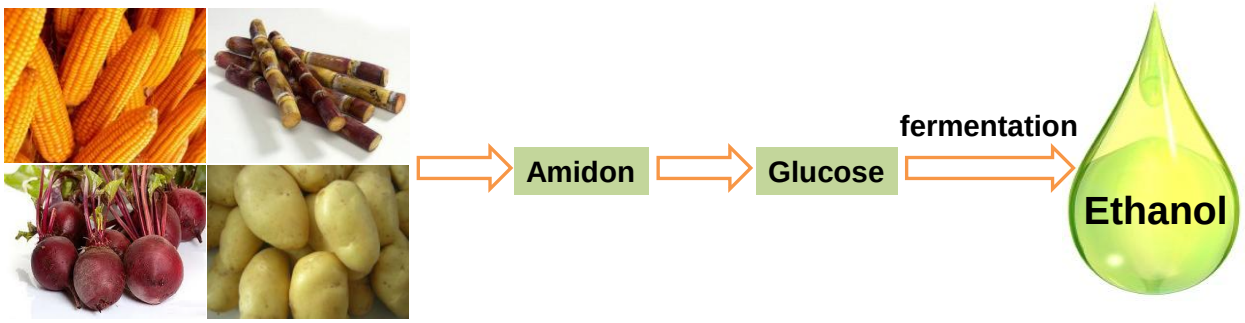

Fig. 2-6 Strategy for ethanol production from sugars and sugar-derived carbohydrates.[16]

2.4.2 Ethanol production from lignocellulosics

As lignocellulosics accounts for about 50% of biomass in the world, there is increasing attention in producing ethanol from lignocellulosic biomass.[45-47] The use of lignocellulosics not only greatly increases the availability of raw materials for ethanol production, but also

considerably reduces the production price. But ethanol production from lignocellulosics is much more difficult than from sugar or sugar-derived materials owing to its more complex molecular structures.[48] Lignocellulosics mainly exist in three forms: cellulose, hemi-cellulose and lignin (**Fig. 2-7**). As cellulose and hemi-cellulose consist of chains of sugar molecules, they can be hydrolyzed to produce monosaccharide that can be used for ethanol production by conversional fermentation.[48]

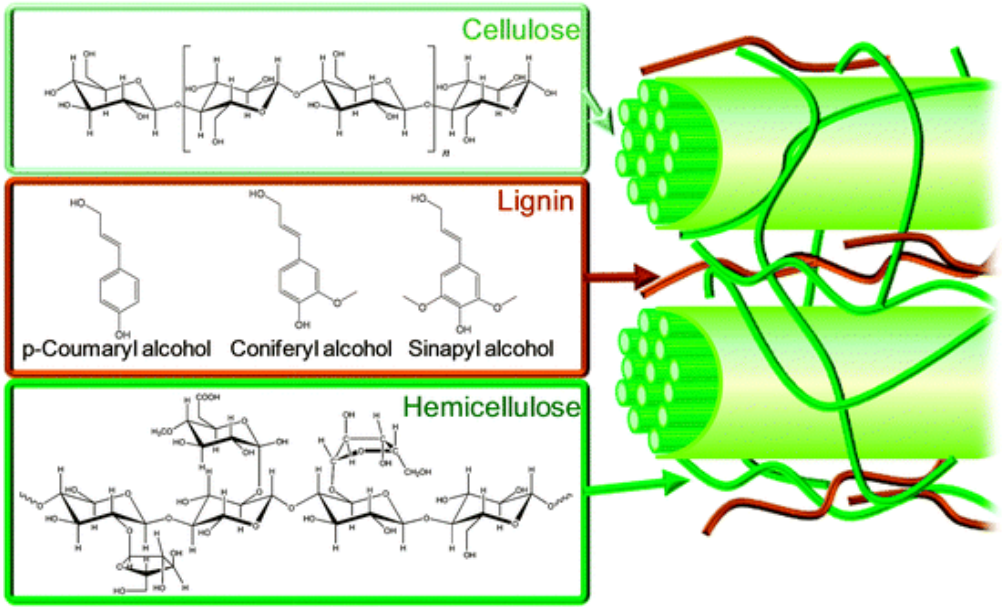

Fig. 2-7 The structure and composition of lignocellulosics.[39]

The main processes for ethanol production from lignocellulosics are illustrated in **Fig. 2-8**.[45] All processes are composed of two steps: i) hydrolysis of cellulose and hemicelluloses to monosaccharide, and ii) subsequent fermentation to produce bio-ethanol. The processes are different in the hydrolysis steps, in which concentrated acid, diluted acid and enzymes are employed.

As acid hydrolysis suffers from equipment corrosion and low glucose yield, there is little research on the technology. Enzymatic hydrolysis is relatively new and has received much more attention.[49]

Compared with separate hydrolysis and fermentation, the simultaneous saccharification and fermentation are more advantageous owing to simpler reactor configuration and enhanced glucose conversion. With the development of genetic engineering, it is expected that bio-ethanol production from lignocellulosic materials will become more efficient and cost-effective.

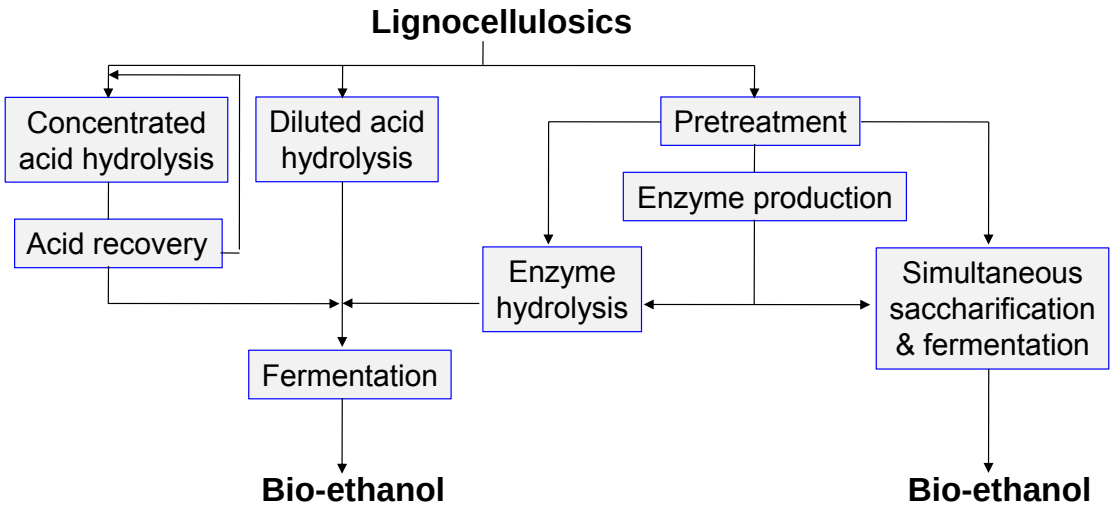

Fig. 2-8 Production of bio-ethanol from lignocellulosics.[16]

2.5 H_2 production from ethanol

2.5.1 H_2 production from steam reforming of ethanol

2.5.1.1 Reactions

The steam reforming of ethanol (SRE) is a very desirable route to produce hydrogen from ethanol. SRE allows producing hydrogen not only from ethanol, but also probably from water. In theory, H_2 production from ethanol can be CO_2 neutral process since all CO_2 produced could be recycled back to plants *via* the photosynthesis reaction. The ideal H_2 production from the steam reforming of ethanol generates only H_2 and CO_2 (**Eq. 2-2**), giving the highest H_2 yield of 6 mol mol_{EtOH}^{-1} in stoichiometry. However, when the steam supply is insufficient, SRE would lead to H_2 and CO (**Eq. 2-3**) with undesirable product and lower H_2 yield.

$$\mathbf{C_2H_5OH + 3\ H_2O \rightarrow 6\ H_2 + 2\ CO_2\ \Delta H^0_{298K} = +174\ KJ\ mol^{-1}} \qquad \textbf{Eq. 2-2}$$

$$C_2H_5OH + H_2O \rightarrow 4\ H_2 + 2\ CO\ \Delta H^0_{298K} = +255\ KJ\ mol^{-1} \qquad \textbf{Eq. 2-3}$$

The steam reforming of ethanol is strongly endothermic reaction with an increase of the number of moles, *i.e.*, 4 mol of reactants lead to 8 mol of gaseous products. Therefore the reaction is favored at high temperature and low pressure.

As a matter of fact, the SRE process involves quite a complicated reaction network accompanied by many possible by-products. Ethanol can undergo some other possible reactions.

Ethanol dehydrogenation to acetaldehyde (**Eq. 2-4**), dehydration to ethylene (**Eq. 2-5**) and cracking (**Eq. 2-6** to **2-8**) are the main possible reaction path ways starting from ethanol.

$$C_2H_5OH \rightarrow CH_3CHO + H_2 \quad \Delta H^0_{298K} = +68 \text{ KJ mol}^{-1} \qquad \textbf{Eq. 2-4}$$

$$C_2H_5OH \rightarrow C_2H_4 + H_2O \quad \Delta H^0_{298K} = +45 \text{ KJ mol}^{-1} \qquad \textbf{Eq. 2-5}$$

$$C_2H_5OH \rightarrow CO + CH_4 + H_2 \quad \Delta H^0_{298K} = +49 \text{ KJ mol}^{-1} \qquad \textbf{Eq. 2-6}$$

$$C_2H_5OH \rightarrow C + CO + 3\ H_2 \quad \Delta H^0_{298K} = +124 \text{ KJ mol}^{-1} \qquad \textbf{Eq. 2-7}$$

$$2\ C_2H_5OH \rightarrow CO_2 + 3\ CH_4 \quad \Delta H^0_{298K} = -74 \text{ KJ mol}^{-1} \qquad \textbf{Eq. 2-8}$$

On the other hand, the gaseous products would also lead to further possible reactions. Acetaldehyde may further decompose to form CO and CH_4 (**Eq. 2-9**), or undergo aldol condensation to acetone (**Eq. 2-10**), or undergo steam reforming to CO and H_2 (**Eq. 2-11**).

$$CH_3CHO \rightarrow CO + CH_4 \qquad \textbf{Eq. 2-9}$$

$$2\ CH_3CHO \rightarrow C_3H_6O + CO + H_2 \qquad \textbf{Eq. 2-10}$$

$$CH_3CHO + H_2O \rightarrow 2\ CO + 3\ H_2 \qquad \textbf{Eq. 2-11}$$

Methane can undergo steam reforming to CO and H_2 (**Eq. 2-12**) at high temperatures, or dehydrogenation to carbon and H_2 (**Eq. 2-13**).

$$CH_4 + H_2O \leftrightarrow CO + 3\ H_2 \qquad \textbf{Eq. 2-12}$$

$$CH_4 \rightarrow C + 2\ H_2 \qquad \textbf{Eq. 2-13}$$

Carbon monoxide can either be transformed to CO_2 *via* the water gas shift reaction (WGS, **Eq. 2-14**), or form carbon through the Boudouard reaction (**Eq. 2-15**). According to thermodynamic analysis, WGS is favored at low temperatures to eliminate CO, while high temperatures facilitate the back reaction of WGS to form CO.

$$CO + H_2O \leftrightarrow CO_2 + H_2 \qquad \textbf{Eq. 2-14}$$

$$2\ CO \rightarrow \text{polymers} \rightarrow C \qquad \textbf{Eq. 2-15}$$

Ethylene derived from ethanol dehydration can easily polymerize and form coke (**Eq. 2-16**), which is also a possible route contributing to carbon formation.

$$n\ C_2H_4 \leftrightarrow C + CO_2 \qquad \textbf{Eq. 2-16}$$

The entire above are the main possible routes existing in the SRE process, in fact, there might be even more possible by-products formed, especially in low temperature range, where some C_3-C_4 products can be generated, such as ethyl acetate and crotonaldehyde. Generally speaking, an ideal SRE is supposed to transform more ethanol and water to CO_2 and H_2, and reduce or avoid the formation of intermediate or by-products products.

In such a context, the crucial factor is to develop highly active, selective, stable and low-cost catalysts that are able to efficiently break the C-C and C-H bonds and promote the subsequent formation of H_2 and CO_2

2.5.1.2 Catalysts for SRE

The steam reforming of bio-ethanol has been comprehensively reviewed by Ni *et al*,[27] de la Piscina and Homs[7], Briens *et al*,[28] and Bion *et al*.[50] A large number of literatures on steam reforming of ethanol has been also synthesized in our laboratory.[51] Therefore, the present thesis will mainly synthesize the very recent literature focusing on Ni-based catalysts regarding several issues, such as steam reforming of raw bio-ethanol, low-temperature high-yield H_2 production from SRE, metal-oxide interaction in metal oxides-supported Ni catalysts for SRE, and Ni-based catalysts involving Mg and Al elements including ex-hydrotalcites for SRE.

Duprez's group performed series of studies on H_2 production from steam reforming of crude bio-ethanol. The effect of various impurities identified in the crude bio-ethanol from sugar beet was studied. The impurities, including acetic acid, diethylamine, butanol, butanal, ethyl acetate and diethylether, were added into a pure ethanol-water mixture (H_2O/EtOH = 4), and then tested over Rh/$MgAl_2O_4$/Al_2O_3 catalyst at 675 °C.[52] The addition of diethylamine or butanal increased ethanol conversion without changing product selectivity, compared to that obtained with pure ethanol-water mixture. The presence of butanol, ethyl acetate and diethylether led to a strong deactivation of the catalyst, moreover H_2 selectivity also decreased; whereas an increase in intermediate products especially ethylene was observed. The deactivation was explained by the coke formation at the catalyst surface. The poisoning effect can be classified in an increasing order: diethylamine < butanal < no impurities < acetic acid < butanol < diethylether < ethyl acetate.[52]

The optimization of catalyst composition with improved stability against various impurities was carried out in the same group.[53,54] In order to disfavor the coke formation, the acidity of the support was decreased by the addition of rare earth elements, the acidic sites being responsible for olefin formation at the origin of coke production were disfavored. The metallic phase was also modified by adding a second metal (Ni, Pt or Pd) favoring either water gas shift or methane reforming reaction. It was shown that the addition of Ni led to the highest H_2 yield. The Rh-Ni/Y-Al_2O_3 catalyst showed good activity, selectivity and stability for steam reforming of crude bio-ethanol, *i.e.*, 97% of ethanol conversion and 3.49 mol mol_{EtOH}^{-1} of H_2 yield were reported after 24 h SRE at 675 °C (H_2O/EtOH = 4).[53,54]

Duprez's group also studied the effect of alcohols as impurities in the steam reforming of crude bio-ethanol over 1 wt% Rh/$MgAl_2O_4$/Al_2O_3 catalyst at 675 °C (H_2O/EtOH = 4).[55] The alcohols studied were methanol, propan-1-ol, butan-1-ol, pentan-1-ol, isopropanol, 2-methyl propan-1-ol, and 3-methyl butan-1-ol. It was shown that ethanol conversion was not modified in the presence of 1% methanol but H_2 yield slightly increased partially due to methanol steam reforming. But addition of linear or branched higher alcohols with more than three carbon atoms led to strong deactivation in conversion and H_2 yield. The effect was more pronounced in the presence of branched alcohols or alcohols with higher number of carbon atoms. It was demonstrated that higher alcohols favored to dehydrate to the corresponding olefin that successively polymerized to yield coke.[55]

Low-temperature high-yield H_2 production from SRE is a very interesting process, which is important and good for the application of hydrogen to fuel cell systems that are regarded as safe and mobile energy generators. However, low-temperature SRE is a very challenging process, as SRE is thermodynamically favored at high temperatures. In the very recent literature, only a few systems have been reported as good candidates for high-yield H_2 production from SRE at very low temperatures ($\leqslant$ 350 °C).

Ciambelli *et al* investigated the effect of the support (Al_2O_3 or CeO_2) on the activity and stability of 1 wt% Pt catalyst for the low temperature SRE.[56,57] Ceria-supported catalyst showed better performance with reference to deactivation rate strictly linked to the greater ability of ceria to release and store oxygen, resulting in higher stability. The characterizations revealed that the presence of very well dispersed PtO_x in ceria, during calcinations step, was stabilized in the highest oxidation state, in contrast to Al_2O_3.[56] The 5 wt% Pt/CeO_2 catalyst was very active and selective, with negligible CO production, and complete ethanol conversion with 35% of H_2 yield

was obtained at 300 °C ($EtOH/H_2O/N_2$ = 0.5/1.5/98).[57] The main promoted reactions were ethanol decomposition, ethanol steam reforming and CO water gas shift. A surface reaction mechanism was proposed involving i) ethanol dissociative adsorption on catalyst surface to form CH_3CHO, ii) decarbonylation to produce mainly H_2, CH_4 and CO, iii) WGS of CO adsorbed on Pt sites to produce H_2 and CO_2.[57]

Chen and the co-workers developed a novel Fe-promoted Rh catalyst for SRE at low temperature. Total conversion and 3.5 mol mol_{EtOH}^{-1} of H_2 yield were reported at 350 °C on the Rh-Fe/Ca- Al_2O_3 catalyst ($EtOH/H_2O/N_2$ = 1.1/11.5/88.4).[58] The Fe oxides in the vicinity of Rh sites reduced the CO adsorption on Rh sites and transferred the adsorbed CO from Rh to COO-formate species on Fe_xO_y for the subsequent water gas shift reaction, leading to a high H_2 yield, extremely low CO selectivity and a long Rh life span.

Huang *et al* compared CeO_2-supported Rh and Co catalysts for low temperature SRE. On Rh/CeO_2 catalyst, the reaction produced a high yield of H_2 production with large amounts of CO and CH_4 mainly by means of adsorbed oxametallacycle decarbonylation (OD) and acetaldehyde steam reforming (ASR). On Co/CeO_2 catalyst, the reaction provided a low H_2 yield with small amounts of CO and CH_4 primarily by ethanol dehydrogenation, ASR and WGS.[59] With a combination of Rh and Co, the reaction followed desired pathway (OD, ASR, and WGS) to result in a small amount of CO, a decreased amount of CH_4, and a high yield of H_2. The bicomponent $(Rh+Co)/CeO_2$ catalyst (Co/Rh = 1.5 in atomic ratio) was reported to obtain CO-free H_2 generation with a H_2 yield of 4.3 mol mol_{EtOH}^{-1} at 300 °C (150 mg of catalyst; $H_2O/EtOH$ = 10).[59]

The metal-support interaction is widely regarded as a very important factor in metal oxides-supported Ni catalysts, such as Ni/CeO_2 and Ni/ZrO_2. The interaction between nickel and oxide support can influence the reducibility, dispersion, catalytic activity and coke resistance of catalysts. Several latest studies focus on improvement of supported Ni catalysts for SRE by enhancement of the metal-oxide interaction.

Ebiad *et al* investigated the activity of nano-sized *x*%$Ni/Ce_{0.74}Zr_{0.26}O$ (*x* = 0, 2, 10, 20) catalysts for H_2 production from SRE.[60] It was found that complete ethanol conversion was obtained at 400 °C over all the catalysts (2 g of catalyst; $H_2O/EtOH$ = 8). H_2 was produced at a very low temperature of 200 °C over 10% and 20% Ni loadings, while a maximum H_2 selectivity (75%) was reached at 600 °C over the 2% $Ni/Ce_{0.74}Zr_{0.26}O$ catalyst. XRD and HRTEM indicated that the interaction between nickel metal and support was greatly strengthened by the small

nickel particle size (2-4 nm) in the 2% Ni/$Ce_{0.74}Zr_{0.26}O$ catalyst, which accounted for its high selectivity.[60]

Li *et al* reported a novel nickel-zirconia (Ni@ZrO_2) nanocomposite for H_2 production *via* SRE.[61] The introduction of nickel particles into the framework of an oxide support with high oxygen mobility could effectively maintain the pore structure of the oxide support and increase the accessibility of the metal particles. Particularly, the size match of the metal and oxide could increase the metal-oxide interface length and strength their interaction. In addition, the confinement effect could effectively prevent metal particles from sintering.[61] The Ni@ZrO_2 nanocomposite showed a nearly complete ethanol conversion during the time on stream over a period of 50 h, at 500 °C and GHSV of 50 000 h^{-1}.

Sharma and the co-workers also studied ZrO_2-supported Ni catalyst with addition of copper for the SRE reaction.[62] Introduction of Cu was found to lower the reduction temperature of the catalyst, which resulted in the increase of dispersion of Ni species indicating the active role of the second component on the alteration of metal-support interaction. At lower loadings, Cu led to an increase surface area and mesoporosity that reflected on the improved catalytic performance of the material. WGS was enhanced and acetaldehyde decomposition as well as reforming was favored in the presence of Cu species. Bimetallic Ni-Cu (3% w/w CuO)/ZrO_2 catalyst was reported to be the most effective towards SRE, exhibiting total ethanol conversion and 84% H_2 selectivity at 600 °C (1 g of catalyst; H_2O/EtOH = 6).[62]

Xu *et al* studied the role of Ni/CeO_2 catalyst under SRE reaction conditions, identified intermediates, and ascertained the reaction pathway leading to the production of hydrogen and the deactivation of the catalyst.[63] Metallic Ni and Ce^{3+} species were demonstrated to be the active components for SRE. Ni helped in the adsorption of ethanol and in the cleavage of C-C bond; while Ce^{3+} species facilitated the decomposition of water with the subsequent formation of OH groups that are essential for reacting with C_xH and C_yO_zH and produce CO_2 and H_2. Both encapsulating carbon and filamentous carbon were formed on the surface of Ni/CeO_2 catalyst. A water-rich atmosphere favored the formation of filamentous carbon which did not lead to the deactivation of the catalyst.[63]

Recently, a new research interest has moved to the Ni-containing mixed oxides obtained from the thermal treatment of hydrotalcite-like compounds (HT-like). The so-called HT-like compounds with a general formula of $[M^{2+}_{1-x}M^{3+}_{x}(OH)_2]^{x+}(A^{n-})_{x/n}\cdot mH_2O$, are the solids that have a structure closely related to that of the mineral hydrotalcite. The structure of HT-like compounds consist of brucite-like layered double hydroxides where the substitution of M^{2+} with M^{3+} cations

leads to a net positive charge, compensated by exchangeable anions in the interlayer space.[64] The oxides obtained from the calcinations of HT-like precursors exhibit several unique properties, such as large surface area, high thermal stability and well-dispersion of metallic particles. As the HT-like compounds can incorporate various metal cations such as Ni^{2+}, Co^{2+} and Cu^{2+}, many researchers have taken them as the catalyst precursor or as the catalyst support.

Resini *et al* studied SRE over Ni-Zn-Al and Ni-Mg-Al catalysts. Ni-Zn-Al catalysts were polyphasic, being a mixture of NiO, ZnO and a spinel $ZnAl_2O_4$ phase. Ni-Mg-Al catalysts were assigned to a monophase of a solid solution of NiO-MgO. IR showed the incorporation of tetrahedrally coordinated Al cations in the mixed oxides.[65] It was reported that total ethanol conversion can be obtained above 750-800 K with only possible products of H_2, CO_2, CO and CH_4. A hydrogen yield of about 5.0 mol mol_{EtOH}^{-1} was obtained at higher than 823 K over the $Ni_{50}Zn_{22}Al_{29}$ catalyst (25 mg of catalyst; EtOH: 2.4 mol%; H_2O: 14.5 mol%).[65]

Li *et al* applied Ni-Mg-Al catalysts for H_2 production from SRE. The catalysts being mainly composed of Ni-Mg-O solid solution phase exhibited good activity and stability for SRE.[66] Ethanol could be completely converted even at 400 °C and hydrogen concentration increased with increasing reaction temperature, gas hourly space velocity (GHSV) and Ni/Mg ratio. It was proposed that Ni^0 phase which was reduced at an optimum temperature of 800 °C was responsible to improve the catalytic activity and stability. Proper amount of Ni^0 species showed good resistance to coke formation.[66]

Yu *et al* studied Cu-promoted NiMgAl catalysts for SRE. The addition of small amounts of Cu to Ni-containing catalysts led to the increase of surface Ni species and the enhancement of Ni^{2+} reducibility.[67] The $Ni_{0.5}Cu_{0.1}Mg_{2.4}Al$ catalyst with Cu/Ni ratio of 0.2 exhibited higher catalytic activity and long-term stability, showing no apparent deactivation during 20 h on stream at 700 °C, *i.e.*, total ethanol conversion and 70% H_2 selectivity (100 mg of catalyst; H_2O/EtOH = 3). This was due to the synergetic effect between Ni and Cu in the bimetallic system providing good metal dispersion, which led to the strong resistance to coke formation and the sintering of Ni particles.[67]

Vizcaíno and the co-workers synthesized a series of NiMAl (M = Mg, Ca, Zn) and NiMgN (N = La, Ce) ex-hydrotalcite catalysts for ethanol steam reforming.[68] NiMgAl mixed oxide exhibited well-stabilized nickel species needing high temperatures to be reduced (around 1100 K). The extent of Ni^{2+} reduction was improved with the replacement of Mg by Ca and Zn or Al by La and Ce. NiMAl (M = Mg, Ca, Zn) catalysts kept almost complete ethanol conversion at 600 °C (315 mg of catalyst; H_2O/EtOH = 3.7), while NiMgN (N = La, Ce) catalysts showed lower

conversion leading to the formation of acetaldehyde. In particular, the presence of Ca resulted in an important dispersing effect over the Ni species, favoring H_2 production (87% of H_2 selectivity) while keeping moderate coke formation.[68] The amount of coke formed varied in the order: NiMgAl >> NiZnAl > NiCaAl > NiMgLa > NiMgCe.

Wu *et al* also reported Ni-CaO-Al_2O_3 multifunctional catalysts for H_2 production *via* sorption enhanced SRE.[69] It was shown uniform distribution of Ni, Ca and Al contributing to the adsorption capacity and reaction activity. In comparison with the mixture of CaO adsorbent and Ni/Al_2O_3 catalyst, this multifunctional catalyst showed higher H_2 concentration and larger CO_2 adsorption capacity. The maximum CO_2 adsorption reached 24.8% at 500 °C over the CA3.5 catalyst, while the CA3.0 catalyst performed the best considering balanced adsorption ability and catalytic activity for SESRE.[69]

Zeng and the co-workers prepared Ni-Mg-Zn-Al ex-hydrotalcite quaternary catalysts for ethanol steam reforming.[70] It was found that catalyst properties and catalytic performance depended on the Mg/Zn molar ratio. The catalyst with a Mg/Zn ratio of 4 improved the Ni dispersion and the average pore diameter, enhanced the NiO-MgO synergetic effect. At 700 °C, the $NiMgZn_4Al$ catalyst exhibited the highest H_2 yield of 4.84 mol mol_{EtOH}^{-1} and the best stability of 100 h on stream (200 mg of catalyst; H_2O/EtOH = 3).[70] Ternary catalyst without Mg suffered severe coke formation.

Coleman *et al* studied Mg-Al mixed oxide-supported Ni catalysts for ethanol steam reforming. A series of 10 wt% Ni/Mg-Al catalysts with different Mg/Al ratios were prepared and the influence of support compositions was analyzed.[71] Catalytic performance was dependent upon the Mg/Al ratio. Ni/Mg-Al catalyst was found to give better activity, H_2 and CO_x selectivity, and stability compared to the pure oxide-supported Ni catalysts. This was illustrated by the incorporation of the pure oxides, MgO and Al_2O_3 into $MgAl_2O_4$ phase. In addition, $MgAl_2O_4$ was shown to be a slight basic material exhibiting moderate acidic and basic site strength and density compared to the pure oxides support.[71] Total ethanol conversion with about 5.1 mol mol_{EtOH}^{-1} of H_2 production was obtained at 650 °C over the Ni/Mg_2Al and Ni/$MgAl_2$ catalysts (50 mg of catalyst; H_2O/EtOH = 8.4).

Szijjártó *et al* also performed studies on $MgAl_2O_4$-supported metal catalysts for SRE, including noble metals of Pt, Pd, Au, and non-noble metals of Ni, Co, Cu, Zn, La, Ce, Zr.[72] It was revealed that practically no noble metal is required in order to achieve high H_2 yield. At 500 °C, a four-component catalyst containing Ni, Co, Ce and Mo led to 4.4 mol mol_{EtOH}^{-1} of H_2 yield (H_2O/EtOH = 9). The strong synergism between Ni and Co was responsible for the high

activity in H_2 production. The addition of Ce to $NiCo/MgAl_2O_4$ system proved to be advantageous, resulting in further improvement in H_2 yield and suppression of coke formation. The presence of Mo hindered all reactions of CO in the temperature range between 320-370 °C (coke formation *via* Boudouard reaction).[72]

In our laboratory, $CeNi_XO_Y$ mixed oxides were developed as active and selective catalysts for H_2 production from SRE.[51,73,74] After *in situ* treatment in H_2 between 200-300 °C, the $CeNi_XO_Y$ solids became hydrogen reservoirs, called oxyhydrides, with the presence of hydrogen species of hydride nature in the anionic vacancies of the solid. Hydrogen can be produced at low temperatures $\leqslant$ 250 °C, *i.e.*, 55% of ethanol conversion and 50 mol% H_2 were obtained on the $CeNi_{0.7}O_Y$ catalyst in the presence of high concentration of ethanol (200 mg of catalyst; $EtOH/H_2O/N_2$ = 14/42/44).[74] The active Ni species belonged to NiO crystallites and/or to Ce-Ni solid solution where Ni species were in close interaction with Ce species. The presence of small NiO nanoparticles and/or Ce-Ni solid solution allowed optimizing the content of these Ni species presenting the characteristic of being able to be reduced and reoxidized easily and reversibly.[73,74]

2.5.2 H_2 production from oxidative steam reforming of ethanol

2.5.2.1 Reactions

Steam reforming of ethanol (**Eq. 2-2**) is an endothermic process in the absence of O_2 and requires extra energy input to initiate the reactions. Alternatively, hydrogen can be produced by partial oxidation of ethanol (POE) according to the following equation (**Eq. 2-17**). POE is an exothermic process.

$$C_2H_5OH + 1.5\ O_2 \rightarrow 3\ H_2 + 2\ CO_2\ \Delta H^0_{298K} = -545\ KJ\ mol^{-1} \qquad \textbf{Eq. 2-17}$$

However, hydrogen selectivity of POE is generally low. In order to enhance H_2 production, autothermal reforming of ethanol can be applied. Autothermal reforming of ethanol, generally called the oxidative steam reforming of ethanol (OSRE), can be regarded as a combination of SRE and POE, which can be expressed by the following equation (**Eq. 2-18**).

$$\mathbf{C_2H_5OH + (3\text{-}2\delta)\ H_2O + \delta\ O_2 \rightarrow (6\text{-}2\delta)\ H_2 + 2\ CO_2} \qquad \textbf{Eq. 2-18}$$

OSRE has advantages as coke formation can be significantly inhibited by the presence of O_2. Thus, long-term stable operation can be achieved.

2.5.2.2 Catalysts for OSRE

The OSRE reaction is generally studied in the catalytic fixed-bed reactors or the micro-channel membrane reactors.[75-77] The oxidative steam reforming of ethanol in the last decade has been reviewed by Ni *et al*.[27] The relevant literatures have been also synthesized in our laboratory.[51] OSRE *via* membrane reactors has been recently reviewed by Iulianelli *et al*.[76] The present thesis will mainly focus on synthesizing the very recent literatures on OSRE, *i.e.*, metal catalysts fixed-bed systems, including the oxides-supported metal catalysts and Ni-, Co-, Cu-based mixed oxides.

Youn *et al* reported the effect of support acidity on oxides-supported Ni catalysts for OSRE. Ni catalysts supported on pure metal oxides (ZnO, MgO, ZrO_2, TiO_2 and Al_2O_3) with different acidity were prepared and applied to H_2 production from OSRE.[78] Acidity of supports determined by NH_3-TPD increased in the order: MgO < ZnO < TiO_2 < ZrO_2 < Al_2O_3. A correlation between H_2 yield and acidity of supports showed a volcano-shaped curve, *i.e.*, TiO_2 and ZrO_2 with an intermediate acidity were found to be efficient supporting materials. As a result, a series of Ni catalysts supported on TiO_2-ZrO_2 mixed oxides ($Ti_XZr_{1-X}O_2$) with different Ti content (x = 0, 0.2, 0.5, 0.8 and 1) were prepared and studied for OSRE. Ni/$Ti_{0.2}Zr_{0.8}O_2$ with intermediate acidity of support exhibited the best catalytic performance, *i.e.*, total ethanol conversion and 2.6 mol mol_{EtOH}^{-1} of H_2 yield were reported at 500 °C after a 15 h reaction (50 mg of catalyst; H_2O/EtOH/O_2 = 3/1/0.5).[78] $Ti_{0.2}Zr_{0.8}O_2$ support with partial metal substitution favorably served as supporting material for improving nickel dispersion and reducibility of the catalyst, leading to an enhanced catalytic performance.

Hung *et al* investigated the catalytic performance and mechanism of OSRE on a series of Al_2O_3-supported metal catalysts under various conditions (H_2O/EtOH and O_2/EtOH ratios).[79] The reaction over Group 11 metals (Cu, Ag and Au) preferentially followed the oxidation pathway and primarily produced acetaldehyde. The dehydration of ethanol favorably occurred on Co, Ni, Pd and Pt with higher selectivity of ethylene. The C-C bond of ethanol was efficiently ruptured on Ru, Rh and Ir, leading to the highest CO_x formation and the best H_2 yield. In addition, increasing H_2O/EtOH and O_2/EtOH ratios can improve catalytic activity, attributed to atomic oxygen from H_2O (in WGS) and O_2 (in oxidation). This concept led to a CeO_2-modified catalyst, nearly optimum conversion (97%) and H_2 yield (about 3 mol mol_{EtOH}^{-1}) was reported at 600 °C on 1.6 wt% Rh/Ce-Al_2O_3 catalyst (125 mg) with 100% selectivity for C_1 products (H_2O/EtOH/O_2 = 3/1/0.3).[79]

Chen and the co-workers reported OSRE over Ir/CeO_2 catalyst, in which the effect of *in situ* dispersion of Ir was studied.[80] Physicochemical characterizations showed that La_2O_3 was transformed into hexagonal $La_2O_3CO_3$ during the OSRE reaction, which suppressed coking effectively. Reduced Ir metal can strongly react with $La_2O_3CO_3$ leading to the formation of Ir-doped $La_2O_3CO_3$. It dynamically formed and decomposed to release active Ir nanoparticles, thereby preventing the catalyst from sintering and affording high dispersion of Ir/CeO_2 catalyst elevated temperature. The surface Ir concentration was significantly improved using ultrasonic-assisted impregnation method, while the *in situ* dispersion effect inhibited Ir from sintering.[80] The Ir crystallite size in the 9 wt% Ir/CeO_2 catalyst was maintained at 3.2 nm after 100 h OSRE at 650 °C, giving total ethanol conversion and 80% selectivity of H_2 (200 mg of catalyst; $H_2O/EtOH/O_2 = 3/1/0.83$).

Pereira *et al* studied the effect of the addition of Rh and K in Co/CeO_2-ZrO_2 catalyst for H_2 production from OSRE. K addition greatly improved the catalytic behavior of CeO_2-ZrO_2-supported Co or Co-Rh catalysts, *i.e.*, small Co particles formed on monometallic (Co-) or bimetallic (Co-Rh) K-containing catalysts. The addition of Rh facilitated Co reducibility and enhanced activity under OSRE conditions.[81] Although the presence of Rh favored the formation of methane, bimetallic $CoRh/CeO_2$-ZrO_2 catalyst showed high activity at temperature as low as 320 °C. The $Co_{0.02}Rh(K)/ CeO_2$-ZrO_2 catalyst (100 mg) exhibited total ethanol conversion and a stable (40 h) H_2 yield of about 50% with only CH_4 as by-product ($H_2O/EtOH/O_2 = 6/1/0.5$).[81]

Andonava *et al* studied the effect of the Co addition on the structure and redox properties of $Ni/\gamma Al_2O_3$ catalyst for OSRE *via in situ* temperature resolved X-ray absorption near edge structure spectroscopy (XANES).[82] The characterizations clearly indicated that the Co addition into the Ni/Al_2O_3 system had a considerable effect on the metal-support interaction, by assisting the formation of NiO and Co_3O_4 species weakly interacting with Al surface and decreasing the reduction temperature compared to that of the monometallic system. It was found that the reducibility of the metallic oxides species in bimetallic $CoNi/Al_2O_3$ catalysts increased with increasing Co content. The Co addition to the Ni/Al_2O_3 system prevented some of the unfavorable aspects related to the partial oxidation of metallic particles during OSRE. This was due to the synergetic effect between the Ni and Co components which reflected to a significant extent on the ability of Ni and Co oxides species to be reduced with hydrogen produced during OSRE. The $6CoNi/Al_2O_3$ catalyst was reported to exhibit the best performance, *i.e.*, total ethanol conversion at 500 °C with about 64 mol% of H_2 formation ($H_2O/EtOH/O_2 = 6/1/0.5$).[82]

Cai and the co-workers performed a systematic study for identifying the relationship between the catalyst morphology/structure and catalytic performance in OSRE over a series of Ir/CeO_2 catalysts.[83] The dispersion of both the ceria support and Ir phase was shown to strictly control key parameters, such as diffusion of oxygenated adspecies along the ceria surface, the surface basicity, and the concentration of coupled sites formed at the metal-support interface between peripheral ceria defects and Ir coordinately unsaturated sites (CUS). All the above factors were found to be critical for ethanol conversion, H_2 selectivity and resistance to aging upon long-term testing. It was demonstrated that OSRE on Ir/CeO_2 catalysts was a structure sensitive reaction, leading to either an effective bifunctional or a more monofunctional mechanism depending on the domain of ceria and Ir dispersion.[83] Well-dispersed active phases therefore led to stable and selective catalysts. Total ethanol conversion and 50 mol% of H_2 formation were obtained at 450 °C on the 1.9 wt% Ir/CeO_2 (ceria support calcined at 400 °C) catalyst (300 mg of catalyst; $H_2O/EtOH/O_2 = 1.8/1/0.6$).

Up to date, only a few mixed oxide catalysts have been reported for H_2 production from OSRE. Velu *et al* applied CuNiZnAl ex-hydrocalcite mixed oxides to the OSRE.[84] CuZnAl and NiZnAl catalysts were equally active, exhibiting an ethanol conversion close to 100% at 300 °C (100 mg of catalyst; $H_2O/EtOH/O_2 = 3/1/0.4$). CuZnAl produced acetaldehyde and H_2 as major products, while NiZnAl or CuNiZnAl produced a mixture of H_2, CO, CO_2, CH_4. The CoNi-based catalysts were found to exhibit better catalytic performance with lower selectivity of undesirable products. Depending on the reaction conditions, a H_2 yield between 2.5 and 3.5 mol mol_{EtOH}^{-1} could be obtained over those catalysts (100 mg of catalyst; $H_2O/EtOH/O_2 = 3/1/0.4$).[84]

Velu and the co-workers then used *in situ* XPS technique to further understand the active species of $Cu_{1-x}Ni_xZnAl$ catalysts involved in OSRE.[85] A combined XPS and XAES investigation clearly indicated the existence of Cu^{2+}, Ni^{2+} and Zn^{2+} species on the calcined materials. Upon *in situ* H_2-reduction the Cu^{2+} was fully reduced to Cu^0 and Ni^{2+} reduced partially (fully) to Ni^0 at 300 °C (500 °C). The extent of Ni metal cluster formation increased with decreasing Cu-content at 300 °C.[85] XPS results demonstrated the existence of a well dispersed Cu on mostly ZnO support. This scenario progressively changed to well dispersed active metals (Cu and Ni) on $ZnO + Al_2O_3$ support with some metal-support interactions on Cu + Ni systems. For Ni-rich system, the interaction with support was relatively higher than the above Cu-containing systems and Ni was somewhat decorated preferentially by Al and Zn.[85] The addition of Ni to CuZnAl-system did not influence ethanol conversion significantly and it remained about 90% at 300 °C on all the catalysts, irrespective of the composition. H_2 yield (selectivity) varied

between 2.6-3.0 mol mol_{EtOH}^{-1} independent of catalyst composition (100 mg of catalyst; $H_2O/EtOH/O_2$ = 3/1/0.4).

Guil-López *et al.* studied series of Co, Ni and Cu oxides derived from hydrotalcite-like precursors for OSRE.[86] It was shown that the particle size of the segregated active metal oxide decreased upon the increasing of the crystallinity of HT-like precursors. Moreover those small particle sizes favored the strong interactions between active metals and the amorphous matrix of Al-modified cations, causing a high stabilization of the active metal phases. The $CoAl_{0.7}$, $CoZn_{2.4}Al_{1.9}$, $CoMg_{2.2}Al_{1.9}$ and $NiMg_{2.3}Al_{1.9}$ catalysts could all compeletely convert ethanol between 450 and 575 °C with H_2 formation of about 55 mol% during 4 h ($H_2O/EtOH/O_2$ = 2.28/1/0.36).[86] The best catalyst for H_2 production was CoZnAl, in which the Zn presence increased the reducibility of Co^{2+}. This was attributed to cause the higher H_2 selectivity on CoZnAl at 575 °C.

Lima *et al.* applied $La_{1-x}Ce_xNiO_3$ perovskite-type oxides to OSRE, the $La_{0.9}Ce_{0.1}NiO_3$ oxide allowed obtaining total conversion with about 45 mol% of H_2 formation at 500 °C ($H_2O/EtOH/O_2$ = 3/1/0.5).[87] The higher resistance to carbon formation on the $La_{0.9}Ce_{0.1}NiO_3$ catalyst was due to the smaller Ni crystallite size. Furthermore, the support also played an important role on catalyst stability during OSRE. The reduced $La_{0.9}Ce_{0.1}NiO_3$ oxide exhibited the highest amount of oxygen vacancies, which decreased as ceria content increased. This highly mobile oxygen reacted with carbon species as soon as it formed, and thus keeps the metal surface free of carbon, inhibiting deactivation.[87]

In our laboratory, a novel $CeNiH_ZO_Y$ nano-oxyhydride was developed as highly efficient and stable catalyst for H_2 production from OSRE at room temperature.[88] This promising technology can dramatically save energy by means of a smart combination of the strong exothermic reaction between the hydride species in the catalyst and O_2 (chemical energy) and the exothermic reaction between ethanol and O_2 (POE). The $CeNiH_ZO_Y$ nano-oxyhydride catalyst turned out to be able to simultaneously activate ethanol, produce hydrogen at room temperature, and provide hydride species to sustain the chemical reaction with O_2. Total conversion and 45 mol% H_2 were obtained with an oven temperature of only 60 °C (30 mg of catalyst; $H_2O/EtOH/O_2$ = 3/1/1.6).[88] The $CeNiH_ZO_Y$ nano-oxyhydride catalyst showed remarkable catalytic stability at least for 70 h OSRE.

2.6 Objective of the thesis

In summary, catalytic transformation of ethanol in the presence of water (bio-ethanol) is a very desirable route to produce H_2. In the literature, Ni-based catalysts have been widely reported for H_2 production from catalytic transformation of ethanol based on its excellent activity to break the C-C and C-H bonds. However, Ni-based catalysts easily suffer deactivation caused by metal sintering and coke formation with the time on stream. Hence the objective of the present thesis is to develop highly active, selective, stable and low-cost Ni-based catalysts to produce high yield of H_2 from ethanol. The transformation is performed *via* two routes, steam reforming of ethanol and oxidative steam reforming of ethanol.

Ni-containing mixed oxides derived from hydrotalcite-like compounds have several attractive properties. It allows obtaining the materials with large surface area, good thermal stability and uniform dispersion of each metal component. Ni-based ex-hydrotalcite catalysts enable to enhance the interactions between Ni species and other metal cations, leading to the strong synergetic effect in multicomponent catalyst, which can suppress nickel sintering and carbon formation.

In our laboratory, Ce-Ni mixed oxides have been studied owing to the strong interactions between Ni and Ce species. As a fluorite-type oxide, CeO_2 has been applied to various reactions in order to take advantage of its oxygen storage capacity and/or oxygen diffusion property. The release and uptake of oxygen by CeO_2 allow it to participate in the redox reactions, and the enhancement of the formation of oxygen vacancies attributed to the replacement of cerium cations by nickel cations (in solid solution) and also to the reduction of cerium cations.

Herein in the present thesis, two types of Ni-based catalysts, $CeNi_XO_Y$ and $Ni_XMg_2AlO_Y$, were studied for H_2 production from ethanol *via* steam reforming and oxidative steam reforming. Numerous physicochemical techniques were used to characterize the catalysts. Many different reaction parameters were comprehensively analyzed. The correlation between the catalytic performances and the catalysts properties were established. The active phase, active sites and possible mechanism were discussed.

2.7 References

[1] G. W. Huber, S. Iborra and A. Corma, *Chem. Rev.*, 2006, **106**, 4044.

[2] R. Kothari, D. Buddhi and R. L. Sawhney, *Renewable Sustainable Energy Rev.*, 2008, **12**, 553.

[3] M. T. Balta, I. Dincer and A. Hepbasli, *Int. J. Hydrogen Energy*, 2009, **34**, 2925.

[4] E. Kirtay, *Energy Conversion and Management*, 2011, **52**, 1778.

[5] H. Arakawa, M. Aresta, J. N. Armor, M. A. Barteau, E. J. Beckman, A. T. Bell, J. E. Bercaw, C. Creutz, E. Dinjus, D. A. Dixon, K. Domen, D. L. DuBois, J. Eckert, E. Fujita, D. H. Gibson, W. A. Goddard, D. W. Goodman, J. Keller, G. J. Kubas, H. H. Kung, J. E. Lyons, L. E. Manzer, T. J. Marks, K. Morokuma, K. M. Nicholas, R. Periana, L. Que, J. Rostrup-Nielson, W. M. H. Sachtler, L. D. Schmidt, A. Sen, G. A. Somorjai, P. C. Stair, B. R. Stults and W. Tumas, *Chem. Rev.*, 2001, **101**, 953.

[6] D. Chen and L. He, *ChemCatChem*, 2011, **3**, 490.

[7] P. R. de La Piscina and N. Homs, *Chem. Soc. Rev.*, 2008, **37**, 2459.

[8] N. H. Florin and A. T. Harris, *Chem. Eng. Sci.*, 2008, **63**, 278.

[9] R. C. Saxena, D. Seal, S. Kumar and H. B. Goyal, *Renewable Sustainable Energy Rev.*, 2008, **12**, 1909.

[10] S. Sato, S.-Y. Lin, Y. Suzuki and H. Hatano, *Fuel*, 2003, **82**.561.

[11] L. He, J. M. S. Parra, E. A. Blekkan and D. Chen, *Energy Environ. Sci.*, 2010, **3**, 1046.

[12] S. Satyapal, *DOE Hydrogen Prohram-FY 2009 Annual Progress Report*, Department of Energy, USA, 2009.

[13] S. Brethauer and C. E. Wyman, *Bioreour. Technol.*, 2010, **101**, 4862.

[14] V. Monedero, G. Perez-Martinez and M. J. Yebra, *Appl. Microbiol. Biotechnol.*, 2010, **86**, 1003.

[15] D. Mohan, C. U. Pittman and P. H. Steelle, *Energy Fuels*, 2006, **20**, 848.

[16] M. Li, D. Y. C. Leung, M K. H. Leung and K. Sumathy, *Fuel Process. Technol.*, 2006, **87**, 461.

[17] J. R. Rostrup-Nielsen and R. Nielsen, *Catal. Rev. Sci. Eng.*, 2004. **46**, 247.

[18] L. Garcia, R. French, S. Czernik and E. Chornet, *Appl. Catal. A*, 2000, **201**, 225.

[19] C. Wu and R. H. Liu, *Int. J. Hydrogen Energy*, 2010, **35**, 7386.

[20] Y. Kalinci, A. Hepbasli and I. Dincer, *Int. J. Hydrogen Energy*, 2009, **34**, 8799.

[21] K. J. Ptasinski, *Biofuels, Bioprod. Biorefin.*, 2008, **2**, 239.

[22] J. Corella, J. M. Toledo and G. Molina, *Ind. Eng. Chem. Res.*, 2006, **45**, 6137.

[23] J. Fermoso, F. Rubiera and D. Chen, *Energy Environ. Sci.*, 2012, **5**, 6358.

[24] A. A. Peterson, F. Vogel, R. P. Lachance, M. Floring, M. J. Antal and J. W. Tester, *Energy Environ. Sci.*, 2008, **1**, 32.

[25] Y. Guo, S. Z. Wang, D. H. Xu, Y. M. Gong, H. H. Ma and X. Y. Tang, *Renewable Sustainable Energy Rev.*, 2010, **14**, 334.

[26] L. Devi, K. J. Ptasinski and F. Jassen, *Biomass Bioenergy*, 2003, **24**,125.

[27] M. Ni, D. Y. C. Leung and M. K. H. Leung, *Int. J. Hydrogen Energy*, 2007, **32**, 3238.

[28] C. Briens, J. Piskorz and F. Berruti, *Int. J. Chem. React. Eng.*, 2008, **6**.

[29] C. H. C. Zhou, J. N. Beltramini, Y. X. Fan and G. Q. M. Lu, *Chem. Sco. Rev.*, 2008, **37**, 527.

[30] P. D. Vaidya and A. E. Rodrigues, *Chem. Eng. Technol.*, 2009, **32**, 1463.

[31] W. Cai, N. Homs and P. Ramirez de la Piscina, *Green Chem.*, 2012, **14**, 1035.

[32] M. El Doukkali, A. Iriondo, P. L. Arias, J. F. Cambra, I. Gandarias and V. L. Barrio, *Int. J. Hydrogen Energy*, 2012, **37**, 8298.

[33] A. Iriondo, V. L. Barrio, M. El Doukkali, J. F. Cambra, M. B. Güemez, J. Requies, P. L. Arias, M. C. Sánchez-Sánchez, R. Navarro and J. L. G. Fierro, *Int. J. Hydrogen Energy*, 2012, **37**, 2028.

[34] M. Marquevich, S. Czernik, E. Chornet and D. Montane, *Energy Fuels*, 1999, **13**, 1160.

[35] S. Czernik, R. French, C. Feik and E. Chornet, *Ind. Eng. Chem. Res.*, 2002, **41**, 4209.

[36] K. Sato, K. Kawano, A. Ito, Y. Takita and K. Nagaoka, *ChemSusChem*, 2010, **3**, 1364.

[37] M. El Doukkali, A. Iriondo, P. L. Arias, J. Requies, I. Gandarías, L. Jalowiecki-Duhamel and F. Dumeignil, *Appl. Catal. B*, 2012, **125**, 516.

[38] M. El Doukkali, A. Iriondo, J. F. Cambra, L. Jalowiecki-Duhamel, A. S. Mamede, F. Dumeignil and P. L. Arias, *J. Mol. Catal. A: Chem.*, 2013, **368–369**, 125.

[39] D. M. Alonso, S. G. Wettstein and J. A. Dumesic, *Chem. Soc. Rev.*, 2012, **41**, 8075.

[40] C. T. Tye and K. J. Smith, *Catal. Today*, 2006, **116**, 461.

[41] L. He and D. Chen, *ChemSusChem*, 2012, **5**, 587.

[42] P. Leung, A. Tsolakis, J. Rodriguez-Fernandez and S. Golunski, *Energy Environ. Sci.*, 2010, **3**, 780.

[43] A. Iulianelli and A. Basile, *Catal. Sci. Technol.*, 2011, **1**, 366.

[44] L. Wang, R. Templer and R. J. Murphy, *Energy Environ. Sci.*, 2012, **5**, 8281.

[45] M. Galbe and G. A. Zacchi, *Appl. Microbiol. Biotechnol.*, 2002, **59**, 618.

[46] B. C. Dien, M. A. Cotta and T. W. Jeffries, *Appl. Microbiol. Biotechnol.*, 2003, **63**, 258.

[47] K. Nakashima, K. Yamaguchi, N. Taniguchi, S. Arai, R. Yamada, S. Katahira, N. Ishida, H. Takahashi, C. Ogino and A. Kondo, *Green Chem.*, 2011, **13**, 2948.

[48] Y. Sun and J. Y. Cheng, *Bioresource Technol.*, 2002, **83**, 1.

[49] M. L. Rabinovich, *Appl. Biochem. Microbiol.*, 2006, **42**, 1.

[50] N. Bion, D. Duprez and F. Epron, *ChemSusChem*, 2012, **5**, 76.

[51] C. Pirez, *Thèse*, Univ. Lille 1, décembre 2010.

[52] A. Le Valant, A. Garron, N. Bion, F. Epron and D. Duprez, *Catal. Today*, 2008, **138**, 169.

[53] A. Le Valant, F. Can, N. Bion, D. Duprez and F. Epron, *Int. J. Hydrogen Energy*, 2010, **35**, 5015

[54] A. Le Valant, N. Bion, F. Can, D. Duprez and F. Epron, *Appl. Catal. B*, 2010, **97**, 72.

[55] A. Le Valant, A. Garron, N. Bion, D. Duprez and F. Epron, *Int. J. Hydrogen Energy*, 2011, **36**, 311.

[56] P. Ciambelli, V. Palma and A. Ruggiero, *Appl. Catal. B*, 2010, **96**, 18.

[57] P. Ciambelli, V. Palma and A. Ruggiero, *Appl. Catal. B*, 2010, **96**, 190.

[58] L. Chen, C. K. S. Choong, Z. Zhong, L. Huang, T. P. Ang, L. Hong and J. Lin, *J. Catal.*, 2010, **276**, 197.

[59] L. Huang, C. Choong, L. Chen, Z. Wang, Z. Zhong, C. Campos-Cuerva and J. Lin, *ChemCatChem*, 2013, **5**, 220.

[60] M. A. Ebiad, D. R. Abd El-Hafiz, R. A. Elsalamony and L. S. Mohamed, *RSC Adv.*, 2012, **2**, 8145.

[61] S. Li, C. Zhang, Z. Huang, G. Wu and J. Gong, *Chem. Commun.*, 2013, **49**, 4226.

[62] P. K. Sharma, N. Saxena, A. Bhatt, C. Rajagopal and P. K. Roy, *Catalysis Science & Technology*, 2013, **3**, 1017.

[63] W. Xu, Z. Liu, A. C. Johnston-Peck, S. D. Senanayake, G. Zhou, D. Stacchiola, E. A. Stach and J. A. Rodriguez, *ACS Catal.*, 2013, **3**, 975.

[64] D. P. Debecker, E. M. Gaigneaux and G. Busca, *Chem. Eur. J.*, 2009, **15**, 3920.

[65] C. Resini, T. Montanari, L. Barattini, G. Ramis, G. Busca, S. Presto, P. Riani, R. Marazza, M. Sisani, F. Marmottini and U. Costantino, *Appl. Catal. A*, 2009, **355**, 83.

[66] M. Li, X. Wang, S. Li, S. Wang and X. Ma, *Int. J. Hydrogen Energy*, 2010, **35**, 6699.

[67] X.-P. Yu, W. Chu, N. Wang and F. Ma, *Catal. Lett.*, 2011, **141**, 1228.

[68] A.J. Vizcaíno, M. Lindo, A. Carrero and J.A. Calles, *Int. J. Hydrogen Energy*, 2012, **37**, 1985.

[69] G. Wu, C. Zhang, S. Li, Z. Huang, S. Yan, S. Wang, X. Ma and J. Gong, *Energy Environ. Sci.*, 2012, **5**, 8942.

[70] G. Zeng, Q. Liu, R. Gu, L. Zhang and Y. Li, *Catal. Today*, 2011, **78**, 206.

[71] L.J.I. Coleman, W. Epling, R.R. Hudgins and E. Croiset, *Appl. Catal. A*, 2009, **363**, 52.

[72] G.P. Szijjártó, A. Tompos and J.L. Margitfavi, *Appl. Catal. A*, 2011, **391**, 417.

[73] L. Jalowiecki-Duhamel, C. Pirez, M. Capron, F. Dumeignil and E. Payen, *Catal. Today*, 2010, **157**, 456.

[74] L. Jalowiecki-Duhamel, C. Pirez, M. Capron, F. Dumeignil and E. Payen, *Int. J. Hydrogen Energy*, 2010, **35**, 12741.

[75] B. Neltner, B. Peddie, A. Xu, W. Doenlen, K. Durand, D. S. Yun, S. Speakman, A. Peterson and A. Belcher, *ACS Nano*, 2010, **4**, 3227.

[76] A. Iulianelli and A. Basile, *Catal. Sci. & Technol.*, 2011, **1**, 366.

[77] N. Zhu, X. Dong, Z. Liu, G. Zhang, W. Jin and N. Xu, *Chem. Commun.*, 2012, **48**, 7137.

[78] M. H. Youn, J. G. Seo, H. Lee, Y. Bang, J. S. Chung and I. K. Song, *Appl. Catal. B*, 2010, **98**, 57.

[79] C.-C. Hung, S.-L. Chen, Y.-K. Liao, C.-H. Chen and J.-H. Wang, *Int. J. Hydrogen Energy*, 2012, **37**, 4955.

[80] H. Chen, H. Yu, F. Peng, H. Wang, J. Yang and M. Pan, *J. Catal.*, 2010, **269**, 281.

[81] E. B. Pereira, P. Ramírez De La Piscina, S. Martí and N. Homs, *Energy Environ. Sci.*, 2010, **3**, 487.

[82] S. Andonova, C. N. de Ávila, K. Arishtirova, J. M. C. Bueno and S. Damyanova, *Appl. Catal. B*, 2011, **105**, 346.

[83] W. Cai, F. Wang, C. Daniel, A. C. van Veen, Y. Schuurman, C. Descorme, H. Provendier, W. Shen and C. Mirodatos, *J. Catal.*, 2012, **286**, 137.

[84] S. Velu, N. Satoh, C. S. Gopinath and K. Suzuki, *Catal. Lett.*, 2002, **82**, 145.

[85] S. Velu, K. Suzuki, M. Vijayaraj, S. Barman and C. S. Gopinath, *Appl. Catal. B*, 2005, **55**, 287.

[86] R. Guil-López, R. M. Navarro, M. A. Peña and J. L. G. Fierro, *Int. J. Hydrogen Energy*, 2011, **36**, 1512.

[87] S. M. de Lima, A. M. da Silva, L. O. O. da Costa, J. M. Assaf, L. V. Mattos, R. Sarkari, A. Venugopal and F. B. Noronha, *Appl. Catal. B*, 2012, **121–122**, 1.

[88] C. Pirez, M. Capron, H. Jobic, F. Dumeignil and L. Jalowiecki-Duhamel, *Angew. Chem. Int. Ed*, 2011, **50**, 10193.

3 Preparation and characterization of catalysts

Ni-based catalysts are the most attractive and extensively studied systems for ethanol steam reforming among all the non-noble metal catalysts. In our laboratory, the binary $CeNi_XO_Y$ mixed oxides have been studied because of the strong interactions between nickel and cerium species leading to interesting properties of the materials.[1,2] $CeNi_XO_Y$ mixed oxides have been reported as active catalyst for H_2 production from the transformation of ethanol in the presence of water at low temperatures.[3,4] Studying the preparation methods for Ce-Ni compounds allows better understanding this material, moreover it may bring about promising catalytic performances.

On the other hand, a recent research interest has focused on nickel-containing mixed oxides obtained from the thermal treatment of hydrotalcite-like compounds. HT-like compounds can incorporate various metal cations, such as Ni^{2+}, Cu^{2+} and Co^{2+}, which are largely used as catalyst precursors. The ex-hydrocalcite materials embrace several significant properties, such as large surface area, well-dispersed metallic particles and high thermal stability.

In the present thesis, two types of Ni-based catalysts are synthesized and studied. Ce-Ni catalysts are prepared by different methods, namely co-precipitation (CP), impregnation (IMP) and incipient wetness impregnation (IWI) methods. Ni-Mg-Al ternary mixed oxides are prepared by CP method. Various physicochemical techniques, such as N_2 physisorption, XRD, Raman, H_2-TPR, XPS, *in situ* XRD in H_2 and INS, are employed to systematically characterize the properties of the catalysts. As the Ce-Ni have been studied, some characterizations have been already published. Therefore, all the physicochemical characterizations are not systematically involved to analyze these compounds.

3.1 Catalyst preparation

3.1.1 Ce-Ni catalysts

The catalyst samples denoted as $CeNi_XO_Y$, *x*-Ni/CeO_2-IMP and *x*-Ni/CeO_2-IWI (where x corresponds to the Ni/Ce molar ratio, *x* corresponds to the Ni wt%) were prepared by the co-precipitation (CP), impregnation (IMP) and incipient wetness impregnation (IWI) methods, namely.

The $CeNi_XO_Y$ nano-compounds were prepared by the co-precipitation of the corresponding hydroxides from mixtures of nickel and cerium nitrates by using triethylamine (TEA) as a precipitating agent in the presence of methanol. After filtration, the solids were dried at 100 °C for 24 h and calcined in air at 500 °C for 4 h.

The *x*-Ni/CeO_2-IMP catalysts were prepared by adding the support of CeO_2 into the corresponding nickel nitrate solution (20 mL), after stirring overnight, the slurry was dried under vacuum and calcined in air at 500 °C for 4 h. The CeO_2 support comes from commercial samples (S.d Fine Chem LTD-Mumbai).

For the *x*-Ni/CeO_2-IWI catalysts, very small quantity of corresponding nickel nitrate solution was slowly added into the support of CeO_2, followed by standing overnight. Then the wet support was dried under vacuum and calcined in air at 500 °C for 4 h. The CeO_2 support comes from commercial samples (S.d Fine Chem LTD-Mumbai).

3.1.2 $Ni_XMg_2AlO_Y$ catalysts

The Ni-Mg-Al hydrotalcite-like precursors were prepared by the co-precipitation method by using NaOH/Na_2CO_3 as precipitant. An aqueous mixed solution (1 M) of nitrate metal with a proper molar ratio of Ni/Mg/Al = x/2/1 was added drop-wise into NaOH (1 M) and Na_2CO_3 (0.5 M) mixed solution at room temperature. Then the slurry was kept stirring at 80 °C for 18 h. The solids were recovered by filtration, followed by thorough washing to pH = 7. And then the solids were dried at 120 °C overnight. Finally the $Ni_XMg_2AlO_Y$ catalysts were obtained by the calcination in air at 500 °C for 4 h.

3.2 Catalyst characterizations

Elemental analysis:

For all the catalysts, the Ni, Ce, Mg and Al wt% were analyzed by the ICP-MS technique (Central d'Analyses CNRS Vernaison). The Ni/M_T molar ratio is the nickel molar proportion in all the metals. For Ce/Ni catalyst, $M_T = x + 1$, Ni/$M_T = x/(x + 1)$. For Ni/Mg/Al catalyst, $M_T = x + 3$, Ni/$M_T = x/(x + 3)$

XRD:

X-ray powder diffraction analysis was carried out with a Bruker D8 Advance x-ray diffractometer equipped with a fast detector type LynxEye with a copper anticathode. The XRD

patterns were registered in the 2θ domain (10-90 °) with a measured step of 0.02 °, and the time integration was fixed to 0.3 s. The crystallite size was calculated based on the Scherrer equation.

Textural analysis:

The textural properties were measured by N_2 physisorption at 77 K using a Micromeritics TriStar II 3020 Surface-Area and Porosimetry analyzer. Samples were previously out-gassed under vacuum at 150 °C for 3 h.

Raman:

Raman spectra were acquired on a Labram Infinity HORIBA JOBIN YVON Raman spectrometer using a visible laser with an output laser power of λ = 532 nm at room temperature.

XPS:

X-ray photoelectron spectroscopy was performed on a Thermo VG Escalab 220 XL spectrometer under ultrahigh vacuum, using a twin Al x-ray source (1486.6 eV) at a pass energy of 40 eV. The solids in the form of pellets were fixed on a copper holder with copper tape. The charge effect was adjusted by reference to the C 1s peak at 284.5 eV.

H_2-TPR:

Temperature-programmed reduction was performed on a Micromeritics Autochem II Chemisorption analyzer, and the hydrogen consumption was measured by a TCD detector. 50 mg of the sample was treated in the 5 vol% H_2-95 vol% Ar mixture with a flow rate of 30 mL min^{-1}. The temperature was increased to 1000 °C at a heating rate of 10 °C min^{-1}.

***In situ* XRD in H_2:**

In situ XRD in H_2 was performed on a Bruker D8 Advance type HT1200N x-ray diffractometer equipped with a fast detector type VANTEC with a copper anticathode. A mixture of 3 vol% H_2-97 vol% Ar is employed with a heating rate of 10 °C min^{-1}.

INS:

Inelastic neutron scattering experiments were carried out on the IN1 Lagrange spectrometer at the Institut Laue Langevin, Grenoble France. 36 g of the solid was placed in a stainless steel container and treated in high purity H_2 (10 h). INS was analyzed at 10 K by using a Cu monochromator. The scattering cross-section is much greater for hydrogen (80 barns) than for other elements (5 barns); therefore, INS emphasizes the motions of hydrogen species.

3.3 Results and discussion

3.3.1 Elemental analysis and textural properties

3.3.1.1 Ce-Ni catalysts

The precise Ni loadings and the specific surface areas of Ce-Ni catalysts are analyzed and summarized in **Table 3-1**. Three series of Ce-Ni catalysts with the corresponding Ni loadings are synthesized by the different preparation methods. All the $CeNi_XO_Y$ catalysts have a relatively large surface area no less than 75 $m^2\ g^{-1}$, specifically the $CeNi_{0.5}O_Y$ and $CeNi_1O_Y$ nano-compounds present the highest specific areas in the range of about 110-120 $m^2\ g^{-1}$.

Compared to that, the *x*-Ni/CeO_2-IMP and *x*-Ni/CeO_2-IWI catalysts obviously show much smaller specific surface areas. No matter what the Ni loading is, the values measured are about 7 $m^2\ g^{-1}$. The surface areas of the IMP and IWI compounds are certainly related to the surface area of the commercial CeO_2 support.

Table 3-1 Ni loading, specific surface area and crystallite size of Ce-Ni catalysts prepared by different methods.

Catalyst	Ni loading/ wt%	Ni/M_T	S_{BET}/ $m^2\ g^{-1}$	*d* NiO/ nm	*d* CeO_2/ nm
$CeNi_{0.02}O_Y$	0.3	0.02	76	—	6
$CeNi_{0.3}O_Y$	7.9	0.23	79	—	5
$CeNi_{0.5}O_Y$	12.2	0.31	109	8	5
$CeNi_1O_Y$	24.0	0.50	119	11	4
$CeNi_5O_Y$	52.8	0.85	84	10	4
6-Ni/CeO_2-IMP	6.1	0.16	6	20	35
13-Ni/CeO_2-IMP	13.4	0.32	7	30	37
18-Ni/CeO_2-IMP	17.9	0.41	8	34	37
23-Ni/CeO_2-IMP	22.6	0.49	6	38	38
6-Ni/CeO_2-IWI	6.2	0.16	6	19	37
12-Ni/CeO_2-IWI	12.0	0.30	7	27	36
18-Ni/CeO_2-IWI	18.4	0.42	7	26	38
22-Ni/CeO_2-IWI	21.9	0.50	7	38	36

3.3.1.2 Ni_XMg_2Al HT-like compounds

Table 3-2 lists the Ni/Mg/Al molar ratios and BET surface areas of the HT-like compounds (catalyst precursors). The real Ni/Mg/Al molar ratios are precisely measured by the ICP-MS

technique and are proved to be very close to the theoretical values, which illustrates that there is not significant loss of any component during the co-precipitation procedure. The Ni_XMg_2Al HT-like compounds do not exhibit regular textural parameters depending on the Ni content. Surface areas are found in the range of about 40-80 $m^2\ g^{-1}$, except the $Ni_{12}Mg_2Al$ sample which possesses a higher surface area of 137 $m^2\ g^{-1}$.

Table 3-2 Ni/Mg/Al molar ratio, specific surface area and interlayer distance of Ni_XMg_2Al HT-like compounds.

Samples	Ni loading / wt%	Ni/Mg/Al molar ratio	Ni/M_T	S_{BET}/ $m^2\ g^{-1}$	Interlayer distance / nm
Mg_2Al	0	0/2/1	0	63	0.77
$Ni_{0.5}Mg_2Al$	9.6	0.5/2.1/1	0.14	38	0.77
Ni_1Mg_2Al	15.4	1/2.2/1	0.24	76	0.77
Ni_2Mg_2Al	25.6	2/1.7/1	0.43	40	0.77
Ni_3Mg_2Al	31.4	3/1.5/1	0.55	46	0.76
Ni_4Mg_2Al	33.7	4/1.6/1	0.61	56	0.76
$Ni_{12}Mg_2Al$	42.0	11.7/1.7/1	0.81	137	0.73

3.3.1.3 $Ni_XMg_2AlO_Y$ catalysts

The molar compositions and specific surface areas of $Ni_XMg_2AlO_Y$ catalysts that are obtained by the calcination of the HT-like compounds are also investigated (**Table 3-3**). The precise Ni/Mg/Al molar ratios are almost the same as those measured for the precursors. The specific surface areas largely expend after the thermal treatment of HT-like precursors at 500 °C. There is a global increase in the surface area with the higher Ni content, and the $Ni_{12}Mg_2AlO_Y$ catalyst still exhibits the maximum value of 196 $m^2\ g^{-1}$.

Table 3-3 Ni/Mg/Al molar ratio, specific surface area and crystallite parameters of $Ni_XMg_2AlO_Y$ catalysts.

Catalysts	Ni loading / wt%	Ni/Mg/Al molar ratio	Ni/M_T	S_{BET} / $m^2\ g^{-1}$	*d* NiO and/or $NiMgO_2$/ nm	Lattice parameter / nm
Mg_2AlO_Y	0	0/2.1/1	0	106	3.2	0.42
$Ni_{0.5}Mg_2AlO_Y$	13.2	0.5/2.1/1	0.14	95	3.4	0.42
$Ni_1Mg_2AlO_Y$	21.9	1/2.1/1	0.24	127	3.6	0.41
$Ni_2Mg_2AlO_Y$	35.7	2/1.7/1	0.43	146	3.7	0.39
$Ni_3Mg_2AlO_Y$	43.7	3/2/1	0.50	168	3.9	0.38
$Ni_4Mg_2AlO_Y$	48.2	4/1.8/1	0.60	180	4.0	0.36
$Ni_{12}Mg_2AlO_Y$	61.4	12/2/1	0.80	196	5.9	0.26

3.3.2 XRD studies

3.3.2.1 Ce-Ni catalysts

The structure and crystalline phase of Ce-Ni catalysts are investigated by XRD analysis. **Fig. 3-1** shows the XRD patterns of the $CeNi_XO_Y$ nano-compounds with various Ni contents. A ceria-like phase (34-0394 JCPDS file) with similar intensity is clearly detected in each sample, while the NiO crystalline phase (4-0835 JCPDS file) starts to be emerging when $x \geqslant 0.5$ (corresponding to the Ni loading of $x \geqslant 13$ wt%). Furthermore, the diffraction peaks of crystallized NiO become more intense for the samples with higher Ni content.

As already reported, the addition of nickel has an effect not only on the broadness of CeO_2 peaks, but also on their positions, which was attributed to the substitution of Ce^{4+} cations by Ni^{2+} cations inside the CeO_2 lattice and was interpreted by the formation of the cerium-nickel solid solution.[1] In fact, the nickel cation ionic radius (0.07 nm) is smaller than that of cerium cation (0.09 nm). It has been reported that the $CeNi_XO_Y$ compounds can be ascribed to a mixture of the nanoparticles consisting of CeO_2 and NiO, and to a solid solution where cerium and nickel species can coexist when $x < 1$.[1,3,4] Thereby, our current results reach agreement with the literature.

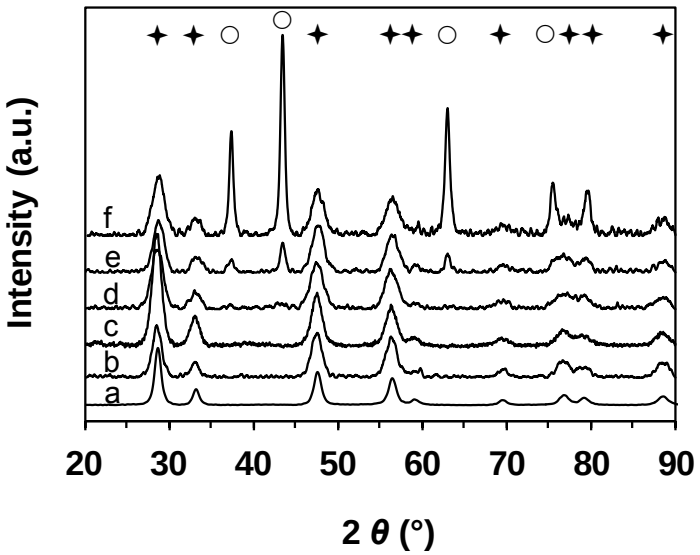

Fig. 3-1 XRD patterns of $CeNi_XO_Y$ catalysts. a) x = 0 (CeO_2), b) x = 0.02, c) x = 0.3, d) x = 0.5, e) x = 1, f) x = 5. CeO_2 (✦), NiO (○).

The diffraction patterns become much more intense and narrower when the impregnation and incipient wetness impregnation methods are employed (**Fig. 3-2** and **Fig. 3-3**), suggesting that very well crystallized materials are formed, which is related to the well-crystallized ceria support used. Diffraction lines assigned to CeO_2 phase are detected in each sample, and the characteristic diffractions of NiO phase emerge when $x \geqslant 13$ wt %. The given XRD patterns are likely to be characteristic of a mixture of NiO and CeO_2 phases in various proportions depending on the Ni loading. Almost the same XRD patterns are obtained over Ni/CeO_2-IWI and Ni/CeO_2-IMP catalysts.

The crystallite sizes of NiO and CeO_2 particles are estimated from the diffraction lines, taking into account of the (111), (200) and (220) peaks. The results are summarized in **Table 3-1**. For $CeNi_XO_Y$ catalysts, the average CeO_2 particles size is around 5 nm, presenting only a slight decrease with the Ni content. With regard to NiO particles, the average crystallites size grows slightly larger, from 8 nm to 11 nm with increasing Ni content. It is necessary to recall that the crystallites smaller than 2 nm cannot be examined by XRD technique due to the detection limit. However, such small sized NiO nanoparticles have been evidenced to be present in the $CeNi_XO_Y$ nano-compounds.[2,5]

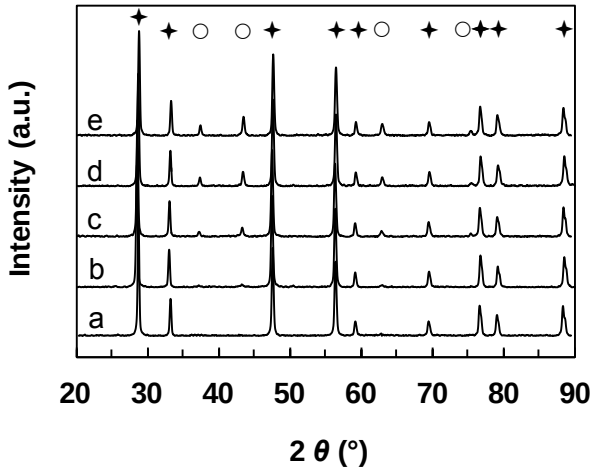

Fig. 3-2 XRD patterns of *x*-Ni/CeO_2-IMP catalysts. a) $x = 0$ (CeO_2), b) $x = 6$, c) $x = 13$, d) $x = 18$, e) $x = 23$. CeO_2 (✦), NiO (○).

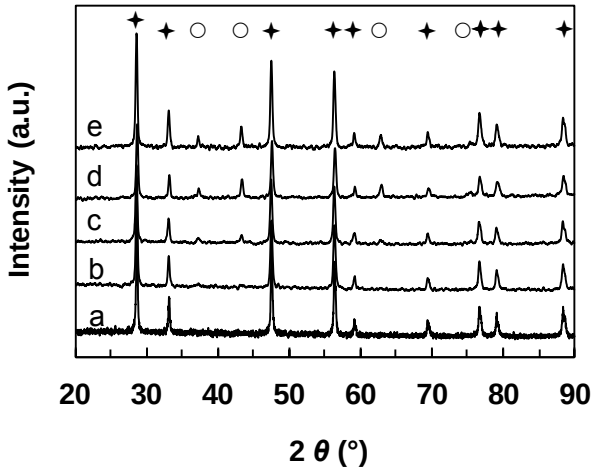

Fig. 3-3 XRD patterns of *x*-Ni/CeO_2-IWI catalysts. a) $x = 0$ (CeO_2), b) $x = 6$, c) $x = 12$, d) $x = 18$, e) $x = 22$. CeO_2 (✦), NiO (○).

Ni/CeO_2-IMP and Ni/CeO_2-IWI catalysts have quite similar crystallites size of CeO_2, about 37 nm is measured for each sample independent on the Ni loading (**Table 3-1**). But NiO particles size exhibits a global increase in the same series with higher Ni loadings. The IMP and IWI methods lead to the materials possessing relatively larger NiO particles ranging from 20 nm up to 40 nm (**Table 3-1**). Compared to these two types of catalysts, the CP method allows to obtaining the nano-compounds with much smaller NiO and CeO_2 nanoparticles sizes.

3.3.2.2 Ni_XMg_2Al HT-like compounds

The XRD patterns of Ni_XMg_2Al HT-like compounds are shown in **Fig. 3-4**. crystallized materials are successfully synthesized by the co-precipitation method. All the precursors exhibit the characteristic diffractions of the layered double hydrotalcite or HT-like compounds for (003), (006), (012), (015), (018), (110) and (113) planes, according to 70-2151 JCPDS file. There is no trace of any other oxide or hydroxide phases detected for the Mg_2Al, $Ni_{0.5}Mg_2Al$ and Ni_1Mg_2Al compounds.

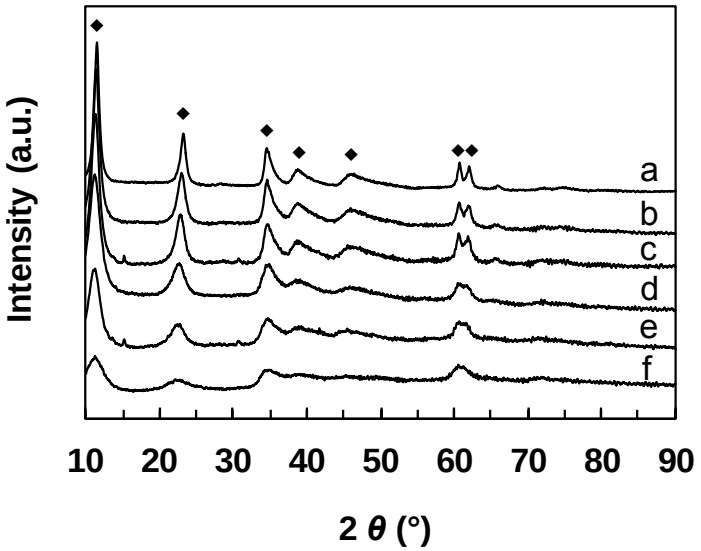

Fig. 3-4 XRD patterns of Ni_XMg_2Al HT-like compounds. a) Mg_2Al, b) $Ni_{0.5}Mg_2Al$, c) Ni_1Mg_2Al, d) Ni_2Mg_2Al, e) Ni_3Mg_2Al, f) Ni_4Mg_2Al. HT-like phase and/or α nickel hydroxide phase (◆).

The ternary Ni_XMg_2Al HT-like compounds appear less crystalline than hydrotalcite (Mg_2Al), which is proved by the shape and broadness of the diffraction peaks depending on the Ni content. This can be interpreted by the presence of α nickel hydroxide phase (38-0715 JCPDS file) in the solids by increasing the Ni loading.

But in fact the diffraction peaks of hydrotalcite and *α* nickel hydroxide would nearly overlap each other. With a very high Ni content, the $Ni_{12}Mg_2Al$ compound clearly shows more *α* nickel hydroxide phase instead of hydrotalcite structure (**Fig. 3-5**).

The interlayer distance as measured from the position of (003) plane (the first peak), is found to be 0.77 nm for Mg_2Al hydrotalcite, and in the range of 0.76-0.77 nm for Ni-containing HT-like compounds (**Table 3-2**). These data are quite similar to the value (0.76 nm for Mg_2Al HT) provided by Ogawa,[6] and the data (0.77 nm for Ni-Mg-Al HT-like precursor) reported by Li.[7]

Apart from that, the $Ni_{12}Mg_2Al$ compound provides a different interlayer distance from the series certainly due to its different diffraction patterns. The value obtained at 0.73 nm is as the same as the interlayer distance of α nickel hydroxide studied by Bae.[8]

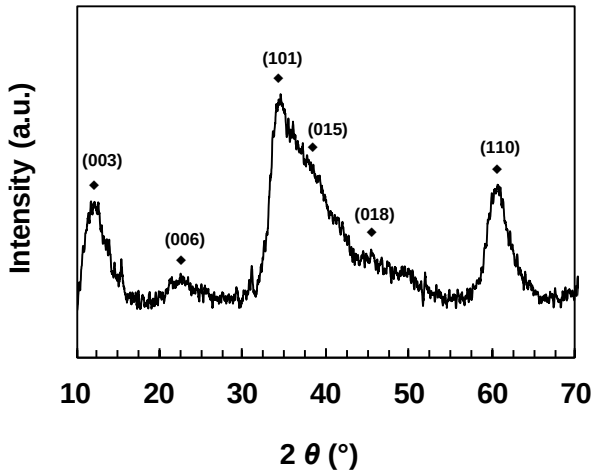

Fig. 3-5 XRD patterns of the $Ni_{12}Mg_2Al$ compound. *α* Nickel hydroxide phase (◆).

3.3.2.3 $Ni_XMg_2AlO_Y$ catalysts

The crystalline phase and structure of $Ni_XMg_2AlO_Y$ catalysts are studied by XRD analysis. After calcination at 500 °C, the HT-like structures are destroyed and the precursors are transformed into oxides. As presented in **Fig. 3-6**, the diffraction patterns of $Ni_XMg_2AlO_Y$ catalysts can be attributed to a mixture of MgO (44-1159 JCPDS file), $NiMgO_2$ solid solution (24-0712 JCPDS file) and NiO (47-1049 JCPDS file). As a matter of fact, the diffraction peaks of MgO, $NiMgO_2$ and NiO almost overlap each other, and cannot be distinguished. None of the

relevant peaks corresponding to Al_2O_3 is discovered, which can be due to the high dispersion, amorphous phase of the aluminum species and/or the insertion of Al species in the $NiMgO_2$ phase forming a Ni-Mg-Al-O solid solution.

A careful examination reveals that the addition of nickel affects not only the intensity of the peaks, but also their broadness. It can be attributive to the incorporating Ni species into MgO phase *via* the formation of $NiMgO_2$ solid solution even doped with Al^{3+} cations.[9] The diffraction patterns become more intense and thinner by increasing the Ni content, which is in good agreement with the growing average crystallites size of NiO and/or $NiMgO_2$ (**Table 3-3**).

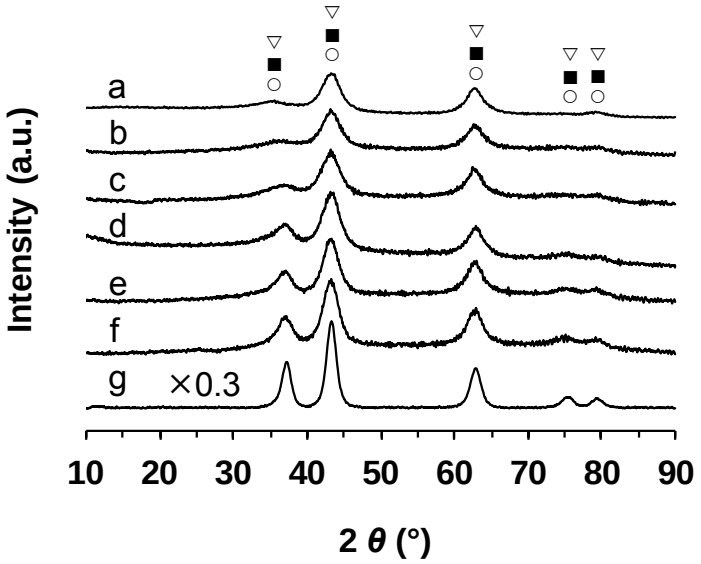

Fig. 3-6 XRD patterns of $Ni_XMg_2AlO_Y$ catalysts. a) Mg_2AlO_Y, b) $Ni_{0.5}Mg_2AlO_Y$, c) $Ni_1Mg_2AlO_Y$, d) $Ni_2Mg_2AlO_Y$, e) $Ni_3Mg_2AlO_Y$, f) $Ni_4Mg_2AlO_Y$, g) $Ni_{12}Mg_2AlO_Y$. MgO (○), $NiMgO_2$ (■), NiO (▽).

The lattice parameter α of the cubic MgO phase in $Ni_XMg_2AlO_Y$ catalysts is smaller than that of the pure MgO (0.42 nm), moreover, the values present a reduction when the Ni loading increases (**Table 3-3**), which is in agreement with the formation of a solid solution.[9] A lattice parameter α of 0.41 nm is calculated for the $Ni_1Mg_2AlO_Y$ catalyst; nevertheless it decreases to 0.26 nm for the $Ni_{12}Mg_2AlO_Y$ catalyst. It may be owing to the substitution of Mg^{2+} cations by Ni^{2+} cations, which leads to the reduction of the average distance of metal ions within the oxides, as a result, the lattice parameter α decreases. In fact, Ni^{2+} radius (0.69 Å) is smaller than that of Mg^{2+} (0.72 Å).

3.3.3 Raman studies

The $CeNi_XO_Y$ nano-compounds are also characterized by Raman spectroscopy. The results show a strong frequency shift and broadening for the first-order F_{2g} ceria peak located near 460 cm^{-1} (**Fig. 3-7**) related to fluorite nano-crystalline CeO_2.[10,11] It shifts to lower frequencies of 438 cm^{-1} compared to those reported previously on the cerium-nickel mixed oxides (443 cm^{-1}).[12] This behavior can be interpreted as a result of the solubility of nickel species into the ceria, which is in agreement with the presence of a solid solution.[13] It appears that in the present case the distortion of the lattice and the creation of oxygen vacancies are higher.

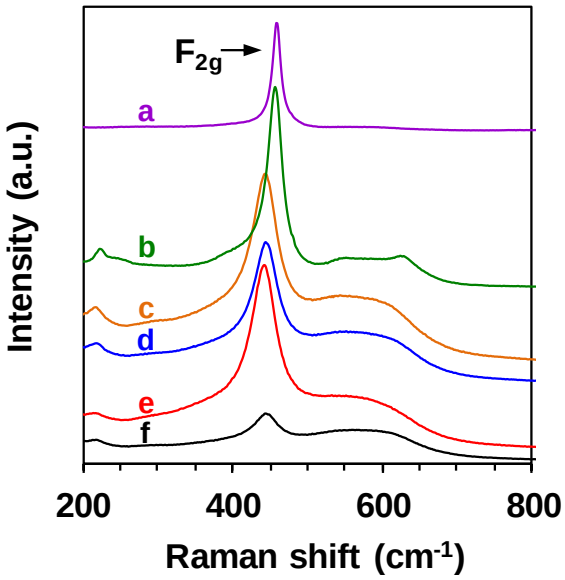

Fig. 3-7 Raman spectra of $CeNi_XO_Y$ catalysts. a) x = 0 (CeO_2), b) x = 0.02, c) x = 0.3, d) x = 0.5, e) x = 1, f) x = 5.

Secondary peak at about 230 cm^{-1} assigned to ceria nanostructures are also observed.[12] The phonon mode at 570 cm^{-1} is characteristic of oxygen vacancies in the ceria lattice.[14] As a matter of fact, weak shoulders between 500 cm^{-1} and 650 cm^{-1} were observed on doped cerium oxides and attributed to oxygen vacancies created by the incorporation of the dopant.[15] Two modes positioned at 540 cm^{-1} and 600 cm^{-1} were related to the local vibrations of different oxygen vacancy (V_O) complexes. It has been reported that the mode at 600 cm^{-1} originates from the existence of Ce^{3+}–V_O complexes in the ceria lattice.[13] As a consequence, the broad NiO signal at about 520 cm^{-1} cannot be very well detected, also due to a shadowing effect by the long tail of the

first-order F_{2g} ceria peak. However, for very low Ni content two peaks at 540 cm^{-1} and 620 cm^{-1} are observed.

3.3.4 TPR studies

3.3.4.1 Ce-Ni catalysts

The reductive properties of Ce-Ni catalysts are analyzed by H_2-TPR. **Fig. 3-8** reports the TPR profiles of $CeNi_XO_Y$ catalysts. For a low Ni content, only one peak related to nickel species is observed at around 270 °C. When the Ni/Ce molar ratio increases from 0.02 up to 1, a main reduction peak at about 370 °C becomes more intense, and slightly shifts towards higher temperature of 390 °C.

Furthermore, it is commonly accepted that the TPR analysis of CeO_2 present two peaks at approximately 500 °C and 820 °C, hence the reduction peak obtained at around 820 °C is assigned to the reduction of bulk Ce^{4+} to Ce^{3+}.

For the reduction temperatures lower than 600 °C, a linear relationship can be established between the total hydrogen consumption during TPR and the Ni content of $CeNi_XO_Y$ nano-compounds (**Fig. 3-9**), showing that H_2 is nearly completely consumed in order to reduce the nickel species in this range of temperatures.

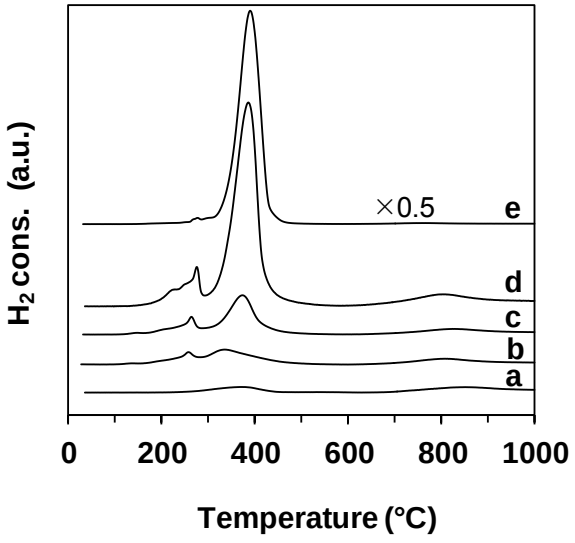

Fig. 3-8 TPR profiles of $CeNi_XO_Y$ catalysts. a) x = 0.02, b) x = 0.3, c) x = 0.5, d) x = 1, e) x = 5.

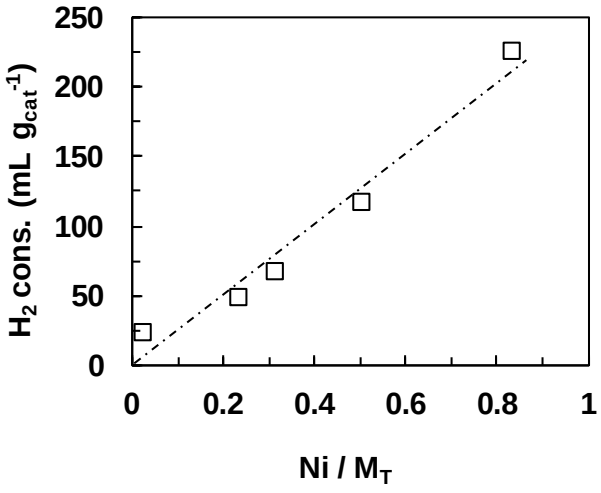

Fig. 3-9 H_2 consumption in TPR as a function of the Ni content of $CeNi_XO_Y$ catalysts.

Moreover, the reduction peak at low temperature was attributed to nickel species: i) belonging to the solid solution and/or to ii) small NiO particles, easily reducible, but with the simultaneous reoxidation of a part of these species by reduction of the Ce^{4+} cations in their vicinity into Ce^{3+} cations as the existence of a redox system was established (**Eq. 3-1** and **Eq. 3-2**),[1,2] then larger NiO crystallites are reduced when temperature increases.

$$Ni^{2+} + O^{2-} + H_2 \rightarrow Ni^0 + H_2O + \square \text{ (}\square\text{: anionic vacancy)} \qquad \textbf{Eq. 3-1}$$

$$2\ Ce^{4+} + Ni^0 \leftrightarrow 2\ Ce^{3+} + Ni^{2+} \qquad \textbf{Eq. 3-2}$$

The reductive properties of Ce-Ni catalysts prepared by different methods but with the approximately same Ni loading of 23 wt% are compared in **Fig. 3-10**. The main reduction peak is found at around 400 °C for all types of catalysts, and this peak slightly shifts towards lower temperature for the $CeNi_1O_Y$ catalyst. More interestingly, the small peak at about 270 °C is only clearly presented on the $CeNi_1O_Y$ nano-compound, but not observed on the 23-Ni/CeO_2-IMP and the 22-Ni/CeO_2-IWI catalysts. This unique result confirms the attribution of the reduction peak of 270 °C to the presence of the nickel species in small NiO nanoparticles and/or in the solid solution.[5] It has to be remarked that this phenomenon has been verified for different Ni loadings.

Apart from that, the H_2 consumptions for different types of Ce-Ni catalysts are displayed in **Fig. 3-11**. No matter what kind of preparation method is involved, a linear relationship can be also found between the total H_2 consumption for temperatures lower than 600 °C and the Ni content of Ce-Ni catalysts. Very close values are measured for the catalysts differently prepared but with the similar Ni loadings. $CeNi_XO_Y$ nano-compounds consume slightly more H_2 in TPR compared to the other two types of catalysts. This result reveals that H_2 is mainly consumed to reduce the nickel species in this range of temperatures.

Therefore, the CP method allows to obtaining the $CeNi_XO_Y$ nano-compounds with much smaller NiO and CeO_2 particle sizes which are able to enhance the strong interactions between nickel and cerium species. As a result, the $CeNi_XO_Y$ nano-compounds can be easily and reversibly reduced and reoxidized.

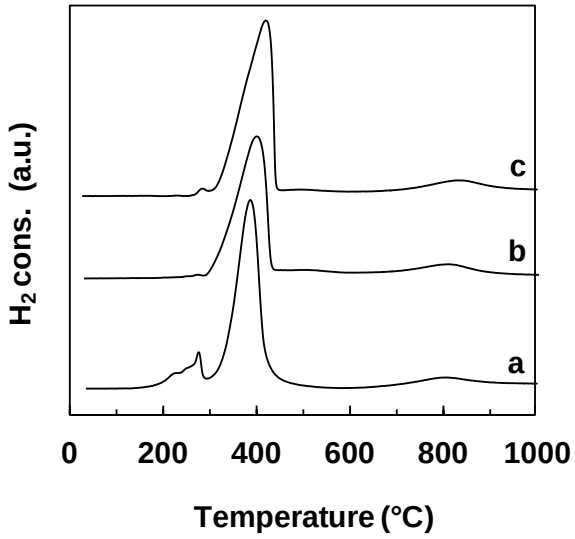

Fig. 3-10 Comparison of the TPR profiles of Ce-Ni catalysts prepared by different methods. a) Ce Ni_1O_Y, b) 23-Ni/CeO_2-IMP, c) 22-Ni/CeO_2-IWI.

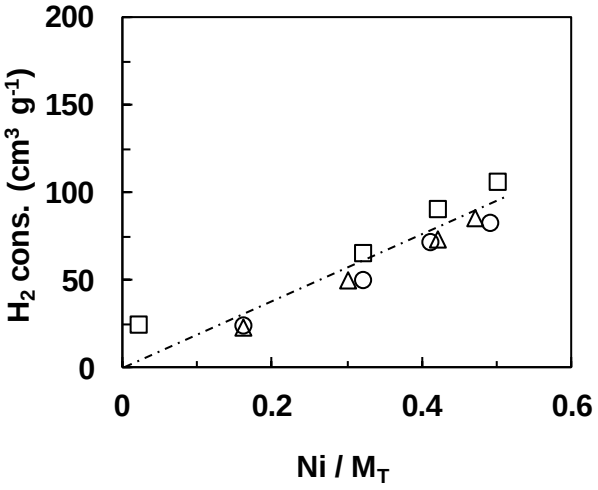

Fig. 3-11 H_2 consumption in TPR *versus* the Ni content of Ce-Ni catalysts. CP (□), IMP (○), IWI (△).

3.3.4.2 Ni_XMg_2Al HT-like compounds

H_2-TPR is used to characterize the reductive properties of Ni_XMg_2Al HT-like compounds. As shown in **Fig. 3-12**, for low Ni content, the $Ni_{0.5}Mg_2Al$ (Ni/M_T = 0.14) compound presents only one broad reduction peak located at high temperature of about 814 °C. This main peak significantly shifts towards lower temperatures with higher Ni content, for example, on the $Ni_{12}Mg_2Al$ (Ni/M_T = 0.81) compound, this peak already shifts to 410 °C.

In the mean time, if the Ni content increases, a shoulder peak starts to emerge at lower temperatures but still in the shape of the main peak. Furthermore, this shoulder peak exhibits more intense and shift towards lower temperatures when the Ni content increases. The shoulder peak is first visible at about 515 °C on the Ni_1Mg_2Al (Ni/M_T = 0.24) compound, whereas it shifts to 414 °C for the Ni_4Mg_2Al (Ni/M_T = 0.61) compound. In that case, it already becomes the main reduction peak.

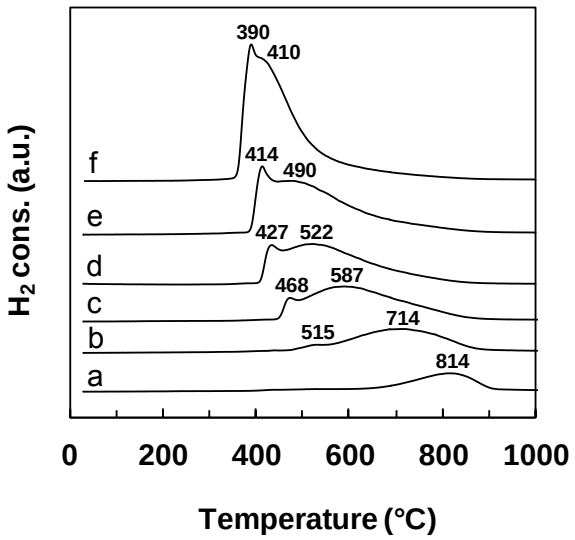

Fig. 3-12 TPR profiles obtained for Ni_XMg_2Al HT-like compounds. a) $Ni_{0.5}Mg_2Al$, b) Ni_1Mg_2Al, c) Ni_2Mg_2Al, d) Ni_3Mg_2Al, e) Ni_4Mg_2Al, f) $Ni_{12}Mg_2Al$.

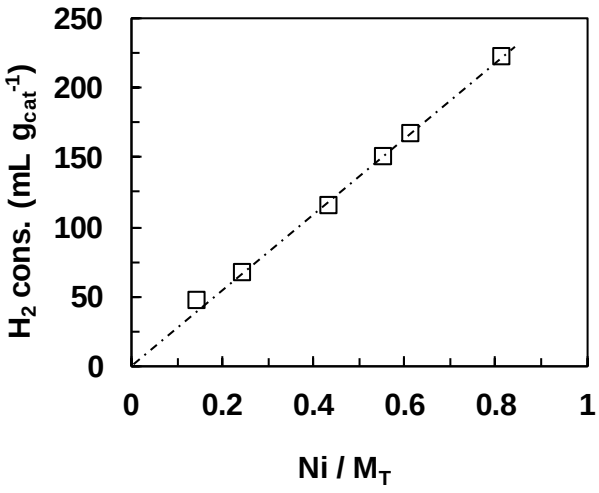

Fig. 3-13 H_2 consumption of Ni_XMg_2Al HT-like compounds during TPR as a function of the Ni content.

Some quantitative TPR features can provide additional information. The H_2 consumption of Ni_XMg_2Al HT-like compounds during TPR is plotted in **Fig. 3-13** as a function of Ni molar ratio. Obviously, a very well linear relationship can be established between the total H_2 consumption during TPR and the Ni content of Ni_XMg_2Al HT-like compounds, revealing that hydrogen is almost completely consumed in order to reduce the nickel species.

In the literature, it was reported for the reductive procedure of nickel hydroxide in TPR by one step at about 370 °C, [16] according to **Eq. 3-3**. Hence the reduction peak located at lower temperatures, ranging 390-515 °C, can be ascribed to the reduction of nickel hydroxide that has different interactions with Mg-Al layer depending on the Ni content.

Besides the reduction peak visible at higher temperatures can be assigned to nickel species that have different chemical surroundings (Ni/Mg/Al molar ratios) related to the Ni content. In fact, these two reduction peaks apparently become closer when the Ni content increases.

It is important to remark that the quantity of H_2 consumed during the whole TPR is higher than what required for the reduction of Ni^{2+} species, the nH_2/nNi molar ratio is of 1.27. This can be due to the migration of some hydrogen into the compounds.

$$Ni(OH)_2 + H_2 \rightarrow Ni + 2\ H_2O \qquad \textbf{Eq. 3-3}$$

3.3.4.3 $Ni_XMg_2AlO_Y$ catalysts

The H_2-TPR profiles of $Ni_XMg_2AlO_Y$ catalysts are reported in **Fig. 3-14**. A main single broad peak is observed for each sample, no matter what the Ni content is. This main reduction peak is located in the temperature range of 560-844 °C; moreover the reduction temperature is clearly associated to the Ni content of the catalyst.

The peak shifts towards lower temperatures by increasing the Ni content. The $Ni_{0.5}Mg_2AlO_Y$ catalyst presents the reduction peak at 844 °C, whereas that of the $Ni_{12}Mg_2AlO_Y$ catalyst appears at much lower temperature of 560 °C. In other words, the catalyst with higher Ni content is easier to reduce.

Besides, it is found that a shoulder peak is emerging in the shape of the curve for higher Ni loadings. A very small reduction peak at about 160 °C is only recorded for the catalysts with $Ni/M_T \geqslant 0.5$, which has been assigned in the literature to the reduction of Ni^{3+} species.[17]

It can be remarked that the quantity of H_2 consumed during the whole TPR is higher than what required for the reduction of NiO species, the nH_2/nNi molar ratio is of 1.22 (**Eq. 3-4**).

$$NiO + H_2 \rightarrow NiO + H_2O \qquad \textbf{Eq. 3-4}$$

It is known that the isolated NiO basically shows a single broad reduction peak centered at approximately 370 °C, spanning from 250 to 430 °C.[7, 18] The existence of NiO phase in $Ni_XMg_2AlO_Y$ catalysts is in agreement with the XRD analysis, and the proportion of NiO species grows with the higher Ni loadings. It is reasonable to ascribe the small shoulder peak at around 400 °C to the reduction of NiO in $Ni_XMg_2AlO_Y$ catalysts, and this peak shifts towards lower temperatures when Ni content increases, which is probably due to the different chemical environment surrounded the NiO species.

In the literature,[7,19-21] Ni-Mg-Al ex-hydrotalcite catalysts basically exhibited a single broad reduction peak at high temperatures ranging from 750 to 850 °C, which was interpreted by the strong incorporation of Ni into the Mg-Al support to form $NiMgO_2$ and/or $NiAl_2O_4$ solid solutions.

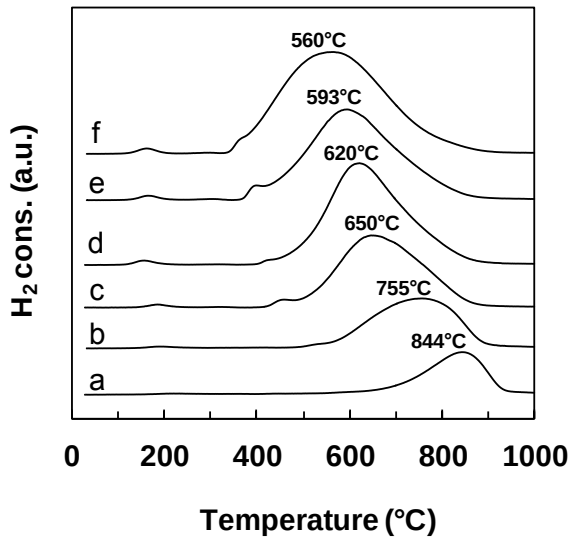

Fig. 3-14 TPR profiles of $Ni_XMg_2AlO_Y$ catalysts. a) $Ni_{0.5}Mg_2AlO_Y$, b) $Ni_1Mg_2AlO_Y$, c) $Ni_2Mg_2AlO_Y$, d) $Ni_3Mg_2AlO_Y$, e) $Ni_4Mg_2AlO_Y$, f) $Ni_{12}Mg_2AlO_Y$.

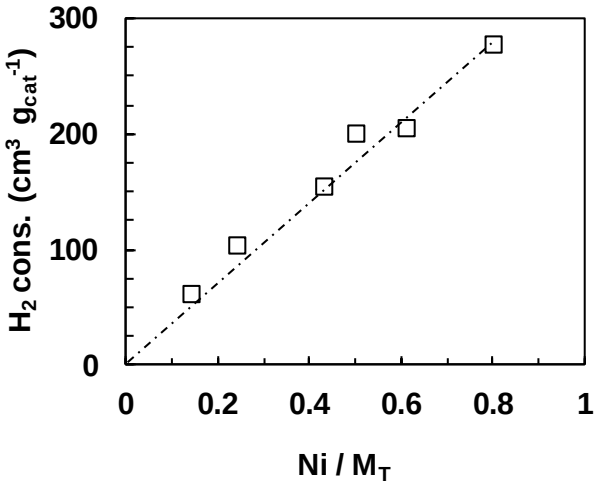

Fig. 3-15 H_2 consumption of $Ni_XMg_2AlO_Y$ catalysts during TPR *versus* Ni content.

It has to be noted that TPR on the Ni-Mg-Al ex-hydrotalcite compound with very high Ni loading have not been reported in the literature. The components composition (Ni/Mg/Al molar ratio) has an effect on the reducibility of nickel species. In the current study, the interactions between Ni species and Mg or/and Al species can be significantly modified by tuning the Ni loading; as a consequence, the catalysts with higher Ni loadings are more easily reduced.

Further analysis discloses that a linear relationship can be established between the total hydrogen consumption during TPR and the Ni content of $Ni_XMg_2AlO_Y$ catalysts (**Fig. 3-15**), showing that hydrogen is nearly completely consumed so as to reduce the nickel species in this range of temperatures.

Therefore, the relatively low-temperature reduction peaks ($\leqslant$ 650 °C) can be assigned to the reduction of Ni species; whereas the $Ni_{0.5}Mg_2AlO_Y$ and $Ni_1Mg_2AlO_Y$ catalysts present the classic reduction peaks in the range of 750-850 °C, which is in good agreement with the literature.[7,19-21]

3.3.5 XPS studies

3.3.5.1 Ni_XMg_2Al HT-like compounds

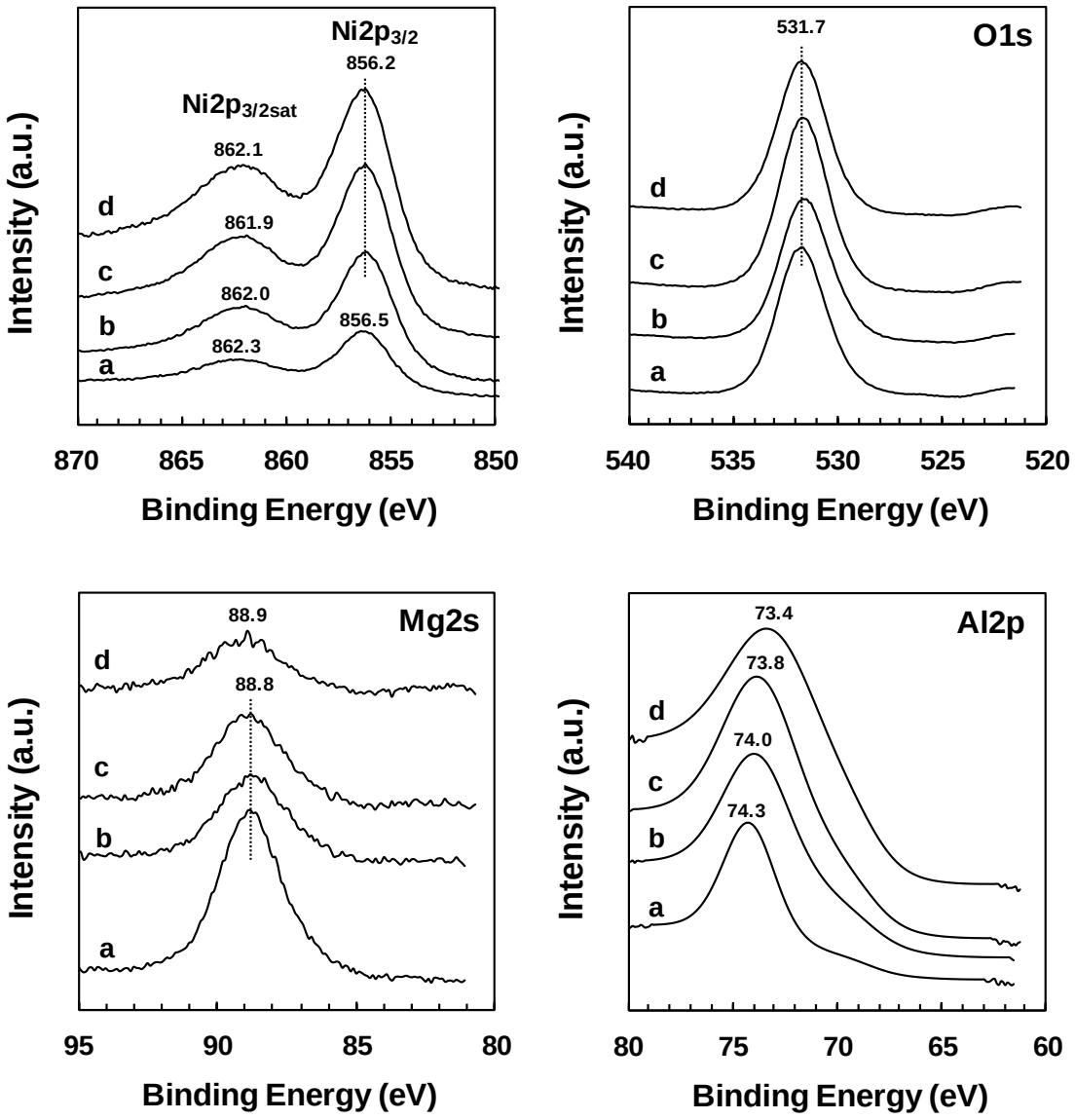

Fig. 3-16 Ni2p, O1s, Mg2s and Al2p XPS spectra of Ni_XMg_2Al HT-like compounds a) Ni_1Mg_2Al, b) Ni_3Mg_2Al, c) Ni_4Mg_2Al, d) $Ni_{12}Mg_2Al$.

XPS is used to study the surface properties of Ni_XMg_2Al HT-like compounds. The Ni2p core-level spectra are shown in **Fig. 3-16**. The binding energies obtained from XPS spectra are summarized in **Table 3-4**. A main emission peak in the $Ni2p_{3/2}$ region is observed for all the Ni_XMg_2Al compounds analyzed. The BE found for $Ni2p_{3/2}$ is 856.5 eV on the Ni_1Mg_2Al sample, while it slightly shifts to lower BE of 856.2 eV for Ni_XMg_2Al compounds with higher Ni content.

Moreover a careful examination of the $Ni2p_{3/2}$ peak shapes of Ni_XMg_2Al compounds show a line broadening effect by increasing the Ni content (**Table 3-4**). This phenomenon can be due to the different types of Ni species coexisting on the surface.

These values are higher than the BE reported for pure NiO (about 854.6 eV) and also higher than Ni^{2+} in Al_2O_3 (855.4 eV),[22] as a matter of fact, no NiO phase is detected by XRD analysis on HT compounds. In the literature, the BE of 856.1 ± 0.1 eV has been obtained for $Ni2p_{3/2}$ XPS spectra on Ni hydroxide ($Ni(OH)_2$) and assigned to Ni^{2+} cations.[22,23] Hence the BE obtained on Ni_XMg_2Al HT-like compounds in the present study can be attributed to the Ni^{2+} species. And with the high Ni loading, almost the same value is obtained compared to $Ni(OH)_2$. The shift to higher energies (856.5 eV) can be explained by the existence of strong interactions between Ni cations and other cations.

The $Ni2p_{3/2}$ core-level satellite lines are also seen at around 862.1 eV, about 6 eV up to the main peak. This 6 eV satellite has been interpreted by a predominant surface plasmon loss due to a two hole $c3d^94s^2$ (c is a core hole) final state effect.[24] The satellite lines are related to Ni^{2+} species, showing the presence of Ni^{2+} species.

This assignment is in good agreement with the XRD and TPR results. XRD shows the presence of $Ni(OH)_2$ phase coexisting with HT-like structure for Ni_XMg_2Al compounds with high Ni content ($x \geqslant 3$). TPR discloses that the first peak at around 400 °C is due to the reduction of $Ni(OH)_2$ species having different interactions with Mg-Al layer depended on Ni content.

Table 3-4 XPS parameters of Ni_XMg_2Al HT-like compounds.

Sample	$Ni2p_{3/2}$ / eV	FWHM ($Ni2p_{3/2}$)/ eV	$Ni2p_{3/2satllite}$ / eV	Mg2s / eV	Al2p / eV	O1s / eV	FWHM (O1s) / eV
Ni_1Mg_2Al	856.6	3.06	862.3	88.8	74.3	531.7	2.73
Ni_3Mg_2Al	856.2	3.28	862.0	88.8	74.0	531.7	2.82
Ni_4Mg_2Al	856.2	3.28	861.9	88.8	73.8	531.7	2.75
$Ni_{12}Mg_2Al$	856.2	3.50	862.1	88.9	73.4	531.7	2.79

The O1s, Mg2s and Al2p XPS spectra are also reported in **Fig. 3-16**. Only one peak is appearing at BE of 531.7 eV obtained for O1s spectra, which is in good agreement with the presence of oxygen species related to the hydroxyl groups. In such a case, the BE is higher than the typical O^{2-} lattice oxygen species (529.1 eV) . The Mg2s line shows typical Mg^{2+} species with the BE at 88.8 eV. The Al2s line ranging 73.4-74.3 eV is observed which is lower than the value

reported for aluminum species (74.5 eV) in Al_2O_3.[25] Al2s line shifts to lower BE when the Ni content increases due to the growing influence of the Ni peak, which is in agreement with XRD and TPR results.

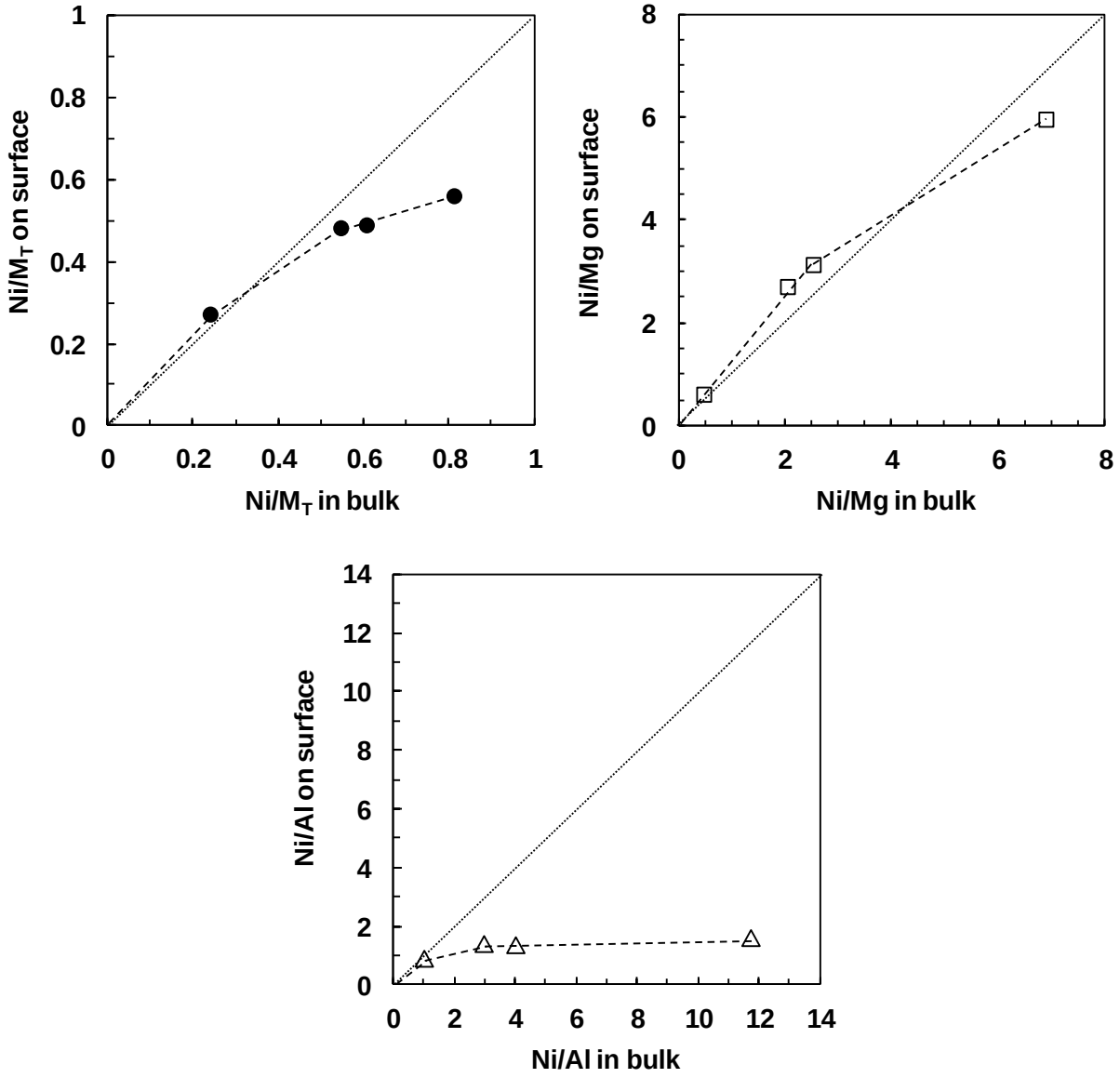

Fig. 3-17 Variation of surface Ni molar ratios as a function of bulk Ni molar ratios in Ni_XMg_2Al HT-like compounds.

The surface Ni molar ratio obtained by XPS is compared to the bulk Ni molar ratio analyzed by ICP-MS (**Fig. 3-17**), thus the variation of Ni concentration between the surface and the bulk of the Ni_XMg_2Al HT-like compounds may be investigated. The 45 ° diagonal line in **Fig. 3-17** is corresponding to the case of an ideal homogeneous distribution of nickel species inside the solid. It can be seen that the Ni/M_T and Ni/Mg ratios on surface are close to those in bulk, showing

relatively well homogeneous distribution of nickel species. But the surface Ni/M_T ratio starts to deviate from the ideal model in the compounds with high Ni content ($Ni/M_T \geqslant 0.61$) may be due to some segregation effect of Al species on to the surface (**Fig. 3-17**).

3.3.5.2 $Ni_XMg_2AlO_Y$ catalysts

The surface information of $Ni_XMg_2AlO_Y$ catalysts are studied by XPS analysis. The Ni2p core-level spectra are presented in **Fig. 3-18**, and the binding energies obtained from the XPS spectra are listed in **Table 3-5**. The $Ni_1Mg_2AlO_Y$, $Ni_3Mg_2AlO_Y$ and $Ni_{12}Mg_2AlO_Y$ catalysts as examples exhibit a main emission peak in the $Ni2p_{3/2}$ region. The BE found for this peak is about 855.7 eV for the $Ni_3Mg_2AlO_Y$ and $Ni_{12}Mg_2AlO_Y$ catalysts, which is very similar to that reported for the Ni-Mg-Al mixed oxides (855.5 eV).[26] While the $Ni_1Mg_2AlO_Y$ catalyst presents a slightly higher BE at 856.1 eV. This value is higher than the BE of pure NiO (853.7-854.6 eV) in the literature, but very close to those observed for $NiAl_2O_4$ (856 eV).[2,24,27] These results demonstrate the strong interactions between Ni^{2+} species with Al^{3+} species and/or Mg^{2+} species due to the different electron-transfer effects.

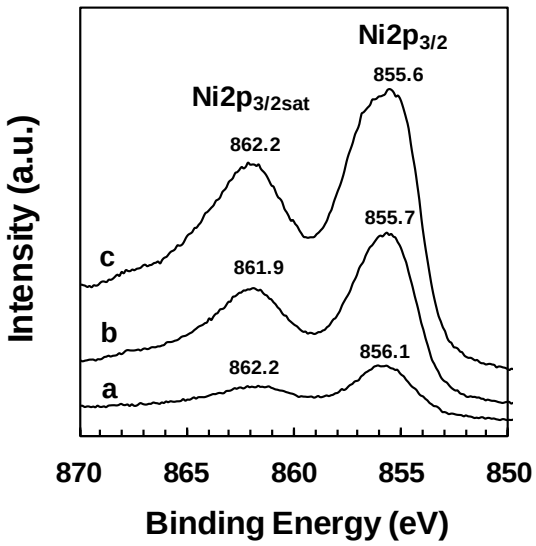

Fig. 3-18 Ni2p XPS spectra of $Ni_XMg_2AlO_Y$ catalysts. a) $Ni_1Mg_2AlO_Y$, b) $Ni_3Mg_2AlO_Y$, c) $Ni_{12}Mg_2AlO_Y$.

The XRD and TPR results have shown the existence of strong interactions between Ni species and Mg and/or Al species due to the formation of Ni-Mg-O and/or Ni-Mg-Al-O solid solution. The XPS results are in good agreement with XRD and TPR results. The electron transfer from nickel to magnesium or aluminum in the structure would thus lead to the shift to a

higher BE of 855.7 eV. Besides, for this $Ni2p_{3/2}$ core-level, satellite lines are visible at around 862.1 eV, about 6 eV up to the main peak. This 6 eV satellite has been interpreted by a predominant surface plasmon loss due to a two hole $c3d^9 4s^2$ (c is a core hole) final state effect.[24] All the results show the presence of Ni^{2+} species. Moreover, a careful examination of the $Ni2p_{3/2}$ band shapes of the $Ni_XMg_2AlO_Y$ mixed oxides shows a line broadening effect when the Ni content increases (**Table 3-5**).

Table 3-5 XPS parameters of $Ni_xMg_2AlO_Y$ catalysts.

Catalyst	$Ni2p_{3/2}$ / eV	FWHM ($Ni2p_{3/2}$)/ eV	$Ni2p_{3/2satllite}$ / eV	Mg1s / eV	Al2s / eV	O1s / eV	FWHM (O1s)/ eV
Mg_2AlO_Y	—	—	—	1303.6	119.4	531.7	2.48
$Ni_1Mg_2AlO_Y$	856.1	3.34	862.2	1303.6	119.1	531.7	2.93
$Ni_3Mg_2AlO_Y$	855.7	3.62	861.9	1303.6	119.4	530.6/531.7	3.08
$Ni_{12}Mg_2AlO_Y$	855.6	4.10	862.2	1303.6	119.5	530.6/531.7	3.42

The O1s, Mg1s and Al2s spectra are also analyzed and reported in **Fig. 3-19**. The O1s core level presents one peak at BE of 531.7 eV for the Mg_2AlO_Y and $Ni_1Mg_2AlO_Y$ compounds, whereas two peaks at BE of 530.6 eV and 531.7 eV are observed for the $Ni_3Mg_2AlO_Y$ and $Ni_{12}Mg_2AlO_Y$ compounds. The first peak at 531.7 eV has been already found in the Ni_XMg_2Al dried solids (**Table 3-4**), which is no doubt assigned to the oxygen species in OH^- groups. The new peak at BE of 530.6 eV can be attributed to the typical O^{2-} lattice oxygen species in oxides of NiO and/or MgO and/or in the Ni-Mg-(Al)-O solid solution.[2,26]

The Mg1s line (1303.6 eV) and Al2s line (119.4 eV) present almost no variation with the Ni content. The value of 119.4 eV is higher than the one reported on CeNi-Mg/AlO compounds (118.1 eV), showing higher interactions in the present study.[26] In fact, no relevant peaks to Al_2O_3 phase is detected by XRD, which is probably attributive that aluminum species are highly dispersed and/or amorphous or even inserted into the Ni-Mg-O solid solution.

However, some quantitative XPS features can provide additional information. **Fig. 3-20** compares the surface Ni molar ratios determined by XPS to the bulk Ni molar ratios measured by ICP-MS, where the variation of Ni concentration with depth in the $Ni_XMg_2AlO_Y$ catalysts may be observed. The 45 ° diagonal line corresponds to the ideal case of a homogeneous distribution of nickel inside the catalysts.

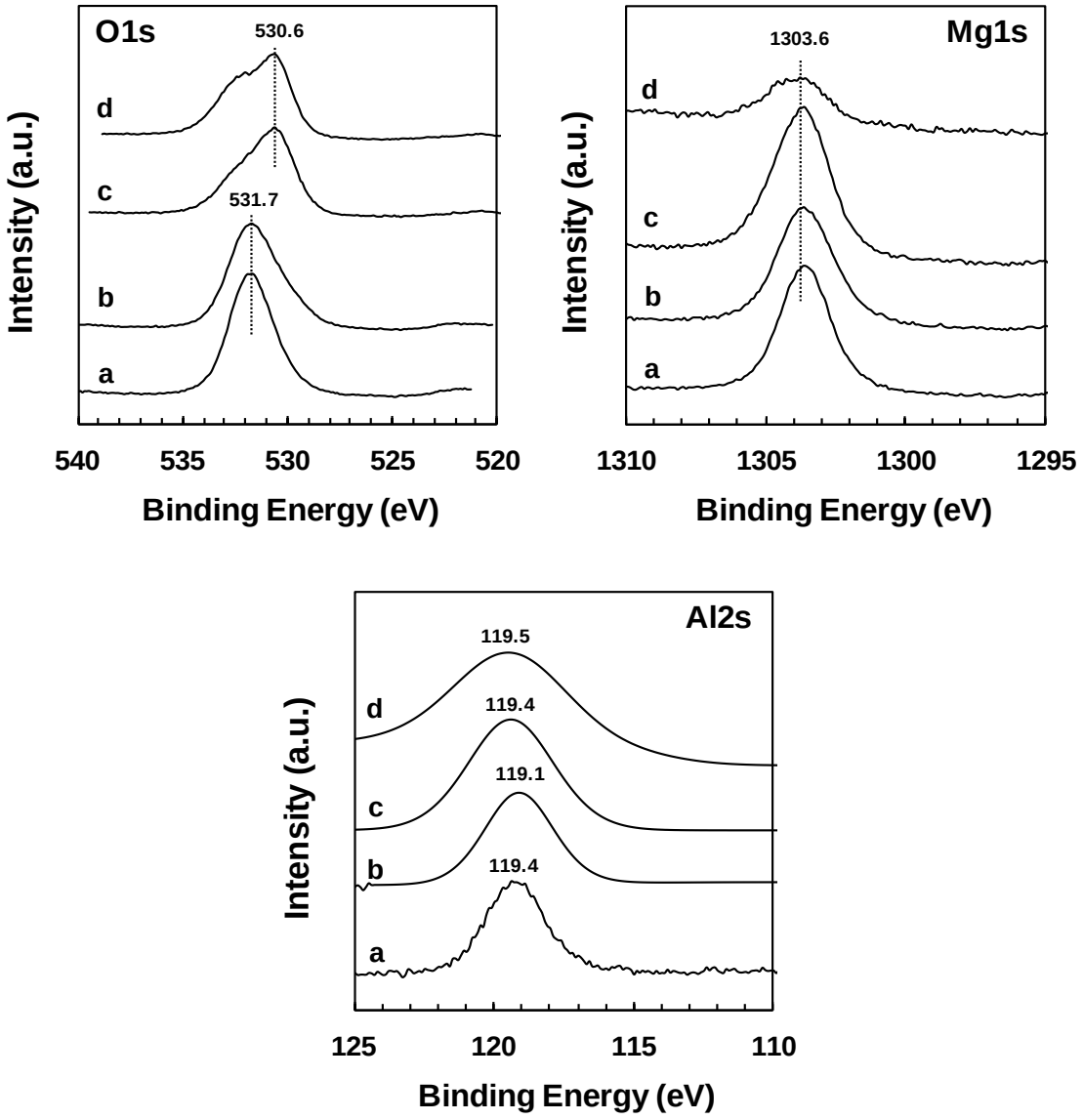

Fig. 3-19 O1s, Mg1s and Al2s XPS spectra of $Ni_XMg_2AlO_Y$ catalysts. a) Mg_2AlO_Y, b) $Ni_1Mg_2AlO_Y$, c) $Ni_3Mg_2AlO_Y$, d) $Ni_{12}Mg_2AlO_Y$.

It is possible to see that the Ni/M_T ratio on surface is relatively lower than that in bulk, showing a relative surface segregation. On the other hand, the surface Ni/M_T and Ni/Mg ratios still well respect to the Ni content, presenting a linear relationship. But the Ni/Al ratio on surface appears significantly lower than the value in bulk, it becomes more pronounced for a higher Ni content ($Ni/M_T \geqslant 0.5$). As observed previously on HT-like compounds, this result reveals that the variations of Ni molar ratios between the surface and the bulk are may be due to the surface segregation of Al species. This is related to the increase in particles sizes with the higher Ni

content (**Table 3-3**). Compared to the Ni_XMg_2Al HT-like compounds (**Fig. 3-17**), $Ni_XMg_2AlO_Y$ catalysts obtained after calcination exhibit still lower Ni concentration on the surface due to the thermal treatment.

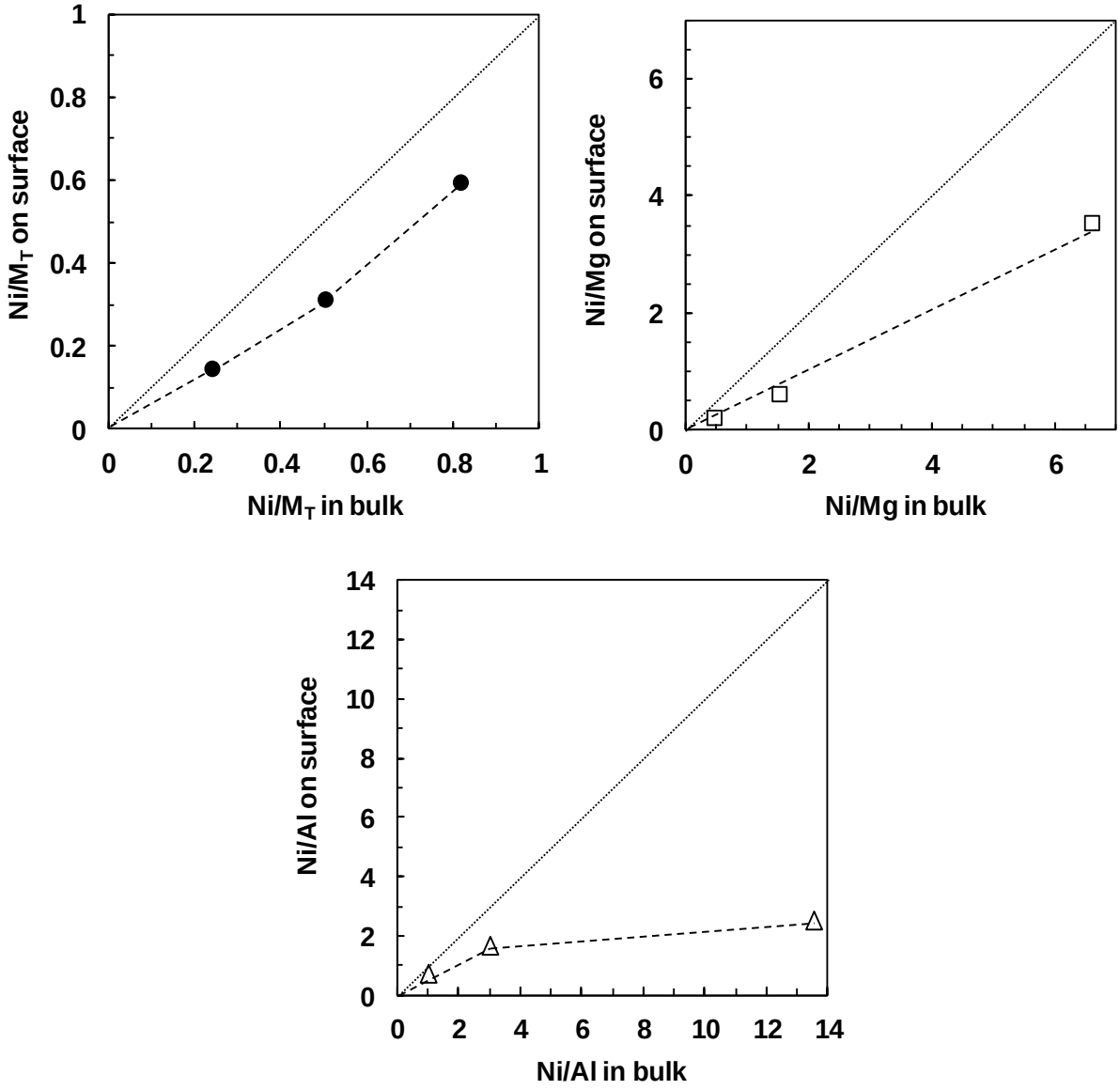

Fig. 3-20 Variation of surface Ni molar ratios as a function of bulk Ni molar ratios in $Ni_XMg_2AlO_Y$ catalysts.

The XRD analysis provide the patterns of MgO, NiO and/or Ni-Mg-O solid solution even doped with Al^{3+} cations, which can correspond to a mixture as the peaks related to these phases are overlapping each other and no phase related to aluminum is observed. In the TPR profiles, the catalysts with low Ni content exhibit a reduction peak above 750 °C assigned to the reduction of

thermal stable phases involving very strong interactions between cations. Thus the XRD, TPR and XPS results reach very good agreement.

3.3.6 *In situ* XRD in H_2

Fig. 3-21 displays the XRD profiles of the $Ni_3Mg_2AlO_Y$ catalyst obtained from the *in situ* treatment in H_2. The crystalline phase and structure are carefully analyzed at some selected temperatures. Compared to the fresh $Ni_3Mg_2AlO_Y$ catalyst, none difference is observed in the diffraction patterns obtained at lower temperature than 450 °C in the presence of H_2. There is a very clear evidence that the metallic Ni^0 phase at 2θ = 44.5 ° and 51.8 ° (70-1849 JCPDS file) starts to be detected from the treatment at 450 °C for 10 h, which can be respectively attributed to (111) and (200) planes of the metallic nickel. These two diffraction peaks become slightly more intense by further increasing the temperature to 560 °C and 620 °C. In addition, a new peak relevant to Ni (220) plane emerges at 76.2 °.

All the patterns maintain the diffraction lines of NiO and/or $NiMgO_2$ and/or MgO after treatment in H_2 whatever the temperature, even if the intensity slightly decreases, which implies that the Ni^{2+} species are partially reduced under the analysis conditions examined.

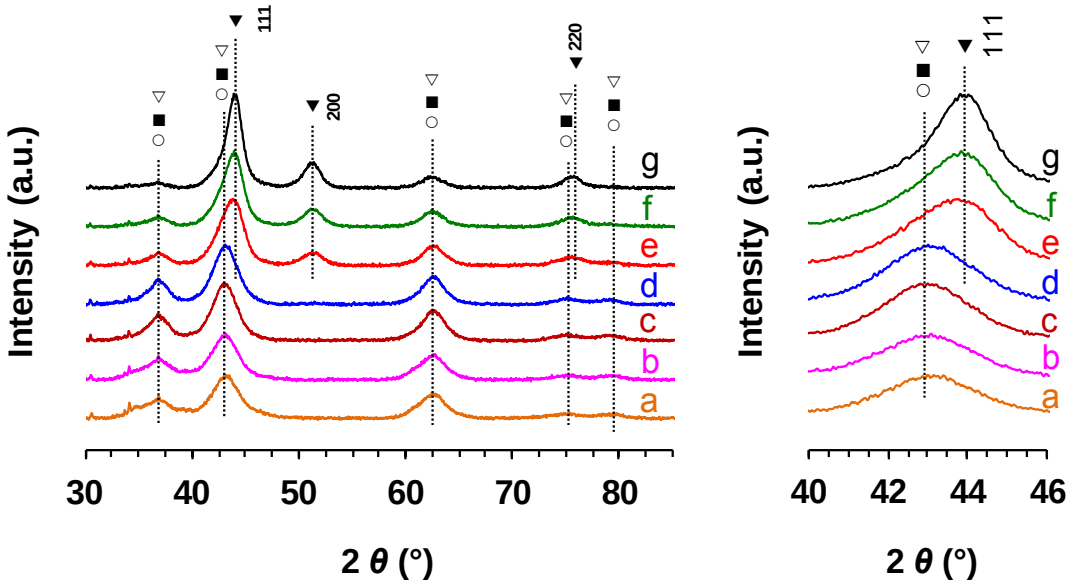

Fig. 3-21 *In situ* XRD patterns in H_2 for the $Ni_3Mg_2AlO_Y$ catalyst. a) room temperature, b) 164 °C, c) 365 °C, d) 450 °C, e) 450 °C for 10 h, f) 560 °C, g) 620 °C. MgO (○), $NiMgO_2$ (■), NiO (▽), Ni (▼).

Table 3-6 lists the average sizes of Ni-related nanoparticles in the $Ni_3Mg_2AlO_Y$ catalyst during the *in situ* XRD in H_2. The Ni^0 nanoparticle size is first found about 4.0 nm after the treatment in H_2 at 450 °C for 10 h. And then, the particle slightly grows with temperature, finally it reaches about 4.9 nm at 620 °C. With regard to NiO and/or $NiMgO_2$ nanoparticles, the average size also exhibits a slight growth depending on the temperature, ranging 3.2-4.0 nm. The values are almost the same as that of the fresh $Ni_3Mg_2AlO_Y$ catalyst.

Table 3-6 Average sizes of Ni-related nanoparticles in the $Ni_3Mg_2AlO_Y$ catalyst during the *in situ* XRD in H_2.

Temperature in H_2	*d* NiO and/or $NiMgO_2$/ nm [a]	*d* Ni^0/ nm [b]
Room temperature	3.2	—
163 °C	3.2	—
365 °C	3.7	—
450 °C	3.9	—
450 °C for 10 h	4.0	4.0
560 °C	4.0	4.5
620 °C	4.0	4.9

[a] Calculated from (200) plane. [b] Calculated from Ni (200) plane.

As a good supplement, the *in situ* H_2-XRD result reaches good agreement with the H_2-TPR result. It provides phase and structural information to prove that the TPR peak at 620 °C is mainly ascribed to the reduction of Ni species. More importantly, it deeply reveals that treatment in H_2 at 450 °C for 10 h leads to small nanoparticles of NiO accompanied with a small amount of nanoparticles of metallic nickel species Ni^0 (4 nm).

Fig. 3-22 shows the XRD patterns of the $Ni_{12}Mg_2AlO_Y$ catalyst obtained from the *in situ* treatment in H_2. It is obvious to find out that the (111) and (200) plane of the metallic nickel phase at 2θ = 44.5 ° and 51.8 ° (70-1849 JCPDS file) starts to be detected from the treatment at 450 °C. These two diffraction peaks appear more intense by maintaining 450 °C for 10 h. In addition, a new peak relevant to Ni (220) plane clearly emerges at 76.2 °. The same patterns are recorded when the temperature further rises to 560 °C.

All the patterns maintain the diffraction lines of NiO, $NiMgO_2$ and/or MgO during the whole analysis, which suggests that the Ni^{2+} species are partially reduced under the analysis conditions employed. Compared to the $Ni_3Mg_2AlO_Y$ catalyst, the $Ni_{12}Mg_2AlO_Y$ nano-compound begins to exhibit Ni^0 phase at lower temperatures. This result is in good agreement with the TPR analysis, that is, the catalyst with higher Ni content is reduced at lower temperature.

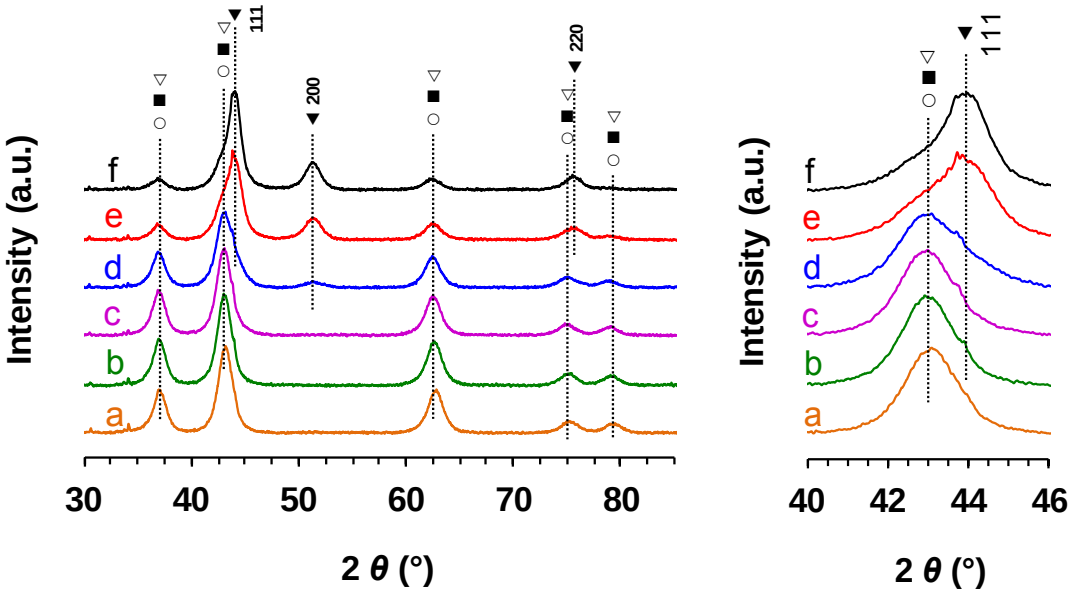

Fig. 3-22 *In situ* XRD patterns in H_2 for the $Ni_{12}Mg_2Al$ catalyst. a) room temperature, b) 163 °C, c) 365 °C, d) 450 °C, e) 450 °C for 10 h, f) 560 °C. MgO (○), $NiMgO_2$ (■), NiO (▽), Ni (▼).

The mean crystallites size of the metallic Ni^0 nanoparticles is calculated and listed in **Table 3-7**. The average particles size is found at about 4.9 nm at 450 °C. And then, it maintains at 5.0 nm after staying at 450 °C for 10 h. Finally the particles size slightly grows to 5.5 nm at 560 °C. This *in situ* XRD analysis reveals that at 450 °C some Ni species have been already reduced from the $Ni_{12}Mg_2AlO_Y$ catalyst, which requires more mild conditions than the $Ni_3Mg_2AlO_Y$ compound.

Table 3-7 Crystallite sizes of the $Ni_{12}Mg_2AlO_Y$ catalyst during the *in situ* XRD in H_2.

Temperature in H_2	*d* NiO and/or $NiMgO_2$/ nm [a]	*d* Ni^0/ nm [b]
Room temperature	5.8	—
163 °C	5.5	—
365 °C	5.6	—
450 °C	5.9	4.9
450 °C for 10 h	5.5	5.0
560 °C	5.6	5.5

[a] Calculated from (200) plane. [b] Calculated from Ni (200) plane.

3.3.7 INS studies

Inelastic neutron scattering (INS) spectroscopy is a technique that allows the vibration spectra of solid materials to be obtained. Particularly the active areas include catalysis, hydrogen-in-metals, hydrogen-bonding, magnetism, polymers and fullerenes.[28] INS has been shown as a powerful technique to obtain the information of the nature of hydrogen species.[29]

In our laboratory, it was shown that some materials presenting very good catalytic activities, such as Ce-Ni based mixed oxides that are able to store very high quantities of catalytic hydrogen. This phenomenon was related to the presence of anionic vacancies which allow the formation and storage of hydride species.[1,4,30,31] Over Ce-Ni compounds INS experiments have been already performed and published. Herein $Ni_XMg_2AlO_Y$ catalysts are also studied by INS to explore the existence and nature of hydrogen species in the solids.

3.3.7.1 INS spectra obtained by treatment under vacuum

The $Ni_XMg_2AlO_Y$ compounds are first analyzed by treatment under vacuum at 200 °C for 2 h. The INS spectra of $Ni_XMg_2AlO_Y$ solids treated in vacuum (**Fig. 3-23**) clearly evidence that some hydrogen species are already present in the calcined compounds, which is related to the preparation method and the calcination temperature applied. All the vibration bonds observed are listed in **Table 3-8**. It is important to note that the solids have been pumped under vacuum at 200°C to eliminate physisorbed water.

The spectrum for the $Ni_1Mg_2AlO_Y$ compound is complex, a broad and large peak including the main peaks at 645 cm^{-1} and 822 cm^{-1} is observed; besides a shoulder peak at 419 cm^{-1} is visible. When x =3 ($Ni_3Mg_2AlO_Y$), the main peaks are found at 423 cm^{-1} and 641 cm^{-1}, while a shoulder at 560 cm^{-1} starts to emerge but the peak at 822 cm^{-1} becomes weak. For the $Ni_{12}Mg_2AlO_Y$ compound, three peaks at 419 cm^{-1}, 560 cm^{-1} and 640 cm^{-1} can be reported.

The $Ni_XMg_2AlO_Y$ compounds after calcination and pumping under vacuum all exhibit two peaks at about 420 cm^{-1} and 640 cm^{-1} associated with hydrogen vibration bonds, which can be assigned to hydroxyl groups (OH^-), as previously also observed on cerium-nickel mixed oxides.[32] These mixed oxides contain some hydroxyl groups before the treatment in H_2. This observation is in agreement with the XPS results obtained on the $Ni_XMg_2AlO_Y$ compounds after calcineation with the presence of OH^- groups.

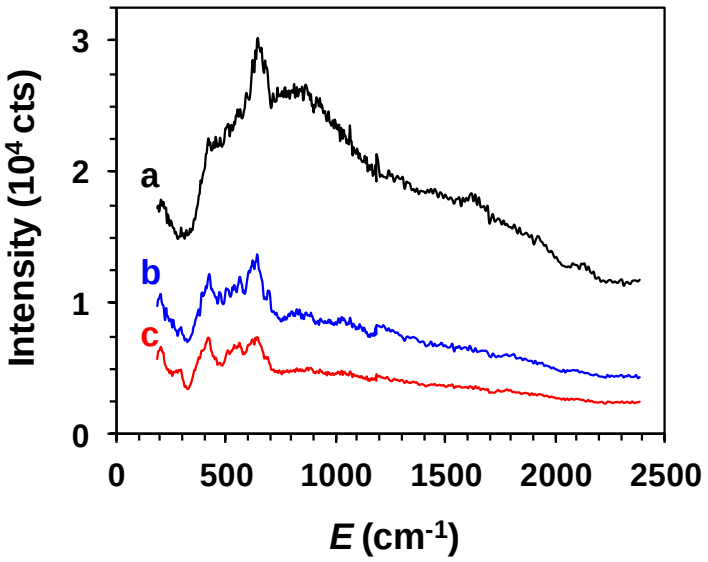

Fig. 3-23 INS spectra of $Ni_XMg_2AlO_Y$ compounds treated under vacuum at 200 °C for 2 h. a) x = 1 (black), b) x = 3 (blue), c) x = 12 (red).

The spectrum level decreases with the increase of Ni content (**Fig. 3-23**). It is important to recall that the spectrum level is proportional to the hydrogen concentration. It is clearly seen that the broad peak at 822 cm^{-1} drastically decreases when Ni content rises. On the other hand, the peaks at about 420 cm^{-1} and 560 cm^{-1} seem to become more intense for higher Ni content; while the peak at about 640 cm^{-1} appears less intense by increasing Ni content. It appears that in the oxidized state (calcined compounds), the concentration of hydrogen decreases when the Ni content increases. Therefore, it appears that the amount of hydroxyl groups (H^+ species) decreases with the increase of Ni content.

3.3.7.2 INS spectra obtained by treatment in H_2

As reported in **Fig. 3-24**, after the treatment in H_2 at 450 °C for 10 h, the shape of the INS spectra of $Ni_XMg_2AlO_Y$ compounds changes, showing the modification of the compounds. First of all, the treatment in H_2 leads to an increase in the spectrum level for the $Ni_3Mg_2AlO_Y$ and $Ni_{12}Mg_2AlO_Y$ compounds, indicating new hydrogen species are inserted into the solids. But as an exception case, the $Ni_1Mg_2AlO_Y$ compound exhibits lower intensity in the spectrum level, showing that this solid contains less hydrogen species after the treatment in H_2. It is probably due to a loss of hydroxyl groups (OH^-) at 450 °C compared to the treatment in vacuum that has been performed at 200°C.

Two main peaks at about 420 cm^{-1} and 640 cm^{-1} are visible on all the $Ni_XMg_2AlO_Y$ compounds treated in H_2. When x = 1 ($Ni_1Mg_2AlO_Y$), the peaks are found at 420 cm^{-1}, 564 cm^{-1}, 640 cm^{-1} and 822 cm^{-1}. For the $Ni_3Mg_2AlO_Y$ compound, the peaks are observed at 419 cm^{-1}, 556 cm^{-1}, 640 cm^{-1}, 834 cm^{-1}, and 927 cm^{-1}. When x =12, the peaks at 419 cm^{-1}, 641 cm^{-1} and 834 cm^{-1} can be reported. For comparison, the Mg_2AlO_Y solid without the presence of nickel is also analyzed. It shows three peaks at 423 cm^{-1}, 645 cm^{-1} and 822 cm^{-1}. Therefore, the common peaks presented on all the compounds at about 420 cm^{-1}, 640 cm^{-1} and 820 cm^{-1} are related to the Mg_2AlO_Y solid.

Careful examinations (**Table 3-8**) reveal that if the Ni content increases, the peaks at about 420 cm^{-1} and 640 cm^{-1} seem to become less intense; in the meantime, both peaks slightly shift to lower frequency. The shoulder peak at about 560 cm^{-1} becomes weak for higher Ni content. Apart from that, the peak at 822 cm^{-1} is found to shift to higher frequency at 834 cm^{-1} when $x \geqslant 3$. To be noted, a new peak at 927 cm^{-1} is clearly emerging only on the $Ni_3Mg_2AlO_Y$ compound.

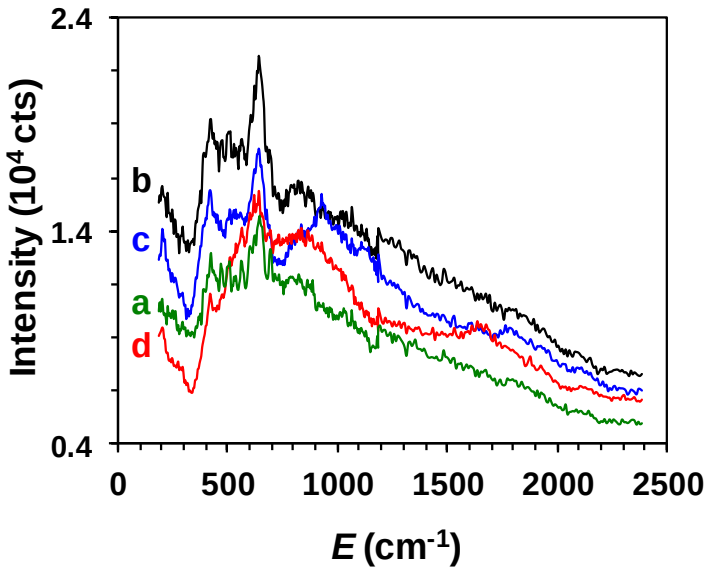

Fig. 3-24 INS spectra of $Ni_XMg_2AlO_Y$ compounds treated in H_2 at 450 °C for 10 h. a) x = 0 (green), b) x = 1 (black), c) x = 3 (blue), d) x = 12 (red).

Table 3-8 INS parameters of $Ni_XMg_2AlO_Y$ compounds.

Conditions	Sample	*E*/ cm^{-1}						
		Peak 1	Peak 2	Peak 3	Peak 4	Peak 5	Peak 6	Peak 7
Vacuum 200 °C 2 h (V)	$Ni_1Mg_2AlO_Y$	419	—	645	822	—	—	—
	$Ni_3Mg_2AlO_Y$	423	560	641	822	—	—	—
	$Ni_{12}Mg_2AlO_Y$	419	560	640	—	—	—	—
H_2 450 °C 10 h (T)	Mg_2AlO_Y	423	—	645	822	—	—	—
	$Ni_1Mg_2AlO_Y$	420	564	640	822	—	—	—
	$Ni_3Mg_2AlO_Y$	419	556	641	834	927	—	—
	$Ni_{12}Mg_2AlO_Y$	419	—	641	834	—	—	—
Oxidation after H_2 450 °C (O)	$Ni_1Mg_2AlO_Y$	419	—	641	818/834	—	—	—
	$Ni_3Mg_2AlO_Y$	419	552	641	822/834	—	—	—
	$Ni_{12}Mg_2AlO_Y$	419	560	641	822	—	—	—
Subtraction (T-V)	$Ni_3Mg_2AlO_Y$	—	—	653	—	927	1140	1765
	$Ni_{12}Mg_2AlO_Y$	—	—	641	790		—	1676

The spectra obtained are complex, but clearly hydride species are inserted into the compounds. In order to be able to report the precise values of the energy, the unity that has been used is cm^{-1}, however, the energy can be also reported in meV (1 meV = 8.065 cm^{-1}).

For easy comparison with the literature, the spectra obtained are reported in **Fig. 3-25** and **Fig. 3-26** by using meV. It has been reported in the literature that aluminum hydride (AlH_3) leads to a very large spectrum with 5 peaks between 76 and 128 meV (namely, 76, 104, 117, 123, and 127 meV),[33] while 2 peaks between 60 and 80 meV have been observed on magnesium hydride (MgH_2).[34]

Therefore, it is understandable to observe a complex spectrum with the $Ni_3Mg_2AlO_Y$ hydrogenated compound that presents INS peaks at about 55.5 meV, 83 meV and 117 meV. It appears that, globally, the shape of the spectrum obtained on the hydrogenated $Ni_{12}Mg_2AlO_Y$ compound looks relatively similar to what has been observed by INS on nickel hydride.

The very high Ni loading (61.4 wt%) in this compound allows obtaining peaks at about 83 meV, 100 meV and 200 meV, which leads to a spectrum shape relatively close to what has been largely reported on NiH.[35,36]

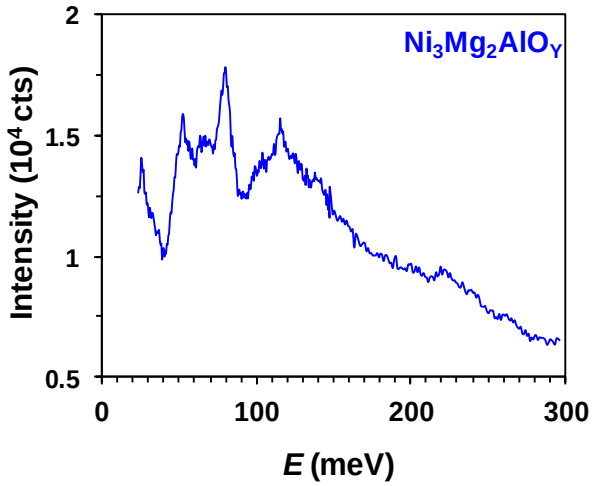

Fig. 3-25 INS spectrum of $Ni_3Mg_2AlO_Y$ compound treated in H_2 at 450 °C for 10 h.

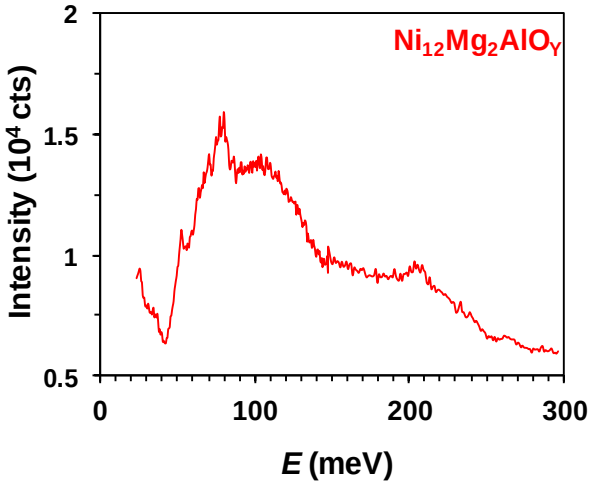

Fig. 3-26 INS spectrum of $Ni_{12}Mg_2AlO_Y$ compound treated in H_2 at 450 °C for 10 h

3.3.7.3 INS spectra obtained by treatment of oxidation

The $Ni_XMg_2AlO_Y$ compounds are also studied by oxidation of the solids treated in H_2. It is important to note that the oxidation is performed on place (ILL) by opening the cells after INS analysis, followed by a pumping (but not at 200 °C). As shown in **Fig. 3-27**, all the compounds exhibit three main peaks at 419 cm^{-1}, 641 cm^{-1} and about 820 cm^{-1}. The shoulder peak at about 560 cm^{-1} is only visible when $x \geqslant 3$. A peak at 834 cm^{-1} is observed for the $Ni_1Mg_2AlO_Y$ and $Ni_3Mg_2AlO_Y$ compounds, and this peak has been already found in the solids treated in H_2 but only when $x \geqslant 3$ (**Table 3-8**).

It could be the same oxidized state for the calcined solids and the solids oxidized after the treatment in H_2, it may be of interest to see some differences in the INS spectra. But it has to be recalled that the treatment in H_2 is performed at 450 °C, so the solids have been analyzed at this temperature; moreover the pumping condition applied after oxidation is not performed at 200 °C but at room temperature. Compared to the spectra of the solids pumped in vacuum at 200 °C (**Fig. 3-23**), the oxidation after the treatment in H_2 leads to an increase in the spectrum level for the $Ni_3Mg_2AlO_Y$ compounds, while the $Ni_1Mg_2AlO_Y$ compound shows a lower spectrum level (**Fig. 3-27**). Besides, all the main peaks at about 420 cm^{-1}, 640 cm^{-1} and 820 cm^{-1} appear more intense, especially the peak at about 820 cm^{-1}.

It appears clearly that the hydride species formed during the treatment in H_2 disappear during the oxidation process in air. Moreover, it has been experimentally proved that the reaction is significantly exothermic, which is in good agreement with the chemical reaction of highly reactive hydride species (H^-) reacting with O_2 to form hydroxyl groups (**Eq. 3-5**). With the $Ni_1Mg_2AlO_Y$ compound nearly the same spectrum is obtained because almost no hydride species are certainly inserted. For the $Ni_3Mg_2AlO_Y$ solid, the spectrum level decreases a little and for the $Ni_{12}Mg_2AlO_Y$ compound, it decreases much more, showing that a large amount of hydride species are eliminated because they reacted with O_2. This is in very good agreement with the very high reactivity of hydride species with O_2, which confirms their existence and the strong exothermicity of the reaction.

$$H^- + 0.5\ O_2 \rightarrow OH^- \qquad \textbf{Eq. 3-5}$$

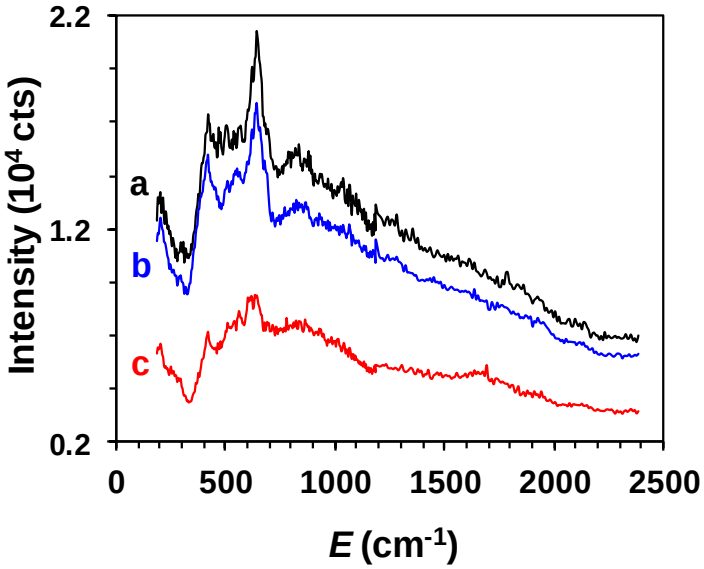

Fig. 3-27 INS spectra of $Ni_XMg_2AlO_Y$ compounds obtained by oxidation of the solids treated in H_2 at 450 °C for 10 h. a) x = 1 (black), b) x = 3 (blue), c) x = 12 (red).

3.3.7.4 Influence of treatment conditions and Ni content

For better visualization, the INS spectra of $Ni_XMg_2AlO_Y$ compounds treated in different conditions are separately analyzed in the above text and the influence of Ni content is also partially discussed. For better understanding the influence of treatment conditions and Ni content, the INS spectra are reported for each compound obtained by different treatments.

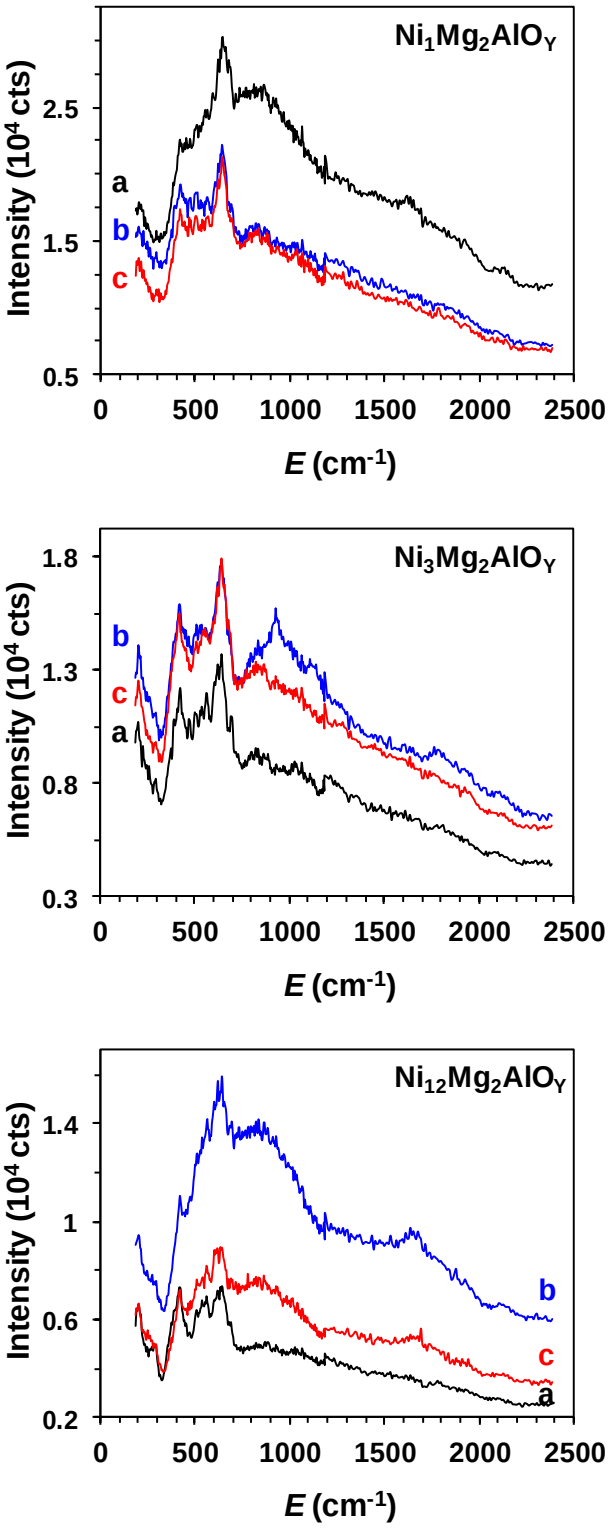

Fig. 3-28 INS spectra of $Ni_XMg_2AlO_Y$ compounds obtained by different treatments. a) under vacuum at 200 °C for 2 h (black); b) in H_2 at 450 °C for 10 h (blue); c) oxidation after treatment in H_2 (red).

From **Fig. 3-28**, it can be seen that the spectra (blue) of the solids treated in H_2 at 450 °C exhibit differences in both the shape and the spectrum level, compared to the spectra (black) of the calcined solids pumped in vacuum at 200 °C. Higher spectrum level is obtained on the $Ni_3Mg_2AlO_Y$ and $Ni_{12}Mg_2AlO_Y$ compounds, showing the insertion of hydrogen species into the solids. On the contrary, the $Ni_1Mg_2AlO_Y$ compound shows a lower spectrum level after the treatment in H_2. It can be due to the loss of hydroxyl groups (OH^-) at 450 °C but without certain insertion of hydrogen species into the solid.

However, the deeper reason is related to the reductive property depending on the Ni content. Unlike the $CeNi_XO_Y$ mixed oxides exhibiting nearly the same location of TPR peaks (**Fig. 3-8**) independent on Ni content, the $Ni_XMg_2AlO_Y$ compounds have different reduction peaks which are strongly associated with Ni content (**Fig. 3-14**). The compounds with higher Ni content are easier to reduce. In other words, each compound requires an optimized treatment temperature. As already reported previously 450 °C is not suitable to the $Ni_1Mg_2AlO_Y$ compound, which is may be not high enough to insert hydrogen species into the solid by treated in H_2.

Compared with the spectra (blue) of solids treated in H_2, the INS spectra (red) obtained by oxidation after H_2 treatment show a decrease intensity in the spectrum level with increasing Ni content (**Fig. 3-28**). The $Ni_1Mg_2AlO_Y$ compound exhibits two nearly overlapping spectra, whereas the $Ni_{12}Mg_2AlO_Y$ compound apparently presents two spectra in different intensity. This result suggests more hydrogen species can be inserted into the solids with higher Ni content.

The INS spectra (red) obtained by oxidation after H_2 treatment and the spectra obtained by treatment under vacuum does not perfectly overlap each other (**Fig. 3-28**). As a matter of fact, both of the solids analyzed are in oxidized state. The two spectra exhibit similar shapes but different spectrum levels. This result has been already noted and explained previously, but it can also suggest that some hydrogen species inserted into the solids by H_2 treatment were not removed by reoxidizing the solids.

3.3.7.5 Influence of treatment in H_2

In our previous studies on $CeNi_XO_Y$ compounds, it has been reported that H_2 treatment at 250 °C modifies the INS peaks related to hydroxyl groups (H^+ species) and generates the emergence of new peaks. In particular, a large band at about 480 cm^{-1} is observed in the H_2

treated solids, due to the insertion of hydride species (H^-).[37] These experiments helped us successfully develop the $CeNiH_ZO_Y$ nano-oxyhydride compound.[38]

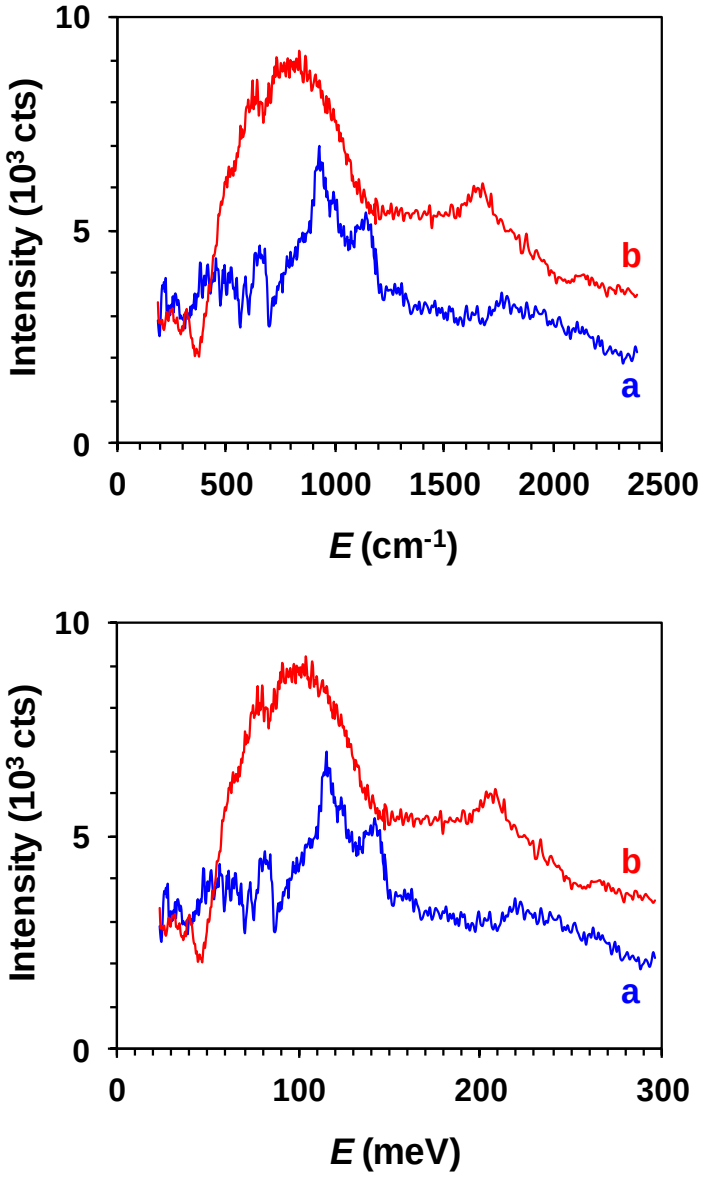

Fig. 3-29 INS spectra of $Ni_XMg_2AlO_Y$ compounds treated in H_2 at 450 °C after subtraction of the spectrum obtained by treatment under vacuum at 200 °C. a) x = 3, b) x = 12.

In order to extract the signals due to the new type of hydrogen species inserted into the $Ni_XMg_2AlO_Y$ compounds by the treatment in H_2 at 450 °C, the spectrum obtained with the corresponding compound (oxidized state: calcined compound) is subtracted to the spectrum obtained with the H_2 treated solid. As presented in **Fig. 3-29**, the $Ni_3Mg_2AlO_Y$ compound clearly shows three new peaks at 927 cm^{-1}, 1140 cm^{-1} and 1765 cm^{-1}, which are related to the vibration

bands of new hydrogen species. For the $Ni_{12}Mg_2AlO_Y$ compound, the spectrum is more complex. A very broad peak at about 790 cm^{-1} is presented, and another new peak at 1676 cm^{-1} emerges. It seems that the common peak at around 640 cm^{-1} is still visible for both compounds. These results clearly show the spectra of the nano-oxyhydride compounds that are formed during the treatment in H_2 at 450 °C (**Fig. 3-29**).

3.4 Conclusion

Two types of Ni-based catalysts, $CeNi_XO_Y$ binary mixed oxides and $Ni_XMg_2AlO_Y$ ternary mixed oxides, are prepared by the co-precipitation method (CP). CeO_2 supported Ni catalysts (Ni/CeO_2) are also prepared by the impregnation (IMP) and incipient wetness impregnation (IWI) methods, respectively. The above Ni-based catalysts are studied by different physicochemical techniques, such as ICP-MS, N_2 physisorption, XRD, Raman, H_2-TPR, XPS, *in situ* XRD in H_2 and INS.

$CeNi_XO_Y$ compounds prepared by CP method are ascribed to a mixture of NiO and CeO_2 nanoparticles, and to a cerium-nickel solid solution when $x < 1$, according to XRD analysis. Ni/CeO_2 catalysts prepared by IMP and IWI methods are well-crystallized compounds exhibiting characteristic of a mixture of NiO and CeO_2 oxides. CP method allows obtaining $CeNi_XO_Y$ nano-compounds with small NiO (about 10 nm) and CeO_2 (about 5 nm) nanoparticles. $CeNi_XO_Y$ nano-compounds have relatively large surface areas ranging between 75-120 $m^2\ g^{-1}$, whereas Ni/CeO_2-IMP and Ni/CeO_2-IWI catalysts have small surface areas of about 7 $m^2\ g^{-1}$ related to the CeO_2 support used. Moreover, IMP and IWI methods lead to materials with much larger NiO (20-40 nm) and CeO_2 (about 37 nm) particles sizes.

XRD evidences that Ni-containing Ni_XMg_2Al hydrotalcite-like compounds are formed by CP method, and α nickel hydroxide phase emerges for higher Ni proportions ($x \geqslant 3$). After calcination at 500 °C, the precursor is transformed to $Ni_XMg_2AlO_Y$ mixed oxides. $Ni_XMg_2AlO_Y$ catalysts are assigned to a mixture of nanoparticles of NiO, MgO and/or to the solid solution of Ni-Mg-(Al)-O. Very small and uniform nanoparticles ranging between 3-6 nm are obtained depending on the Ni content. Ternary $Ni_XMg_2AlO_Y$ nano-compounds have large surface areas between 100 and 200 $m^2\ g^{-1}$.

TPR analysis discloses that $CeNi_XO_Y$ nano-compounds provide similar TPR peaks assigned to the reduction of Ni species. $CeNi_XO_Y$ solids possess high proportions of very active Ni species

which present the characteristic reduction peak at about 270 °C. Such Ni species are able to be reduced and reoxidized easily and reversibly, which is due to the existence of strong interactions between nickel and cerium species in $CeNi_XO_Y$ solids. This characteristic TPR peak at 270 °C is not clearly visible on Ni/CeO_2 catalysts prepared by IMP and IWI methods. $Ni_XMg_2AlO_Y$ mixed oxides show a single broad TPR peak at between 560 and 844 °C assigned to the reduction of Ni species. Moreover, TPR peaks clearly shift to low temperature when the Ni content increases. For low Ni content the strong interactions between nickel species and other cations either in Ni-Mg-(Al)-O solid solution and/or at the interfaces between small nanoparticles of NiO, MgO and/or Ni-Mg-(Al)-O make the solid difficult to reduce; while if the Ni content increases, the reducibility of the solid becomes closer to that of bulk NiO. However, there are still strong interactions existing between Ni cations and some other cations, because the required temperature for reduction of Ni species is still much higher than the one necessary to reduce bulk NiO (560 °C for the $Ni_{12}Mg_2AlO_Y$ compound compared to 390 °C for NiO).

In situ XRD analysis demonstrates that the treatment in H_2 at 450 °C for 10 h leads to small nanoparticles of NiO accompanied with a small amount of nanoparticles of metallic nickel species Ni^0 in the $Ni_3Mg_2AlO_Y$ (dNi^0: 4 nm) and $Ni_{12}Mg_2AlO_Y$ compounds (dN^0: 5 nm), but all the oxidized phases related to NiO, MgO and $NiMgO_2$ still maintain.

Raman spectra reveal that nano-crystalline CeO_2 and oxygen vacancies created by the incorporation of the dopant are observed presenting the solubility of nickel species into ceria, as a proof to the existence of the strong interactions between nickel and cerium species.

XPS analysis proves the presence of Ni^{2+} species in hydroxides ($Ni(OH)_2$) on the surface of Ni_XMg_2Al HT-like compounds (dried solids without calcination). For $Ni_XMg_2AlO_Y$ compounds, Ni^{2+} species are still evidenced on the surface of the solids, which is in agreement with the main formation of Ni-Mg-(Al)-O solid solution.

INS experiments discover that some hydrogen species already exist in the calcined $Ni_XMg_2AlO_Y$ compounds (before H_2 treatment) which are assigned to the OH^- groups. After the treatment in H_2 at 450 °C for 10 h, new peaks are observed in the solids, proving the insertion of new type of hydrogen species into the solids. Ni content and treatment conditions have influences on the nature and concentration of hydrogen species stored in the solids. The formation of nano-oxyhydrides during the treatment in H_2 is shown by INS spectra. No hydride species are inserted

into the $Ni_1Mg_2AlO_Y$ compound after treatment in H_2 at 450 °C; whereas the $Ni_3Mg_2AlO_Y$ and $Ni_{12}Mg_2AlO_Y$ compounds are able to store hydride species after treatment in H_2 at 450 °C.

3.5 References

[1] C. Lamonier, A. Ponchel, A. D'Huysser and L. Jalowiecki-Duhamel, *Catal. Today*, 1999, **50**, 247.

[2] A. Ponchel, A. Huysser, C. Lamonier and L. Jalowiecki-Duhamel, *Phys. Chem. Chem. Phys*., 2000, **2**, 303.

[3] L. Jalowiecki-Duhamel, C. Pirez, M. Capron, F. Dumeignil and E. Payen, *Int. J. Hydrogen Energy*, 2010, **35**, 12741.

[4] L. Jalowiecki-Duhamel, C. Pirez, M. Capron, F. Dumeignil and E. Payen, *Catal. Today*, 2010, **157**, 456.

[5] L. Jalowiecki-Duhamel, H. Zarrou and A. D'Huysser, *Int. J. Hydrogen Energy*, 2008, **33**, 5527.

[6] M. Ogawa and H. Kaiho, *Langmuir*, 2002, **18**, 4240.

[7] M. Li, X. Wang, S. Li, S. Wang and X. Ma, *Int. J. Hydrogen Energy*, 2012, **35**, 6699.

[8] H.-S. Bae, E.-H. Shim, J. Hoon Park and H. Jung, *J. Phys. Chem. Solids*, 2012, **73**, 1456.

[9] C. Resini, T. Montanari, L. Barattini, G. Ramis, G. Busca, S. Presto, P. Riani, R. Marazza, M. Sisani, F. Marmottini and U. Costantino, *Appl. Catal. A*, 2009, **355**, 83.

[10] G. Li, R. L. Smith, Jr. and H. Inomata. *J. Am. Chem. Soc.*, 2001, **123**, 11091.

[11] S.-L. Zhong, L.-F. Zhang, L. Wang, W.-X. Huang, C.-M. Fan and A.-W. Xu. *J. Phys. Chem. C*, 2012, **116**, 13127.

[12] L. Barrio, A. Kubacka, G. Zhou, M. Estrella, A. Martínez-Arias, J. C. Hanson, M. Fernández-García and J. A. Rodriguez. *J. Phys. Chem. C*, 2010, **114**, 12689.

[13] N. Paunović, Z. Dohčević-Mitrović, R. Scurtu, S. Aškrabić, M. Prekajski, B. Matović and Z. V. Popović, *Nanoscale*, 2012, **4**, 5469.

[14] A. Mineshige, T. Taji, Y. Moroi, M. Kobune, S. Fujii, N. Nishi, M. Inaba and Z. Ogumi, *Solid State Ionics*, 2000, **135**, 481.

[15] M. Palard, J. Balencie, A. Maguer and J.-F. Hochepied, *Materials Chemistry and Physics*, 2010, **120**, 79.

[16] C. Wang, G. Gau, S. Gau, C. Tang and J. Bi, *Catal. Lett.*, 2005, **101**, 241.

[17] B. Mile, D. Stirling, M. A. Zammitt, A. Lovell and M. Webb, *J. Catal.*, 1988, **114**, 217.

[18] L. J. I. Coleman, W. Epling, R. R. Hudgins and E. Croiset, *Appl. Catal. A*, 2009, **363**, 52.

[19] A. J. Vizcaíno, M. Lindo, A. Carrero and J. A. Calles, *Int. J. Hydrogen Energy*, 2012, **37**, 1985.

[20] Q. Wang, W. Ren, X. Yuan, R. Mu, Z. Song and X. Wang, *Int. J. Hydrogen Energy*, 2012, **37**, 11488.

[21] G. Zeng, Q. Liu, R. Gu, L. Zhang and Y. Li, *Catal. Today*, 2011, **178**, 206.

[22] A. F. Carley, S. D. Jackson, J. N. O'Shea and M. W. Roberts, *Surf. Sci.*, 1999, **440**, 868.

[23] L. M. Moroney, R. St. C. Smart and M. W. Roberts, *J. Chem. Sco. Faraday Trans.*, 1983, **79**, 1769.

[24] A. P. Grosvenor, M. C. Biesinger, R. St. C. Smart and N. S. McIntyre, *Surf. Sci.*, 2006, **600**, 1771.

[25] T. E. Madey, C. D. Wagner and A. Joshi, *J. Electron. Spectros. Relat. Phenomena.*, 1977, **10**, 359.

[26] A. F. Lucrédio, J. D. A. Bellido and E. M. Assaf, *Appl. Catal. A*, 2010, **388**, 77.

[27] M. C. Biesinger, B. P. Payne, L. W. M. Lau, A. Gerson and R. St. C. Smart, *Surf. Interface Anal.*, 2009, **41**, 324.

[28] S. F. Parker, *Handbook of Vibrational Spectroscopy*, John Wiley & Sons, Ltd, 2006.

[29] H. Jobic, *Handbook of Heterogeneous Catalysis*, Eds. G. Ertl, H. Knözinger, F. Schüth, J. Weitkamp, Wiley-VCH, 2008, **2nd Ed.**, pp. 971.

[30] L. Jalowiecki-Duhamel, *Int. J. Hydrogen Energy*, 2006, **31**, 191.

[31] L. Jalowiecki-Duhamel, J. Carpentier and A. Ponchel, *Int. J. Hydrogen Energy*, 2007, **32**, 2439.

[32] C. Lamonier, E. Payen, P. C. H. Mitchell, S. Parker, J. Mayers and J. Tomkinson, *Studies in Surface Science and Catalysis*, Elsevier, 2000, **130**, pp. 3161.

[33] A. I. Kolesnikov, M. Adams, V. E. Antonov, N. A. Chirin, E. A. Goremychkin, G. G. Inikhova, Yu E. Markushkin, M. Prager and I. L. Sashi, *J. Phys.: Condens. Matter*., 1996, **8,** 2529.

[34] J. R. Santisteban, G. J. Cuello, J. Dawidowski, A. Fainstein, H. A. Peretti, A. Ivanov and F. J. Bermejo, *Phys. Rev. B*, 2000, **62**, 37.

[35] V. E. Antonov, B. Dormer, K. E. Fedokov, G. Grosse, A. S. Ivanaov, A. S. Kodesnikov and F. E. Wagner, *Neutron spectroscopy of high pressure hydrides*. *In Hydrogen materials science and chemistry of metal hydrides*. Ichms Eds D.V. Schur, S. Yu Zaginaichenko. 2001, pp. 184.

[36] V. E. Antonov, V. K. Fedotov, B. A. Gnesin, G. Grosse, A. S. Ivanov, A. I. Kolesnikov and F. E. Wagner. *Europhys. Lett.*, 2000, **51** (2), 140.

[37] L. Jalowiecki-Duhamel, S. Debeusscher, H. Jobic and E. Payen, *Int. J. Nuclear Hydrogen Production and Applications*, 2009, **2**, 148.

[38] C. Pirez, M. Capron, H. Jobic, F. Dumeignil and L. Jalowiecki-Duhamel, *Angew. Chem. Int. Ed*, 2011, **50**, 10193.

4 Steam reforming of ethanol on Ni-based catalysts

The steam reforming of ethanol (SRE) is a very ideal route to produce H_2 (**Eq. 4-1**), since SRE can be CO_2 neutral process in theory due to that all CO_2 produced could be recycled back during biomass growth. The ideal SRE reaction generates only H_2 and CO_2. But as a matter of fact, SRE involves quite a complicated reaction network accompanied by many possible by-products, which mainly depends on the catalyst employed.

$$C_2H_5OH + 3\ H_2O \rightarrow 6\ H_2 + 2\ CO_2\ \Delta H^0_{298K} = 174\ KJ\ mol^{-1} \qquad \textbf{Eq. 4-1}$$

On the other hand, the SRE reaction is a strong endothermic process that requires extra energy (**Eq. 4-1**),[1,2] so that SRE is basically performed at high temperatures ($\geqslant$ 650 °C). In such a context, the crucial factor is to develop highly active, selective, stable and low-cost catalysts which are able to efficiently break the C-C and C-H bonds and promote the subsequent formation of H_2 and CO_2.

Nickel-based catalysts have been extensively and widely studied for the steam reforming of ethanol because of their good capability in the C-C bond rupture. However, it has been often reported that nickel favors coke deposition leading to deactivation of the catalyst. Meanwhile, carbon can exist in different forms, and if formation of coke is often seen as a problem, another type of carbon such as carbon nano-materials are considered as strategic materials in nano-technologies. Recently, it has been shown that chemical decomposition of biomass materials like ethanol is another way to produce hydrogen and few works reported the production of carbon nanotubes (CNTs) accompanied by hydrogen production during ethanol decomposition.[3,4]

It is shown that tuning the catalyst may allow obtaining not only a very active catalyst for H_2 production, but also for the formation of carbon nano-materials, as an added bonus. To our knowledge, the production of carbon nanofibers (CNFs) and carbon nanotubes (CNTs) accompanied by high-yield hydrogen production during ethanol steam reforming has not been reported under mild conditions ($\leqslant$ 650 °C). Compared to ethanol decomposition, working in the presence of water allows for the use of bio-ethanol and avoids some of the costly steps involved in purification.

In our laboratory, the Ce-Ni mixed oxides have been studied due to the strong interactions existing between nickel and cerium species inside the solid.[5-7] It is well known that the metal-

support interactions play an important role during the preparation step and the thermal treatment, since both of them are able to define the properties of final catalysts: reducibility, resistance to thermal sintering of the active sites or metallic dispersion. Better catalytic performances with high stability and high hydrogen selectivity can be expected over a support such as CeO_2 which is able to maintain smaller metal catalyst particles by strong metal-support bonding.[8] Moreover, the reducibility, catalytic activity and coking resistant behaviors of catalysts are affected by their surface and structural properties, so that the methodology involved in the preparation step can lead to the obtainment of materials with important properties for applications in catalytic processes, such as the steam reforming of ethanol. There is no report on the preparation methodology of Ce-Ni materials for H_2 production from ethanol reforming.

On the other hand, recently an alternative research interest focused on Ni-based catalysts that are derived from the thermal treatment of the hydrotalcite-like compounds.[9-12] Hydrotalcites (HTs), with a general formula of $[M^{2+}_{1-x}M^{3+}_{x}(OH)_2]^{x+}(A^{n-})_{x/n}\cdot mH_2O$, are synthetic or natural layered materials made of positively charged two-dimensional sheets of mixed hydroxides with water and exchangeable charge-compensating anions. Hydrotalcite can be synthesized with several reducible bivalent (Co, Ni, Cu) and trivalent (Cr, Fe) cations in the structure together with the classical ones (Mg, Al, Zn) serving as precursors for the preparation of various mixed oxides to be catalyst or support.[13] After thermal treatment, the mixed oxides obtained show several unique properties. It allows obtaining materials with large surface areas and uniform dispersion of each metal component. In this sense, Ni-based ex-hydrotalcite catalysts are able to bring benefit to catalytic process, such as H_2 production from the steam reforming of the biomass-derived hydrocarbon sources.

It has been reported recently that Co-Ni/HTls, Pd/Co-Ni, Ni-Sn-Al and Ni-Mg-Al systems are active catalysts for H_2 production from glycerol, lignocellulosic biomass, ethylene glycol and landfill gas, namely.[14-17] Still, the mainstream studies are the SRE reaction. In the past few years, various ternary and quaternary mixed oxide catalysts derived from the HT-like materials have been applied to the SRE reaction, such as ternary Ni-M-Al (M = Mg, Ca, Zn) and Ni-Mg-N (N = La, Ce) catalysts,[10-12] and Cu-, Zn-, La-, Ce-promoted Ni-Mg-Al quaternary catalysts.[9,18,19] The common features of these catalytic systems are found to be the intensive exploration in the H_2 production efficiency at temperatures higher than 650 °C. A H_2 yield of 6 mol mol_{EtOH}^{-1} is equivalent to 100% in theory, but it can never be achieved in reality. The H_2 yields between 4.0

and 5.1 mol mol_{EtOH}^{-1} are reported from the above catalytic systems under very harsh conditions where a huge amount of energy is consumed.

In the present study, two types of Ni-based catalysts are studied for SRE (H_2O/EtOH = 3). The Ce-Ni catalysts are synthesized by using different preparation methods to explore the factors which benefit the reaction process. The $Ni_XMg_2AlO_Y$ ex-hydrotalcite catalysts are prepared by the co-precipitation method. Different parameters are analyzed, including reaction temperature, calcination temperature effect, *in situ* activation in H_2, Ni content, influence of preparation method, catalyst dilution effect, water partial pressure effect and ethanol concentration effect.

All the above analysis are performed under hard conditions in the presence of high concentration of ethanol (14 mol%), because it is more interesting to use ethanol in high concentration in the practical applications, *e.g.*, bio-ethanol from wheat straw contains about 18 mol% ethanol;[20] besides, it allows easily seeing the differences in the catalytic performances for SRE. The efficiency of Ni-based catalysts towards H_2 production (H_2 yield in mol mol_{EtOH}^{-1}) is also studied under diluted conditions involving low concentration of ethanol (EtOH: 1 mol% or 3 mol%).

Herein, in this chapter, $CeNi_XO_Y$ and $Ni_XMg_2AlO_Y$ mixed oxides are reported as highly active, efficient and low-cost catalysts for production of hydrogen from the steam reforming of ethanol. The correlations between the catalyst properties, the catalytic performances and the characterizations are thoroughly discussed.

4.1 Studies on reaction temperature

4.1.1 $CeNi_XO_Y$ catalysts

In our laboratory, $CeNi_XO_Y$ catalysts have been already studied for H_2 production from transformation of ethanol in the presence of water at low temperatures (H_2O/EtOH = 3). Some parameters have been analyzed.[5,6] In order to show the continuity of this study, some typical results are necessary to recall in this part.

The influence of reaction temperature was analyzed in the range of 200-500 °C. When the $CeNi_{0.5}O_Y$ catalyst (200 mg), as an example, is previously *in situ* treated in H_2 at 200 °C for 10 h, there is globally an increase *versus* temperature but with the existence of an optimum of conversion at about 30 % at 250 °C. Finally total conversion is reported at 400 °C with about 50

mol% H_2 formation among the gas phase products.[5] The other products obtained in the outlet gas stream are CO_2, acetaldehyde, CO and CH_4. Acetaldehyde decreases with temperature and disappears at 400 °C. CO and CH_4 formation present optimum at 250 °C.[5]

4.1.2 $Ni_XMg_2AlO_Y$ catalysts

As an example, the reaction temperature is reported on the $Ni_4Mg_2AlO_Y$ catalyst under hard conditions, *i.e.*, high concentration of ethanol (14 mol%). 100 mg catalyst is pre-treated in H_2 at 550 °C (T_T) and then applied to the SRE reaction. As shown in **Fig. 4-1**, a very good activity of 40% ethanol conversion is obtained at very low temperature of 200 °C. Activity increases with reaction temperature and approaches to 100% at 400 °C, exhibiting high activity for SRE. H_2 molar fraction relative to all the gas phase products (dry basis) maintains about 55% (in mol.). This result is better compared to the recent values reported on Ni-Mg-Al catalyst, in which $Ni_{0.5}Mg_{2.5}Al$ catalyst (100 mg) gave about 85% ethanol conversion at 300 °C and reached total conversion at 450 °C in the presence of 9 mol% ethanol.[19]

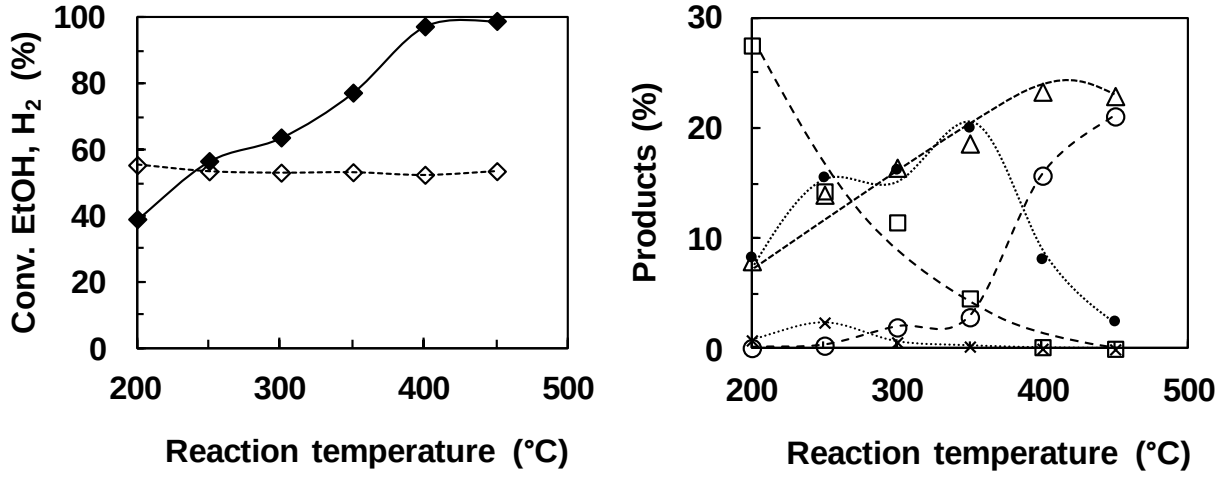

Fig. 4-1 SRE over the $Ni_4Mg_2AlO_Y$ catalyst (treated in H_2 at 550 °C) as a function of reaction temperature. Ethanol conversion (◆), H_2 (◇), CO_2 (○), CH_3CHO (□), CO (●), CH_4 (△) and acetone (×) formation. Reaction conditions: catalyst: 100 mg; $EtOH/H_2O/N_2$ = 14/42/44; time: 5 h for each temperature.

Acetaldehyde formation shows a significant decline with increasing reaction temperature, and finally eliminates at 400 °C. Only trace of CO_2 is examined in the outlet gases at temperatures lower than 300 °C. CO_2 formation starts to rise from 350 °C and rapidly reaches to about 20% at 450 °C. Some other undesirable products, such as CO, CH_4 and acetone, are

obtained in the outlet gas. Acetone decreases to zero at 350 °C. CO formation presents a maximum of about 20% at 350 °C; afterwards it declines, which is certainly due to the coke formation from the disproportionation of CO. CH_4 undergoes a global increase with reaction temperature and reaches a maximum of about 20% at 450 °C.

Fig. 4-2 reports the catalytic performance of the $Ni_3Mg_2AlO_Y$ catalyst using lower mass (50 mg) *versus* reaction temperature, as an example. By *in situ* treating in H_2 at 450 °C (T_T), the $Ni_3Mg_2AlO_Y$ catalyst converts 27% ethanol at very low temperature of 200 °C. As expected, there is a global increase in the conversion depending on reaction temperature. Ethanol conversion starts to increase from 300 °C, and then reaches and maintains about 75% from 400 °C, showing very good catalytic activity. For all the temperatures investigated ranging from 200 to 450 °C, H_2 formation basically keeps about 55% (in mol.) among all the gas phase products (dry basis).

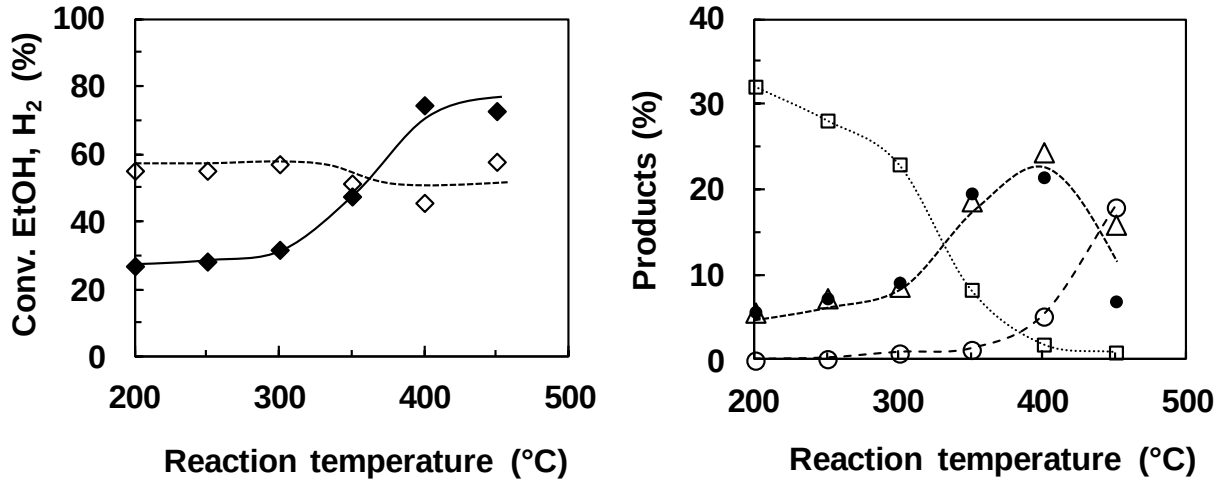

Fig. 4-2 SRE over the $Ni_3Mg_2AlO_Y$ catalyst (T_T = 450 °C) as a function of reaction temperature. Ethanol conversion (◆), H_2 (◇), CO_2 (○), CH_3CHO (□), CO (●) and CH_4 (△) formation. Reaction conditions: catalyst: 50 mg; $EtOH/H_2O/N_2$ = 14/42/44; time: 5 h for each temperature.

The other products are CO_2, CH_3CHO, CO and CH_4. CO_2 formation retains less than 1% below 250 °C so as expected; because the SRE process is thermodynamically not favorable at these low temperatures. It begins to dramatically rise from 350 °C, and reaches the value of about 20% at 450 °C. CH_3CHO formation declines with reaction temperature, from about 30% at 200 °C down to lower than 1% at 400 °C. Meanwhile CO and CH_4 display very similar evolution. Both present the maxima of about 23% at 400 °C, but then decrease at 450 °C. Carbon formation is observed after the whole reaction at 450 °C, and it is measured by mass variation at 0.15 g.

Fig. 4-3 shows the catalytic results obtained over the $Ni_{12}Mg_2AlO_Y$ catalyst as a function of reaction temperature. Under the same conditions (50 mg; T_T = 450 °C), the $Ni_{12}Mg_2AlO_Y$ catalyst clearly shows the higher ethanol conversion at each corresponding temperature compared to the $Ni_3Mg_2AlO_Y$ catalyst. At 200 °C, 37% of ethanol conversion is analyzed over the $Ni_{12}Mg_2AlO_Y$ catalyst. As expected, there is a global increase in the conversion *versus* reaction temperature, but with the existence of an optimum at 250 °C, where ethanol conversion could reach 51%. Finally, almost total ethanol conversion is obtained at 400 °C. The present $Ni_{12}Mg_2AlO_Y$ catalyst shows much better activity compared to the result recently reported on Ni-Mg-Al catalyst with high Ni content. In that case, $Ni_{50}MgAl$ catalyst (25 mg) exhibited activity lower than 30% when reaction temperature is below 450 °C in the presence of a lower ethanol concentration of 9.2 mol%.[10]

For all the temperatures investigated ranging from 200 to 450 °C, H_2 formation always keeps about 55% (in mol.) among the gas phase products (dry basis). As a matter of fact, considering the trend and variation of the products concentration, the H_2 production is enhanced in terms of ethanol conversion with increasing reaction temperature.

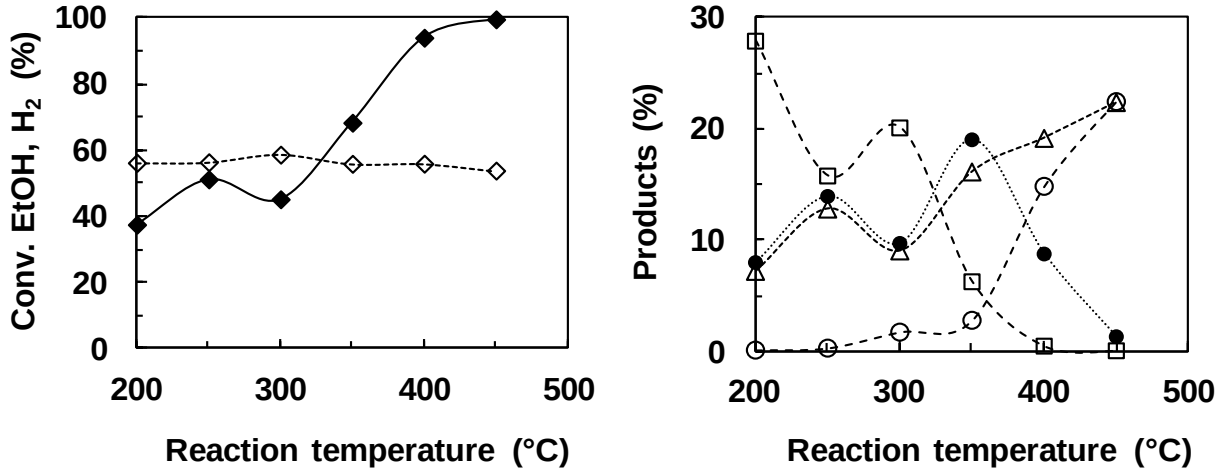

Fig. 4-3 SRE over the $Ni_{12}Mg_2AlO_Y$ catalyst (T_T = 450 °C) as a function of reaction temperature. Ethanol conversion (◆), H_2 (◇), CO_2 (○), CH_3CHO (□), CO (●) and CH_4 (△) formation. Reaction conditions: catalyst: 50 mg; $EtOH/H_2O/N_2$ = 14/42/44; time: 5 h for each temperature.

The other gas phase products produced by the $Ni_{12}Mg_2AlO_Y$ catalyst are CO_2, CH_3CHO, CO and CH_4. Acetaldehyde formation decreases with reaction temperature, while CO_2 formation increases (**Fig. 4-3**). Acetaldehyde reduces from about 30% at 200 °C to lower than 1% at 400 °C. None of ethylene, ethyl acetate or acetone is observed. Meanwhile, CO_2 formation retains less than 1% below 250 °C, as expected.[2,22] From 350 °C, CO_2 concentration begins to dramatically

rise, and reaches about 20% at 450 °C. During the whole temperature range analyzed, the $Ni_{12}Mg_2AlO_Y$ catalyst constantly shows a lower CH_3CHO formation and a higher CO_2 formation than the $Ni_3Mg_2AlO_Y$ catalyst.

Both CO and CH_4 formation are observed at about 7% at 200 °C, and then present an optimum value of around 14% at 250 °C (**Fig. 4-3**), which follows the evolution of ethanol conversion and reaches agreement with the variation of CH_3CHO at 250 °C. The unique phenomenon at 250 °C may be attributed to that the $Ni_{12}Mg_2AlO_Y$ catalyst leads to higher ethanol conversion, as well as higher CO and CH_4 formation, as a result the concentration of CH_3CHO is lower. Carbon formation is observed after the whole reaction at 450 °C, and it is measured at 0.6 g. It appears that carbon formation increases with Ni content, when comparing to the carbon formed over the $Ni_3Mg_2AlO_Y$ catalyst.

Based on the above results, the influence of reaction temperature on $Ni_XMg_2AlO_Y$ catalyst for SRE can be discussed. It seems that the dehydrogenation and decomposition are the main reactions when temperature is lower than 350 °C. It is disclosed that ethanol is more feasible to dehydrogenate to form CH_3CHO and H_2 over the basic catalyst (**Eq. 4-2**); whereas dehydration to ethylene (**Eq. 4-3**) most likely occurs on acidic sites.[21] Basic oxides, such as CeO_2, or ex-hydrotalcite $MgAl_2O_4$ favor the acetaldehyde route of ethanol transformation.[21] Acetaldehyde could further decompose to CO and CH_4 (**Eq. 4-4**). In addition, it is possible that ethanol directly decomposes into CH_4, CO and H_2 over the catalyst possessing strong capability in breaking the C-C bond (**Eq. 4-5**), *e.g.* Ni-based catalyst.[2,5,6] It was pointed out that ethanol decomposition may successively undergo a pathway of ethanol dehydrogenation and acetaldehyde decomposition.[22] Acetone can be obtained by the dehydrogenation of ethanol followed by aldol condensation. (**Eq. 4-6**).

When reaction temperature is higher than 350 °C, CO_2 and CH_4 increase while CH_3CHO fast declines; CO exhibits a maximum between 350-400 °C, then it goes down fast and approaches to zero at 450 °C. It is probably due to that SRE starts to be the main reaction. In fact, it is known that high temperatures facilitate SRE, while CO transformation by water gas shift (**Eq. 4-7**) is favored at low temperatures. H_2 formation is found to maintain about 55% which can be probably explained by the high concentrations of gas products formed from the high conversion of ethanol in a concentrated feed ($EtOH/H_2O/N_2$ = 14/42/44). The products distribution is in agreement with the thermodynamic analysis *via* response reactions studied by Fishtik.[22]

$$C_2H_5OH \rightarrow CH_3CHO + H_2 \quad \textbf{Eq. 4-2}$$

$$C_2H_5OH \rightarrow C_2H_4 + H_2O \quad \textbf{Eq. 4-3}$$

$$CH_3CHO \rightarrow CO + CH_4 \quad \textbf{Eq. 4-4}$$

$$C_2H_5OH \rightarrow CO + CH_4 + H_2 \quad \textbf{Eq. 4-5}$$

$$2\ CH_3CHO \rightarrow C_3H_6O + CO + H_2 \quad \textbf{Eq. 4-6}$$

$$CO + H_2O \rightarrow CO_2 + H_2 \quad \textbf{Eq. 4-7}$$

4.2 Studies on calcination effect

It is well known that the thermal treatment of catalysts can influence the metal-support interactions, leading to the different properties of the final catalysts: reducibility, resistance to thermal sintering of the active sites or metallic dispersion. In such a context, it is of interest to study the influence of calcination on Ni-based catalysts for SRE. **Fig. 4-4** reports the catalytic performances of the $CeNi_{0.5}O_Y$ catalyst as an example, which is calcined at different temperatures (300-500 °C). A regular evolution of ethanol conversion and products distribution is found depending on the calcination temperature.

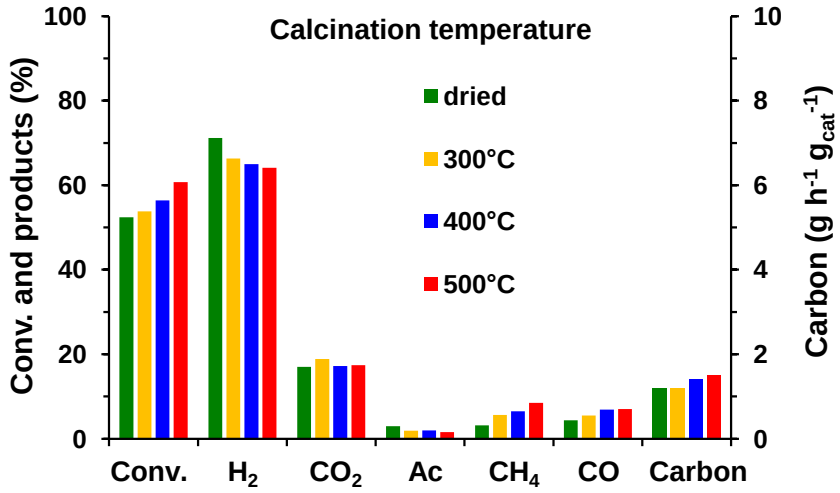

Fig. 4-4 Influence of calcination temperature on the $CeNi_{0.5}O_Y$ (T_T = 250 °C) catalyst for SRE at 450 °C. Reaction conditions: catalyst: 50 mg; $EtOH/H_2O/N_2$ = 14/42/44; time: 5 h.

Conversion slightly increases when the solid is calcined at higher temperatures. The dried $CeNi_{0.5}O_Y$ solid without any calcination exhibits about 50% conversion, whereas the $CeNi_{0.5}O_Y$ catalyst calcined at 500 °C provides higher value of 60%. There are also some differences in the products distribution. H_2 formation slightly decreases with the calcination temperature, which is certainly associated with the increasing conversion. Higher conversion leads to higher amount of gases produced, thus H_2 molar fraction would be diluted. Acetaldehyde is more likely to decompose into CH_4 and CO on the solid calcined at higher temperatures. Besides carbon production is also relatively pronounced with a higher calcination temperature process. But it must be noted that carbon formation is not linear with the time on stream. Therefore, in the following study unless it is precized, the catalysts are all obtained by calcination at 500 °C by default.

4.3 Studies on *in situ* activation in H_2

4.3.1 $CeNi_XO_Y$ catalysts

The influence of *in situ* treatment of $CeNi_XO_Y$ catalysts in H_2 has been analyzed in our laboratory. The SRE reaction was studied as a function of treatment temperature in H_2 and the conditions were optimized.[5,6] It was reported that for low-temperature SRE at 250 °C, the $CeNi_{0.7}O_Y$ catalyst pre-treated in H_2 at 275 °C (corresponding to the first TPR peak) exhibits the highest ethanol conversion of about 50 % with 55 mol% H_2 formation. CO and CH_4 follow the same evolution, presenting optima with T_T at around 275 °C.[5] The $CeNi_XO_Y$ mixed oxides possess good dehydrogenation properties, once the solids are activated in H_2 at a temperature (T_T) ranging between 250-300 °C, the ethanol decomposition can be accentuated at 250 °C. When T_T is higher than 300 °C, conversion decreases.[5]

The optimization of the treatment temperature at about 250 °C is tested and verified for $CeNi_XO_Y$ catalysts with different Ni loadings, and for SRE at different temperatures (200-450 °C).[23] As a matter of fact, it was disclosed by chemical titration that $CeNi_XO_Y$ mixed oxides show optimum hydrogen storage by pre-treatment at 250-300°C in H_2, while for higher T_T the hydrogen content decreases.[6]

4.3.2 $Ni_XMg_2AlO_Y$ catalysts

The influence of treatment temperature in H_2 is investigated over the $Ni_1Mg_2AlO_Y$ catalyst, as an example. As illustrated in **Fig. 4-5**, ethanol conversion and products distribution show strong dependence on the treatment temperature. Conversion undergoes a slow growth from 20% to 33% with treatment temperatures lower than 450 °C. By further increasing treatment temperature up to 550 °C, conversion tremendously goes up to 93% and reaches 100% with T_T = 700 °C. H_2 formation first stays relatively stable around 65% and then decreases to about 47% when $T_T \geqslant 550$ °C.

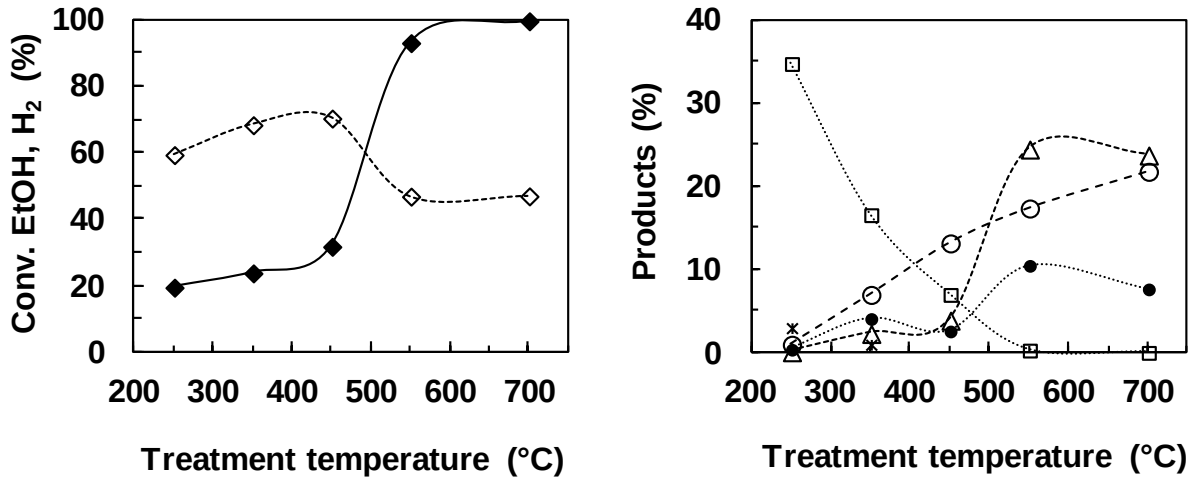

Fig. 4-5 Dependence of SRE at 450 °C *versus* the treatment temperature over the $Ni_1Mg_2AlO_Y$ catalyst. Ethanol conversion (◆), H_2 (◇), CO_2 (○), CH_3CHO (□), CO (●), CH_4 (△) and C_2H_4 (∗) formation. Reaction conditions: catalyst: 50 mg; $EtOH/H_2O/N_2$ = 14/42/44; time: 5 h for each temperature.

CH_3CHO formation apparently declines and CO_2 formation increases with the treatment temperature. CO and CH_4 formation follow similar evolution as conversion, that is, there is no big variation when $T_T \leqslant 450$ °C but the maximum values are obtained with T_T = 550 °C. Ethylene formation of about 3% is detected when T_T = 250 °C, which derives from the dehydration of ethanol, and it diminishes to less than 1% when T_T = 350 °C. Solid carbon is observed when $T_T \geqslant 450$ °C. The carbon formation is measured, namely, 0.1 g (T_T = 450 °C), 0.35 g (T_T = 550 °C) and 0.6 g (T_T = 700 °C). Carbon formation follows the increase in ethanol conversion.

The activation of Ni-based catalysts in H_2 is widely accepted as an important factor to influence the ethanol conversion, as well as the products distribution. In the literature, the

majority of the pre-treatment procedures were performed at very high temperatures (⩾ 700 °C) in order to obtain the metallic nickel species which were believed to be the active sites.[11,12,17,18]

However, such high treatment temperatures could bring several disadvantages. On one hand, it gives rise to the nickel sintering, a main cause of the deactivation of Ni-based catalyst. On the other hand, a high concentration of metallic nickel species obtained by reduction at high temperatures could simultaneously exhibit highly activity toward producing carbon deposition which usually makes troubles to the catalytic stability. Furthermore, plenty of energy is consumed during the high-temperature treatment procedure.

It was reported that high treatment temperature can even lead to a fast deactivation of Ni-Mg-Al catalyst in SRE at 650 °C.[11] The $Ni_{0.3}Mg_{2.7}Al$ catalyst treated in H_2 at 700 °C led to the formation of undesirable products, such as ethylene (18.4 mol%) and ethane (1.3 mol%).[11]

As high treatment temperatures are shown to generate large amounts of carbon (**Fig. 4-5**), the catalytic performances of the $Ni_3Mg_2AlO_Y$ catalyst are only compared after treatment in H_2 at 450 °C and 560 °C. From **Fig. 4-6**, it reveals that even if slightly better catalytic performance can be obtained by using a higher treatment temperature of 560 °C, much more solid carbon (0.83 g) is produced. Comparable good catalytic results are reported with T_T = 450 °C, but in that case significantly lower formation of carbon species (0.2 g) is measured.

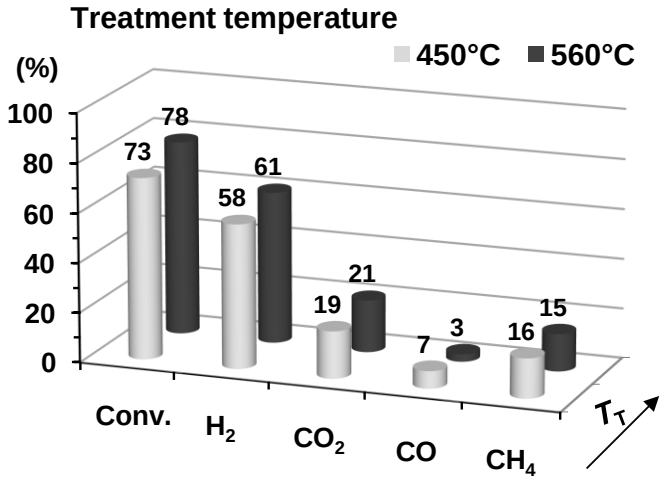

Fig. 4-6 Dependence of SRE at 450 °C *versus* the treatment temperature over the $Ni_3Mg_2AlO_Y$ catalyst. Reaction conditions: catalyst: 50 mg; $EtOH/H_2O/N_2$ = 14/42/44; time: 5 h for each temperature.

Further studies on the activation in H_2 are performed on the $Ni_{12}Mg_2AlO_Y$ catalyst. It has been shown by H_2-TPR of $Ni_XMg_2AlO_Y$ nano-compounds that the reduction peaks clearly shift to

lower temperatures, that is, catalyst with higher Ni loading requires lower treatment temperature for reduction **(Fig. 3-14)**. The $Ni_{12}Mg_2AlO_Y$ compound presents a reduction peak at about 560 °C. First of all, the catalytic performances are compared as a function of reaction temperature, between the catalyst treated at 450 °C and without treatment. It can be clearly seen in **Fig. 4-7** that the activation in H_2 has a strong effect on the conversion and products distribution. The $Ni_{12}Mg_2AlO_Y$ catalyst without treatment is not able to convert any ethanol at low temperatures ($\leqslant$ 250 °C). Conversion starts to be detectable from 300 °C. Very low conversion of about 10% is obtained at 400 °C; even it can approach to 20% at 450 °C. Hydrogen and acetaldehyde are the only products obtained during the whole temperatures range investigated. It is no doubt that only ethanol dehydrogenation can take place on the $Ni_{12}Mg_2AlO_Y$ catalyst without treatment in H_2.

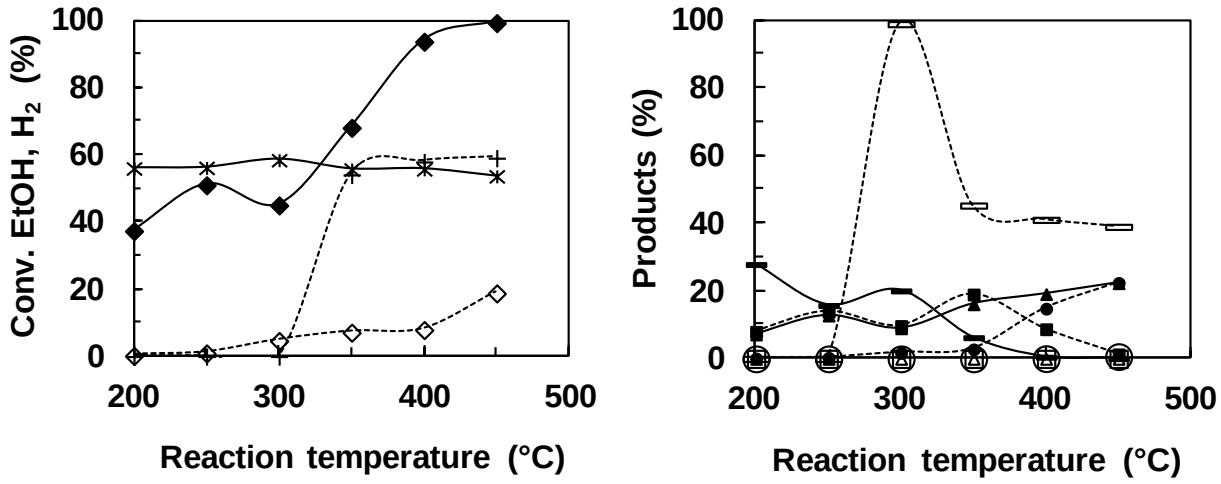

Fig. 4-7 SRE over the $Ni_{12}Mg_2AlO_Y$ catalyst *versus* reaction temperature. Fresh (white) and treated in H_2 at 450 °C (black). Ethanol conversion (◇,◆), H_2 (+,∗), CO_2 (○,●), CH_3CHO (▫,▪), CO (□,■) and CH_4 (△,▲) formation. Reaction conditions: catalyst: 50 mg; $EtOH/H_2O/N_2$ = 14/42/44; time: 5 h for each temperature.

On the contrary, the $Ni_{12}Mg_2AlO_Y$ catalyst pre-treated in H_2 at 450 °C enables to provide about 40% ethanol conversion with 55% H_2 formation at only 200 °C. Conversion undergoes a global increase with reaction temperature and reaches almost 100% at 400 °C. Acetaldehyde formation exhibits much lower at each corresponding temperature, in the meantime CH_4 and CO are observed even from very low temperature of 200 °C, showing that the decomposition of acetaldehyde (and/or ethanol) is much more pronounced on the catalyst once treated at 450 °C.

In the present study, after the treatment in H_2 (T_T) at 450 °C, the $Ni_{12}Mg_2AlO_Y$ catalyst exhibits very good catalytic performance in low temperature range ($\leqslant$ 300 °C). An optimum of

ethanol conversion (51%) is discovered at low temperature of 250 °C. As a matter of fact, similar phenomenon has been reported over the $CeNi_XO_Y$ catalyst, a unique dependence of the catalytic activity upon the treatment temperature. In previous studies, the $CeNi_{0.7}O_Y$ catalyst allowed obtaining about 50% conversion and 55% H_2 also at 250 °C but with the use of a higher catalyst mass (200 mg).[5]

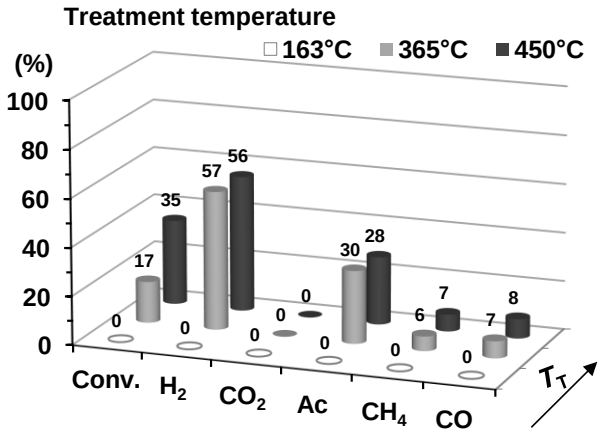

Fig. 4-8 Dependence of SRE at 200 °C *versus* the treatment temperature on the $Ni_{12}Mg_2AlO_Y$ catalyst. Reaction conditions: catalyst: 50 mg; $EtOH/H_2O/N_2$ = 14/42/44; time: 5 h.

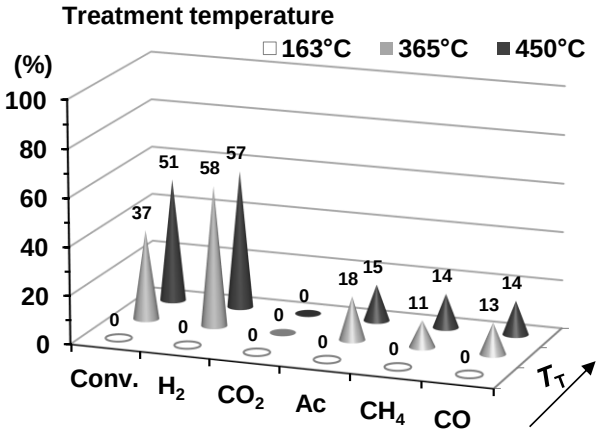

Fig. 4-9 Dependence of SRE at 250 °C *versus* the treatment temperature on the $Ni_{12}Mg_2AlO_Y$ catalyst. Reaction conditions: catalyst: 50 mg; $EtOH/H_2O/N_2$ = 14/42/44; time: 5 h.

So the catalytic performance of the $Ni_{12}Mg_2AlO_Y$ catalyst at low temperatures is further studied by investigating the influence of treatment temperature. Some specific treatment temperatures are selected, following an interesting way to the first small peak (163 °C), the shoulder peak (365 °C) and the initial stage of the main peak (450 °C) of the TPR profile. As shown in **Fig. 4-8** and **Fig. 4-9**, no ethanol is converted into any products at lower than 250 °C, when the $Ni_{12}Mg_2AlO_Y$ catalyst is treated at 163 °C. For reaction temperature of 250 °C, ethanol conversion rapidly increases to 37% with T_T = 365 °C, and keeps rising to 51% with the treatment at 450 °C. Although ethanol conversion follows relatively similar evolution for reaction temperature at 200 °C, the values clearly appear lower, 35% conversion is obtained with T_T = 450 °C.

The products distribution exhibits very similar evolution relatively independent of the treatment temperature. H_2 formation maintains about 57% and CO_2 constantly stays zero whatever the reaction temperature. It makes sense that the strong endothermic SRE reaction hardly takes place at these low temperatures. CO and CH_4 formation clearly present higher values

at higher reaction temperature of 250 °C compared to 200 °C, while it is the inverse for CH_3CHO. This is in agreement with the discussion on the influence of reaction temperature (**Part 4.1**). Below 250 °C, ethanol dehydrogenation and decomposition are the main reactions. The decomposition reactions (**Eq. 4-3** and **Eq. 4-6**) are accentuated at 250 °C when the $Ni_{12}Mg_2AlO_Y$ catalyst is activated in H_2 at 450 °C.

The treatment temperatures higher than 450 °C are not studied, because it can be predicted that a big amount of solid carbon would be produced by using high treatment temperature, even if better activity might be obtained. In fact, high Ni content and high treatment temperature can promote the formation of carbon. It has been proved that treatment of the $Ni_3Mg_2AlO_Y$ catalyst at 560 °C (compared to 450 °C) leads to significantly much more carbon formation (**Fig. 4-6**).

The physicochemical properties of catalyst play an important role in the evolution of surface reaction. In the transformation of ethanol at lower than 250 °C, both the dehydrogenation of ethanol to acetaldehyde or the dehydration of ethanol to ethylene could take place upon the nature of the catalyst. Obviously in the current study, the well tunable $Ni_XMg_2AlO_Y$ catalysts are evidenced to possess quite good capabilities for the dehydrogenation and cleavage of ethanol. The $Ni_{12}Mg_2AlO_Y$ catalyst enables to achieve 51% ethanol conversion and 56% H_2 production at only 250 °C under very hard conditions, *e.g.*, catalyst: 50 mg, $EtOH/H_2O/N_2$ = 14/42/44. The other products are CH_3CHO (16%), CO (14%) and CH_4 (14%).

The attractive result is related to the physicochemical properties of $Ni_{12}Mg_2AlO_Y$ catalyst. XRD shows a mixture of nanoparticles of NiO and/or MgO and/or Ni-Mg-(A)-O with small size of about 6 nm (**Table 3-3**). TPR presents a reduction peak at lower temperature of about 560 °C, compared to the compounds with lower values of x, due to the presence of active Ni species which have strong interactions with other cations (Mg, Al) that can be easily reduced at 450 °C in H_2 (**Fig. 3-14**). The $Ni_{12}Mg_2AlO_Y$ compound has the largest surface area of 196 $m^2\ g^{-1}$ while it also possesses the highest surface Ni molar ratio evidenced by XPS (**Fig. 3-20**). Therefore, it can present the highest amount of accessible active Ni species at the surface.

4.4 Studies on Ni content

4.4.1 $Ni_XMg_2AlO_Y$ catalysts

Fig. 4-10 demonstrates the influence of Ni content on the catalytic performances of $Ni_XMg_2AlO_Y$ catalysts which are *in situ* treated in H_2 at 450 °C. Ethanol conversion, as well as products distribution, is strongly associated with the Ni content. At 450 °C the Mg_2AlO_Y compound, without the presence of nickel, provides 8% ethanol conversion with 43% H_2, 40% CH_3CHO and 17% C_2H_4 formation. The products composition discloses that the main reactions over the Mg_2AlO_Y catalyst are ethanol dehydrogenation and dehydration. As solid inorganic base, Mg-Al hydrotalcites are widely applied to the condensation and idolization reactions because of the dehydrogenation and dehydration properties.[13]

When small quantity of nickel is added into Mg_2AlO_Y compound, the $Ni_{0.5}Mg_2AlO_Y$ catalyst provides clearly different catalytic result. Ethanol conversion goes up to 24%, H_2 formation also grows to 64%; while CH_3CHO decreases to 26%, specifically C_2H_4 formation nearly eliminates. Meanwhile, CO_2 (4%), CO (2%) and CH_4 (1%) are observed, suggesting SRE and decomposition start occurring with the presence of nickel.

With the increase of Ni content, ethanol conversion and CO_2 formation undergo a global rise, showing that higher Ni content facilitates the SRE process (**Fig. 4-10**). Total conversion and about 22% CO_2 are observed at $Ni/M_T = 0.8$. H_2 formation maintains around 55%.

Besides, CH_3CHO formation rapidly declines to zero when Ni/M_T equals 0.5, while CH_4 follows similar evolution of CO_2, CO formation exhibits an optimum at $Ni/M_T = 0.43$. The results demonstrate that higher Ni content promotes the decomposition of acetaldehyde and/or ethanol. Carbon formation starts to be detected from $Ni/M_T = 0.24$ and accelerates with Ni content. 0.1 g carbon production is measured with $Ni/M_T = 0.24$, when Ni/M_T comes to 0.8, the carbon formation grows fast to 0.3 g.

The activity appears to increase with the growth of Ni content, which is in good agreement with the characterizations on the fresh catalysts. In fact, it has been shown in Chapter 3 that the surface area of $Ni_XMg_2AlO_Y$ catalysts expand by increasing Ni content, while the particles sizes of NiO and/or $NiMgO_2$ are well maintained between 3.4-5.9 nm (**Table 3-3**). In addition, XPS proves that the Ni molar ratio on surface also respect to the rising Ni content (**Fig. 3-20**). TPR

peaks show a shift towards lower temperatures with increasing Ni content due to a higher proportion of active Ni species obtained in the compounds with higher Ni content (**Fig. 3-14**).

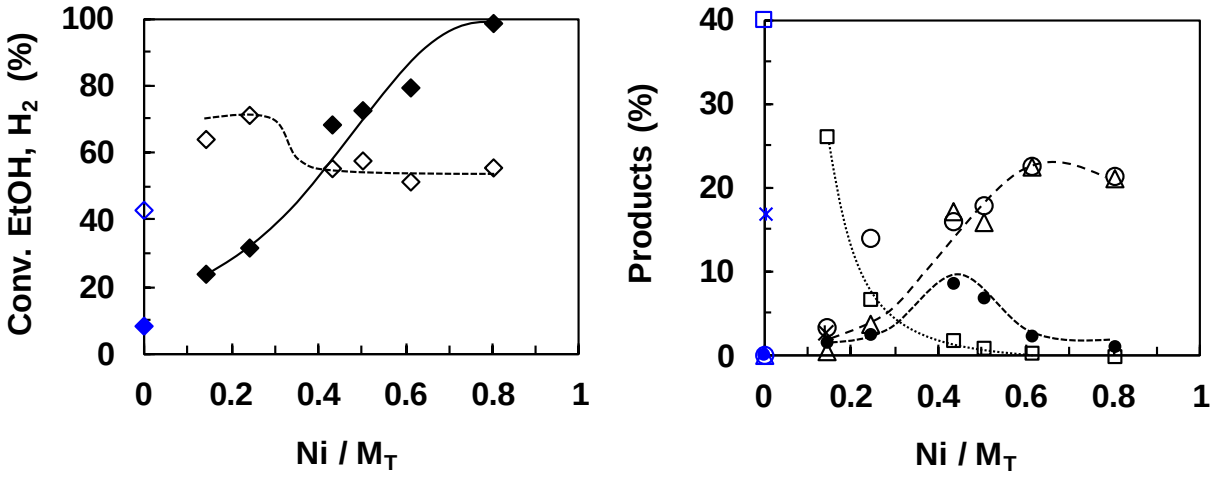

Fig. 4-10 SRE at 450 °C over $Ni_XMg_2AlO_Y$ catalysts (treated in H_2 at 450 °C) as a function of the Ni content. Ethanol conversion (◆), H_2 (◇), CO_2 (○), CH_3CHO (□), CO (●), CH_4 (△) and C_2H_4 (∗) formation. Reaction conditions: catalyst: 50 mg; $EtOH/H_2O/N_2$ = 14/42/44; time: 5 h for each catalyst. Blue symbols represent Mg_2AlO_Y catalyst without the presence of nickel.

Due to the difficulty in seeing the real catalytic behavior of the $Ni_{12}Mg_2AlO_Y$ catalyst when the conversion reaches 100% at 450 °C, the catalyst is tested with a low mass of 8 mg (**Table 4-1**). Total conversion and a very high H_2 production of 7.7 g h^{-1} g_{cat}^{-1} can be reported in the initial stage after 1 h by default because in such a case the starting flow rate is taken into account, in fact there is a large increase of the flow rate (due to the production of a higher number of moles during the reaction **Eq. 4-1**) that is not measured because the products are analyzed online. Afterwards the activity decreases with the time on stream and stabilizes after 5 h (40%), showing a H_2 production of 4.7 g h^{-1} g_{cat}^{-1} (taking into account the starting flow rate). This value is very high compared to the literature,[21] but with a high carbon formation of 0.2 g after 1 h (**Table 4-1**).

Table 4-1 SRE at 450 °C over the $Ni_{12}Mg_2AlO_Y$ catalyst (T_T = 450 °C).

Time/ h	EtOH Conv./ %	Products/ %					H_2 production/ g h^{-1} g_{cat}^{-1}
		H_2	CO_2	CO	CH_4	CH_3CHO	
1	98	58	11	14	17		7.7
5	40	73	12	5	5	5	4.7[a]

Reaction conditions: catalyst: 8 mg; $EtOH/H_2O/N_2$ = 14/42/44. [a] Carbon formation: 0.2 g.

4.4.2 Ce-Ni catalysts

In order to investigate the influence of Ni content on the SRE reaction, a series of $CeNi_XO_Y$ catalysts with different Ni contents (treated in H_2 at 250 °C) are evaluated at 450 °C by using 50 mg of the solid. In the mean time, some Ni/CeO_2 catalysts with different Ni loadings prepared by the impregnation (IMP) and incipient wetness impregnation (IWI) methods are also tested. Finally the results are compared to the curve of the $CeNi_XO_Y$ catalysts.

It shows clearly in **Fig. 4-11** that the catalytic activity strongly depends on the Ni content of the Ce-Ni catalysts, no matter what kind of preparation method is employed. Ethanol conversion increases with Ni content and reaches 100% when the Ni/M_T molar ratio is higher or equal to 0.5 (corresponding to about 23 wt% of Ni loading). H_2 formation decreases from about 70 mol% down to around 45% when increasing the Ni/M_T molar ratio.

The gas phase products distribution follows relatively similar evolutions as plotted in **Fig. 4-11**. Acetone and acetaldehyde are only formed over the catalysts with low Ni contents and disappear when $Ni/M_T \geqslant 0.5$. CO_2 formation exhibits a gradual increase with the Ni content; whereas CO and CH_4 formation present a maximum at $Ni/M_T = 0.5$, where the CO_2 and CO products do not fit to the curve. This phenomenon is certainly due to the very high conversion of ethanol over the $CeNi_1O_Y$ catalysts leading to a higher concentration of CO_2.

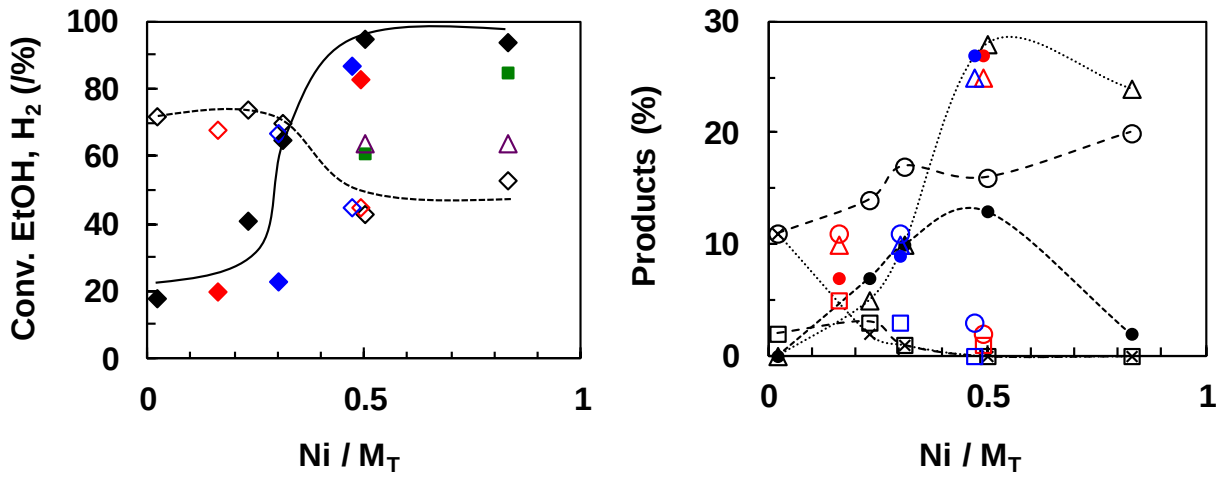

Fig. 4-11 SRE at 450 °C on Ce-Ni catalysts (treated in H_2 at 250 °C) prepared by different methods as a function of the Ni content. Ethanol conversion (◆), H_2 (◇), CO_2 (○), CH_3CHO (□), CO (●), CH_4 (△) and acetone (×) formation. CP (black), IMP (red), IWI (blue). Reaction conditions: catalyst: 50 mg; $EtOH/H_2O/N_2$ = 14/42/44; time: 5 h. For 8 mg of the $CeNi_XO_Y$ catalysts, ethanol conversion (■), H_2 formation (△) are reported after 1 h.

Due to the difficulty to compare the catalytic results of $CeNi_XO_Y$ catalysts when ethanol conversion approaches to 100%, the $CeNi_1O_Y$ and $CeNi_5O_Y$ catalysts are analyzed by using low mass of 8 mg. It is clearly presented in **Fig. 4-11** (green symbols) that ethanol conversion increases with Ni content, and H_2 formation is found at the same value of about 64%.

The other gas phase products distribution also exhibits some differences depending on the Ni content (**Table 4-2**). By increasing the Ni content, CO formation rises while CH_3CHO formation declines. In such conditions, even if the higher H_2 production of 7.0 g h^{-1} g_{cat}^{-1} can be reported over the $CeNi_5O_Y$ catalyst, the carbon formation (80 mg) is so high that the reaction has to be stopped on this compound after 1 h due to an increase of the pressure in the catalytic system. But with regard to the $CeNi_1O_Y$ catalyst, a H_2 production of 2.8 g h^{-1} g_{cat}^{-1} can be obtained at 450 °C at a relatively stable state after 5 h. However, in such a case some CO and acetaldehyde are also formed, which is certainly owing to the low amount of catalyst used. Regardless of the carbon formation and catalytic stability, the H_2 production obtained on the present $CeNi_XO_Y$ catalysts are comparable and even much better than the values reported in recent literature.[21]

Table 4-2 SRE at 450 °C over $CeNi_XO_Y$ catalysts (T_T = 250 °C).

Catalyst	EtOH Conv./ %	Products/ %					H_2 production/ g h^{-1} g_{cat}^{-1}
		H_2	CO_2	CO	CH_4	CH_3CHO	
$CeNi_1O_Y$	61	64	8	14	10	4	5.9[a]
$CeNi_1O_Y$	38	70	10	7	5	8	2.8[b]
$CeNi_5O_Y$	85	64	5	20	11	—	7.0[a]

Reaction conditions: catalyst: 8 mg; $EtOH/H_2O/N_2$ = 14/42/44. [a] Time: 1 h. [b] Time: 5 h.

4.5 Studies on preparation method

The catalytic performances of the Ce-Ni catalysts prepared by the CP, IMP and IWI methods are firstly compared in a group of catalysts with approximately the same Ni loading (23 wt%). Over a high catalyst mass of 200 mg, very similar results are obtained regardless of the preparation method (**Fig. 4-12**). It is obvious that there is almost no difference between the catalysts prepared by different methods.

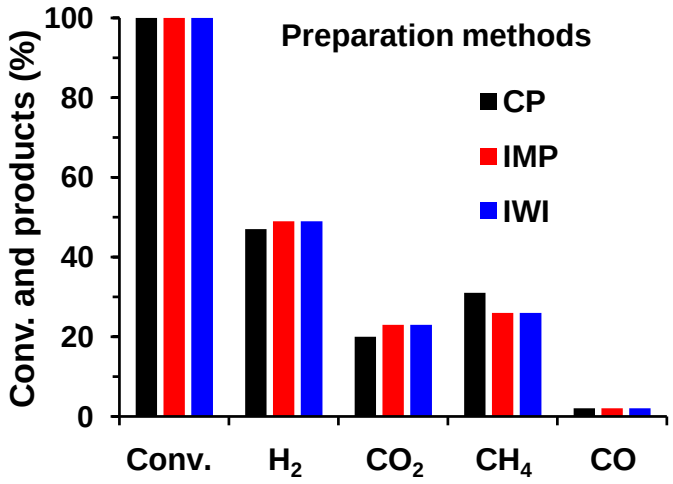

Fig. 4-12 Comparison of SRE at 450 °C over the Ce-Ni catalysts (T_T = 250 °C) prepared by different methods. $CeNi_1O_Y$ (black), 23-Ni/CeO_2-IMP (red), 22-Ni/CeO_2-IWI (blue). Reaction conditions: catalyst: 200 mg; EtOH/H_2O/N_2 = 14/42/44; time: 5 h.

Ethanol conversions all reach 100% at 450 °C over 200 mg of the catalysts. The gas phase products are H_2, CO_2, CH_4 and CO, and the products distribution also exhibits good similarity. Carbon species are observed after the reaction, but the values are not reported under these conditions. It is important to note that under the present conditions, the catalytic activity maintains stable after 5 h of reaction for all the types of catalysts.

Based on the above results, no difference in catalytic activity and stability is found by using 200 mg catalyst. The real influence of preparation method can be seen over lower mass of the catalyst. **Fig. 4-13** compares the catalytic performances of Ce-Ni catalysts (Ni loading: 23 wt%) prepared by different methods evaluating 50 mg of catalyst. The $CeNi_1O_Y$ catalyst enables to provide a very high activity for SRE to our interest. Ethanol is almost completely converted at 450 °C. While the catalysts prepared by the IMP and IWI methods show a relatively lower ethanol conversion, although the values are already very promising of about 85%.

The main products detected in the gas phase are H_2, CO_2, CO and CH_4. The same products distribution is observed on the 23-Ni/CeO_2-IMP and 22-Ni/CeO_2-IWI catalysts. Compared to that, the $CeNi_1O_Y$ catalyst presents a much higher CO_2 formation and a lower CO formation.

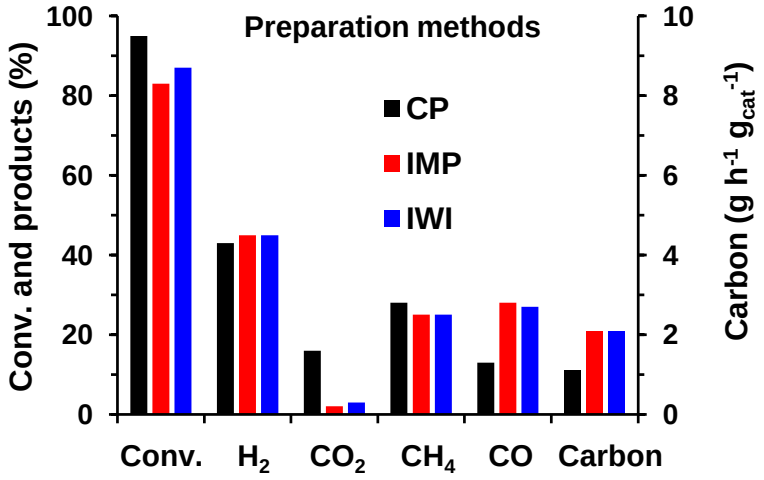

Fig. 4-13 Comparison of the catalytic performances at 450 °C of the Ce-Ni catalysts (T_T = 250 °C) prepared by different methods. $CeNi_1O_Y$ (black), 23-Ni/CeO_2-IMP (red), 22-Ni/CeO_2-IWI (blue). Reaction conditions: catalyst: 50 mg; EtOH/H_2O/N_2 = 14/42/44; time: 5 h for CP, 1 h for IMP and IWI.

Carbon species are found after the reaction and precisely measured. On the $CeNi_1O_Y$ catalyst, a carbon formation of 1.1 g h^{-1} g_{cat}^{-1} is measured after 5 h of reaction, but none deactivation is detected. On the contrary, the 23-Ni/CeO_2-IMP and 22-Ni/CeO_2-IWI catalysts produce much higher carbon formation with the same rate of 2.1 g h^{-1} g_{cat}^{-1} after 1 h of reaction. It is important to recall that solid carbon is not linearly formed with the time on stream, in particular, the carbon production rate is higher at the beginning of the reaction, but the carbon formation can be roughly compared for different systems as a function of time.

It must be emphasized that all the results reported on the $CeNi_XO_Y$ catalysts are obtained at least after 5 h of the reaction. Carbon species are observed as expected, but the catalytic system exhibits good stability. In contrast, when the IMP and IWI catalysts are tested, a dramatic increase of the pressure inside the catalytic system takes place, which requires stopping the catalytic reaction after 1 hour. This phenomenon is also observed over other IMP and IWI catalysts with different Ni loadings, showing that $CeNi_XO_Y$ catalysts behave far more stable than the other two types of catalysts. It can be expected that different types of carbonaceous species are formed.

Compared to the cases when 200 mg of catalyst is evaluated, there is not any significant difference in either catalytic activity or catalytic stability, whatever the preparation method. It seems that when the catalyst mass is higher than what required for the total conversion of ethanol, a part of the catalyst can be used to remove or help to remove the carbon species. However, in

that case, it is impossible to tell the differences with the total conversion of ethanol. Therefore, the main influence of the preparation method on Ce-Ni catalysts for SRE is the catalytic stability. Compared with the Ni/CeO_2-IMP and Ni/CeO_2-IWI catalysts, the $CeNi_XO_Y$ catalysts prepared by CP method is able to provide slight higher catalytic activity, but exhibit much better catalytic stability.

4.6 Studies on catalyst dilution

In the present studies, in order to conveniently collect the spent catalysts for further characterizations, the catalysts are evaluated without the presence of carborundum (SiC). However, in the literature, in some cases the catalysts were diluted by SiC and/or sandwiched by two-layer of SiC.[10,11,18,24] As a matter of fact, the catalyst dilution may have an effect on the catalytic performance, which is mainly related to the following matters: i) in order to obtain the same GHSV for different catalysts with different volume densities; ii) in order to obtain a uniform temperature distribution of the catalyst bed especially for the reaction with strong thermal effect. In such a context, the influence of catalyst dilution is analyzed by using 8 mg of the $CeNi_1O_Y$ catalyst diluted by SiC.

From **Fig. 4-14**, it can be seen that the $CeNi_1O_Y$ catalyst is very active at 450 °C to convert ethanol (70%) to mainly produce H_2 (63%), CO_2 (8%), CH_4 (12%), CO (14%) and CH_3CHO (2%) after 1 h of the reaction. Then it undergoes a deactivation but starts to become much more stable after 4 h. About 35% ethanol conversion accompanied with 72% H_2, 14% CO_2, 3% CH_4, 6% CO, and 4% CH_3CHO formation is obtained after 5 h.

When reaction temperature further increases up to 650 °C, total conversion is achieved. Afterwards the catalyst show similar evolution and exhibits stability. About 76% conversion and 71% H_2 formation are reported after 5 h at 650 °C. The other products in gas phase are CO_2 (14%), CH_4 (5%), CO (6%), CH_3CHO (3%) and C_2H_4 (1%). Solid carbon is observed after the whole test at 650 °C and it is measured at 0.3 g.

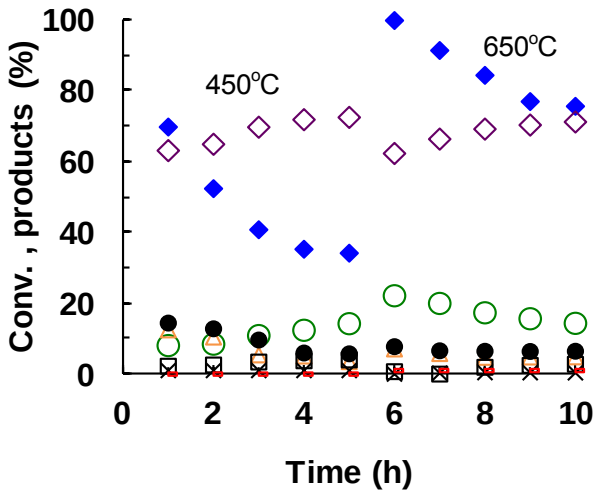

Fig. 4-14 SRE over the $CeNi_1O_Y$ catalyst (8 mg; T_T = 250 °C; $EtOH/H_2O/N_2$ = 14/42/44) diluted by SiC. Ethanol conversion (◆), H_2 (◇), CO_2 (○), CO (●), CH_4 (△), CH_3CHO (□), acetone (×) and C_2H_4 (▫) formation. The catalyst was diluted by SiC (250 μm, 10 mg), and then was sandwiched by two-layer of SiC (500 μm, 50 mg).

Compared with the catalytic results reported in **Table 4-2** (without the presence of SiC), the influence of catalyst dilution by SiC on the $CeNi_1O_Y$ catalyst for SRE is shown in **Fig. 4-15**. Generally there is no apparent difference in catalytic performances, that is, very similar results are obtained whatever the catalyst is diluted or not. This small difference can be due to the uncertainty on the catalyst mass that is very low.

At 450 °C, $CeNi_1O_Y$ catalyst exhibits good activity in the initial stage, giving about 65% ethanol conversion and 65% H_2 formation. Followed a deactivation with the time on stream, the catalyst becomes relatively stable after 5 h or reaction. In such case, a lower ethanol conversion of about 35% and H_2 formation about 70% can be reported. However, some undesirable products are also formed, such as CH_3CHO, CH_4, and CO, which is certainly due to the very low amount of catalyst used. Besides, trace of C_2H_4 formation (1%) is observed only on the $CeNi_1O_Y$ catalyst in the presence of carborundum.

Therefore all the other catalytic results in the present thesis are reported without the presence of carborundum as a catalyst dilution. This allows a faster response in case of deactivation and also to be able to analyze the catalyst after test.

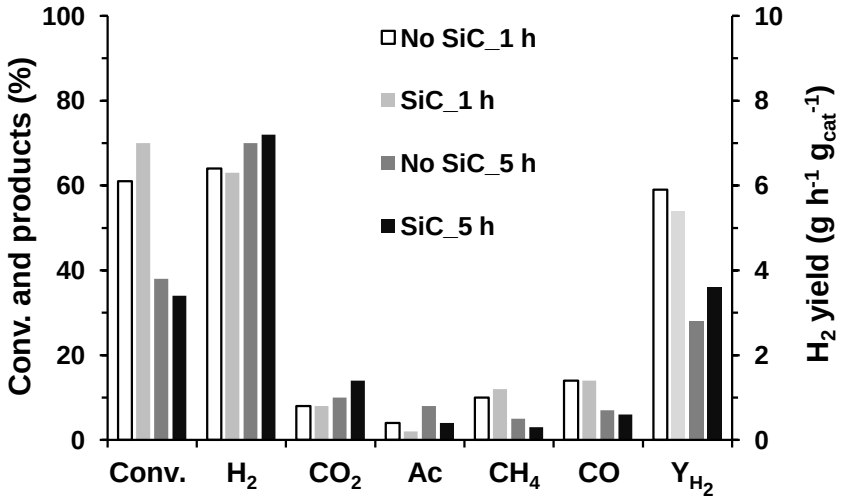

Fig. 4-15 Influence of catalyst dilution on SRE at 450 °C over the $CeNi_1O_Y$ catalyst (T_T = 250 °C). Reaction conditions: catalyst: 8 mg; $EtOH/H_2O/N_2$ = 14/42/44. The catalyst was diluted by SiC (250 μm, 10 mg), and then was sandwiched by two-layers of SiC (500 μm, 50 mg).

4.7 Studies on efficiency of Ni-based catalysts towards hydrogen production

4.7.1 Low-temperature high-yield H_2 production

A very important and interesting application of hydrogen is for clean power generation in fuel cell systems, which are viewed as safe and mobile energy generators. With the rapid growth of the global market demand for fuel cells in the near future, much attention is focused on the H_2 production technology.[25,26] Polymer exchange membrane fuel cells (PEMFCs) and solid oxide fuel cells (SOFCs) powered by hydrogen are suitable for on-board and stationary application. However, the operation requires low temperatures, which could furthermore not only reduce the energy-consumption at high temperatures, but also avoid the deactivation due to metal sintering and carbon deposition. In such a context, it is still very challenging.

In the recent literature, only a few systems have been reported as good candidates for high-yield H_2 production from SRE at very low temperatures ($\leqslant$ 350 °C). Ciambelli *et al.* reported low temperature SRE over Pt/CeO_2 catalyst under highly diluted conditions ($EtOH/H_2O/N_2$ = 0.5/1.5/98), the 5 wt% Pt/CeO_2 catalyst can provide full conversion with 38% H_2 yield at 300 °C.[27,28] Chen *et al.* found Rh-Fe/Ca-Al_2O_3 catalyst for CO-free H_2 generation, total

conversion and 3.5 mol mol_{EtOH}^{-1} H_2 yield were reported at 350 °C under highly diluted conditions and with the presence of a large amount of water ($EtOH/H_2O/N_2$ = 1.1/11.5/88.4).[29] Huang *et al.* reported that (Rh+Co)/CeO_2 catalyst can lead to CO-free H_2 generation with an initial yield of 4.3 mol mol_{EtOH}^{-1} at 300 °C under also highly diluted conditions and high H_2O/EtOH ratio of 10.[30]

The $Ni_{12}Mg_2AlO_Y$ catalyst has been shown to be highly active for low-temperature SRE in the presence of high concentration of ethanol (14 mol%), among the whole series of $Ni_XMg_2AlO_Y$ catalysts (**Fig. 4-9**). Therefore the efficiency towards H_2 production at low temperatures (⩽ 300 °C) is further investigated on the $Ni_{12}Mg_2AlO_Y$ catalyst under highly diluted conditions.

The efficiency of the $Ni_{12}Mg_2AlO_Y$ catalyst towards H_2 production ($EtOH/H_2O/N_2$ = 1/3/96) is shown in **Fig. 4-16**. Total ethanol conversion is achieved at either 250 °C or 300 °C, and only H_2, CO_2 and CH_4 are formed in the gas phase products without the formation of CO. At 250 °C, about 51% H_2, 19% CO_2 and 30% CH_4 are obtained in the gas phase. Methane transformation is logically more pronounced at 300 °C compared to 250 °C; as a result, a higher proportion of H_2 (61%) is observed at this temperature, while CH_4 formation decreases to about 20%. The H_2 yield reaches 3 mol mol_{EtOH}^{-1} at 300 °C.

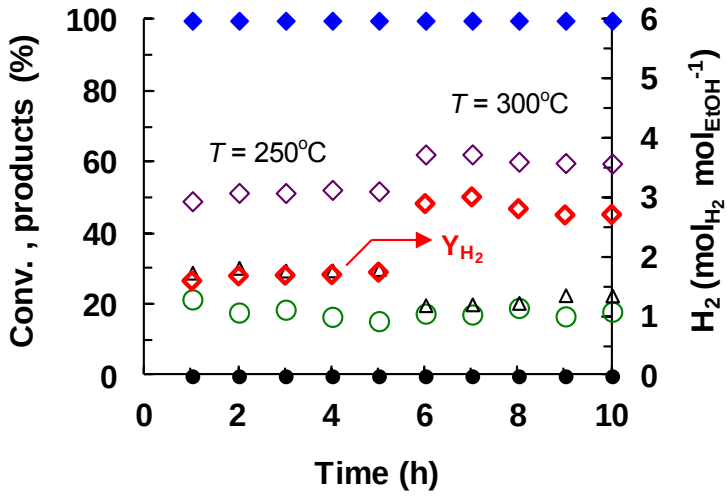

Fig. 4-16 Efficiency of the $Ni_{12}Mg_2AlO_Y$ catalyst (T_T = 450 °C) towards H_2 production in the SRE reaction. Conversion (◆), H_2 (◇), CO_2 (○), CO (●), CH_4 (△) and H_2 yield (◇). Reaction conditions: catalyst 50 mg; $EtOH/H_2O/N_2$ = 1/3/96.

As is known that increasing the amount of water allows increasing H_2 yield, the performance obtained here with a H_2O/EtOH ratio of 3 is very high compared to the results reported in the literature even over noble metal based catalysts.[21,27-31]

Even if very recently it has been reported that (Rh+Co)/CeO_2 catalyst can lead to CO-free H_2 yield of 4.3 mol mol_{EtOH}^{-1} at 300 °C,[30] the value has been obtained with much higher catalyst mass (150 mg) and with a very high H_2O/EtOH ratio of 10. Moreover the value corresponds to an initial state obtained after only 25 min. The H_2 yield already decreases to 3 mol mol_{EtOH}^{-1} after 4 h, in that case, 11% CO formation is obtained in the outlet gases.[30] Rh-Fe/Ca-Al_2O_3 catalyst has also been reported as highly efficient catalyst for CO-free H_2 generation, with total conversion and a H_2 yield of 3.5 mol mol_{EtOH}^{-1} at 350 °C, but a large amount of water (EtOH/H_2O/N_2 = 1.1/11.5/88.4) was also used.[29] The present catalytic system exhibits stable activity during at least 10 h certainly due to the very low carbon formation of only 9 mg at 300 °C. The type and morphology of the carbon species formed need further characterizations.

4.7.2 Influence of ethanol concentration

In practical applications it would be more interesting to use alcohol in high concentration. However, it has been already presented before that H_2 formation stays around 50 mol% when a large amount of gases are produced from the high conversion of ethanol in a concentrated feed (EtOH/H_2O/N_2 = 14/42/44). Highly diluted conditions are usually employed in the literature in order to analyze and compare the catalysts activities; mainly because this allows avoiding problems due to the big variation of volume in the outlet gases, as the SRE reaction (**Eq. 4-1**) leads to the formation of higher number of moles.

Here is an example displayed to show how ethanol concentration influences the catalytic performance. **Fig. 4-17** compares the catalytic results obtained on the $Ni_{12}Mg_2AlO_Y$ catalyst at 250 °C by feeding different concentrations of ethanol. The H_2O/EtOH ratio is always maintained at 3. Increasing the ethanol concentration in the reactant mixture clearly leads to a decrease of the activity. 100% of conversion is obtained with EtOH/H_2O/N_2 = 1/3/96, but lower conversion of about 60% can be reported with a higher concentration of ethanol (EtOH/H_2O/N_2 = 3/9/88).

The ethanol concentration also has an effect on the products distribution. Under a lower ethanol concentration (1 mol%), only H_2 (52%), CO_2 (18%) and CH_4 (30%) are obtained, without the formation of CO. Whereas increasing ethanol concentration up to 3 mol%, H_2 (70%) and

acetaldehyde (28%) are the main products, CO_2 formation is very low (2%); no CH_4 and CO are formed, suggesting dehydrogenation of ethanol is the dominant reaction happening in such conditions. As a general consequence, the H_2 yield of 1.1 mol mol_{EtOH}^{-1} obtained with a $EtOH/H_2O/N_2$ = 3/9/88 mixture is lower than the value of 1.7 mol mol_{EtOH}^{-1} obtained with the presence of more diluted ethanol-water mixture ($EtOH/H_2O/N_2$ = 1/3/96).

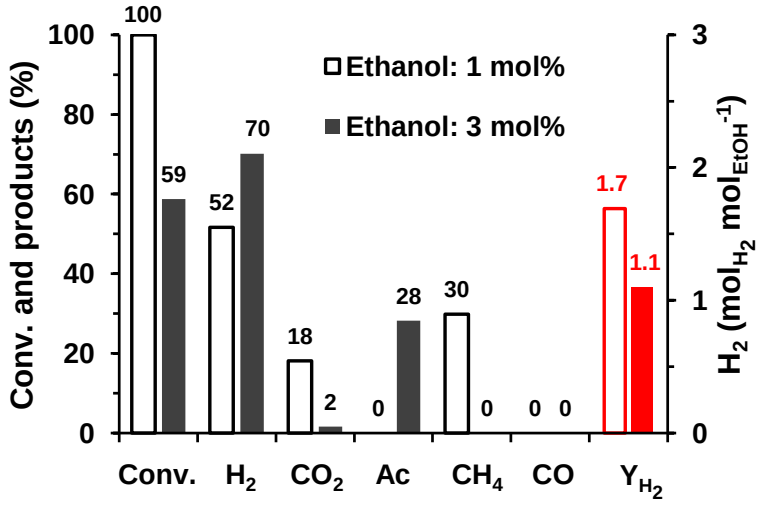

Fig. 4-17 Influence of ethanol concentration on SRE at 250 °C over the $Ni_{12}Mg_2AlO_Y$ catalyst (T_T = 450 °C). Reaction conditions: catalyst 50 mg; time 5 h. Hollow columns: $EtOH/H_2O/N_2$ = 1/3/96; solid columns: $EtOH/H_2O/N_2$ = 3/9/88; Ac: acetaldehyde.

Furthermore the evolution of the $Ni_{12}Mg_2AlO_Y$ catalyst at 250 °C with time on stream can be seen by working with higher proportion of ethanol (3 mol%). From **Fig. 4-18**, a deactivation is observed with the time on stream. Total conversion is observed after 1 h; however, the activity falls to 60% after 5 h (**Fig. 4-18**). This evolution is not observed by feeding lower concentration of ethanol (1 mol%, **Fig. 4-16**). Because in that case the activity is saturated even if a deactivation of activity might exist. In the literature, H_2 yield is basically reported and compared with total ethanol conversion, even though a deactivation might take place.[10,24] In order to avoid problems due to volume variation which allows reporting high values for H_2 yield, quite highly diluted conditions: very low concentration of ethanol and/or a big amount of water are frequently used.[9,10] Such conditions are extremely mild. It would be much more interesting in practical use to involve higher concentrations of ethanol.

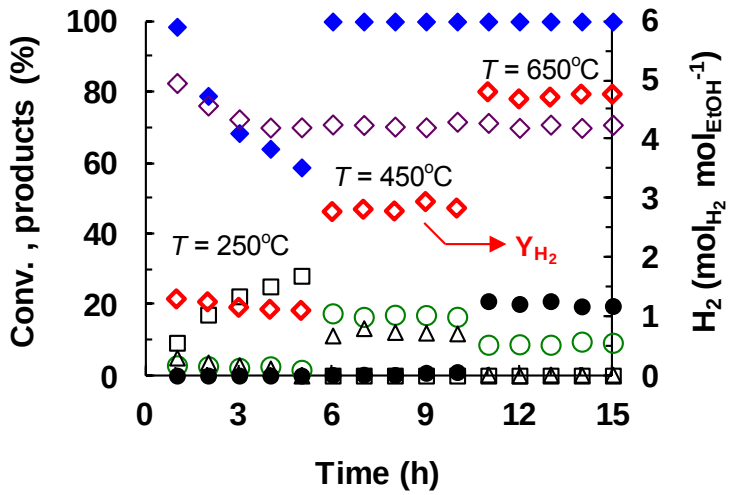

Fig. 4-18 Efficiency of the $Ni_{12}Mg_2AlO_Y$ catalyst (T_T = 450 °C) towards H_2 production in the SRE reaction. Conversion (◆), H_2 (◇), CO_2 (○), CO (●), CH_4 (△), H_2 yield (◇). Reaction conditions: catalyst 50 mg; $EtOH/H_2O/N_2$ = 3/9/88.

The influence of ethanol concentration is more pronounced when the ethanol concentration further increases to 14 mol% (**Fig. 4-3**). At 250 °C H_2 formation is comparable to the value reported previously in our laboratory, over the very active $CeNi_{0.7}O_Y$ mixed oxide which allowed obtaining 50% ethanol conversion with 55 mol% H_2 formation under hard conditions ($EtOH/H_2O/N_2$ = 14/42/44), but with the use of a higher catalyst mass (200 mg).[5] To be recalled, the H_2O/EtOH molar ratio is constantly fixed at 3 whatever the ethanol concentration. In such conditions, total conversion can be obtained at 450 °C on the $Ni_{12}Mg_2AlO_Y$ catalyst, and the main products obtained in gas phase are H_2, CO_2 and CH_4, without the formation of CO (**Fig. 4-3**).

4.7.3 Influence of reaction temperature

As expected, higher temperatures allow obtaining higher H_2 yield. Moreover the catalyst sustains harder conditions. The catalytic activity remains stable even under higher concentration of reaction mixture. In the presence of a higher ethanol concentration ($EtOH/H_2O/N_2$ = 3/9/88), over the $Ni_{12}Mg_2AlO_Y$ catalyst, H_2 yield reaches 2.8 mol mol_{EtOH}^{-1} at 450 °C (**Fig. 4-18**) without the formation of CO. The other gas phase products are CO_2 (17%) and CH_4 (13%). By increasing reaction temperature up to 650 °C, H_2 yield reaches 4.8 mol mol_{EtOH}^{-1} with a $EtOH/H_2O/N_2$ = 3/9/88 mixture. At 650 °C the SRE reaction can be performed with the transformation of water which allows obtaining yield to hydrogen higher than 3 mol mol_{EtOH}^{-1}. However, at this

temperature water gas shift is less favorable and CO (20%) is observed among the products. The activity is stable during at least 10 h certainly due to the low carbon formation of 19 mg.

Herein the efficiency of the $Ni_3Mg_2AlO_Y$ catalyst towards H_2 production is carefully explored. **Fig. 4-19** reports the time course for the SRE reaction under diluted conditions ($EtOH/H_2O/N_2$ = 3/9/88). At 450 °C, the $Ni_3Mg_2AlO_Y$ catalyst is able to completely convert ethanol and provide a CO-free H_2 production of 3.0 mol mol_{EtOH}^{-1}. The other products are CO_2 and CH_4. By further increasing the reaction temperature to 650 °C, CH_4 formation decreases from about 10% down to zero; meanwhile CO formation starts to rise to about 11%. This phenomenon is in good agreement with the thermodynamic features of methane reforming and water gas shift reactions depending on the temperatures. As a result, the H_2 yield significantly increases up to 5.0 mol mol_{EtOH}^{-1} at 650 °C, and the catalyst exhibits good stability. Carbon species are measured with a low quantity of 19 mg after 10 h. The type and morphology of carbon species formed are analyzed and the results are discussed later.

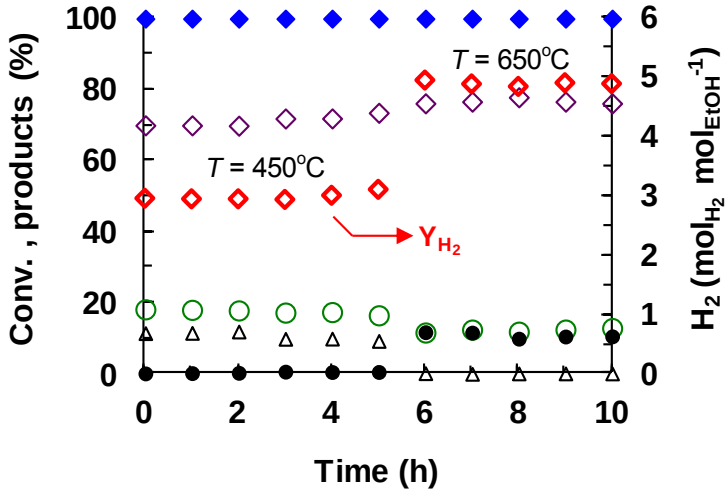

Fig. 4-19 Efficiency of the $Ni_3Mg_2AlO_Y$ catalyst (T_T = 450 °C) towards H_2 production in the SRE reaction. Conversion (◆), H_2 (◇), CO_2 (○), CO (●), CH_4 (△), H_2 yield (◇). Reaction conditions: catalyst 50 mg; $EtOH/H_2O/N_2$ = 3/9/88.

The efficiency of the $CeNi_XO_Y$ catalysts is also deeply studied by their capacity of producing hydrogen from SRE. **Fig. 4-20** reports H_2 yield and the gas phase products with the time on stream over the $CeNi_1O_Y$ catalyst. Similar catalytic performance is obtained. At 450 °C, the $CeNi_1O_Y$ catalyst enables to totally convert ethanol to H_2 production with a yield of 2.9 mol mol_{EtOH}^{-1}. The other gas phase products are CO_2 and CH_4. CO formation is not observed.

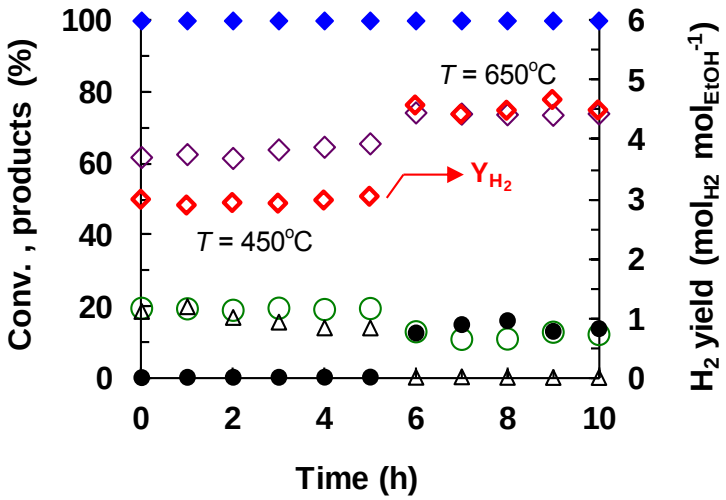

Fig. 4-20 Efficiency of the $CeNi_1O_Y$ catalyst (T_T = 450 °C) towards H_2 production for SRE. Ethanol conversion (◆), H_2 (◇), CO_2 (○), CO (●), CH_4 (△), H_2 yield (◇). Reaction conditions: catalyst: 50 mg; $EtOH/H_2O/N_2$ = 3/9/88.

By further increasing the reaction temperature from 450 °C up to 650 °C, CO formation starts to rise to about 13%, while CH_4 formation gradually decreases from 20% down to zero. It is due to methane reforming favored at high temperatures and CO transformation by water gas shift favored at low temperatures, as already mentioned. As a result, the yield to hydrogen significantly increases to 4.6 mol mol_{EtOH}^{-1} at 650 °C (**Fig. 4-20**). Moreover the catalyst performs considerable stability. It has to be noted that a very low carbon formation of 8 mg is measured on the $CeNi_1O_Y$ catalyst after 10 h of the reaction at 650 °C under diluted conditions.

To the best of our knowledge, the $CeNi_XO_Y$ and $Ni_XMg_2AlO_Y$ catalysts studied in the present thesis are highly efficient for H_2 production from ethanol. The H_2 yield of about 5 mol mol_{EtOH}^{-1} obtained on the above two types of Ni-based catalysts is one of the best and very competitive result that has been ever reported for SRE. It is important to remark that the formation of CO and CH_4 limits the yield to hydrogen to no more than 90% (corresponding to 5.4 mol mol_{EtOH}^{-1}) in the best conditions. In fact, working at high temperature water gas shift equilibrium does not allow such a yield to increase, while at lower temperature the yield is also limited by the methane steam reforming equilibrium.

Up to date, some H_2 yields between 4.0 and 5.1 mol mol_{EtOH}^{-1} have been reported over Ni-based catalysts at temperatures higher than 650 °C. But the reaction conditions applied were such as the ethanol concentration was highly diluted and/or the H_2O/EtOH molar ratio was much higher than 3, which has been well known as a promotion to H_2 yield. The value of about 5.0 mol

mol_{EtOH}^{-1} with the present $CeNi_XO_Y$ and $Ni_XMg_2AlO_Y$ catalysts can be considered as better than those measured on other Ni-based ternary and quaternary mixed oxide catalysts if taking into account the experimental conditions, typically such as 4.5 mol mol_{EtOH}^{-1} (150 mg LaNiMgAl catalyst),[9] 4.9 mol mol_{EtOH}^{-1} (200 mg $NiMg_4ZnAl$ catalyst, 700 °C),[18] 5.0 mol mol_{EtOH}^{-1} ($Ni_{50}ZnAl$ catalyst, H_2O/EtOH = 6)[10] and 5.1 mol mol_{EtOH}^{-1} (Ni/Mg_2Al catalyst, H_2O/EtOH = 8.4).[24]

4.8 Characterizations on the spent catalysts

4.8.1 XRD

Studying and comparing the structure and crystalline phase of the fresh and spent catalysts allow further understanding the correlations between the catalysts properties and catalytic performances, *i.e.*, possible active phase, active sites and mechanism.

Fig. 4-21 and **Fig. 4-22** show the XRD patterns of the $Ni_3Mg_2AlO_Y$ and $Ni_{12}Mg_2AlO_Y$ catalysts obtained before reaction, *in situ* treatment in H_2, and after reaction in highly diluted conditions. The fresh catalysts (calcined at 500 °C) show mixture phases of nanoparticles of NiO, MgO and/or $NiMgO_2$ solid solution. The diffraction peaks of NiO, MgO and $NiMgO_2$ nearly overlap each other, and cannot be distinguished. The particles sizes of NiO and/or $NiMgO_2$ are measured at 3.9 nm for the $Ni_3Mg_2AlO_Y$ compound and at 5.9 nm for the $Ni_{12}Mg_2AlO_Y$ compound (**Table 4-3**).

Table 4-3 Crystallite sizes of $Ni_XMg_2AlO_Y$ catalysts. [a] Calculated from (200) plane. [b] Calculated from Ni (200) plane.

Catalyst	Conditions	*d* NiO and/or $NiMgO_2$/ nm [a]	*d* Ni^0/ nm [b]
$Ni_3Mg_2AlO_Y$	calcined at 500 °C	3.9	—
	treated in H_2 at 450 °C for 10 h	4.0	4.0
	after SRE at 650 °C	4.4	4.3
$Ni_{12}Mg_2AlO_Y$	calcined at 500 °C	5.9	—
	treated in H_2 at 450 °C for 10 h	5.5	5.0
	after SRE at 300 °C	5.4	5.0

After the treatment in H_2 at 450 °C for 10 h, metallic Ni^0 phase is detected at 2θ = 44.5 °, 51.8 ° and 76.2 ° for Ni (111), (200), (220) plane, namely (**Fig. 4-21** and **Fig. 4-22**). The Ni

particle size is measured at 4.0 nm for $Ni_3Mg_2AlO_Y$ and at 5.5 nm for $Ni_{12}Mg_2AlO_Y$ (**Table 4-3**). All the phases related to NiO and/or MgO and/or $NiMgO_2$ are maintained, the crystallite sizes are very close to the values measured in the calcined compounds (**Table 4-3**).

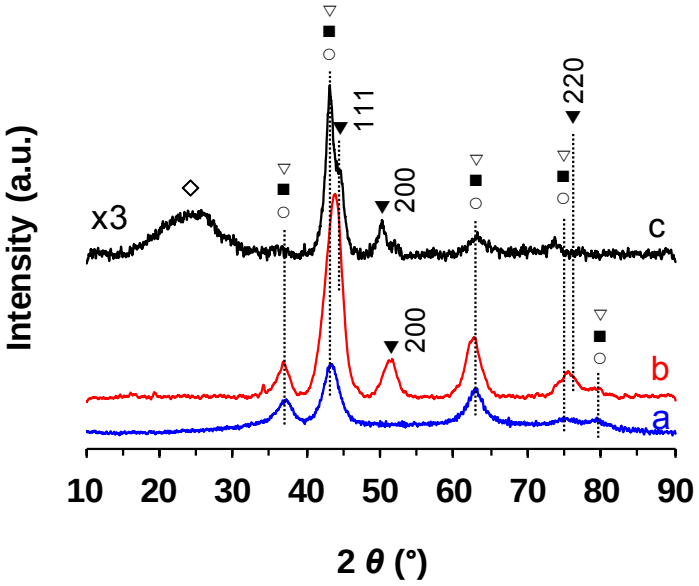

Fig. 4-21 XRD patterns of the $Ni_3Mg_2AlO_Y$ catalyst. a) calcined at 500 °C, b) treated in H_2 at 450 °C for 10 h, c) after SRE at 650 °C. (Reaction conditions: catalyst: 50 mg; $EtOH/H_2O/N_2$ = 3/9/88; time: 10 h.). MgO (○), $NiMgO_2$ (■), NiO (▽), Ni (▼) and C (◇).

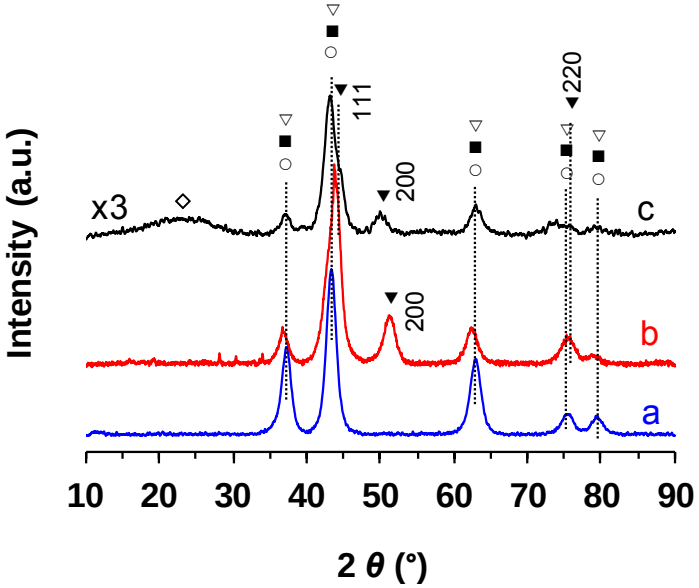

Fig. 4-22 XRD patterns of the $Ni_{12}Mg_2AlO_Y$ catalyst. a) calcined at 500 °C, b) treated in H_2 at 450 °C for 10 h, c) after SRE at 300 °C. (Reaction conditions: catalyst: 50 mg; $EtOH/H_2O/N_2$ = 1/3/96; time: 10 h.). MgO (○), $NiMgO_2$ (■), NiO (▽), Ni (▼) and C (◇).

After the reaction in highly diluted conditions (EtOH: 1 mol% or 3 mol%), the spent catalysts largely present the structure of the fresh catalysts (**Fig. 4-21** and **Fig. 4-22**). All the phases attributed to NiO, MgO and $NiMgO_2$ are still well maintained. However, the solid appear less crystallized. Compared with the patterns obtained in H_2 treatment, Ni^0 phase for (111) and (200) plane is also visible in the spent catalysts, but Ni (220) plane becomes less visible. Moreover, the Ni (111) plane reduces after reaction, and this is observed for both $Ni_3Mg_2AlO_Y$ and $Ni_{12}Mg_2AlO_Y$ catalysts. It was reported that Ni (111) exhibited good reactivity towards many molecules including ethylene, methane and water which could be effectively dissociated into H, CH, CH_3, OH and O on Ni (111) surface, most of which are H-contributors.[32,33] Ni (200) plane is found a slight shift to low diffraction angle for both $Ni_3Mg_2AlO_Y$ and $Ni_{12}Mg_2AlO_Y$. The Ni particles sizes are estimated at 4.3 nm for $Ni_3Mg_2AlO_Y$ and 5.0 nm for $Ni_{12}Mg_2AlO_Y$ compounds. These values appear nearly the same as the Ni particles sizes obtained in H_2 treatment at 450 °C whatever $Ni_3Mg_2AlO_Y$ and $Ni_{12}Mg_2AlO_Y$ catalysts (**Table 4-3**). A new peak at 2θ = 26 ° is visible on the catalysts after reaction, which is identified to graphitic carbon.

$Ni_XMg_2AlO_Y$ catalysts after SRE at 450 °C in the presence of high concentration of ethanol (EtOH: 14 mol%) are also analyzed by XRD. As displayed in **Fig. 4-23**, all the phases related to NiO and/or MgO and/or $NiMgO_2$ still maintain, but the intensity of some lines diminishes showing that the compounds become more amorphous compared to the fresh catalysts (**Fig. 4-24**). This phenomenon is more pronounced for the high Ni content.

Metallic Ni^0 species are also detected for (111) and (200) plane, but the intensity is much lower than that obtained by the treatment in H_2 at 450 °C, and also lower than that obtained after SRE in highly diluted conditions (**Fig. 4-21** and **Fig. 4-22**).

This phenomenon can be probably due to relatively high quantity of solid carbon generated after test compared to the catalyst used (50 mg), thus a strong diffraction peak due to the graphitic carbon is visible at 2θ = 26 °. It has to be remarked that it is much more difficult to separate the spent catalyst from a big amount of solid carbon, compared to the case with low formation of carbon in the presence of low concentration of ethanol (EtOH: 1 mol% or 3 mol%).

The intensity of carbon lines become more intense on the catalysts with higher Ni content, which is in agreement with the carbon formation depended on the Ni loading. Therefore, higher Ni content leads to higher carbon formation, which is in agreement with the increase of ethanol conversion by increasing the Ni content (**Fig. 4-10**).

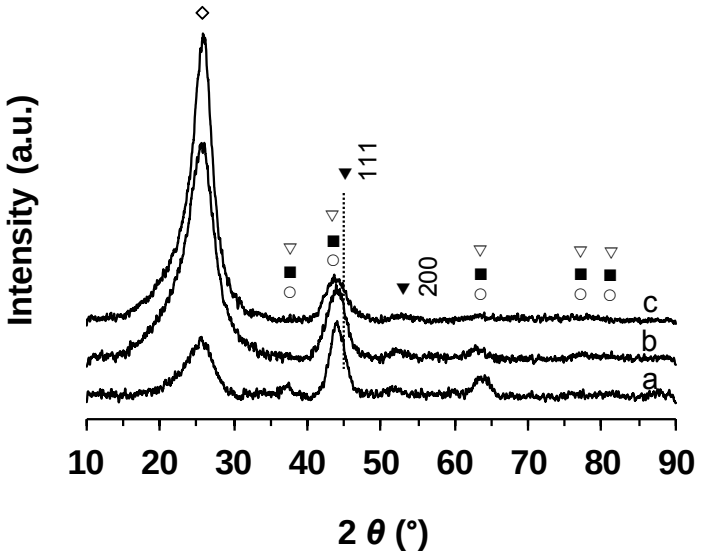

Fig. 4-23 XRD patterns of $Ni_XMg_2AlO_Y$ catalysts (T_T = 450 °C) after SRE at 450 °C. a) $Ni_1Mg_2AlO_Y$, b) $Ni_3Mg_2AlO_Y$, c) $Ni_{12}Mg_2AlO_Y$. MgO (○), $NiMgO_2$ (■), NiO (▽) and Ni (▼). Reaction conditions: catalyst: 50 mg; $EtOH/H_2O/N_2$ = 14/42/44; time: 5 h.

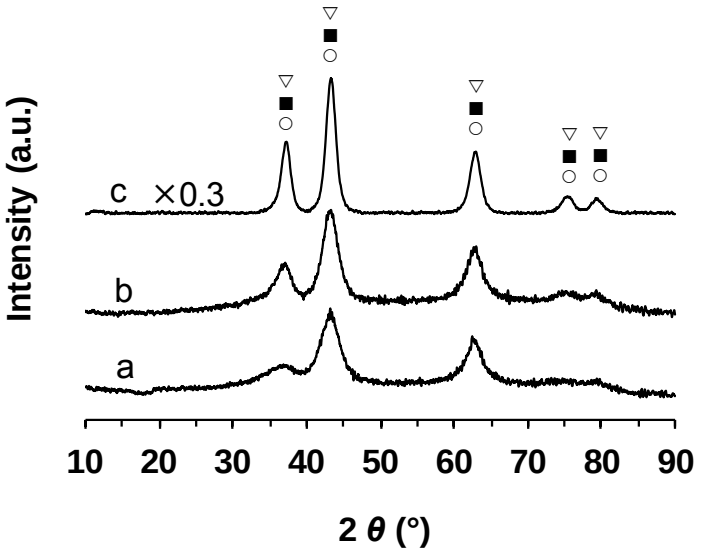

Fig. 4-24 XRD patterns of $Ni_XMg_2AlO_Y$ catalysts (calcined at 500 °c). a) $Ni_1Mg_2AlO_Y$, b) $Ni_3Mg_2AlO_Y$, c) $Ni_{12}Mg_2AlO_Y$. MgO (○), $NiMgO_2$ (■) and NiO (▽).

4.8.2 XPS

The $CeNi_1O_Y$, $Ni_3Mg_2AlO_Y$ and $Ni_{12}Mg_2AlO_Y$ catalysts after SRE are analyzed by XPS. The Ni2p core-level spectra are shown in **Fig. 4-25**. The binding energies obtained from XPS are summarized in **Table 4-4** and **Table 4-5**. A main emission peak in $Ni2p_{3/2}$ region is observed for

all the spent catalysts analyzed. Compared to the calcined compounds the binding energies shift to higher values after reaction. However, for all the studied solids, a BE at 856.5 ± 0.1 eV is observed for the $Ni2p_{3/2}$ main peak after SRE. The shift is higher on the $CeNi_1O_Y$ compound compared to the $Ni_XMg_2AlO_Y$ compounds. As a matter of fact, a value of 854.5 eV has been reported for the calcined Ce-Ni mixed oxide. [34] Besides, almost no variation of the FWHM is observed. Concerning the $Ni_XMg_2AlO_Y$ compounds, the values of the BE obtained after reaction (856.5 eV) become very close to the one obtained on the dried compounds (856.2 eV), in agreement with the value obtained for Ni^{2+} species in $Ni(OH)_2$ (856.2 eV) (**Table 4-4** and **Table 4-5**). This can be well explained by the presence of hydroxyl groups at the surface of the catalyst after reaction in the presence of ethanol and water. Moreover, the characteristic satellite lines of Ni^{2+} species are clearly visible at about 6 eV up to the main peak. The small shoulder peak at lower energy is assigned to metallic Ni^0 species on the surface, which is in agreement with the BE of pure Ni^0 species (852.6 eV). [35]

These results are in very good agreement with the XRD analysis of the spent catalysts (**Fig. 4-21** and **Fig. 4-22**), where all the oxidized phases are well maintained accompanied with a small amount of metallic Ni phase. The surface Ni molar ratios are found lower but still very close to the values obtained on the dried compounds and fresh catalysts (**Table 4-4** and **Table 4-5**), showing that the homogeneous distribution of Ni species in the catalysts after SRE is relatively well maintained.

The O1s spectra are also reported in **Fig. 4-25**. Concerning the $Ni_XMg_2AlO_Y$ compounds, while two peaks are obtained on the calcined compounds, only one is presented after SRE. The value of the BE obtained after reaction (531.7 eV) shifts to higher value (+ 1.1 eV) compared to the calcined compounds and becomes the same as the one obtained on the dried compounds, even if the full width at half-maximum (FWHM) is higher. This contribution is assigned to oxygen species in OH^- groups. On the $CeNi_1O_Y$ catalyst, two peaks are observed after SRE. The BE of 530.3 ± 0.2 eV is also higher (+ 1.2 eV) than the data obtained on the calcined catalyst. The value is close to the one attributed to the typical O^{2-} lattice oxygen species, however, as there is a shift to higher values, the presence of hydroxyl groups can be also proposed. Both the higher BE at 532.3 ± 0.1 eV and the line broadening effect of O1s line demonstrate the presence of different oxygen species. It is highly probably due to the oxygen species in the surface-absorbed organic functional groups. It was reported that O1s line at between 531.9-533.1 eV is the contribution of

different O-containing organic functional groups.[36,37] Moreover, the surface O/Ni ratios after SRE in the present work is much higher than 2, showing the different oxygen species coexist on the surface of the spent catalysts. As a matter of fact, O-containing organic functional groups can exist on the surface of the catalysts after reaction in the presence of ethanol and water.

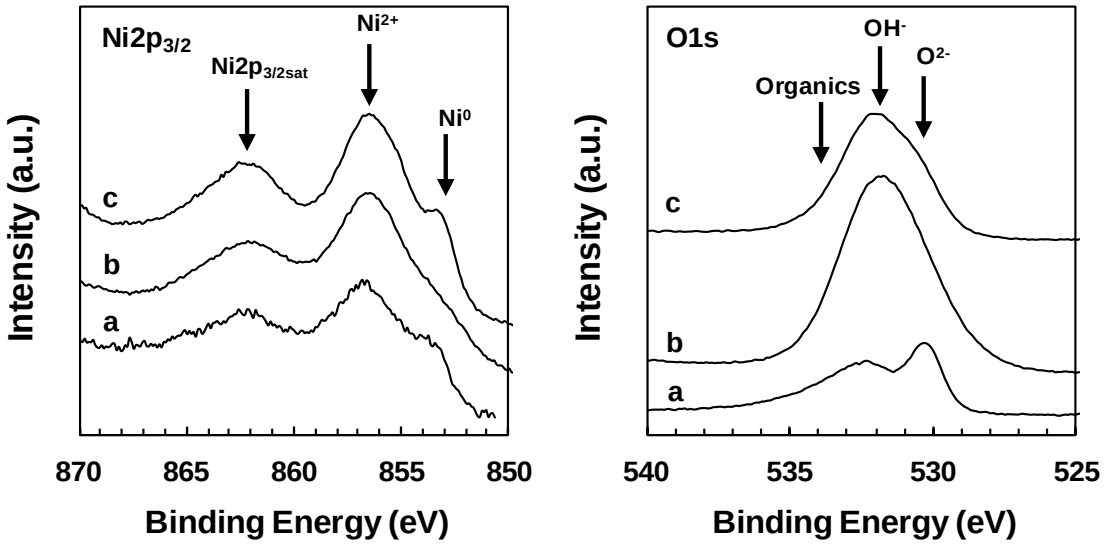

Fig. 4-25 Ni2p and O1s XPS spectra of $CeNi_XO_Y$ and $Ni_XMg_2AlO_Y$ catalysts after SRE. a) $CeNi_1O_Y$ after SRE at 650 °C (catalyst: 50 mg; $EtOH/H_2O/N_2$ = 3/9/88; time: 10 h.), b) $Ni_3Mg_2AlO_Y$ after SRE at 650 °C (catalyst: 50 mg; $EtOH/H_2O/N_2$ = 3/9/88; time: 10 h.), c) $Ni_{12}Mg_2AlO_Y$ after SRE at 300 °C (catalyst: 50 mg; $EtOH/H_2O/N_2$ = 1/3/96; time: 10 h.).

Table 4-4 Binding energies and surface Ni molar ratios of the $CeNi_1O_Y$ catalyst obtained under different conditions. The full width at half-maximum (FWHM) values of the lines are reported in parentheses.

Conditions	$Ni2p_{3/2}$/ eV	O1s/ eV	Ni/M_T
calcined at 500 °C[a]	854.5 (4.8)	529.1 (3.2)	0.38
after SRE at 650 °C	856.6 (4.9)	530.3/532.3 (4.0)	0.46

[a] The XPS parameters of the calcined $CeNi_1O_Y$ catalyst are from reference [34].

Table 4-5 Binding energies and surface Ni molar ratios of $Ni_XMg_2AlO_Y$ catalysts obtained under different conditions. The full width at half-maximum (FWHM) values of the lines are reported in parentheses.

Catalyst	Conditions	$Ni2p_{3/2}$/ eV	O1s/ eV	Ni/M_T
$Ni_3Mg_2AlO_Y$	dried without calcination	856.2 (3.3)	531.7 (2.8)	0.41
	calcined at 500 °C	855.7 (3.6)	530.6/531.7 (3.1)	0.31
	after SRE at 650 °C	856.5 (5.1)	531.7 (3.7)	0.33
$Ni_{12}Mg_2AlO_Y$	dried without calcination	856.2 (3.5)	531.7(2.8)	0.56
	calcined at 500 °C	855.6 (4.1)	530.6/531.7 (3.4)	0.60
	after SRE at 300 °C	856.5 (5.5)	531.7 (3.4)	0.51

4.9 Characterizations on carbonaceous species

It has been shown that Ce-Ni catalysts prepared by different methods have similar catalytic activities, but exhibit quite different catalytic stabilities (**Fig. 4-11**), which can be probably related to the different carbon species formed. Hence it can be helpful to analyze the carbon species formed to in turn provide information about the Ni-based catalysts, *i.e.*, catalytic activity and stability. In the following analysis, carbon species are manually separated from the spent catalysts without any further purification by acid because this procedure can influence the results.

4.9.1 TPO

Carbon species formed on Ni-based catalysts during SRE are analyzed by O_2-TPO; the spectra are shown in **Fig. 4-26** to **Fig. 4-28**. In the literature, the types of carbonaceous species can be identified by the numbers and position of TPO peaks associated with different reactivity towards oxidation.[38-40]

Primarily, there is no peak presented at the temperatures lower than 400 °C for all the carbon analyzed, which is assigned to the amorphous carbon that is highly reactive and easily oxidized from the nickel surface.[38,39]

It is widely reported that the single broad peak at around 600 °C is attributed to more graphitic filamentous carbon which is more stable and oxidizes at higher temperatures.[38,40] However, careful examinations allow observing some differences in the shape and position.

The oxidation peaks obtained on the 23-Ni/CeO_2-IMP and 22-Ni/CeO_2-IWI catalysts look quite similar; whereas the peak of the $CeNi_1O_Y$ catalyst appears broader and shifts towards lower temperatures (**Fig. 4-26**), showing a higher reactivity of carbon and the presence of the different types of carbon species. It can be predicted that some specific differences may exist in the carbon species formed on Ce-Ni catalysts, although all of them are roughly attributed to the filamentous carbon.

In the literature,[38,40] temperatures around 510 °C were assigned to the combustion of single walled carbon nanotubes (SWNTs), and temperatures around 610 °C to multiwalled carbon nanotubes (MWNTs). Carbon nanofibers (CNFs) were supposed to burn off at lower temperatures than SWNTs.[38]

A single broad and asymmetric oxidation peak is also obtained for $Ni_XMg_2AlO_Y$ catalysts (**Fig. 4-27**), which can be generally due to the mixtures of CNFs possibly with some CNTs.

Carbon species formed under highly diluted reactant mixture (EtOH: 1 mol% or 3 mol%) lead to a narrower and more symmetric single TPO peak at around 610 °C (**Fig. 4-28**), indicating that there might be relatively higher proportion of CNTs in the carbon materials formed. Besides there is a shift to higher temperature for the solid carbon formed at higher reaction temperature of 650 °C, moreover the peak exhibits more symmetric (**Fig. 4-28**).

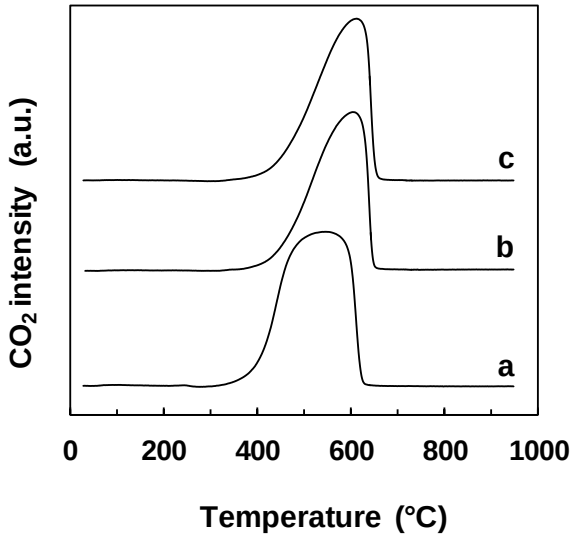

Fig. 4-26 TPO profiles of carbon formed on a) $CeNi_1O_Y$, b) 23-Ni/CeO_2-IMP, c) 22-Ni/CeO_2-IWI. (Catalyst: 50 mg; EtOH/H_2O/N_2 = 14/42/44; T_R = 450 °C; time: 5 h for CP, 1 h for IMP and IWI.)

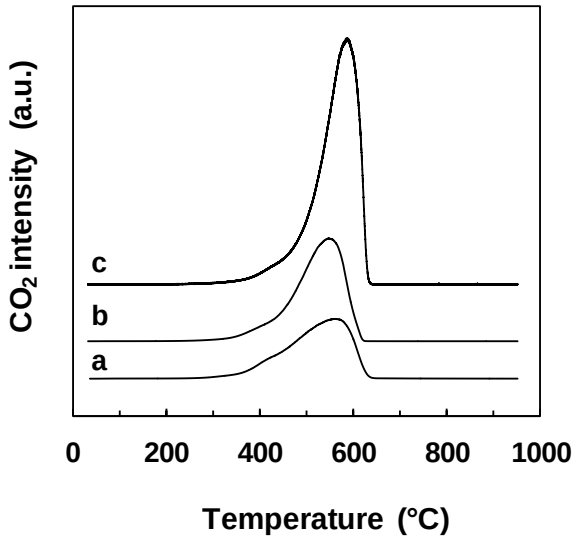

Fig. 4-27 TPO profiles of carbon formed on a) $Ni_1Mg_2AlO_Y$, b) $Ni_3Mg_2AlO_Y$, c) $Ni_{12}Mg_2AlO_Y$. (Catalyst: 50 mg; EtOH/H_2O/N_2 = 14/42/44; T_R = 450 °C; time: 5 h.)

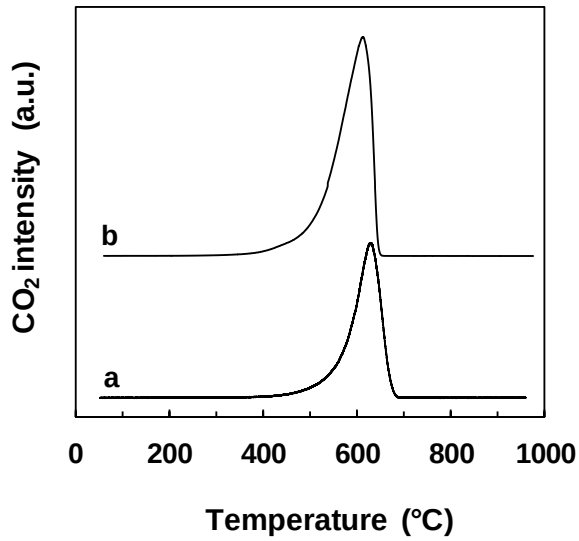

Fig. 4-28 TPO profiles of carbon formed on a) $Ni_3Mg_2AlO_Y$. (Catalyst: 50 mg; EtOH/H_2O/N_2 = 3/9/88; T_R = 650 °C; time: 10 h) b) $Ni_{12}Mg_2AlO_Y$. (Catalyst: 50 mg; EtOH/H_2O/N_2 = 1/3/96; T_R = 300 °C; time: 10 h.)

4.9.2 Raman

Raman spectroscopy has been shown to be an available and powerful technique for characterizing the structure of carbonaceous materials.[41,42] As displayed in **Fig. 4-29** to **Fig. 4-31**, two main peaks well known as the D-bond and G-bond are visible on all the carbon species analyzed. The D-bond observed between 1330 and 1346 cm^{-1} is ascribed to the vibration of the sp^3 hybridized carbon atom with the dangling bonds in the disordered carbonaceous species; while the G-bond observed between 1596 and 1600 is assigned to the stretching mode of the sp^2 hybridized carbon atom in the ordered graphite. The way to distinguish CNFs and CNTs was reported by comparison of the frequency shift, but only slight differences could be verified. The D-bond obtained at 1350 cm^{-1} was for CNFs and 1355 cm^{-1} for CNTs; while the G-bond was observed at 1592 cm^{-1} on CNFs and 1582 cm^{-1} on CNTs.[43]

The same type of Raman spectrum was observed on MWCNTs, and the degree of graphitization can be quantified by the intensity of the D to G bands.[44] Hence I_D/I_G is characteristic of the degree of ordered carbon materials. Lower I_D/I_G ratio suggests higher order degree of substances. It is of interest to find out that I_D/I_G ratios depend on both the Ni content and reaction conditions, following the order below: 1.08 ($Ni_{12}Mg_2AlO_Y$) > 1.00 ($CeNi_1O_Y$) > 0.99 ($Ni_3Mg_2AlO_Y$) > 0.95 ($Ni_3Mg_2AlO_Y$ in highly diluted conditions at 300 °C) > 0.91 ($Ni_1Mg_2AlO_Y$) > 0.82 ($Ni_3Mg_2AlO_Y$ in highly diluted conditions at 650 °C).

Generally lower I_D/I_G ratio is obtained on the catalyst with lower Ni content or on the catalyst tested under highly diluted reactant mixture. Besides reaction temperature also impacts the graphitization of carbon materials formed. The Raman results are in good agreement with the TPO analysis: the presence of G-bond and TPO peak at the high temperatures around 600 °C match well, proving the formation of the graphitic filamentous carbon on $CeNi_XO_Y$ and $Ni_XMg_2AlO_Y$ catalysts during the SRE reaction. As a matter of fact, such type of carbon filaments related to CNFs and/or CNTs can explain the catalytic stability of $CeNi_XO_Y$ catalysts for H_2 production from ethanol.[7,18]

The I_D/I_G ratios measured between 0.8 and 1.1 in our present studies, are comparable to the value obtained from ethanol decomposition over Fe-based catalysts.[44] G. Wang *et al.* recently proposed that H_2 and MWCNTs can be produced from ethanol decomposition at high temperature.[44] However, in this work, it is shown for the first time that similar results can be obtained but *via* the steam reforming process, *i.e.* in the presence of water. As observed

previously under decomposition conditions, the type of carbon species formed explained the good catalytic stability.

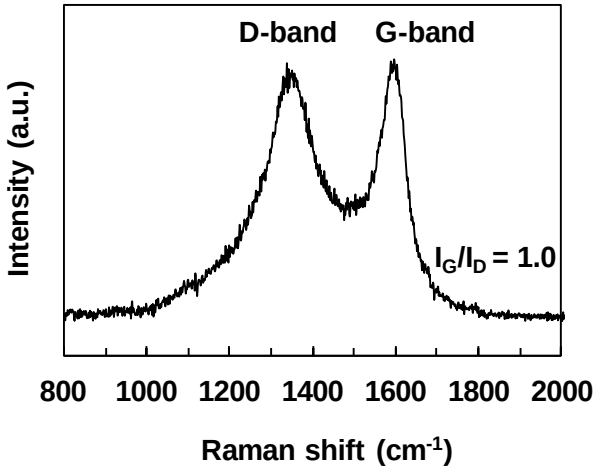

Fig. 4-29 Raman spectrum of carbon formed on the $CeNi_1O_Y$ catalyst. (Catalyst: 50 mg; $EtOH/H_2O/N_2$ = 14/42/44; T_R = 450 °C; time: 5 h.)

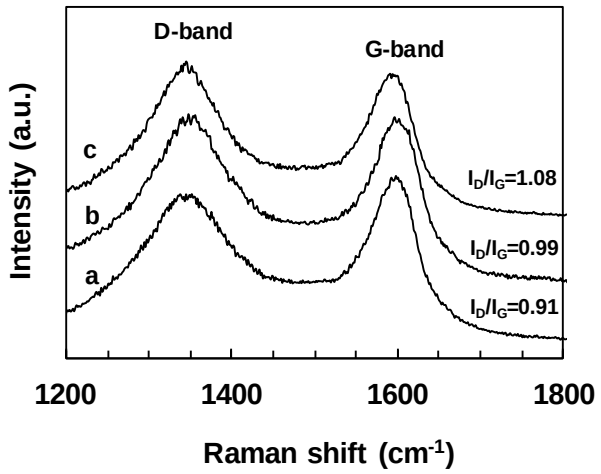

Fig. 4-30 Raman spectra of carbon formed on a) $Ni_1Mg_2AlO_Y$, b) $Ni_3Mg_2AlO_Y$, c) $Ni_{12}Mg_2AlO_Y$. (Catalyst: 50 mg; $EtOH/H_2O/N_2$ = 14/42/44; T_R = 450 °C; time: 5 h.)

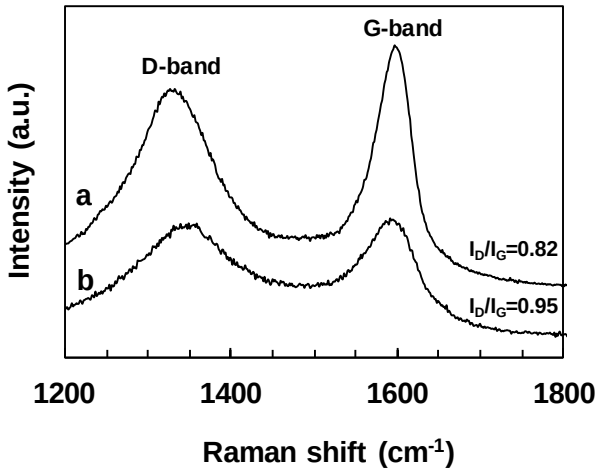

Fig. 4-31 Raman spectra of carbon formed on a) $Ni_3Mg_2AlO_Y$. (Catalyst: 50 mg; $EtOH/H_2O/N_2$ = 3/9/88; T_R = 650 °C; time: 10 h.) b) $Ni_{12}Mg_2AlO_Y$. (Catalyst: 50 mg; $EtOH/H_2O/N_2$ = 1/3/96; T_R = 300 °C; time: 10 h.)

4.9.3 TEM

As a complementary characterization to TPO and Raman, transmission electron microscopy (TEM) allows to directly observing the morphology of carbon species and the nickel particles on the spent catalysts. After SRE at 450 °C under high concentration reactant mixture

(EtOH/H_2O/N_2 = 14/42/44), the filamentous carbon is clearly seen on the $CeNi_1O_Y$ (**Fig. 4-32** (A)-(B)) $Ni_3Mg_2AlO_Y$ (**Fig. 4-33**) and $Ni_{12}Mg_2AlO_Y$ catalysts (**Fig. 4-34**), as examples. Some CNTs are also formed on $CeNi_1O_Y$ (**Fig. 4-32** (B)). The images confirm the TPO results. It was reported that carbon filaments were formed on Ni-Mg-Al catalysts after SRE at 600 °C although deactivation was not observed due to the formation of carbon nanofibres.[12] The present $CeNi_XO_Y$ and $Ni_XMg_2AlO_Y$ catalysts show good stability for SRE, which can be attributed to the formation of relatively homogeneous filamentous carbon.[45]

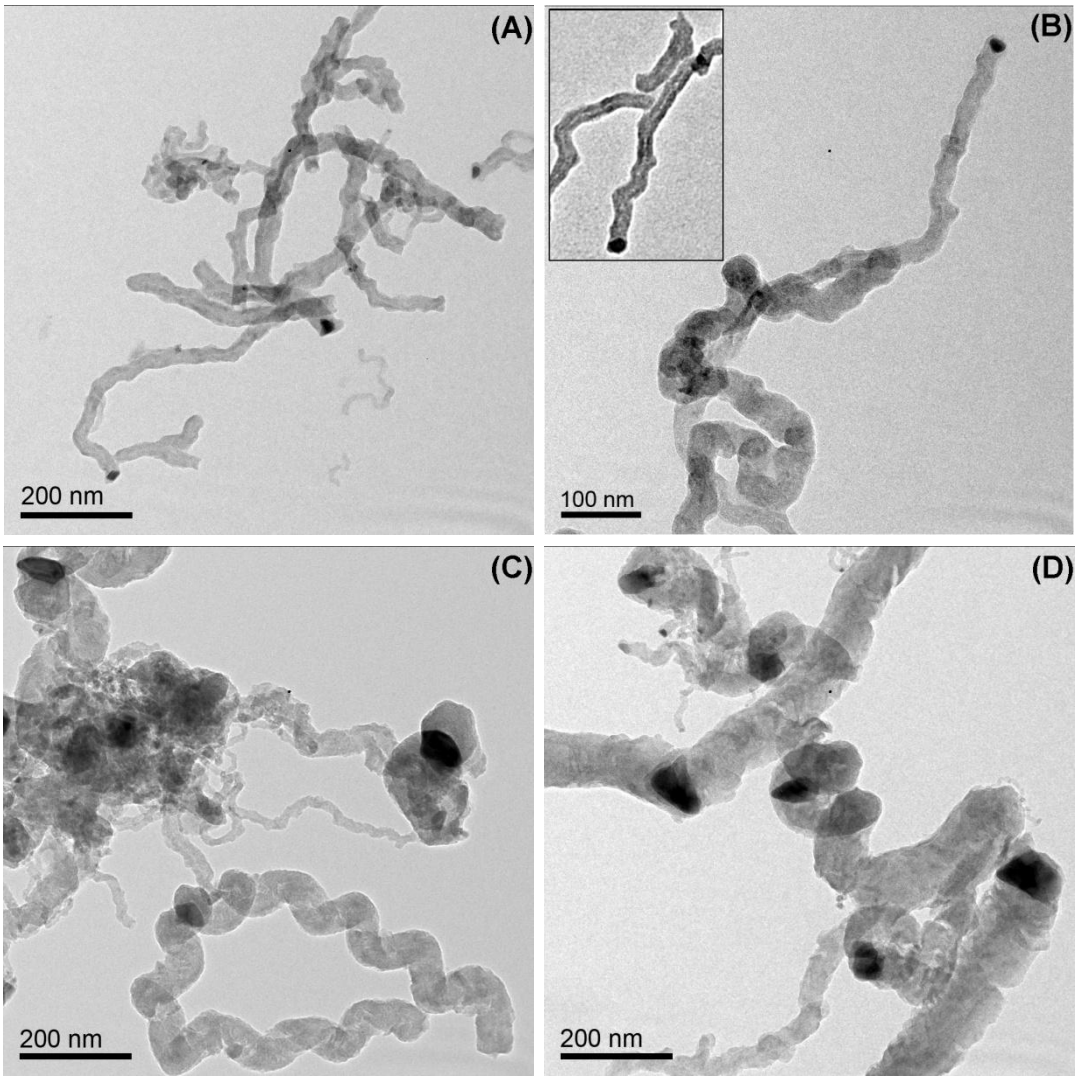

Fig. 4-32 TEM micrographs for the Ce-Ni catalysts prepared by different methods after SRE at 450 °C. (A) and (B) $CeNi_1O_Y$ with (B) a magnification of CNTs; (C) 23-Ni/CeO_2-IMP, (D) 22-Ni/CeO_2-IWI. Reaction conditions: catalyst: 50 mg; time: 5 h for CP, 1 h for IMP and IWI.

Another type of carbon filaments, specifically, the spiral carbon species are clearly found on the 23-Ni/CeO_2-IMP and 22-Ni/CeO_2-IWI catalysts after SRE at 450 °C (**Fig. 4-32** (C)-(D)). This

type of carbon exhibits quite different morphology and size from that grown on the $CeNi_1O_Y$ catalyst. The spiral carbon species present obvious disorder in size, from nano-scale to micro-scale.

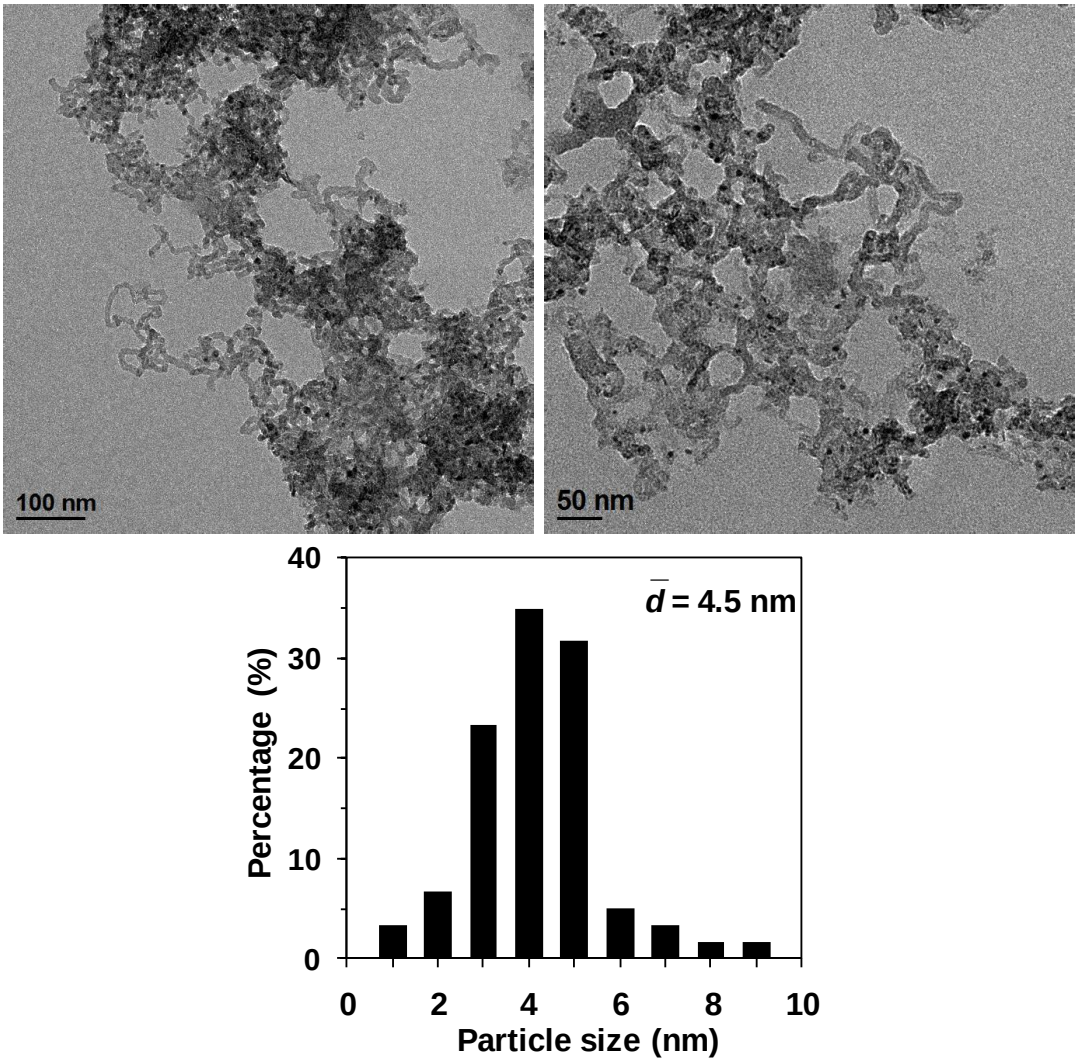

Fig. 4-33 TEM micrographs and corresponding nickel particle size distribution for the $Ni_3Mg_2AlO_Y$ catalyst after SRE at 450 °C. Reaction conditions: catalyst: 50 mg; $EtOH/H_2O/N_2$ = 14/42/44; time: 5 h.

After highly diluted SRE (EtOH: 1 mol% or 3 mol%), not only carbon filaments, but also some CNTs can be apparently examined (**Fig. 4-35** to **Fig. 4-37**). The structure of the carbon filaments are further analyzed by high resolution TEM. Graphitic structure is clearly presented and the filaments are composed of graphite sheets (**Fig. 4-37**). Most of the graphite sheets exhibit some degree of non-parallel, possibly due to an unequal diffusion of graphite sheets through nickel particles.[40] This result is in good agreement with the TPO (**Fig. 4-28**) and Raman (**Fig.**

4-31) results: the presence of the oxidation peak located at higher than 610 °C and the lower I_D/I_G ratio.

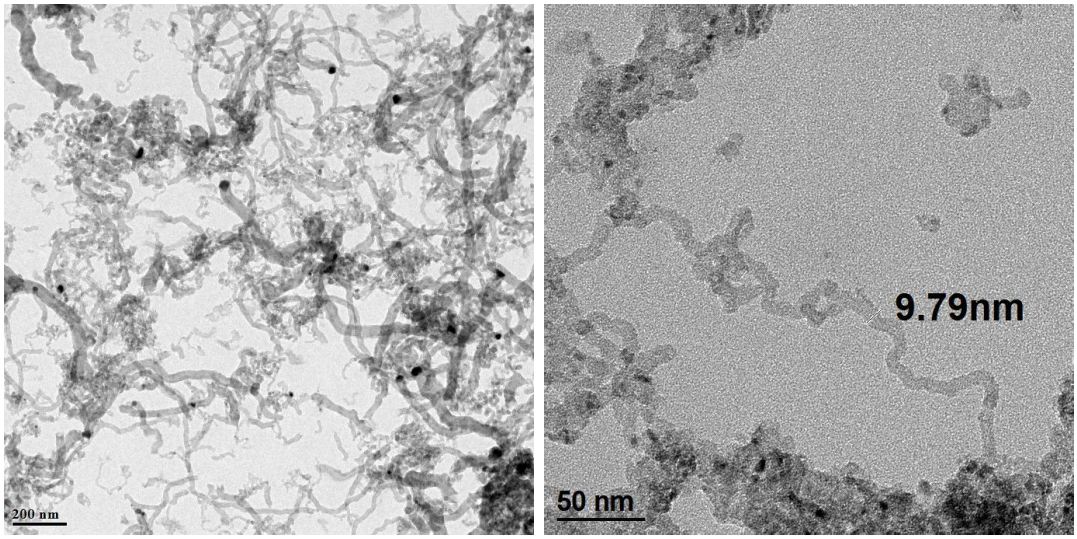

Fig. 4-34 TEM micrographs for the $Ni_{12}Mg_2AlO_Y$ catalyst after SRE at 450 °C. Reaction conditions: catalyst: 50 mg; $EtOH/H_2O/N_2$ = 14/42/44; time: 5 h.

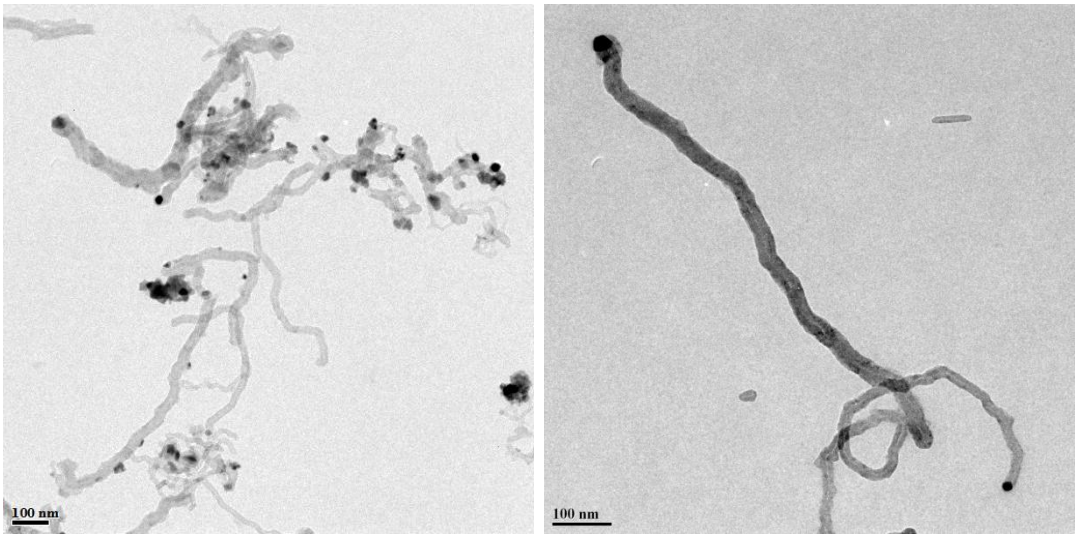

Fig. 4-35 TEM micrographs for the spent $CeNi_1O_Y$ catalyst. Reaction conditions: $EtOH/H_2O/N_2$ = 3/9/88. T_R = 650 °C; time: 10 h.

In addition, Ni nanoparticles are found to be fixed at the tip of the carbon filaments formed on the Ni-based catalysts prepared by CP method, as seen in **Fig. 4-32** (B), **Fig. 4-34** and **Fig. 4-35**, which was reported in the literature as a proof to the stable catalytic system.[24] On the contrary, big Ni particles (about 40 nm) are found to be blocked inside the spiral carbon species formed on 23-Ni/CeO_2-IMP and 22-Ni/CeO_2-IWI catalysts (**Fig. 4-32** (C)-(D)). As a matter of

fact, it has been demonstrated that the growth rates of the filamentous carbon increases with increasing the nickel particle size.[18,46]

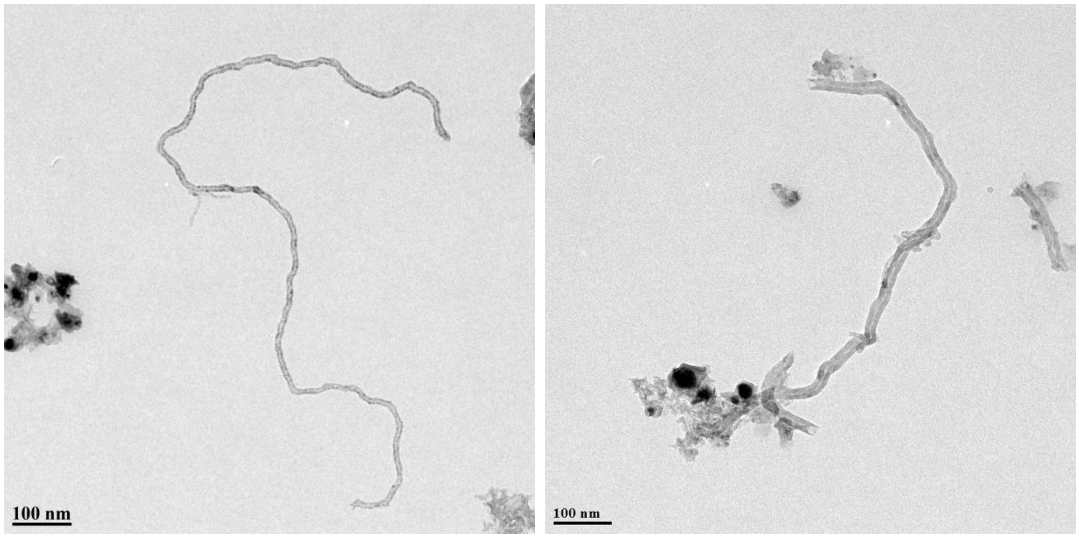

Fig. 4-36 TEM micrographs for the spent $Ni_3Mg_2AlO_Y$ catalyst. Reaction conditions: catalyst: 50 mg; $EtOH/H_2O/N_2$ = 3/9/88; T_R = 650 °C; time: 10 h.

Ni particles sizes are estimated from the spent catalysts. An average size of about 10 nm are estimated on the spent $CeNi_1O_Y$ catalyst (**Fig. 4-32** (A)-(B)), some very small sized Ni nanoparticles around 3 nm are also observed which is in good agreement with the presence of very small sized NiO nanoparticles on the fresh catalyst evidenced by XPS and the low-temperature TPR peak.[47] Whereas Ni particles of about 40 nm are estimated on the spent 23-Ni/CeO_2-IMP and 22-Ni/CeO_2-IWI catalysts (**Fig. 4-32** (C)-(D)). These values are very close to the sizes of NiO in the fresh catalysts measured by XRD (**Table 3-1**): $CeNi_1O_Y$ (11 nm), 23-Ni/CeO_2-IMP and 22-Ni/CeO_2-IWI (38 nm).

Ni nanoparticles on the spent $Ni_3Mg_2AlO_Y$ and $Ni_{12}Mg_2AlO_Y$ catalysts show narrow size distributions. The average particle size is estimated at 4.5 nm for $Ni_3Mg_2AlO_Y$ (**Fig. 4-33**), and 6.0 nm for $Ni_{12}Mg_2AlO_Y$ (**Fig. 4-37**). These values are close to NiO nanoparticles sizes ($Ni_3Mg_2AlO_Y$: 3.9 nm, $Ni_{12}Mg_2AlO_Y$: 5.0 nm) measured by XRD for the fresh compounds; and also very close to Ni nanoparticles sizes obtained after the *in situ* treatment in H_2 at 450 °C ($Ni_3Mg_2AlO_Y$: 4.0 nm, $Ni_{12}Mg_2AlO_Y$: 5.9 nm), suggesting almost no nickel sintering. Besides very small nickel nanoparticles no more than 2 nm are also observed by TEM, but which cannot be detected by XRD due to the detection limit.

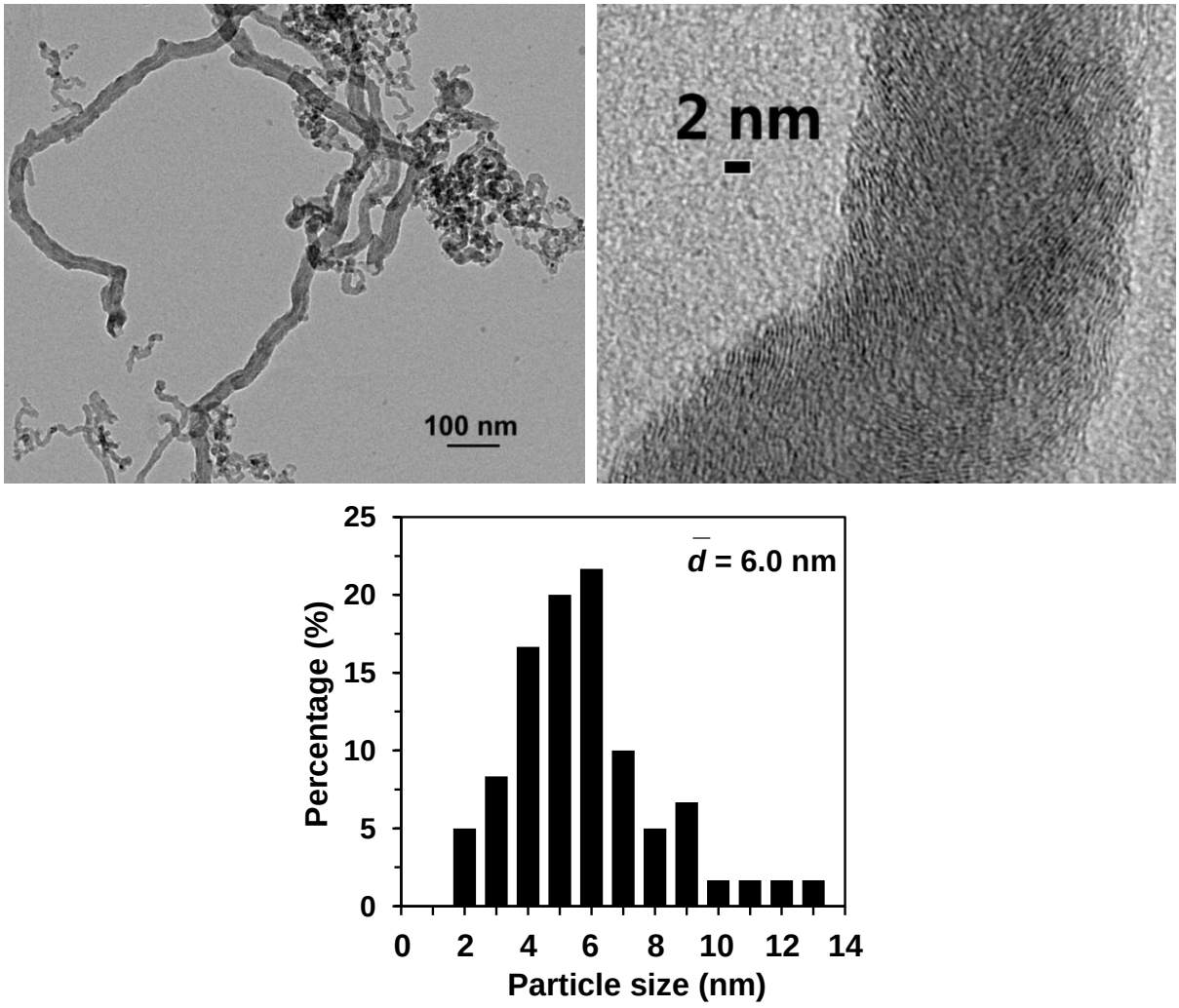

Fig. 4-37 TEM micrographs and corresponding nickel particle size distribution for the spent $Ni_{12}Mg_2AlO_Y$ catalyst. Reaction conditions: catalyst: 50 mg; $EtOH/H_2O/N_2$ = 1/3/96; T_R = 300 °C; time: 10 h.

The present $CeNi_XO_Y$ and $Ni_XMg_2AlO_Y$ catalytic systems show good stability probably due to the formation of relatively homogeneous filamentous carbon species and the location of Ni nanoparticles on the carbon filaments. The formed nanofibrous carbon materials can be regarded as an added value, as CNFs and CNTs are strategic materials in various fields, and in particular, they are very interesting catalyst support materials for various catalytic applications.

4.10 Conclusion

Two types of Ni-based catalysts, $CeNi_XO_Y$ and $Ni_XMg_2AlO_Y$, are studied for the steam reforming of ethanol (SRE, $H_2O/EtOH$ = 3). Many parameters are carefully analyzed by using high concentration of reactant mixture ($EtOH/H_2O/N_2$ = 14/42/44), including reaction

temperature, *in situ* activation in H_2, Ni content, preparation method effect, calcination effect, catalyst dilution effect, water partial pressure effect and ethanol concentration effect. Moreover, the efficiency of $CeNi_XO_Y$ and $Ni_XMg_2AlO_Y$ catalysts towards H_2 production are studied under highly diluted conditions (EtOH: 1 mol% or 3 mol%).

Reaction temperature influences ethanol conversion and products distribution. Conversion increases with reaction temperature and total conversion is obtained at 450 °C when the catalysts (50 mg) are *in situ* treated in H_2, *i.e.*, $CeNi_XO_Y$ at 250 °C, $Ni_XMg_2AlO_Y$ at 450 °C. The gas phase products (dry basis) are H_2 (about 50 mol%), CO_2 and CH_4, without the formation of CO. Solid carbon is formed after SRE at 450 °C. Undesirable products, such as acetaldehyde and acetone that can be produced from dehydrogenation and decomposition, are obtained when reaction temperature is lower than 350 °C. SRE is favored with high temperatures.

The activation in H_2 is evidenced as an important factor to influence the catalytic performance. The treatment temperature optimized for $CeNi_XO_Y$ catalysts with different Ni content is of about 250 °C which corresponds to the first TPR peak. It is attributed to the reduction of very active Ni species being able to be reduced and reoxidized easily and reversibly in $CeNi_XO_Y$ compounds. When treatment temperature is higher than 300 °C, conversion decreases. The optimum treatment temperature for $Ni_XMg_2AlO_Y$ catalysts can be different which depends on the Ni content as it has been shown that TPR peak shifts to low temperature with higher Ni content. Treatment temperature influence is analyzed between 160 °C and 700 °C, the optimum temperature can be proposed at 450 °C taking into account ethanol conversion, products distribution and carbon formed. A big amount of solid carbon is produced when $Ni_XMg_2AlO_Y$ compound is treated in H_2 at a temperature higher than 550 °C.

Ni content strongly affects ethanol conversion and products distribution. Conversion globally increases with Ni content, and total conversion is obtained at 450 °C over $CeNi_XO_Y$ catalysts (treated in H_2 at 250 °C) when $Ni/M_T \geqslant 0.5$ ($Ni/M_T = x/(1+x)$), and over $Ni_XMg_2AlO_Y$ catalysts (treated in H_2 at 450 °C) when $Ni/M_T \geqslant 0.8$ ($Ni/M_T = x/(3+x)$). H_2 formation maintains around 50 mol% when $Ni/M_T \geqslant 0.5$, while CO_2 and CH_4 globally increase with Ni content. Acetaldehyde declines to zero when $Ni/M_T \geqslant 0.5$, while CO presents a maximum at $Ni/M_T = 0.5$. Ethylene and acetone are obtained over the catalysts with low Ni content ($Ni/M_T \leqslant 0.24$), whereas solid carbon starts to generate when $Ni/M_T \geqslant 0.24$ and increases with Ni content.

The influence of preparation method is studied on Ce-Ni catalysts prepared by different methods, namely, co-precipitation, impregnation and incipient wetness impregnation method. It is shown that Ce-Ni catalysts prepared by different methods but with similar Ni loading exhibit relatively similar catalytic activity, but exhibit quite different catalytic stability. $CeNi_XO_Y$ mixed oxides show much better stability than the other two types of Ni/CeO_2 catalysts, which is ascribed to the large surface area and small NiO and CeO_2 nanoparticles obtained by the co-precipitation method. Besides, the small and homogeneous graphitic filamentous carbon species formed on $CeNi_XO_Y$ catalyst contribute to the catalytic stability.

The calcination effect and catalyst dilution effect (by SiC) are analyzed on $CeNi_XO_Y$ compounds, the results show no apparent influence of these two parameters on the ethanol conversion and products distribution. Therefore the Ni-based catalysts studied in the present thesis are calcined at 500 °C, and SRE is performed without the presence of SiC in order to analyze the catalyst without the influence of the diluents and be able to conveniently analyze the catalysts after test.

The present $CeNi_XO_Y$ and $Ni_XMg_2AlO_Y$ mixed oxides are reported as highly active and efficient catalysts for H_2 production from SRE. The $Ni_{12}Mg_2AlO_Y$ catalyst (treated in H_2 at 450 °C) allows obtaining CO-free H_2 production of 3 mol mol_{EtOH}^{-1} ($EtOH/H_2O/N_2$ = 1/3/96) at 300 °C. The $Ni_3Mg_2AlO_Y$ (treated in H_2 at 450 °C) and $CeNi_1O_Y$ (treated in H_2 at 250 °C) catalysts are able to completely convert ethanol at 450 °C to produce CO-free H_2 of about 3 mol mol_{EtOH}^{-1} even with higher ethanol concentration ($EtOH/H_2O/N_2$ = 3/9/88). A very high H_2 production of about 5 mol mol_{EtOH}^{-1} is reported at 650 °C.

The high activity to ethanol and the high selectivity to hydrogen of the present $CeNi_XO_Y$ and $Ni_XMg_2AlO_Y$ catalysts are closely related to their physicochemical properties. The simple co-precipitation method allows producing $CeNi_XO_Y$ and $Ni_XMg_2AlO_Y$ mixed oxides with large surface areas, and with small nanoparticles of NiO, CeO_2, and/or Ni-Mg-(Al)-O. Once treated in H_2 ($CeNi_XO_Y$: 250 °C, $Ni_XMg_2AlO_Y$: 450 °C), the very active Ni species either in the solid solution of Ce-Ni and Ni-Mg-(Al)-O and/or at the interface of small nanoparticles of NiO, CeO_2, or Ni-Mg-(Al)-O, can be easily reduced and reoxidized due to the strong interactions between Ni species and other cations (Ce^{4+}, Mg^{2+} and Al^{3+}). XRD shows the $Ni_XMg_2AlO_Y$ catalysts after SRE present all the oxidized phases related to NiO, MgO and $NiMgO_2$, and the phase of Ni^0 species. The crystallite sizes of NiO and/or $NiMgO_2$ are very close to the values obtained in the

fresh catalyst (calcined at 500 °C), and the average nanoparticles size of Ni^0 is also very close to the value measured from the compounds treated in H_2 at 450 °C. Clearly the Ni species are the active phase, however the other cations in presence have also an influence on the catalytic results.

4.11 Experimental

4.11.1 Catalytic reaction

The catalytic performances were conducted under atmospheric pressure in a fixed-bed flow quartz reactor (inner diameter: 8 mm or 4 mm). Heating of the reactor was provided by a programmable oven. The catalyst (50 mg by default, or 200 mg, or 8 mg) was previously *in situ* treated in H_2 for 10 h. The treatment temperature for Ce-Ni catalysts is 250 °C by default, and for $Ni_XMg_2AlO_Y$ catalyst is 450 °C by default. The water-ethanol mixture with a stoichiometric molar ratio of 3 was injected into a heating chamber by HPLC pump, and then the steam was fed into the reactor by N_2 as carrier with a total flow rate of 60 mL min^{-1}. In most of the cases, the catalytic reaction was performed under concentrated conditions by default: $EtOH/H_2O/N_2$ = 14/42/44; besides, diluted conditions: $EtOH/H_2O/N_2$ = 3/9/88 or $EtOH/H_2O/N_2$ = 1/3/96 are also involved when reporting H_2 yield (mol mol_{EtOH}^{-1}). The feed and product outlet gases were analyzed online by the gas chromatography (TRACE GC ULTRA) equipped with the thermal-conductivity detector (TCD) and the flame ionization detector (FID).

Catalytic performances were reported after 5 h of reaction based on ethanol conversion (X_{EtOH}), products molar composition (C_i) and hydrogen yield (Y_{H2}), which were calculated by the following equations (**Eq. 4-8** to **Eq. 4-10**).

$$X_{EtOH} = \frac{n_{EtOH,in} - n_{EtOH,out}}{n_{EtOH,in}} \times 100\% \qquad \textbf{Eq. 4-8}$$

where $n_{EtOH,in/out}$ is the molar flow rate of ethanol at the inlet/outlet of the reactor, respectively.

$$C_i = \frac{n_i}{\sum_{products} n_i} \times 100\% \qquad \textbf{Eq. 4-9}$$

where n_i represents the molar flow rate of product *i* at the outlet of the reactor.

$$Y_{H_2} = \frac{n_{H_2}}{n_{EtOH,in} X_{C_2H_5OH}} \leq 6 \qquad \textbf{Eq. 4-10}$$

where a yield of 6 is equivalent to 100% in theory.

4.11.2 Carbon characterizations

O_2-TPO. Temperature-programmed oxidation was performed on a Micromeritics Autochem 2920 analyzer. The sample was treated in the 5 vol% O_2-95 vol% He mixture with a flow rate of 50 mL min^{-1}. The temperature was increased to 1000 °C at a heating rate of 5 °C min^{-1}. The desorption species from the sample were traced by an OmniStar GSD 300 O mass spectrometer.

Raman. Raman spectra were acquired on a Labram Infinity HORIBA JOBIN YVON Raman spectrometer using a visible laser with an output laser power of λ = 532 nm at room temperature.

TEM. Transmission electron microscopy images were obtained by a Philips CM30 transmission electron microscope at an acceleration voltage of 300 kV, and a FEI Tecnai G2 20 transmission electron microscope at an acceleration voltage of 200 kV. The sample was previously ultrasonically dispersed in acetone, and then drops of the suspension were applied onto a copper grid-supported transparent carbon film.

4.12 References

[1] E. Y. García and M. A. Laborde, *Int. J. Hydrogen Energy*, 1991, **16**, 307.

[2] M. Ni, D. Y. C. Leung and M. K. H. Leung, *Int. J. Hydrogen Energy*, 2007, **32**, 3238.

[3] D. Z. Mezalira, L. D. Probst, S. Pronier, Y. Batonneau and C. Batiot-Dupeyrat, *J. Mol. Catal. A: Chem.* 2011, **340**, 15.

[4] G. Wang, H. Wang, W. Li and J. Bai, *RSC Adv.*, 2011, **1**, 1585.

[5] L. Jalowiecki-Duhamel, C. Pirez, M. Capron, F. Dumeignil and E. Payen, *Catal. Today*, 2010, **157**, 456.

[6] L. Jalowiecki-Duhamel, C. Pirez, M. Capron, F. Dumeignil and E. Payen, *Int. J. Hydrogen Energy*, 2010, **35**, 12741.

[7] C. Pirez, M. Capron, H. Jobic, F. Dumeignil and L. Jalowiecki-Duhamel, *Angew. Chem. Int. Ed*, 2011, **50**, 10193.

[8] J. A. Farmer and C. T. Campbell, *Science*, 2010, **329**, 933.

[9] A. F. Lucrédio, J. D. A. Bellido and E. M. Assaf, *Appl. Catal. A*, 2010, **388**, 77.

[10] C. Resini, T. Montanari, L. Barattini, G. Ramis, G. Busca, S. Presto, P. Riani, R. Marazza, M. Sisani, F. Marmottini and U. Costantino, *Appl. Catal. A*, 2009, **355**, 83.

[11] M. Li, X. Wang, S. Li, S. Wang and X. Ma, *Int. J. Hydrogen Energy*, 2012, **35**, 6699.

[12] A .J . Vizcaíno, M. Lindo, A. Carrero and J. A. Calles, *Int. J. Hydrogen Energy*, 2012, **37**, 1985.

[13] D.P. Debecker, E.M. Gaigneaux and G. Busca, *Chem. Eur. J.*, 2009, **15**, 3920.

[14] L. He, J. M. S. Parra, E. A. Blekkan and D. Chen, *Energy Environ. Sci.*, 2010, **3**, 1046.

[15] J. Fermoso, F. Rubiera and D. Chen, *Energy Environ. Sci.*, 2012, **5**, 6358.

[16] G. Pan, Z. Ni, F. Cao and X. Li, *Applied Clay Science*, 2012, **58**, 108.

[17] Q. Wang, W. Ren, X. Yuan, R. Mu, Z. Song and X. Wang, *Int. J. Hydrogen Energy*, 2012, **37**, 11488.

[18] G. Zeng, Q. Liu, R. Gu, L. Zhang and Y. Li, *Catal. Today*, 2011, **178**, 206.

[19] X.-P. Yu, W. Chu, N. Wang, F. Ma, *Catal. Lett.*, 2011, **141**, 1228.

[20] J. Rass-Hansen, R. Johansson, M. Moller and C. H. Christensen, *Int. J. Hydrogen Energy*, 2008, **33**, 4547.

[21] N. Bion, D. Duprez and F. Epron, *ChemSusChem*, 2012, **5**, 76.

[22] I. Fishtik, A. Alexander, R. Datta and D. Geana, *Int. J. Hydrogen Energy*, 2000, **25**, 31.

[23] C. Pirez, *Thèse*, Univ. Lille 1, décembre 2010.

[24] L. J. I. Coleman, W. Epling, R. R. Hudgins, and E. Croiset, *Appl. Catal. A*, 2009, **363**, 52

[25] M. Contestabile, G. J. Offer, R. Slade, F. Jaeger and M. Thoennes, *Energy Environ. Sci.*, 2011, **4**, 3754.

[26] J. C. Ruiz-Morales, D. Marrero-Lopez, J. Canales-Vazquez and J. T. S. Irvine, *RSC Adv.*, 2011, **1**, 1403.

[27] P. Ciambelli, V. Palma and A. Ruggiero, *Appl. Catal. B*, 2010, **96**, 18.

[28] P. Ciambelli, V. Palma and A. Ruggiero, *Appl. Catal. B*, 2010, **96**, 190.

[29] L. Chen, C. K. S. Choong, Z. Zhong, L. Huang, T. P. Ang, L. Hong and J. Lin, *J. Catal.*, 2010, **276**, 197.

[30] L. Huang, C. Choong, L. Chen, Z. Wang, Z. Zhong, C. Campos-Cuerva and J. Lin, *ChemCatChem*, 2013, **5**, 220.

[31] S. Li, C. Zhang, Z. Huang, G. Wu and J. Gong, *Chem. Commun.*, 2013, DOI: 10.1039/c2cc37109j.

[32] M. Pozzo, G. Carlini, R. Rosei and D. Alfe, *The Journal of Chemical Physics*, 2007, **126**, 164706.

[33] S. Nave and B. Jackson, *The Journal of Chemical Physics*, 2009, **130**, 054701.

[34] A. Ponchel, A. Huysser, C. Lamonier and L. Jalowiecki-Duhamel, *Phys. Chem. Chem. Phys.*, 2000, **2**, 303.

[35] M. C. Biesinger, B. P. Payne, L. W. M. Lau, A. Gerson and R. St. C. Smart, *Surf. Interface Anal.*, 2009, **41**, 324.

[36] B. P. Payne, M. C. Biesinger and N. S. McIntyre, *J. Electron. Spectrosc. Relat. Phenom.*, 2009, **175**, 55.

[37] B. P. Payne, M. C. Biesinger and N. S. McIntyre, *J. Electron. Spectrosc. Relat. Phenom.*, 2012, **185**, 159.

[38] A. W. Musumeci, G. G. Silva, W. N. Martens, E. R. Waclawik and R. L. Frost. *J. Therm. Anal. Calorim.*, 2007, **88**, 885.

[39] S. Natesakhawat, R. B. Watson, X. Wang and U. S. Ozkan, *J. Catal.*, 2005, **234**, 496.

[40] P. Wang, E. Tanabe, K. Ito, J. Jia, H. Morioka, T. Shishido and K. Takehira, *Appl. Catal. A*, 2002, **231**, 35.

[41] A. Carrero, J.A. Calles and A.J. Vizcaíno, *Chem. Eng. J.*, 2010, **163**, 395.

[42] G. Wang, H. Wang, Z. Tang, W. Li and J. Bai, *Appl. Catal. B*, 2009, **88**, 142.

[43] Y. Liu, C. Pan and J. Wang, *J. Materials Science*, 2004, **39**, 1091.

[44] G. Wang , H. Wang , W. Li, Z. Ren , J. Bai and J. Bai, *Fuel Processing Technology*, 2011, **92**, 531.

[45] A. L. Alberton, M. M. V. M Souza and M. Schmal, *Catal. Today*, 2007, **123**, 257.

[46] A. Carrero, J.A. Calles, and A.J. Vizcaíno, *Chem. Eng. J.*, 2010, **163**, 395.

[47] L. Jalowiecki-Duhamel, H. Zarrou, and A. D'Huysser, *Int. J. Hydrogen Energy*, 2008, **33**, 5527.

5 Oxidative steam reforming of ethanol on Ni-based catalysts

The steam reforming of ethanol (SRE) is the dominant thermo-chemical technology to transform ethanol to H_2 production. However, as a matter of fact, the strongly endothermic SRE reaction is not thermodynamically favorable at low temperatures (**Eq. 5-1**), and essentially requires an extra energy input.[1,2] Such high temperature operations ($\geqslant$ 650 °C) not only consume plenty of energy, but also bring inconvenience to the application of hydrogen to fuel cells.[3,4] On the other hand, the energy needed can be supplied by adding some O_2 or air into the feed. This idea enables the exothermic partial oxidation of ethanol (POE, **Eq. 5-2**) to thermodynamically take place at low temperatures,[5,6] during which a portion of ethanol is burned to offer the required energy so as to simultaneously achieve the SRE reaction (**Eq. 5-1**).[7,8]

$$C_2H_5OH + 3\ H_2O \rightarrow 6\ H_2 + 2\ CO_2\ \Delta H^0_{298K} = 174\ KJ\ mol^{-1} \qquad \textbf{Eq. 5-1}$$

$$C_2H_5OH + 1.5\ O_2 \rightarrow 3\ H_2 + 2\ CO_2\ \Delta H^0_{298K} = -545\ KJ\ mol^{-1} \qquad \textbf{Eq. 5-2}$$

In such a context, a technology combined with the SRE and POE processes, generally called the oxidative steam reforming of ethanol (OSRE), would be very promising for the on board H_2 production, that is, for the mobile applications that call for the high hydrogen selectivity and rapid response. Moreover, the OSRE reaction could reduce the carbon deposition owing to that the addition of O_2 into the feed allows to eliminating carbon on catalyst particles.[9]

The OSRE reaction is mainly studied in the catalytic fixed-bed reactors[10-14] or the micro-channel membrane reactors.[15-17] The crucial factor is the development of highly efficient, stable and low-cost catalysts, that is, the design of the appropriate active sites which fulfill the above features of the OSRE reaction, especially the design of the non-noble metal catalysts.

Up to date, some metal catalysts fixed-bed systems have been reported for the auto-thermal reforming of ethanol, more generally the OSRE reaction, including the oxide-supported active metal catalysts[10,11,14,18] and the Ni-, Co-, Cu-based mixed oxides.[13,19-21] There is no doubt that the Ni-based catalyst is the most attractive because of its good activity in the cleavage of the C-C and C-H bonds.[2,12] However, the drawback of these above systems is still reflected in the thermal management. An ideal OSRE process desires to develop a catalyst working at low

temperatures in order to build long life and safe reformers which can be employed for the portable applications.[22,23]

Recently, in our laboratory, a novel route for the room temperature H_2 production from ethanol over $CeNiH_ZO_Y$ nano-oxyhydride catalyst has been reported.[12] This promising technology can dramatically save energy by means of a smart combination of the strong exothermic reaction between the hydride species in the catalyst and O_2 (chemical energy) and the exothermic reaction between ethanol and O_2 (POE). The $CeNiH_ZO_Y$ nano-oxyhydride catalyst turns out to be able to simultaneously activate ethanol, produce hydrogen at room temperature, and provide hydride species to sustain the chemical reaction with O_2, which can be considered as a quite remarkable advance in the field.

As an important factor, the influence of O_2/EtOH was reported in a previous publication.[12] The OSRE reaction on the $CeNiH_ZO_Y$ catalyst (Ni: 20 wt%) was studied as a function of O_2/EtOH ratio from 0.5 to 2.5. Addition of O_2 concentration leads to an increase in ethanol conversion while H_2 molar fraction remains nearly constant up to an O_2/EtOH = 1.2. For higher ratios, H_2 formation slightly decreases. Acetaldehyde, CO and CH_4 formation globally decrease with higher O_2 concentration.[12] Therefore the present studies are performed by using the optimized O_2/EtOH ratio at 1.6.

In our laboratory, $CeNi_XO_Y$ nano-compounds have been studied in the SRE reaction due to the strong interactions existing between the nickel and cerium species inside the solid.[2,12,24-26] As a fluorite-type oxide, CeO_2 has been applied to various reactions so as to take advantages of its oxygen storage capacity and/or oxygen diffusion property. The release and uptake of oxygen by CeO_2 allow it to participate in the redox reactions, and the enhancement of the formation of oxygen vacancies attributed to the reduction of cerium cations has been shown to be of importance for catalytic activity.[27] A redox process among Ce^{4+}, Ce^{3+}, Ni^0 and Ni^{2+} species has been proposed.[28 - 31] As a consequence, the active nickel species in the $CeNi_XO_Y$ nano-compounds are characteristically and easily reduced and reoxidized owing to their close interactions with the cerium species.

On the other hand, $Ni_XMg_2AlO_Y$ mixed oxides have been shown to be highly active and efficient catalysts for H_2 production from ethanol steam reforming. The simple co-precipitation method leads to obtaining the mixed oxide with high proportion of very active small NiO and/or

Ni-Mg-(Al)-O nanoparticles which present the characteristic of being able to be easily reduced and reoxidized.

It can be expected that not only the $CeNiH_ZO_Y$ (Ni loading: 20 wt%) nano-oxyhydride catalyst, but also the family of $CeNi_XH_ZO_Y$ oxyhydrides and probably $Ni_XMg_2AlH_ZO_Y$ oxyhydrides could exhibit catalytic activity in the OSRE reaction certainly depending on the Ni content. Furthermore, the $CeNi_XH_ZO_Y$ oxyhydrides with various Ni contents have different hydrogen storage capacities in terms of hydride species[28,29] which are strongly associated with the chemical energy (O_2) consumed to sustain the OSRE reaction at room temperature. For this reason, the effect of Ni content is likely to bring about interesting catalytic behaviors for the OSRE reaction. Concerning the $Ni_XMg_2AlH_ZO_Y$ oxyhydrides, it has been shown by INS experiment in the present study in Chapter 3 that these compounds can be generated after treatment in temperature in H_2. Moreover, the concentration of hydrogen species inserted into the solid during the treatment in H_2 depends also on the Ni content.

Herein, in this chapter, the $CeNi_XH_ZO_Y$ oxyhydrides and $Ni_XMg_2AlH_ZO_Y$ oxyhydrides are reported as highly efficient and stable catalysts for H_2 production from ethanol at room temperature. The unique reaction phenomenon (huge variation of temperatures between the catalytic bed and the oven) is deeply demonstrated in the present study. The correlations among the catalyst properties, the catalytic performances and the characterizations are discussed to better understand this new technology.

5.1 Several examples of Ni-based nano-oxyhydride catalysts for H_2 production from OSRE at room temperature

5.1.1 The $CeNi_1H_ZO_Y$ nano-oxyhydride catalyst

Following an *in situ* treatment of $CeNi_XO_Y$ nano-compounds in H_2 at 250 °C, the active $CeNi_XH_ZO_Y$ nano-oxyhydride catalysts obtained are studied for H_2 production from ethanol in the presence of water and oxygen. The reactant mixture with a molar composition of $H_2O/EtOH/O_2/N_2$ = 3/1/1.6/1.3 are introduced into the reactor in a specific order. The reaction can be activated at some certain temperature, from which the temperature of the catalytic bed ($T_{Cat.}$) rapidly increases until it does not rise any more within a few minutes. The initial and final temperatures in such an activation phenomenon are recorded as $T_{Ini.}$ and $T_{Fin.}$. At the same

moment, the heating supply can be lowered to nearly room temperature, and the variation of reaction temperature between the catalytic bed and the oven ($\Delta T_R = T_{Cat.}$-T_{Oven}) is precisely measured when the catalytic system maintains stable.

Fig. 5-1 shows the ethanol conversion and the gas phase products distribution in the OSRE reaction over the $CeNi_1H_ZO_Y$ (Ni loading: 24 wt%) catalyst, as an example. Full ethanol conversion is achieved, accompanied with the H_2 formation of about 45% (in mol.) relative to all the gas phase products (dry basis). The other products analyzed are mainly CO_2 (41%) and CO (12%); small amounts of CH_4 and CH_3CHO are also detected. To the best of our knowledge, this is still the best result that has been ever reported for a low-cost catalyst.

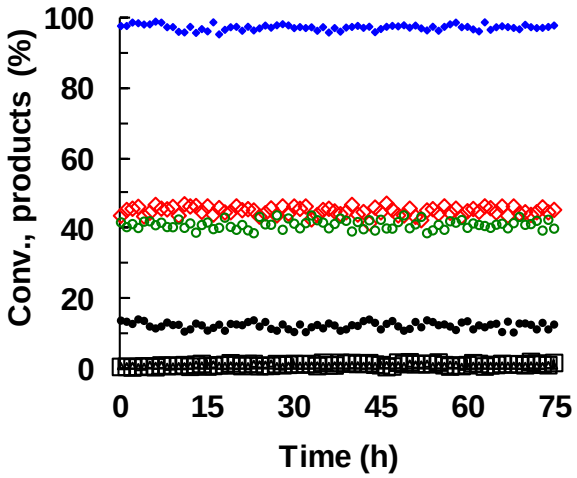

Fig. 5-1 Ethanol conversion and products distribution in OSRE over the $CeNi_1H_ZO_Y$ catalyst. Ethanol conversion (◆), H_2 (◇), CO_2 (○), CO (●), CH_4 (▲) and CH_3CHO (□). Reaction conditions: catalyst: 30 mg; $H_2O/EtOH/O_2/N_2$ = 3/1/1.6/1.3; T_{Oven} = 60 °C; $T_{Cat.}$ = 345 °C.

The reaction temperature ($T_{Cat.}$) is measured at 345 °C, whereas the oven temperature stays at only 60 °C, pretty much lower than what is required. The energy released from the reaction between the hydride species stored in the oxyhydride catalyst and O_2 (chemical energy), and from the exothermic POE reaction, is smartly combined to provide the power necessary to convert ethanol and produce hydrogen. Thereby, only a little extra energy is needed to maintain the reaction. The $CeNi_1H_ZO_Y$ catalyst exhibits remarkable stability after 75 h of reaction, even if a small quantity of carbon species with a formation rate of 28 mg h^{-1} g_{cat}^{-1} is found after the reaction. It must be noted that the carbon formation is not linear as a function of time, but it decreases, this will be discussed later on. A stable activity in SRE reaction over such type of catalyst was attributed to the relatively homogeneous filamentous carbon species produced.[26]

In our previous publication, under the same OSRE conditions, a very high and stable conversion of nearly 100% has been already reported with the main gas phase products of H_2 (44%), CO_2 (31%) and CO (21%) accompanied with about 1 % of CH_4 and 3% of acetaldehyde.[12] In the present study, the products distribution is improved, which can be probably due to (i) a higher Ni content of 24 wt% and (ii) a larger variation of reaction temperature (ΔT_R). Instead of $T_{Cat.}$ of 280 °C obtained previously, a higher $T_{Cat.}$ of 345 °C is observed here. The carbon formation is also diminished compared to the former rate of 63 mg h^{-1} g_{cat}^{-1}. CO formation is also found to decrease, while CO_2 formation increases.

5.1.2 The $Ni_3Mg_2AlH_ZO_Y$ nano-oxyhydride catalyst

As Ni-based ternary mixed oxides, $Ni_XMg_2AlO_Y$ nano-compounds are also expected to be able to support a sustainable H_2 production at room temperature from ethanol by using the same technology. As a matter of fact, in has been shown in Chapter 3 that hydrogen species can be inserted during a treatment in H_2 at 450 °C, in particular when x = 3 and x = 12 (**Fig. 3-29**). The $Ni_XMg_2AlH_ZO_Y$ nano-oxyhydride catalysts are obtained in the similar way by *in situ* treating $Ni_XMg_2AlO_Y$ nano-compounds in H_2 at 450 °C. The treatment temperature plays an important role in achieving such a process. Unlike $CeNi_XO_Y$ nano-compounds, $Ni_XMg_2AlO_Y$ mixed oxides could require different treatment temperatures depending on the Ni content. In fact, it has been reported in Chapter 3 that $Ni_XMg_2AlO_Y$ mixed oxides exhibit different reducibility mainly due to the different Ni loadings (**Fig. 3-14**). The treatment temperature can be optimized for each compound; however, in order to easily compare the catalytic performances of a series of $Ni_XMg_2AlO_Y$ catalysts, the treatment temperature has been fixed at 450 °C in the present study. Following the same reaction procedure, similar activation phenomenon is observed on the $Ni_XMg_2AlH_ZO_Y$ nano-oxyhydride catalysts for OSRE. All the temperatures involved in the reaction process are recorded.

Fig. 5-2 reports the time course of the $Ni_3Mg_2AlH_ZO_Y$ catalyst for OSRE as an example. The significant variation of temperature between the catalyst bed and the oven also are found in this catalytic system, which is mainly attributed to the energy released from the strong exothermic reaction between the hydride species stored in the $Ni_3Mg_2AlH_ZO_Y$ oxyhydride catalyst with O_2, as well as the exothermic POE reaction. The reaction temperature is recorded at about 250 °C, whereas the oven temperature is at only 60 °C.

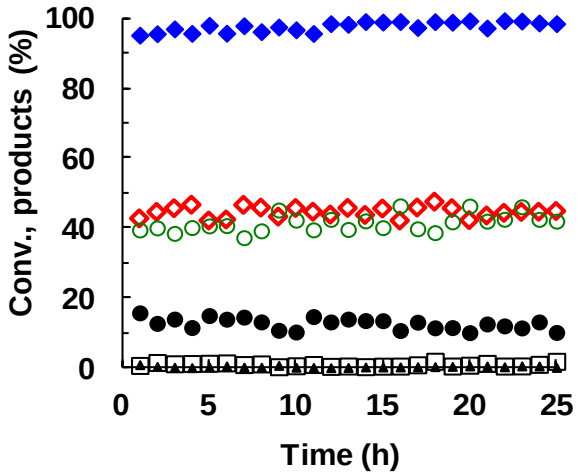

Fig. 5-2 Time course for OSRE on the $Ni_3Mg_2AlH_ZO_Y$ catalyst. Ethanol conversion (◆), H_2 (◇), CO_2 (○), CO (●), CH_4 (▲) and CH_3CHO (□). Reaction conditions: catalyst: 30 mg; $H_2O/EtOH/O_2/N_2$ = 3/1/1.6/1.3; T_{Oven} = 60 °C; $T_{Cat.}$ = 250 °C.

Total ethanol conversion and about 45% H_2 formation among all the gas phase products are obtained. CO_2 (41%) and CO (13%) are the other main products analyzed in the gas phase. Only about 1% of CH_4 and trace of acetaldehyde are detected. The $Ni_3Mg_2AlH_ZO_Y$ catalyst shows considerable stability during 25 h of reaction even if a carbon production of 84 mg h^{-1} g_{cat}^{-1} is observed. It is important to note that carbon formation is not linear with time; it has been observed for several times that it is higher in the initial stage and then it decreases with the time on stream. It can be expected that the good catalytic stability is related to the graphitic filamentous carbon species formed.

5.2 Influence of calcination

5.2.1 $CeNi_XO_Y$ nano-compounds

It is well known that the metal-support interactions play an important role during the preparation procedure and thermal treatment, because both of them are able to define the properties of the final catalysts: reducibility, resistance to thermal sintering of the active sites, or metal dispersion. Accordingly, it is of interest to investigate the catalytic differences coming from the thermal treatment of the catalyst.

Fig. 5-3 shows that the $CeNi_1H_ZO_Y$ catalyst calcined at lower temperature of 300 °C (compared to 500 °C by default) also enables to drive the OSRE reaction with the oven temperature at only 60 °C. It can be clearly seen in **Fig. 5-3** that full ethanol conversion is achieved, and the main gas phase products are H_2, CO_2 and CO. The outstanding catalytic stability is also observed during 40 h of reaction. Therefore the calcination procedure may have an effect mainly on the products distribution.

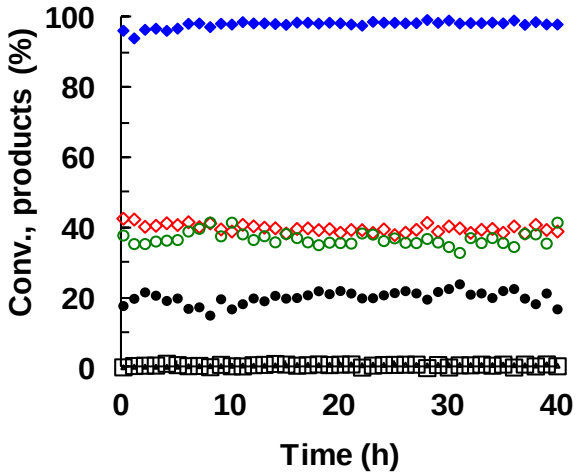

Fig. 5-3 Time course for OSRE on the $CeNi_1H_ZO_Y$ catalyst calcined at 300 °C. Ethanol conversion (◆), H_2 (◇), CO_2 (○), CO (●), CH_4 (▲) and CH_3CHO (□). Reaction conditions: catalyst: 30 mg; $H_2O/EtOH/O_2/N_2$ = 3/1/1.6/1.3; T_{Oven} = 60 °C; $T_{Cat.}$ = 325 °C.

Fig. 5-4 illustrates the influence of the calcination temperature of the $CeNi_1O_Y$ nano-compound on the OSRE reaction. It is no doubt that there is none difference in catalytic activity whatever the calcination temperature, but in the products distribution and the variation of reaction temperature. Nearly total ethanol conversion (98%) is obtained independent on the temperatures involved in the calcination process, in agreement with the fact that the hydrogen species can be inserted into the $CeNi_1O_Y$ mixed oxide to generate oxyhydride group in the catalyst even if the solid is thermal treated at a lower temperature of 300 °C. On the other hand, the real reaction temperature ($T_{Cat.}$) exhibits a gradual increase for the solid calcined at higher temperatures. When the oven temperature (T_{Oven}) is fixed at 60 °C, a group of rising reaction temperature is found for the $CeNi_1O_Y$ mixed oxide calcined at different temperatures, following the order: $T_{Cat.}$ = 325 °C (calcined at 300 °C) < $T_{Cat.}$ = 338 °C (calcined at 400 °C) < $T_{Cat.}$ = 345 °C (calcined at 500 °C).

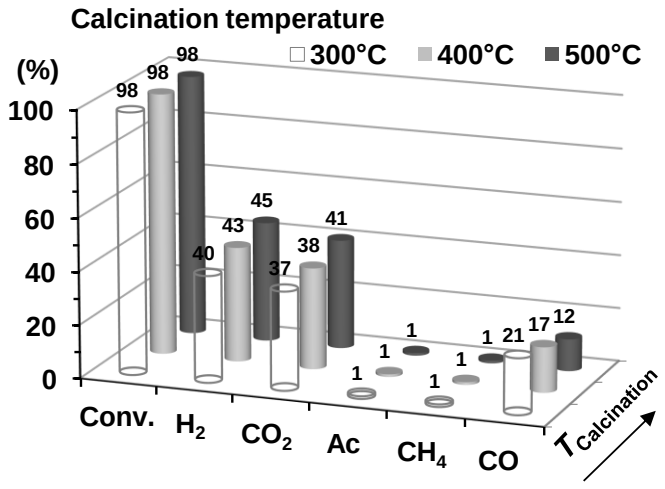

Fig. 5-4 Influence of the calcination temperature of the $CeNi_1O_Y$ nano-compound in OSRE. Reaction conditions: catalyst: 30 mg; $H_2O/EtOH/O_2/N_2$ = 3:1:1.6:1.3; T_{Oven} = 60 °C; t = 40 h.

It can be predicted that a higher reaction temperature would lead to a modification of products composition as already discussed for the SRE reaction over the $CeNi_{0.5}O_Y$ catalysts (**Fig. 4-4**). In fact, the products distribution indeed respects the evolution of reaction temperature ($T_{Cat.}$) which is associated with the calcination procedure. About 45% H_2 production and 12% CO formation are analyzed with the calcination temperature of 500 °C. Compared to that, when the $CeNi_1O_Y$ compound is calcined at 300 °C, less H_2 production of 40% but more CO formation of 21% are produced. CO_2 formation only slightly increases with the calcination temperature. Catalytic systems are found very stable after 40 h of reaction whatever the thermal treatment temperature, affirming no direct correlation between the catalytic stability and the calcination procedure.

5.2.2 $Ni_XMg_2AlO_Y$ nano-compounds

After obtaining the successful example of the $Ni_3Mg_2AlO_Y$ mixed oxide for room temperature H_2 production from ethanol, it is of great interest to explore the possibility of Ni_XMg_2Al HT-like compounds (dried compounds without calcination) applied for this technology. Thus the $Ni_{12}Mg_2Al$ HT-like dried compound is investigated for the OSRE reaction. After treated in H_2 at 450 °C, the catalyst obtained also allows lowering the oven temperature down to almost room temperature to drive the OSRE process. The unique activation phenomenon takes place and the big variation of temperatures between the catalyst bed and the oven is found.

It is therefore certainly possible to form a $Ni_{12}Mg_2AlH_{Z'}O_{Y'}$ nano-oxyhydride catalyst in H_2 treatment but this will have to be confirmed.

The $Ni_{12}Mg_2Al$ HT-like compound treated *in situ* in H_2 at 450 °C is able to completely convert ethanol (**Fig. 5-5**) with a little extra power (T_{Oven} = 60 °C) supplied. H_2 (38%), CO_2 (45%) and CO (16%) are the main products obtained in the gas phase. The rest are trace formation of methane and acetaldehyde. A carbon formation of 49 mg h^{-1} g_{cat}^{-1} is measured after 50 h of reaction but the catalyst shows good stability. This result is very promising in the point view of sustainable chemistry due to that: i) the catalyst without any thermal treatment could still further save energy involved in the catalyst preparation steps; ii) a new type of material, Ni-containing ternary hydroxide compound is discovered to support the room temperature H_2 production from ethanol by the present technology.

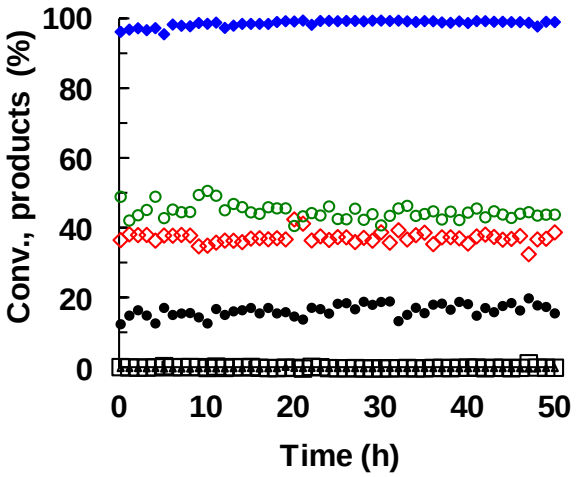

Fig. 5-5 Ethanol conversion and products distribution in OSRE over the $Ni_{12}Mg_2Al$ HT-like compound treated in H_2 at 450 °C. Ethanol conversion (◆), H_2 (◇), CO_2 (○), CO (●), CH_4 (▲) and CH_3CHO (□). Reaction conditions: catalyst: 30 mg; $H_2O/EtOH/O_2/N_2$ = 3/1/1.6/1.3; T_{Oven} = 60 °C; $T_{Cat.}$ = 255 °C.

Fig. 5-6 compares the catalytic results obtained from OSRE on the $Ni_{12}Mg_2Al$ HT-like precursor (dried compound) and the $Ni_{12}Mg_2AlO_Y$ mixed oxide calcined at 500 °C, respectively. Obviously ethanol conversions all reach 100% and CO_2 formation exhibits almost the same value. The only difference is in H_2 and CO formation. A relatively higher proportion of H_2 is obtained on the catalyst calcined at 500 °C, accordingly CO concentration is lower. On the contrary, the dried compound (without calcination) presents relatively lower H_2 composition but higher CO concentration. It is certainly related to the different reaction temperatures obtained during OSRE. Compared to the dried $Ni_{12}Mg_2Al$ compound ($T_{Cat.}$ = 255 °C), CO formation is lower among the

products probably due to the higher reaction temperature of 290 °C obtained on the calcined mixed oxide. However, it is important to note that a much higher loss of weight will be generated over the dried compound during the pretreatment in H_2 at 450 °C. This treatment does not lead to a decrease of activity, showing that the catalyst is enough active to support that.

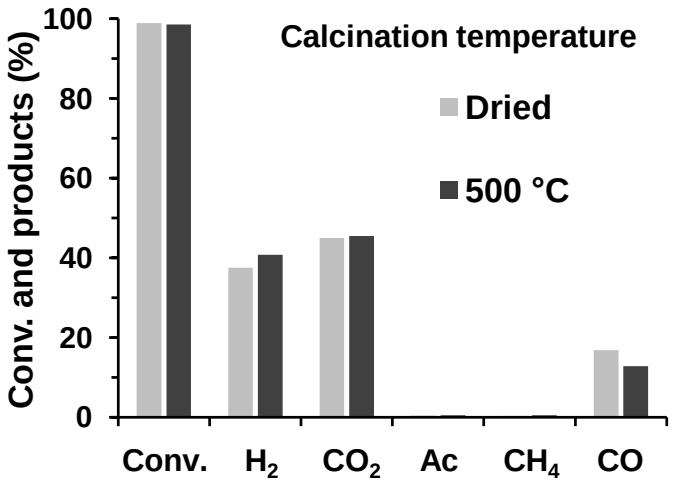

Fig. 5-6 Comparison of the $Ni_{12}Mg_2Al$ HT-like compound (T_T = 450 °C) and $Ni_{12}Mg_2AlH_ZO_Y$ oxyhydride for OSRE. Reaction conditions: catalyst: 30 mg; $H_2O/EtOH/O_2/N_2$ = 3:1:1.6:1.3; T_{Oven} = 60 °C; $T_{Cat.}$ = 255 °C for $Ni_{12}Mg_2Al$ HT-like compound; $T_{Cat.}$ = 290 °C for $Ni_{12}Mg_2AlO_Y$ calcined at 500 °C. Ac: acetaldehyde.

5.3 Influence of Ni content

5.3.1 $CeNi_XH_ZO_Y$ nano-oxyhydride catalysts

The $CeNi_1H_ZO_Y$ nano-oxyhydride catalyst has been shown to be highly efficient for H_2 production from ethanol at room temperature. Thus it can be predicted that the $CeNi_XH_ZO_Y$ oxyhydride family could exibit activity for the OSRE reaction certainly depending on the Ni content. In such a context, a group of $CeNi_XH_ZO_Y$ nano-oxyhydride compounds with different Ni contents are investigated for H_2 production from OSRE and the results are displayed in **Fig. 5-7**.

It is obvious to disclose that the $CeNi_XH_ZO_Y$ oxyhydrides have some common features. Among the compounds studied (x from 0.3 to 5), they are all able to sustain the OSRE process by lowering the oven temperature close to room temperature (60 °C). Ethanol can be completely converted even if a little extra energy is provided. All the $CeNi_XH_ZO_Y$ catalysts investigated show outstanding catalytic stability during long-time OSRE. Whatever the Ni content, the main

products obtained in gas phase are constantly H_2, CO_2 and CO. But the differences in the products distribution can be clearly seen in **Fig. 5-7**. Only traces of acetaldehyde and methane are analyzed in the outles gases.

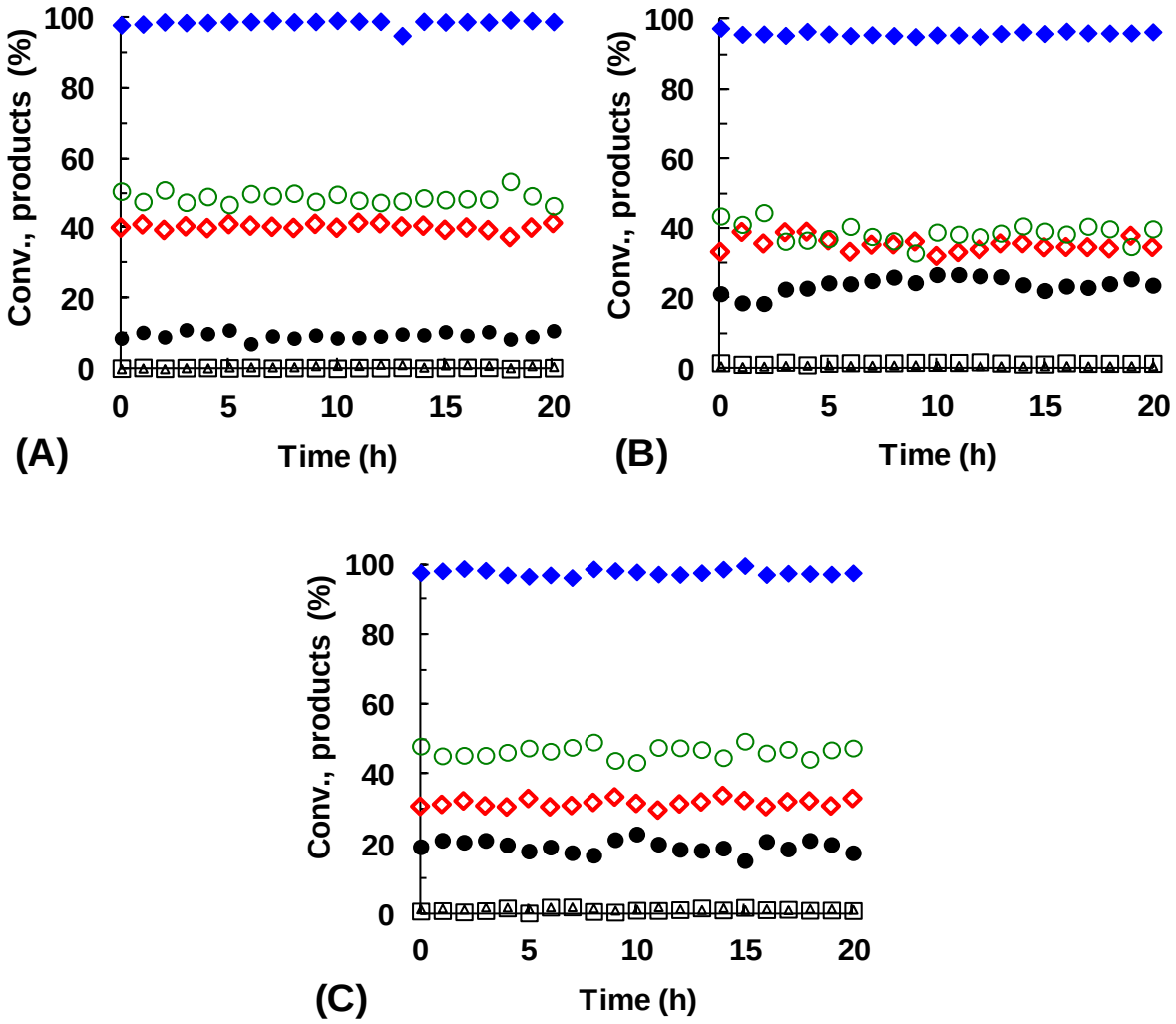

Fig. 5-7 Time course for OSRE on $CeNi_XH_ZO_Y$ nano-oxyhydride catalysts. (A) $CeNi_5H_ZO_Y$, (B) $CeNi_{0.5}H_ZO_Y$, (C) $CeNi_{0.3}H_ZO_Y$. Reaction conditions: catalyst: 30 mg; $H_2O/EtOH/O_2/N_2$ = 3:1:1.6:1.3; T_{Oven} = 60 °C.

It has been reported in our laboratory that $CeNi_XO_Y$ nano-compounds possess different hydrogen storage capacities in form of hydride species depending on the Ni content. This property plays a very important role in achieving this technology because the OSRE process at room temperature is mainly driven by the chemical energy released from the strong exothermic reaction between the hydride species and oxygen. Therefore studying the $CeNi_XH_ZO_Y$

oxyhydride family catalysts with different Ni content allows better understanding this reaction process and the oxyhydride compounds properties.

Fig. 5-8 reports the products composition as a function of the Ni content for the OSRE reaction after 20 h ($Ni/M_T = x/(1+x)$). The results reported in our previous publication are also plotted for comparison.[12] Ethanol is completely converted with an activity constantly higher than 97% over $CeNi_XH_ZO_Y$ catalysts with various Ni contents. Only very small quantities of CH_4 and CH_3CHO are detected in the outlet gases. The total fraction of these two products slightly declines with increasing the Ni content.

The other products in the gas phase do not show monotonic change following the Ni content. About 32% H_2 formation is obtained for the $CeNi_{0.3}H_ZO_Y$ catalyst ($Ni/M_T = 0.23$). Afterward, H_2 molar fraction increases with Ni content and reaches an optimum of about 45% over the $CeNi_1H_ZO_Y$ catalyst. When Ni/M_T ratio further goes up to 0.85 ($CeNi_5H_ZO_Y$), H_2 formation slightly decreases to 40%. CO formation is about 19% as Ni/M_T ratio equals 0.2, and then the maximum value of 24% appears at Ni/M_T ratio of about 0.3, followed by a rapid decrease down to around 11% for higher Ni content. CO_2 molar fraction presents a minimum at Ni/M_T ratio of about 0.4.

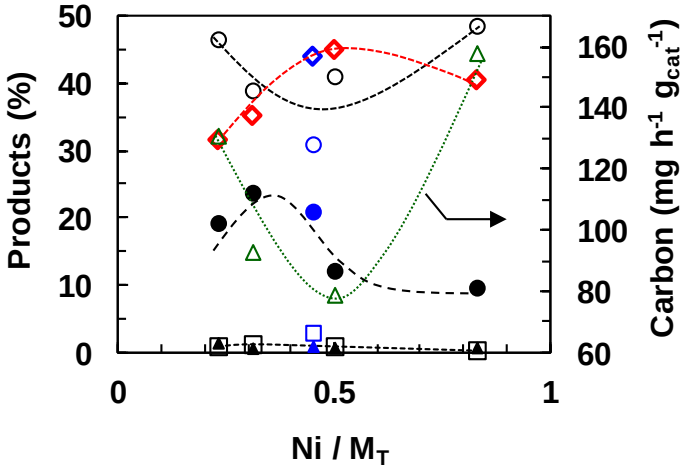

Fig. 5-8 Influence of the Ni content on OSRE over $CeNi_XH_ZO_Y$ catalysts. H_2 (◇), CO_2 (○), CO (●), CH_4 (▲), CH_3CHO (□) and carbon formation (△). Reaction conditions: catalyst: 30 mg; $H_2O/EtOH/O_2/N_2$ = 3/1/1.6/1.3; T_{Oven} = 60 °C; time = 20 h. Ethanol conversion is constantly about 100% independent on the Ni content. For comparison, the blue symbols correspond to the results reported in our previous publication.[12]

In complement to **Eq. 5-1** and **Eq. 5-2** leading to the formation of H_2 and CO_2, different by-products can be obtained due to the co-occurrence of different reactions that can be also involved.

For example, ethanol can be decomposed into a mixture of CO, CH_4 and H_2 (**Eq. 5-3**) at low temperature over the catalysts with strong capability of the C-C bond rupture, like nickel catalyst.[32] Water gas shift (WGS) reaction which is slightly exothermic is favored at low temperature and allows transforming CO (**Eq. 5-4**). Dehydrogenation of ethanol (**Eq. 5-5**) and decomposition of acetaldehyde (**Eq. 5-6**) can happen at the intermediate temperatures (300-350 °C). Moreover, in the presence of O_2 the partial oxidation of methane (**Eq. 5-7**), which is also exothermic, can lead to the formation of H_2 and CO (or CO_2 at higher concentration of O_2).

$$C_2H_5OH \rightarrow CO + CH_4 + H_2 \qquad \textbf{Eq. 5-3}$$

$$CO + H_2O \rightarrow H_2 + CO_2 \qquad \textbf{Eq. 5-4}$$

$$C_2H_5OH \rightarrow CH_3CHO + H_2 \qquad \textbf{Eq. 5-5}$$

$$CH_3CHO \rightarrow CO + CH_4 \qquad \textbf{Eq. 5-6}$$

$$CH_4 + 0.5\ O_2 \rightarrow CO + 2\ H_2 \qquad \textbf{Eq. 5-7}$$

Carbon formation is carefully measured after the reaction and strongly relates to the Ni content (**Fig. 5-8**). The $CeNi_1H_ZO_Y$ catalyst produces the smallest quantity of carbon deposition with a rate of 79 mg h^{-1} g_{cat}^{-1} after 20 h of reaction. Compared with exactly the same catalyst, a much lower carbon formation of 28 mg h^{-1} g_{cat}^{-1} is measured after 75 h.

This result reveals that carbon production is not linearly generated with the time on stream; in contrast, the formation rate is relatively in inverse proportion to the reaction time. It indicates that the majority of carbon deposition is formed in the initial stage and may be before introducing O_2 into the catalytic system. As a matter of fact, solid carbon can be produced by total decomposition of ethanol. Moreover, carbon can be also generated *via* the disproportionation of CO and/or the decomposition of CH_4.[1,33]

In order to understand the interesting products distribution, it is also necessary to investigate the effect of the Ni content on the activation phenomenon which plays a dominant role in the OSRE reaction. As shown in **Fig. 5-9**, when the oven temperature is fixed at 60 °C, the highest reaction temperature ($T_{Cat.}$) of 345 °C is measured over the $CeNi_1H_ZO_Y$ catalyst, while the lowest value of 301 °C is present on the $CeNi_{0.3}H_ZO_Y$ catalyst. It is of importance to notice that none variation of reaction temperature could be observed under exactly the same reaction conditions

on the catalysts without the pre-treatment in H_2. Therefore, the exothermic ethanol partial oxidation (POE) cannot justify the reaction by itself at room temperature. The activation phenomenon is in majority attributed to the strong exothermic reaction (chemical energy) between the hydride species stored in the solid with O_2.

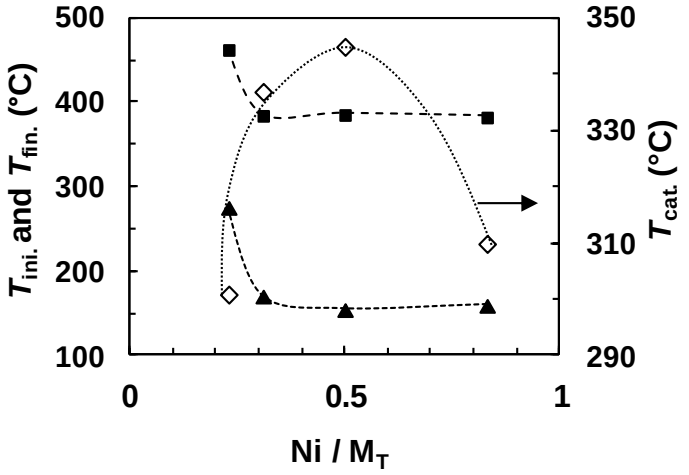

Fig. 5-9 Variation of temperatures *versus* Ni content in the OSRE reaction over $CeNi_XH_ZO_Y$ catalysts. $T_{Cat.}$ (◇), $T_{Ini.}$ (▲) and $T_{Fin.}$ (■). Reaction conditions: catalyst: 30 mg; $H_2O/EtOH/O_2/N_2$ = 3/1/1.6/1.3; T_{Oven} = 60 °C; time = 20 h.

Moreover, whatever the Ni content, total conversion of ethanol is obtained while the variation of temperature exhibits dependence on the Ni content. It appears that the variation of reaction temperature depends on the concentration of the hydrogen stored in the solid in terms of hydride species. As a matter of fact, it has been disclosed by a chemical titration technique that the $CeNi_1O_Y$ nano-compound possesses the highest hydrogen storage capacity among the $CeNi_XO_Y$ series mixed oxides.[29,30]

The evolution of ΔT_R is found to be quite similar respecting to the curve of H_2 formation *versus* the Ni content. A part of hydride species are consumed by O_2 to provide enough chemical energy to drive the catalytic reaction at room temperature, in the meantime the hydride species are continuously generated from ethanol to make the reaction sustainable.

In order to explain how the Ni content affects the carbon formation, the initial and final temperatures during the activation process are investigated (**Fig. 5-9**). It is interesting to find out that the reaction can be activated in the temperature range of 155 to 171 °C over the catalysts with the $Ni/M_T \geqslant 0.5$ after O_2 is added into the feed. And in such a case, the final temperatures are entirely recorded at about 385 °C. When it comes to the lower Ni molar ratio of 0.3, the

reaction has to be activated at much higher temperature of 276 °C (higher more than 100 °C), even if the final temperature is also found higher at about 463 °C.

Among the whole series studied, the $CeNi_1H_ZO_Y$ catalyst still exhibits the optimum behavior, showing the largest variation between the initial and final temperatures during the activation process of the reaction. The variation between the initial and final temperatures is discovered to obey the similar regulation of ΔT_R (**Fig. 5-9**). Thus, it makes sense that the $CeNi_1H_ZO_Y$ catalyst, as well as the $CeNi_{0.5}H_ZO_Y$, enables to inhibit carbon formation because they are able to activate the reaction at lower temperatures (coke formation stage) and drive the reaction at higher temperatures (coke removal and balance stage). On the contrary, the $CeNi_5H_ZO_Y$ and $CeNi_{0.3}H_ZO_Y$ catalysts produce more solid carbon, which can be ascribed to the very high Ni content ($Ni/M_T = 0.8$) and the much higher initial temperature (276 °C), respectively. Regardless of the carbon formation rate, the $CeNi_XH_ZO_Y$ series catalysts all perform excellent catalytic stability.

5.3.2 $Ni_XMg_2AlH_ZO_Y$ nano-oxyhydride catalysts

Followed by the successful application of the $Ni_3Mg_2AlH_ZO_Y$ nano-oxyhydride catalyst for room-temperature hydrogen production from OSRE, it can be speculated that a group of $Ni_XMg_2AlH_ZO_Y$ oxyhydride compounds with different Ni contents could support the OSRE process at room temperature. Hence a series of $Ni_XMg_2AlH_ZO_Y$ nano-oxyhydride catalysts are studied.

Fig. 5-10 reports the time course for a group of $Ni_XMg_2AlH_ZO_Y$ catalysts with various Ni contents for the OSRE reaction. Very excellent catalytic stability is clearly seen after at least 20 h of reaction. Similar to the results obtained over $CeNi_XH_ZO_Y$ oxyhydride compounds, $Ni_XMg_2AlH_ZO_Y$ catalysts are also able to completely convert ethanol with the oven temperature at only 60 °C except the $Ni_1Mg_2AlO_Y$ catalyst, where the reaction has to be maintained with a higher extra energy (T_{Oven} = 215 °C). Whatever the Ni content, the activation phenomenon of the reaction exists, and the variation of temperatures between the catalyst bed and the oven is also observed. The main products in gas phase are H_2, CO_2 and CO. The different distributions are presented in **Fig. 5-10**, which is certainly related to the Ni content. It is of interest to further analyze the influence of the Ni content on the catalytic performances of $Ni_XMg_2AlH_ZO_Y$ catalysts for OSRE at room temperature.

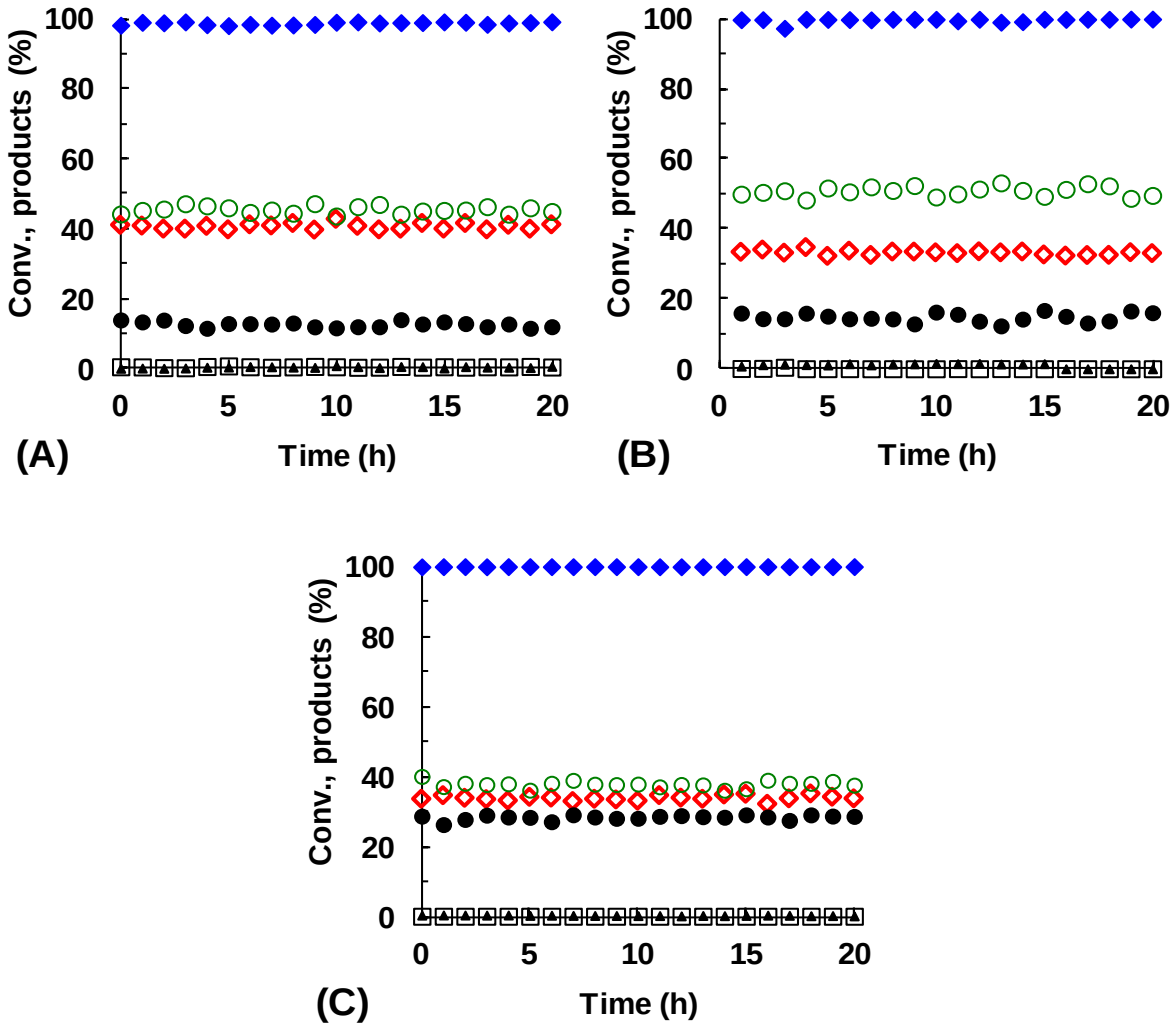

Fig. 5-10 Time course for OSRE on $Ni_XMg_2AlH_ZO_Y$ nano-oxyhydride catalysts. (A) $Ni_{12}Mg_2AlH_ZO_Y$, (B) $Ni_4Mg_2AlH_ZO_Y$, (C) $Ni_1Mg_2AlO_Y$. Reaction conditions: catalyst: 30 mg; $H_2O/EtOH/O_2/N_2$ = 3:1:1.6:1.3; T_{Oven} = 60 °C (for the $Ni_1Mg_2AlO_Y$ catalyst, T_{Oven} = 215 °C).

The products distributions obtained on $Ni_XMg_2AlH_ZO_Y$ catalysts for OSRE are plotted in **Fig. 5-11** as a function of the Ni molar proportion (Ni/M_T). Ethanol conversion is constantly about 100% without the dependence of Ni content. Similar to $CeNi_XH_ZO_Y$ catalysts, only traces of methane and acetaldehyde formation are analyzed for all the $Ni_XMg_2AlH_ZO_Y$ catalysts investigated.

The main products in gas phase, such like H_2, CO_2 and CO, show evolution globally respecting to the Ni content. H_2 formation presents an optimum when Ni/M_T = 0.5. H_2 molar fraction undergoes an apparent increase from Ni/M_T of 0.24 ($Ni_1Mg_2AlO_Y$), and then it remains

at about 45% up to a Ni/M_T ratio of about 0.5 ($Ni_3Mg_2AlH_ZO_Y$). For higher Ni molar ratios, H_2 formation slightly decreases to about 41%.

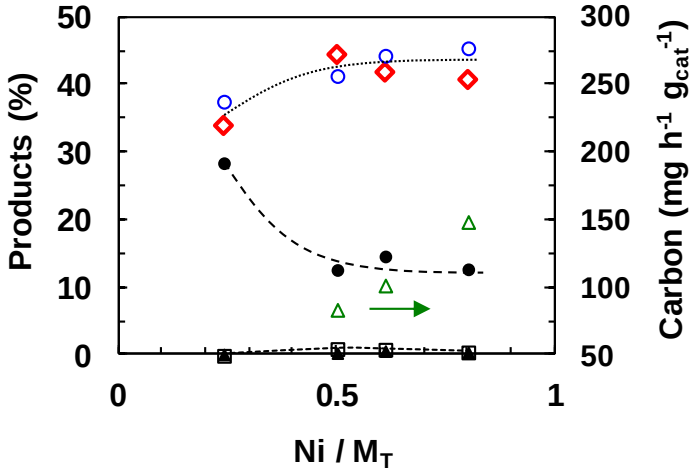

Fig. 5-11 Influence of the Ni content on OSRE over $Ni_XMg_2AlH_ZO_Y$ catalysts. H_2 (◇), CO_2 (○), CO (●), CH_4 (▲), CH_3CHO (□) and carbon formation (△). Reaction conditions: catalyst: 30 mg; $H_2O/EtOH/O_2/N_2$ = 3/1/1.6/1.3; time = 20 h; T_{Oven} = 60 °C (for the $Ni_1Mg_2AlO_Y$ catalyst, T_{Oven} = 215 °C). Ethanol conversion is constantly about 100% independent on the Ni content.

CO_2 formation gradually increases from about 38% to 46% in the Ni/M_T range from 0.24 to 0.8; whereas CO formation first rapidly decreases from about 29% with Ni/M_T = 0.24, then it stays almost constant to 13% when Ni/M_T is higher or equal to 0.5 (**Fig. 5-11**). The evolution of CO formation appears associated with that of CO_2, which is probably due to the water gas shift reaction. In that case, CO is transformed to CO_2 favored at low temperatures.

Solid carbon is observed after test only on the $Ni_XMg_2AlH_ZO_Y$ catalysts with Ni/M_T $\geqslant$ 0.5. Carbon formation is reported in **Fig. 5-11** and found an increase for higher Ni content, though it has been evidenced by the $CeNi_XH_ZO_Y$ catalysts system that carbon production is not linearly generated. For the $Ni_1Mg_2AlO_Y$ catalyst there is no carbon formation obtained after test, which is certainly due to the low Ni loading and the much higher reaction temperature of 405 °C in the presence of O_2. But in return the oven temperature must be no lower than 215 °C to maintain the variation of temperatures between the catalyst bed and the oven.

Analyzing all the temperatures involved in the OSRE process allows to better understanding the correlations among the activation phenomenon, Ni content and products distribution. As shown in **Fig. 5-12**, the reaction has to be activated at higher temperatures ($T_{Ini.}$) for the catalysts having lower Ni content after O_2 is added into the system, however, the tendency appears similar

over the catalysts with the $Ni/M_T \geqslant 0.5$, ranging from 155 to 180 °C. When the Ni molar ratio goes down to 0.24 ($Ni_1Mg_2AlO_Y$), the reaction has to be activated at much higher temperature of 388 °C (higher more than 200 °C). The final temperature ($T_{Fin.}$) shows similar evolution as the initial temperature. For $Ni/M_T \geqslant 0.5$ the final temperatures retains at around 365 °C. Although higher final temperature of 548 °C is recorded on the $Ni_1Mg_2AlO_Y$ catalyst, the variation of temperature during the activation phenomenon is the smallest. Moreover the oven temperature cannot be lowered to 60 °C but must be maintained at 215 °C.

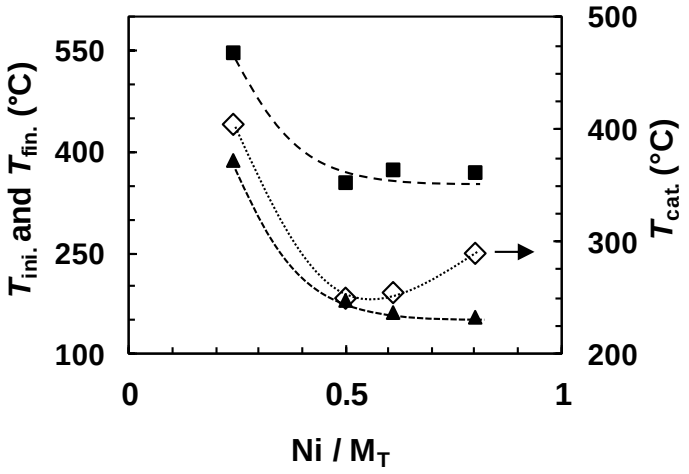

Fig. 5-12 Variation of temperatures *versus* Ni content in the OSRE reaction over $Ni_XMg_2AlH_ZO_Y$ catalysts. $T_{Cat.}$ (◇), $T_{Ini.}$ (▲) and $T_{Fin.}$ (■). Reaction conditions: catalyst: 30 mg, $H_2O/EtOH/O_2/N_2$ = 3/1/1.6/1.3; time = 20 h; T_{Oven} = 60 °C (for the $Ni_1Mg_2AlO_Y$ catalyst, T_{Oven} = 215 °C).

Similar activation phenomenon has been also found on the $CeNi_{0.3}H_ZO_Y$ catalyst (Ni/M_T = 0.23) in the OSRE process. It may be related to the concentration of the hydrogen stored in the solid in the form of hydride species depending on the Ni content. However, it must be noted that the $Ni_1Mg_2AlO_Y$ catalyst is treated in H_2 at 450 °C that is not optimized. It is very important to recall that neither the activation phenomenon nor the variation of temperatures could be observed under exactly the same conditions without the treatment of the catalysts in H_2. As a matter of fact, it has been already disclosed by the TPR profiles depended on the Ni content that the treatment temperature for different $Ni_XMg_2AlO_Y$ nano-compounds can be optimized.

The oven temperature can be lowered to 60 °C for the catalysts with $Ni/M_T \geqslant 0.5$. In that case, the reaction temperatures ($T_{Cat.}$) respect to the Ni content. The $Ni_{12}Mg_2AlH_ZO_Y$ catalyst exhibits the highest $T_{Cat.}$ at 290 °C, while the $Ni_3Mg_2AlH_ZO_Y$ catalyst has a lower value of

250 °C. The $Ni_1Mg_2AlO_Y$ catalyst presents the reaction temperature at 405 °C but with the oven temperature at 215 °C. Generally speaking, the variation of temperatures between the catalyst bed and the oven depends on the Ni content.

INS experiments confirm the insertion of new type of hydrogen species into the $Ni_3Mg_2AlO_Y$ and $Ni_{12}Mg_2AlO_Y$ nano-compounds by the treatment in H_2 at 450 °C (**Fig. 3-29**). The $Ni_{12}Mg_2AlO_Y$ compound exhibits higher spectrum level (compared to $Ni_3Mg_2AlO_Y$) after treatment in H_2 at 450 °C, which is in proportion to the hydrogen concentration in the solids. Whereas the $Ni_1Mg_2AlO_Y$ compound treated in H_2 at 450 °C presents a lower spectrum level than the one obtained on the calcined solid treated in vacuum at 200 °C (**Fig. 3-28**), showing that this solid contains much less hydrogen species after the treatment in H_2. It is highly probably due to a loss of hydroxyl groups (OH^-) after a treatment at higher temperature of 450 °C (compared to 200 °C) without the insertion of new hydrogen species (hydride).

These results can well explain the evolution of variation of temperature between the catalyst bed and oven. Because the extra energy needed is mainly provided by the strong exothermic reaction between hydride species stored in the solids and O_2, thus the oven temperature can be lowered to 60 °C. Hence the $Ni_{12}Mg_2AlO_Y$ catalyst (treated in H_2 at 450 °C) leads to the highest reaction temperature of 290 °C, followed by the $Ni_3Mg_2AlO_Y$ catalyst (treated in H_2 at 450 °C) with $T_{Cat.}$ = 250 °C.

These results are in good agreement with the formation of oxyhydrides during the H_2 treatment at 450 °C (**Fig. 3-29**), and a higher quantity of hydrogen inserted into the $Ni_{12}Mg_2AlO_Y$ solid has been observed by INS spectra in Chapter 3 (**Fig. 3-28**). Higher reaction temperature of 405 °C is recorded on the $Ni_1Mg_2AlO_Y$ catalyst but with a much higher oven temperature at 215 °C, corresponding to a variation of temperature of 190 °C.

$Ni_XMg_2AlO_Y$ nano-compounds have different reduction peaks shown by TPR strongly associated with Ni content, and higher Ni content can promote the reduction (**Fig. 3-14**). In other words, each compound may require an optimized treatment temperature. Apparently 450 °C is not suitable for the $Ni_1Mg_2AlO_Y$ compound, which is not high enough to insert hydrogen species into the solid by treated in H_2; or, this solid is not able to contain a higher quantity of reactive hydrogen species, this needs further investigations.

5.4 Characterizations on the spent catalysts

5.4.1 XRD

The $CeNi_1O_Y$ and $Ni_3Mg_2AlO_Y$ catalysts after ethanol oxidative steam reforming reaction are analyzed by XRD. The patterns obtained are compared with the ones obtained after calcination and after an *in situ* H_2 treatment. As shown in **Fig. 5-13**, the fresh $CeNi_1O_Y$ catalyst (calcined at 500 °C) exhibits a mixture of nanoparticles consisting of NiO and CeO_2. The particles sizes are estimated at 11 nm for NiO and 4 nm for CeO_2 (**Table 5-1**). While the fresh $Ni_3Mg_2AlO_Y$ catalyst (calcined at 500 °C) presents mixture phases of nanoparticles of NiO, MgO and/or $NiMgO_2$ solid solution (**Fig. 5-14**). The crystallites of NiO and/or $NiMgO_2$ are measured at about 3.9 nm, as listed in **Table 5-2**.

After the treatment in H_2 at 250 °C for 10 h, very similar patterns are obtained in the $CeNi_1O_Y$ catalyst (**Fig. 5-13**), compared to the fresh catalyst. However, the *in situ* XRD in H_2 does not evidence the presence of metallic Ni^0 species at a temperature of 250 °C for 10 h (**Fig. 5-13**). On the studied compound, metallic Ni was observed by XRD for a treatment in H_2 at 300 °C in our laboratory.[34] The particles sizes of NiO and CeO_2 are found almost the same values as those in the fresh $CeNi_1O_Y$ catalyst (**Table 5-1**).

Table 5-1 Crystallite sizes of the $CeNi_1O_Y$ catalyst. [a] Calculated taking into account (111), (200) and (220) plane. [b] Calculated taking into account (111) and (200) plane.

Catalyst	Conditions	*d* NiO/ nm [a]	*d* CeO_2/ nm [a]	*d* Ni/ nm [b]
$CeNi_1O_Y$	calcined at 500 °C	11	4	—
	treated in H_2 at 250 °C for 10 h	10	4	—
	after OSRE at 345 °C	26	25	20

Table 5-2 Crystallite sizes of the $Ni_3Mg_2AlO_Y$ catalyst. [a] Calculated from (200) plane. [b] Calculated from (200) plane.

Catalyst	Conditions	*d* NiO and/or $NiMgO_2$/ nm [a]	*d* Ni^0/ nm [b]
$Ni_3Mg_2AlO_Y$	calcined at 500 °C	3.9	—
	treated in H_2 at 450 °C for 10 h	4.0	4.0
	after OSRE at 250 °C	17	22

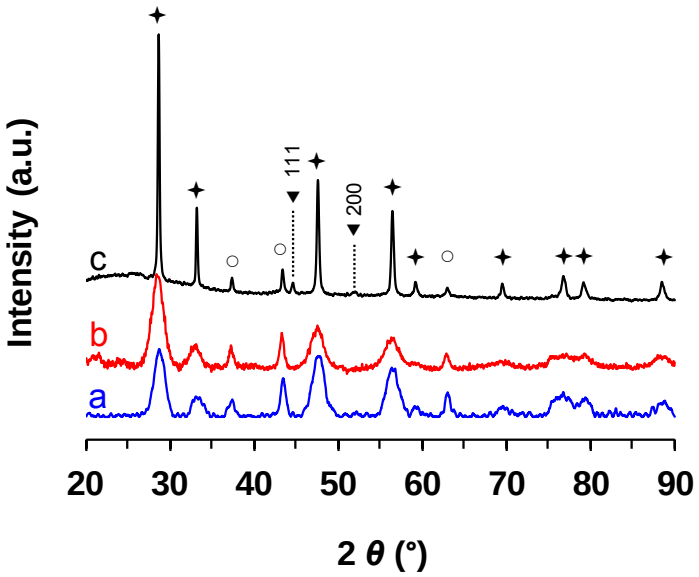

Fig. 5-13 XRD patterns of the $CeNi_1O_Y$ catalyst. a) calcined at 500 °C, b) treated in H_2 at 250 °C for 10 h, c) after OSRE at 345 °C. (Reaction conditions: catalyst: 30 mg; $H_2O/EtOH/O_2/N_2$ = 3/1/1.6/1.3. CeO_2 (✦), NiO (○) and Ni (▼).

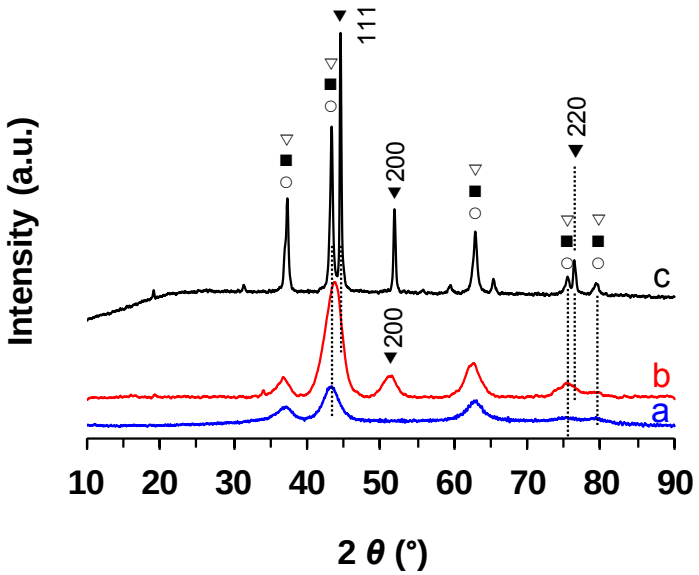

Fig. 5-14 XRD patterns of the $Ni_3Mg_2AlO_Y$ catalyst. a) calcined at 500 °C, b) treated in H_2 at 450 °C for 10 h, c) after OSRE at 250 °C. (Reaction conditions: catalyst: 30 mg; $H_2O/EtOH/O_2/N_2$ = 3/1/1.6/1.3. MgO (○), $NiMgO_2$ (■), NiO (▽) and Ni (▼).

The $Ni_3Mg_2AlO_Y$ catalyst shows metallic nickel phase for Ni (111), (200) and (220) plane when treated in H_2 at 450 °C for 10 h, as presented in **Fig. 5-14**. The Ni particle size is measured at 4.0 nm. All the phase relevant to NiO and/or MgO and/or $NiMgO_2$ are maintained , the crystallite sizes are very close to the values measured in the fresh compound (**Table 5-2**).

After oxidative ethanol steam reforming, it is clearly seen that both the $CeNi_1O_Y$ and $Ni_3Mg_2AlO_Y$ catalysts well maintain the structures and crystalline phases of the fresh catalysts. As shown in **Fig. 5-13** and **Fig. 5-14**, all the oxidized phases are well presented in the spent catalysts. Compared to the patterns obtained after *in situ* H_2 treatment, metallic Ni phase related to the Ni (111) and (200) plane starts to be visible in the spent $CeNi_1O_Y$ catalyst (**Fig. 5-13**), which is not observed in the compound treated in H_2 at 250 °C; while in the spent $Ni_3Mg_2AlO_Y$ catalyst metallic Ni phase due to the Ni (111), (200) and (220) plane is still well presented (**Fig. 5-14**).

The patterns of the spent catalysts are obviously found to appear much more intense and narrower, showing that the catalysts after OSRE become more crystallized, which is probably related to the compounds reacting with the ethanol-water mixture in the presence of O_2, as this phenomenon is not observed in the catalyst after SRE in the absence of O_2 (**Fig. 4-21**). The intensity of ceria phase in the spent $CeNi_1O_Y$ catalyst apparently looks more intense, while NiO phase exhibits similar intensity to that obtained in the calcined compound or after treatment in H_2. In the spent $Ni_3Mg_2AlO_Y$ catalysts, all the crystalline phases appear much stronger intensity compared to those observed either in the fresh compound or after *in situ* H_2 treatment. Hence the Ni crystallites could grow bigger. As reported in **Table 5-1** and **Table 5-2**, the particles sizes of NiO (and/or $NiMgO_2$) are measured at 17 nm for $Ni_3Mg_2AlO_Y$ and at 26 nm for $CeNi_1O_Y$. Ni particles sizes are estimated at 22 nm for $Ni_3Mg_2AlO_Y$ and at 20 nm for $CeNi_1O_Y$. CeO_2 particles also grow to 25 nm in $CeNi_1O_Y$ solid.

5.4.2 XPS

The $CeNi_1O_Y$ and $Ni_3Mg_2AlO_Y$ catalysts after OSRE are also analyzed by XPS. The binding energies obtained on the fresh catalysts and the spent catalysts are listed in **Table 5-3** and **Table 5-4**. The $CeNi_1O_Y$ and $Ni_3Mg_2AlO_Y$ catalysts show a main emission peak in the $Ni2p_{3/2}$ region (**Fig. 5-15**). The BE shifts to higher values after OSRE reaction compared to the calcined state. On the $CeNi_1O_Y$ catalyst, two peaks are obtained for the $Ni2p_{3/2}$, one at the same position as for the calcined state (854.5 eV),[35], and the other one at higher energy (856.3 eV). Therefore the Ni^{2+} species are well maintained but with the formation of Ni^{2+} species interacting with hydroxyl groups. The higher BE at 856.3± 0.1 eV is the same as the BE observed on $Ni(OH)_2$ (856.2 eV). The $Ni2p_{3/2}$ core-level satellite lines related to $Ni^{2+}$are also seen at about 6 eV up to the main

peak. No peak related to metallic Ni^0 is clearly observed. For the $Ni_3Mg_2AlO_Y$ catalyst after OSRE only a very large peak is observed leading to the difficulty in the attribution. This line broadening effect can be due to different types of Ni species coexisting on the surface, or to the remaining organic compounds because the measured reaction temperature is lower (at 250 °C). A small shoulder peak at lower energy is due to the presence of metallic Ni species on the surface.[36] As for the $CeNi_1O_Y$ catalyst, it seems that the Ni^{2+} species are well maintained but with the formation of Ni^{2+} species interacting with hydroxyl groups. The surface Ni molar ratios after OSRE are measured close to the data obtained on the fresh catalysts, which shows the homogeneous distribution of Ni species in the catalysts after reaction.

Table 5-3 Binding energies and surface Ni molar ratios of the $CeNi_1O_Y$ catalyst obtained under different conditions. The full width at half-maximum (FWHM) values of the lines are reported in parentheses.

Conditions	$Ni2p_{3/2}$/ eV	O1s/ eV	Ni/M_T
calcined at 500 °C[a]	854.5 (4.8)	529.1 (3.2)	0.38
after OSRE at 345 °C	854.6/856.3 (4.4)	530.3/531.7 (3.8)	0.33

[a] The XPS parameters of the calcined $CeNi_1O_Y$ catalyst are from reference [35].

Table 5-4 Binding energies and surface Ni molar ratios of the $Ni_3Mg_2AlO_Y$ catalyst obtained under different conditions. The full width at half-maximum (FWHM) values of the lines are reported in parentheses.

Conditions	$Ni2p_{3/2}$/ eV	O1s/ eV	Ni/M_T
dried without calcination	856.2 (3.3)	531.7 (2.8)	0.41
calcined at 500 °C	855.7 (3.6)	530.6/531.7 (3.1)	0.31
after OSRE at 250 °C	855.6/856.1 (10.6)	531.5 (4.4)	0.30

As presented in **Fig. 5-15**, the O1s spectra demonstrates one peak at about 531.5 eV for the spent $Ni_3Mg_2AlO_Y$ catalyst, and two peaks at 530.3 and 531.7 eV for the spent $CeNi_1O_Y$ catalyst. Concerning the $Ni_3Mg_2AlO_Y$ compound, the BE at 531.5± 0.1 eV is very close to one of the values observed on the calcined catalyst (**Table 5-3** and **Table 5-4**), which is in agreement with the presence of oxygen species related to OH^- groups after reaction. For the $CeNi_1O_Y$ catalyst, the lower BE of 530.3 eV is assigned to the typical O^{2-} lattice species which are therefore still present after reaction. Meanwhile hydroxyl groups are formed with the observation of a peak at about 531.7 eV. It can be remarked that this value was also obtained after SRE reaction (**Fig. 4-25**). Both the surface O/Ni molar ratios of higher than 2 and the line broadening effect of O1s line

demonstrate the existence of different oxygen species on the surface of catalysts after OSRE, which is in accordance with the present observation.[37,38] The XPS results are in very good agreement with the XRD analysis on the spent catalysts (**Fig. 5-13** and **Fig. 5-14**), showing that $CeNi_XO_Y$ and $Ni_XMg_2AlO_Y$ catalysts well maintain the oxidized phases and crystalline structures after OSRE with presence of a low quantity of metallic Ni species.

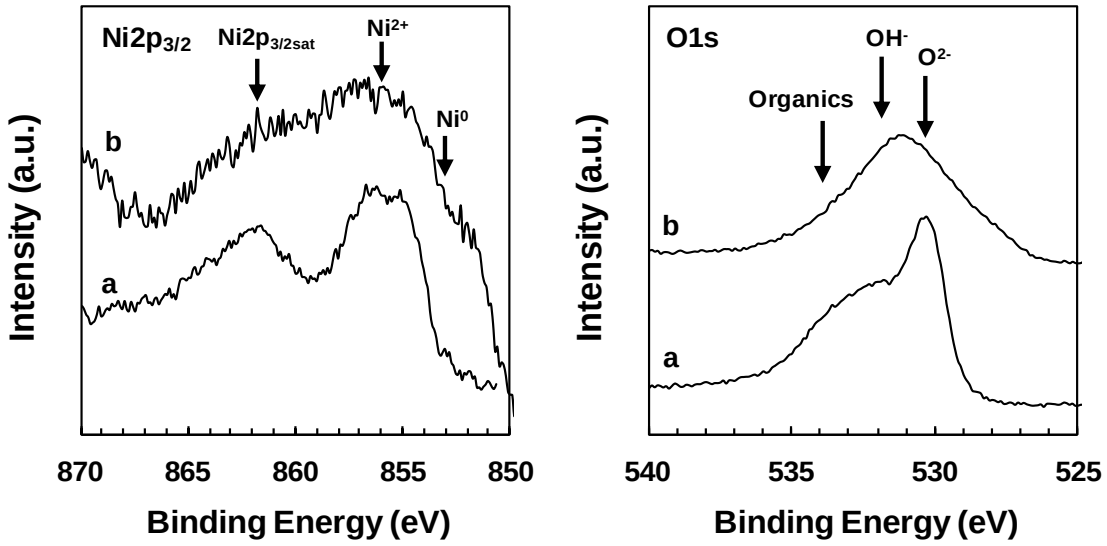

Fig. 5-15 Ni2p and O1s XPS spectra of the $CeNi_1O_Y$ and $Ni_3Mg_2AlO_Y$ catalysts after OSRE. a) $CeNi_1O_Y$ after OSRE at 345 °C (catalyst: 30 mg; $H_2O/EtOH/O_2/N_2$ = 3/1/1.6/1.3; time = 75 h.), b) $Ni_3Mg_2AlO_Y$ after OSRE at 250 °C (catalyst: 30 mg; $H_2O/EtOH/O_2/N_2$ = 3/1/1.6/1.3; time = 25 h.)

Therefore the Ni species are certainly the active phase. However, the largely recovered oxidized phases with a low amount of metallic Ni phase cannot justify the metallic Ni species as the active site. An active site involving an anionic vacancy and an O^{2-} species of the solid can be envisaged for heterolytic dissociation of ethanol, which will be discussed in the following chapter.

In the very recent literature, a few catalytic systems have been reported as good candidates for the OSRE reaction. Pereira *et al.* reported OSRE over K promoted Co-Rh/Ce-Zr catalysts, the stable (40 h) $Co_{0.2}Rh(K)/CeO_2$-ZrO_2 catalyst (100 mg) can lead to CO-free H_2 production (Y_{H2} = 50%) with total conversion at 375 °C using a large amount of water ($H_2O/EtOH/O_2$ = 6/1/0.5).[10] Andovona *et al.* studied Co promoted Ni/Al_2O_3 catalysts for OSRE, the $6CoNi/Al_2O_3$ catalyst gave nearly full conversion and about 64 mol% H_2 formation at 500 °C but during only 30 min ($H_2O/EtOH/O_2$ = 3/1/0.5).[11] Guil-López *et al.* studied series of Co, Ni and Cu *ex*-hydrotalcite catalysts for OSRE, they found that all the $CoAl_{0.7}$, $CoZn_{2.4}Al_{1.9}$, $CoMg_{2.2}Al_{1.9}$ and $NiMg_{2.3}Al_{1.9}$ catalysts could compeletely convert ethanol between 450 and 575 °C with H_2 formation of about

55 mol% during 4 h ($H_2O/EtOH/O_2$ = 2.28/1/0.36).[21] Cai *et al.* reported 1.9 wt% Ir/CeO_2 (300 mg) as active and stable (40 h) catalyst for OSRE, at 450 °C it provided 100% conversion with 50 mol% H_2 formation ($H_2O/EtOH/O_2$ = 1.8/1/0.6).[18] Lima *et al.* applied $La_{1-x}Ce_xNiO_3$ perovskite-type oxides to OSRE, the $La_{0.9}Ce_{0.1}NiO_3$ oxides (20 mg) allowed obtaining total conversion with about 45 mol% at 500 °C ($H_2O/EtOH/O_2$ = 3/1/0.5).[13] Hung *et al.* studied OSRE at 600 °C over a group of Al_2O_3 supported metal catalysts (125 mg), among noble metals 1.6 wt% Rh/Al_2O_3 presented full conversion and 97% H_2 yield; while 1.2 wt% Ni/Al_2O_3 gave full conversion with 23% H_2 yield among non-noble metals ($H_2O/EtOH/O_2$ = 3/1/0.3). To be noted, 100% H_2 yield corresponds to 3 mol mol_{EtOH}^{-1} in this paper.[14]

In the present study, $CeNi_XO_Y$ and $Ni_XMg_2AlO_Y$ catalysts are shown to be highly active, efficient and stable catalysts for H_2 production from OSRE, even if some carbon is formed. The simple co-precipitation method employed allowed preparing the $CeNi_XO_Y$ and $Ni_XMg_2AlO_Y$ nano-compounds which possess a high proportion of very active Ni species either in the solid solutions of Ce-Ni and Ni-Mg-(Al)-O and/or at the interface between small nanoparticles of NiO and nanoparticles of CeO_2 or Mg-(Al)-O. Strong interactions between nickel species (Ni^{2+}) and other cations (Ce^{4+}, Mg^{2+} and Al^{3+}) have been previously evidenced. The INS (inelastic neutron scattering) experiment proves that hydride (H^-) species are inserted into the $CeNi_XO_Y$ and $Ni_XMg_2AlO_Y$ nano-compounds, when x (Ni molar ratio) and the treatment temperature in H_2 are adequately chosen. The INS experiments have shown that the $CeNi_1H_ZO_Y$, $Ni_3Mg_2AlH_ZO_Y$ and $Ni_{12}Mg_2AlH_ZO_Y$ nano-oxyhydrides are formed during the treatment in H_2. The $CeNi_XH_ZO_Y$ and $Ni_XMg_2AlH_ZO_Y$ nano-oxyhydride catalysts can be obtained after an *in situ* treatment in H_2 at 250 °C and 450 °C, respectively.

In this state, the catalysts have been shown to be able to completely convert ethanol to produce H_2 (45 mol%) with only a little extra energy input (oven temperature of 60 °C) by using a very small quantity of catalyst of 30 mg ($H_2O/EtOH/O_2$ = 3/1/1.6). The energy released from the significantly strong exothermic reaction between hydride species stored in the catalyst and O_2 (**Eq. 5-8**) is smartly utilized to continuously drive the OSRE reaction. The results obtained are excellently competitive and better than the ones reported in the literature in the point view of environmentally friendly and sustainable chemistry due to: i) highly active, efficient and stable (75 h) systems; ii) a novel technology remarkably saving energy by requiring only a little extra

power input; iii) low-cost catalysts without the presence of any noble metals; iv) simple preparation method and simple catalyst components.

$$H^- + 0.5\ O_2 \rightarrow OH^- \qquad \textbf{Eq. 5-8}$$

5.5 Characterizations on the carbonaceous species

5.5.1 Raman

The Ni-based nano-oxyhydride catalysts exhibit remarkably catalytic stability for the OSRE reaction. In fact, it has been proved in the SRE reaction that the homogeneous filamentous carbon could contribute to the catalytic stability.[26] Due to the very small quantity of carbon species formed after the reaction, Raman spectroscopy is for sure the most available and powerful technique to characterize the carbonaceous materials.[39,40]

The Raman spectra obtained from the solid carbon grown on $CeNi_XH_ZO_Y$ nano-oxyhydride catalysts in the OSRE reaction are presented in **Fig. 5-16**. Two main peaks well known as the D-band and G-band are visible whatever the Ni content in the catalyst. It has to be noted that the carbon production without the acid treatment in the present result affirmatively provides information coming from the spent catalyst itself. The D-band observed between 1343 cm^{-1} and 1350 cm^{-1}, is assigned to the vibration of the sp^3 hybridized carbon atom with the dangling bonds in the disordered carbonaceous species; while the G-band observed between 1586 cm^{-1} and 1595 cm^{-1} is ascribed to the stretching mode of the sp^2 hybridized carbon atom in the ordered graphite.

In the literature, carbon nanofibers (CNFs) and carbon nanotubes (CNTs) can be distinguished by comparing the Raman frequency shift between the two species, but only very slight differences could be observed. The D-band was obtained at 1350 cm^{-1} for CNFs and 1355 cm^{-1} for CNTs， whereas the G-band was observed at 1592 cm^{-1} on CNFs and 1582 cm^{-1} on CNTs.[40] The marvelous stability of $CeNi_XH_ZO_Y$ catalysts is certainly attributed to the formation of the filamentous carbon species which are probably associated with CNFs and/or CNTs, although this hypothesis requires more evidences from other characterizations, such as TPO and TEM.

The intensity ratio of I_D/I_G can be quantified as a measure of the degree of graphitization. Hence I_D/I_G is characteristic of the degree of order of the carbon materials.[39] Lower I_D/I_G ratio corresponds to higher order degree of substances. It is of interest to find out that the I_D/I_G ratios

do not monotonously depend on the Ni content, but present the minimum value for the $CeNi_1H_ZO_Y$ catalyst. $CeNi_XH_ZO_Y$ catalysts exhibit the I_D/I_G ratios in a declined order of 1.64 (x = 5) > 1.33 (x = 0.3) > 1.23 (x = 0.5) > 0.98 (x = 1). So the optimal behavior of the $CeNi_1H_ZO_Y$ catalyst in both catalytic performance and physicochemical property could be partially explained by the formation of fibrous carbon (CNTs and/or CNFs) with the highest degree of graphitization.

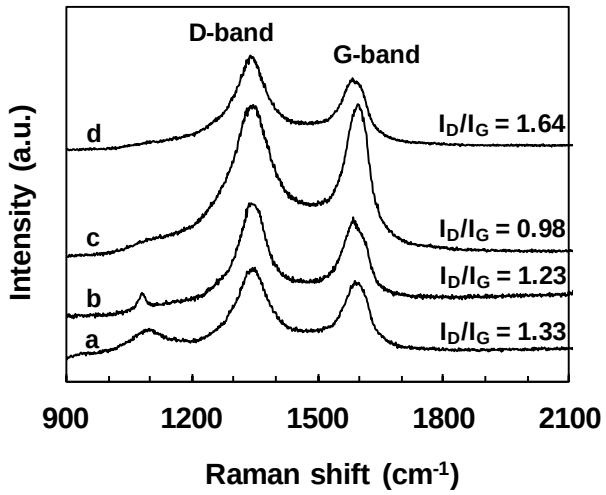

Fig. 5-16 Raman spectra of the carbon species formed on $CeNi_XH_ZO_Y$ nano-oxyhydride catalysts during the OSRE reaction. a) x = 0.3, b) x = 0.5, c) x = 1, d) x = 5. Reaction conditions: catalyst: 30 mg; $H_2O/EtOH/O_2/N_2$ = 3/1/1.6/1.3; time = 20 h.

5.5.2 O_2-TPO

To gain insight to the nature of the carbon species formed on the Ni-based nano-oxyhydride catalysts during the OSRE reaction, temperature-programmed oxidation is used to evaluate the extent of carbon structure, *i.e.*, amorphous and/or graphitic nature. It has been already well established in the literature that the types of carbonaceous species can be identified by the TPO peaks relating to different reactivity towards oxidation.

The TPO profiles obtained on several typical Ni-based nano-oxyhydride catalysts after the OSRE reaction are reported in **Fig. 5-17**, namely the $CeNi_1H_ZO_Y$, $Ni_3Mg_2AlH_ZO_Y$ catalysts and the $Ni_{12}Mg_2Al$ HT-like compound. First of all, it is immediately apparent that no peak is observed at temperatures lower than 400 °C among all the catalysts studied. This low-temperature oxidation peak is attributed to the amorphous carbon species which are highly reactive towards O_2 and easily oxidized from the nickel surface.

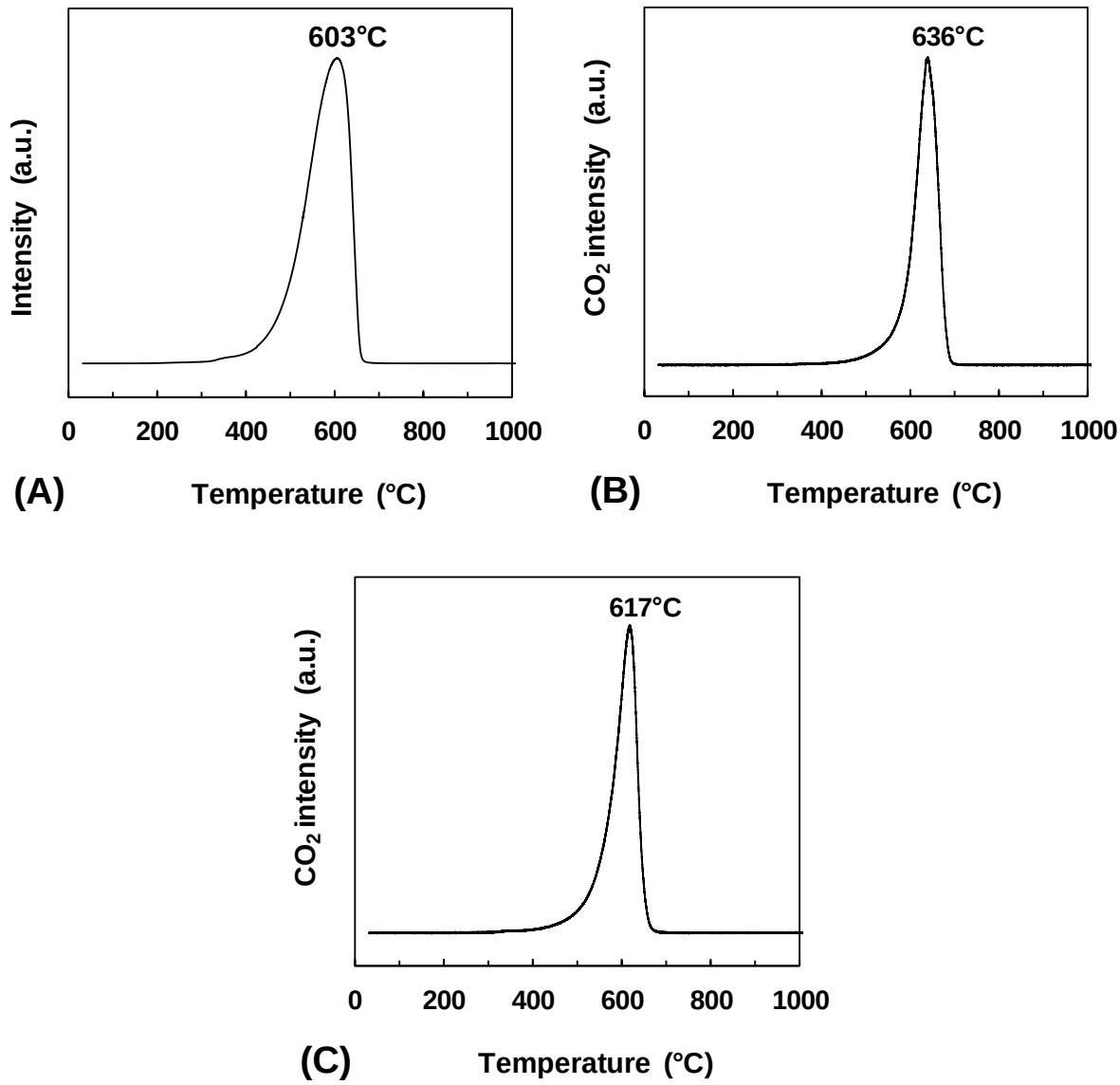

Fig. 5-17 TPO profile of the carbon species formed on Ni-based nano-oxyhydride catalysts during OSRE. (A) $CeNi_1H_ZO_Y$, (B) $Ni_3Mg_2AlH_ZO_Y$, (C) $Ni_{12}Mg_2Al$ HT-like compound. Reaction conditions: catalyst: 30 mg; $H_2O/EtOH/O_2/N_2$ = 3/1/1.6/1.3.

There is only one single oxidation peak presented for all the catalysts analyzed, which is located around 600 °C. This high-temperature oxidation peak is related to the graphitic carbon species in nature. In the literature, it was reported for O_2-TPO analysis of solid carbon that temperatures around 510 °C were assigned to the single walled carbon nanotubes (SWCNTs), while temperatures around 610 °C could be attributed to the multiwalled carbon nanotubes (MWCNTs). Besides, carbon nanofibers (CNFs) were affirmed to burn off in lower temperature

range than SWCNTs.[41] Therefore, the carbon species grown on Ni-based nano-oxyhydride catalysts can be generally ascribed to carbon nanofibers accompanied with some CNTs possibly.

By carefully comparing the shape and broadness of TPO profiles, the peaks obtained on the $Ni_XMg_2AlH_ZO_Y$ catalysts shift towards higher oxidation temperatures, compared to the $CeNi_1H_ZO_Y$ catalyst; and the $Ni_3Mg_2AlH_ZO_Y$ catalyst presents the highest temperature at 636 °C. Moreover the peaks appear narrower and more symmetric than the one obtained on the $CeNi_1O_Y$ catalyst, suggesting that the carbon species formed on the $Ni_XMg_2AlO_Y$ catalysts under the OSRE conditions maybe probably contain more CNTs showing more graphitic in structure.

5.5.3 TEM

The transmission electron microscopy is employed to study the type and morphology of carbonaceous species formed on the $CeNi_1H_ZO_Y$ catalyst during the OSRE reaction, in the meantime, the information related to Ni nanoparticles can be obtained. As a complementary characterization to TPO and Raman, TEM enables to provide direct images of carbonaceous species.

From **Fig. 5-18** the carbonaceous species in the form of filaments are obviously observed on the $CeNi_1H_ZO_Y$ catalyst after the OSRE reaction. It is in accordance with the TPO result which presents an oxidation peak at high temperature of 603 °C without the presence of amorphous carbon species. The filamentous carbon species are found relatively homogeneous in size, even though some large filaments can be seen. Apart from that, some carbon nanotubes (CNTs) are also formed on the $CeNi_1H_ZO_Y$ catalyst, in fact CNTs have been observed even if at lower reaction temperature (300 °C) on the $Ni_{12}Mg_2AlO_Y$ catalyst for highly diluted SRE reaction.

In order to gain insight into the structure of the carbonaceous species formed, an area is selected to analyze under high resolution conditions (HRTEM). The carbon filaments are composed of graphitic sheets that can be clearly seen in **Fig. 5-18**. Most of the graphitic sheets are regularly piled but some degree of non-parallel exists, probably due to an unequal diffusion of graphitic sheets through nickel particles.[42] This result is in very good agreement with the Raman spectrum of the carbon species grown on the $CeNi_1H_ZO_Y$ catalyst, in which the G-band observed at 1595 cm^{-1} is ascribed to the stretching mode of the sp^2 hybridized carbon atom in the ordered graphite. Moreover, the $CeNi_1H_ZO_Y$ catalyst has the minimum I_D/I_G ratio that corresponds to higher order degree of substances.

Nickel related nanoparticles are observed on the spent $CeNi_1H_ZO_Y$ catalyst, and the particles are found located at the tip of the carbon filaments (**Fig. 5-18**). The average particles size is estimated around 10 nm which is very close to the value (11 nm) calculated from XRD patterns for the fresh $CeNi_1O_Y$ compound.

Therefore, the solid carbon produced in the present OSRE process can be seen as an added value, as CNFs and MWCNTs are strategic materials in various fields, and in particular, they are very interesting catalyst support materials for diverse catalytic applications.

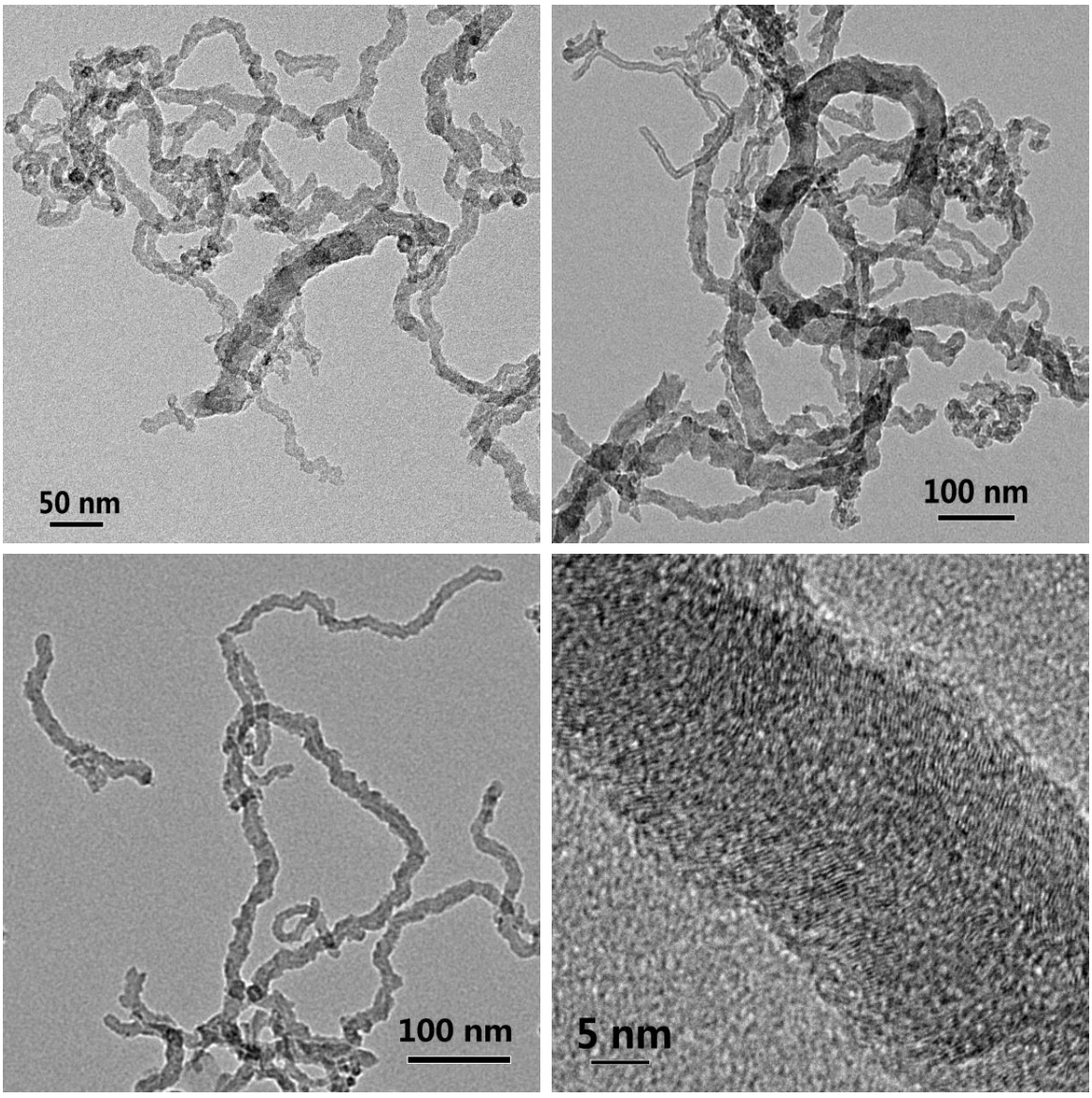

Fig. 5-18 TEM micrographs for the carbon species formed on the $CeNi_1H_ZO_Y$ catalyst. Reaction conditions: catalyst: 30 mg; $H_2O/EtOH/O_2/N_2$ = 3/1/1.6/1.3; time = 75 h.

5.6 Conclusion

A novel catalytic technology is proposed to support a sustainable H_2 production at room temperature from ethanol (and water) with the presence of O_2. Two types of Ni-based catalysts, $CeNi_XO_Y$ and $Ni_XMg_2AlO_Y$ are reported for the oxidative steam reforming of ethanol (OSRE). A simple co-precipitation method is employed to prepare the $CeNi_XO_Y$ and $Ni_XMg_2AlO_Y$ nano-compounds, which possess a high proportion of very active Ni species either in the solid solutions of Ce-Ni and Ni-Mg-(Al)-O and/or at the interfaces of small NiO nanoparticles and CeO_2 or Mg-(Al)-O nanoparticles, which can be reduced and reoxidized easily and reversibly due to the existence of strong interactions between nickel species and other cations (Ce^{4+}, Mg^{2+} and Al^{3+}).

The present new technology enables to remarkably save energy by smartly taking advantages of the energy released from the strong exothermic chemical reaction between the hydride species (H^-) stored in the $CeNi_XH_ZO_Y$ and $Ni_XMg_2AlH_ZO_Y$ catalysts and O_2, together with the exothermic ethanol partial oxidation (POE). A part of hydride species are consumed by O_2 to provide enough chemical energy to drive the catalytic reaction at room temperature, in the meantime the hydride species are continuously generated from ethanol to make the reaction sustainable. Hence, a huge variation of temperature between the catalyst bed and the oven can be observed. Such a unique advantage is able to continuously completely convert ethanol and produce hydrogen with the requirement of only a very small amount of extra power, and allows lowering the oven temperature down to 60 °C. $CeNi_XH_ZO_Y$ and $Ni_XMg_2AlH_ZO_Y$ catalysts show very good catalytic stability owing to the very low formation of the graphitic filamentous carbon species during the reaction.

The Ni content has a significant effect on the products distribution while the activity is mainly related to the hydrogen storage capacity of the solid (hydrogen species inserted into the solids by H_2 treatment) depending also on the Ni content. Total ethanol conversion can be achieved on all the Ni-based oxyhydride catalysts studied, however, the OSRE reaction has to be activated at higher temperatures on the $CeNi_{0.3}O_Y$ and $Ni_1Mg_2AlO_Y$ catalysts. Moreover, the $Ni_1Mg_2AlO_Y$ catalyst needs more energy (T_{Oven} = 215 °C) to maintain the reaction. The $CeNi_1H_ZO_Y$ and $Ni_3Mg_2AlH_ZO_Y$ nano-oxyhydrides are evidenced to be the best catalysts in the series analyzed. Full ethanol conversion and 45% H_2 (in mol.) in all the gas phase products are reported with the oven temperature at only 60 °C. Besides, low carbon species is measured after

reaction. To our knowledge, this is the best result that has been ever reported for a low-cost catalytic system.

5.7 Experimental

5.7.1 Catalytic reaction

The catalytic performances were conducted under the atmospheric pressure in a fixed-bed quartz reactor (inner diameter 8 mm) fitted in a programmable oven. The catalyst (30 mg) was previously *in situ* treated in H_2 for 10 h ($CeNi_XO_Y$ nano-compounds: 250 °C; $Ni_XMg_2AlO_Y$ nano-compounds 450 °C). The water-ethanol mixture with a stoichiometric molar ratio of 3 was pumped and vaporized in the heating chamber. The gas stream of $H_2O/EtOH/O_2/N_2$ = 3/1/1.6/1.3 was then fed to the reactor with a total flow rate of 60 mL min^{-1}. The outlet gases were analyzed online by GC (TRACE GC ULTRA) equipped with the thermal-conductivity detector (TCD) and the flame ionization detector (FID).

The reactants must be introduced in a specific order, and O_2 came at the last to avoid the immediate re-oxidation of the oxyhydride. After all the reactants were fed, the reaction could be activated at some certain temperature, depending on the ability of the oxyhydride catalyst to react with O_2. The heating of the oven could be reduced to room temperature as soon as the measured reaction temperature started to drastically increase and the variation of reaction temperature was recorded.

Catalytic performances were reported based on the ethanol conversion (X_{EtOH}), products molar composition (C_i), which were calculated by the following equations (**Eq. 5-9** and **Eq. 5-10**).

$$X_{EtOH} = \frac{n_{EtOH,in} - n_{EtOH,out}}{n_{EtOH,in}} \times 100\% \qquad \textbf{Eq. 5-9}$$

where $n_{EtOH,in/out}$ is the molar flow rate of ethanol at the inlet/outlet of the reactor, respectively.

$$C_i = \frac{n_i}{\sum_{products} n_i} \times 100\% \qquad \textbf{Eq. 5-10}$$

where n_i represents the molar flow rate of product *i* at the outlet of the reactor.

5.7.2 Carbon characterizations

O_2-TPO. Temperature-programmed oxidation was performed on a Micromeritics Autochem 2920 analyzer. The sample was treated in the 5 vol% O_2-95 vol% He mixture with a flow rate of 50 mL min^{-1}. The temperature was increased to 1000 °C at a heating rate of 5 °C min^{-1}. The desorption species from the sample were traced by an OmniStar GSD 300 O mass spectrometer.

Raman. Raman spectra were acquired on a Labram Infinity HORIBA JOBIN YVON Raman spectrometer using a visible laser with an output laser power of λ = 532 nm at room temperature.

TEM. Transmission electron microscopy images were obtained by a FEI Tecnai G2 20 transmission electron microscope at an acceleration voltage of 200 kV. The sample was previously ultrasonically dispersed in acetone, and then drops of the suspension were applied onto a copper grid-supported transparent carbon film.

5.8 References

[1] E. Y. García and M. A. Laborde, *Int. J. Hydrogen Energy*, 1991, **16**, 307.

[2] G. Zhou, L. Barrio, S. Agnoli, S. D. Senanayake, J. Evans, A. Kubacka, M. Estrella, J. C. Hanson, A. Martínez-Arias, M. Fernández-García and J. A. Rodriguez, *Angew. Chem. Int. Ed*, 2010, **49**, 9680.

[3] M. Z. Jacobson, W. G. Colella and D. M. Golden, *Science*, 2005, **308**, 1901.

[4] J. C. Ruiz-Morales, D. Marrero-Lopez, J. Canales-Vazquez and J. T. S. Irvine, *RSC Adv.*, 2011, **1**, 1403.

[5] J. R. Salge, G. A. Deluga and L. D. Schmidt, *J. Catal.*, 2005, **235**, 69.

[6] S. N. Hsu, J. L. Bi, W. F. Wang, C. T. Yeh and C. B. Wang, *Int. J. Hydrogen Energy*, 2008, **33**, 693.

[7] K. Sato, K. Kawano, A. Ito, Y. Takita and K. Nagaoka, *ChemSusChem*, 2010, **3**, 1364.

[8] S. M. de Lima, I. O. da Cruz, G. Jacobs, B. H. Davis, L. V. Mattos and F. B. Noronha, *J. Catal.*, 2008, **257**, 356.

[9] F. Frusteri, S. Freni, V. Chiodo, S. Donato, G. Bonura and S. Cavallaro, *Int. J. Hydrogen Energy*, 2006, **31**, 2193.

[10] E. B. Pereira, P. Ramírez De La Piscina, S. Martí and N. Homs, *Energy Environ. Sci.*, 2010, **3**, 487.

[11] S. Andonova, C. N. de Ávila, K. Arishtirova, J. M. C. Bueno and S. Damyanova, *Appl. Catal. B*, 2011, **105**, 346.

[12] C. Pirez, M. Capron, H. Jobic, F. Dumeignil and L. Jalowiecki-Duhamel, *Angew. Chem. Int. Ed*, 2011, **50**, 10193.

[13] S. M. de Lima, A. M. da Silva, L. O. O. da Costa, J. M. Assaf, L. V. Mattos, R. Sarkari, A. Venugopal and F. B. Noronha, *Appl. Catal. B*, 2012, **121–122**, 1.

[14] C.-C. Hung, S.-L. Chen, Y.-K. Liao, C.-H. Chen and J.-H. Wang, *Int. J. Hydrogen Energy*, 2012, **37**, 4955.

[15] B. Neltner, B. Peddie, A. Xu, W. Doenlen, K. Durand, D. S. Yun, S. Speakman, A. Peterson and A. Belcher, *ACS Nano*, 2010, **4**, 3227.

[16] A. Iulianelli and A. Basile, *Catal. Sci. & Technol.*, 2011, **1**, 366.

[17] N. Zhu, X. Dong, Z. Liu, G. Zhang, W. Jin and N. Xu, *Chem. Commun.*, 2012, **48**, 7137.

[18] W. Cai, F. Wang, C. Daniel, A. C. van Veen, Y. Schuurman, C. Descorme, H. Provendier, W. Shen and C. Mirodatos, *J. Catal.*, 2012, **286**, 137.

[19] S. Velu, N. Satoh, C. S. Gopinath and K. Suzuki, *Catal. Lett.*, 2002, **82**, 145.

[20] S. Velu, K. Suzuki, M. Vijayaraj, S. Barman and C. S. Gopinath, *Appl. Catal. B*, 2005, **55**, 287.

[21] R. Guil-López, R. M. Navarro, M. A. Peña and J. L. G. Fierro, *Int. J. Hydrogen Energy*, 2011, **36**, 1512.

[22] G. Frenette and D. Forthoffer, *Int. J. Hydrogen Energy*, 2009, **34**, 3578.

[23] P. Leung, A. Tsolakis, J. Rodriguez-Fernandez and S. Golunski, *Energy Environ. Sci.*, 2010, **3**, 780.

[24] L. Jalowiecki-Duhamel, C. Pirez, M. Capron, F. Dumeignil and E. Payen, *Int. J. Hydrogen Energy*, 2010, **35**, 12741.

[25] L. Jalowiecki-Duhamel, C. Pirez, M. Capron, F. Dumeignil and E. Payen, *Catal. Today*, 2010, **157**, 456.

[26] W. Xu, Z. Liu, A. C. Johnston-Peck, S. D. Senanayake, G. Zhou, D. Stacchiola, E. A. Stach and J. A. Rodriguez, *ACS Catal.*, 2013, **3**, 975.

[27] C. Sun, H. Li and L. Chen, *Energy Environ. Sci.*, 2012, **5**, 8475.

[28] C. Lamonier, A. Ponchel, A. D'Huysser and L. Jalowiecki-Duhamel, *Catal. Today*, 1999, **50**, 247.

[29] L. Jalowiecki-Duhamel, *Int. J. Hydrogen Energy*, 2006, **31**, 191.

[30] L. Jalowiecki-Duhamel, J. Carpentier and A. Ponchel, *Int. J. Hydrogen Energy*, 2007, **32**, 2439.

[31] L. Jalowiecki-Duhamel, H. Zarrou and A. D'Huysser, *Int. J. Hydrogen Energy*, 2008, **33**, 5527.

[32] M. A. Ebiad, D. R. Abd El-Hafiz, R. A. Elsalamony and L. S. Mohamed, *RSC Adv.*, 2012, **2**, 8145.

[33] J. Rass-Hansen, C. H. Christensen, J. Sehested, S. Helveg, J. R. Rostrup-Nielsen and S. Dahl, *Green Chem.*, 2007, **9**, 1016.

[34] C. Pirez, *Thèse*, Univ. Lille 1, décembre 2010.

[35] A. Ponchel, A. Huysser, C. Lamonier and L. Jalowiecki-Duhamel, *Phys. Chem. Chem. Phys.*, 2000, **2**, 303.

[36] M. C. Biesinger, B. P. Payne, L. W. M. Lau, A. Gerson and R. St. C. Smart, *Surf. Interface Anal.*, 2009, **41**, 324.

[37 B. P. Payne, M. C. Biesinger and N. S. McIntyre, *J. Electron. Spectrosc. Relat. Phenom.*, 2009, **175**, 55.

[38] B. P. Payne, M. C. Biesinger and N. S. McIntyre, *J. Electron. Spectrosc. Relat. Phenom.*, 2012, **185**, 159.

[39] G. Wang , H. Wang , W. Li, Z. Ren , J. Bai and J. Bai, *Fuel Processing Technology*, 2011, **92**, 531.

[40] Y. Liu, C. Pan and J. Wang, *J. Materials Science*, 2004, **39**, 1091.

[41] A. W. Musumeci, G. G. Silva, W. N. Martens, E. R. Waclawik, and R. L. Frost. *J. Therm. Anal. Calorim.*, 2007, **88**, 885.

[42] P. Wang, E. Tanabe, K. Ito, J. Jia, H. Morioka, T. Shishido and K. Takehira, *Appl. Catal. A*, 2002, **231**, 35.

6 General discussion

In the present thesis, two types of Ni-based catalysts, $CeNi_XO_Y$ binary mixed oxides and $Ni_XMg_2AlO_Y$ ternary mixed oxides, are prepared by the co-precipitation method (CP). CeO_2 supported Ni catalysts (Ni/CeO_2) are also prepared by the impregnation (IMP) and incipient wetness impregnation (IWI) methods, respectively. The above Ni-based catalysts are studied by different physicochemical techniques, such as ICP-MS, N_2 physisorption, XRD, Raman, XPS, H_2-TPR, TEM, *in situ* XRD in H_2 and INS.

$CeNi_XO_Y$ compounds prepared by CP method are ascribed to a mixture of nanoparticles of NiO and CeO_2, according to XRD analysis. Ni/CeO_2 catalysts prepared by IMP and IWI methods are well-crystallized compounds exhibiting characteristic of a mixture of NiO and CeO_2 oxides. CP method allows obtaining $CeNi_XO_Y$ nano-compounds with small NiO (about 10 nm) and CeO_2 (about 5 nm) nanoparticles. $CeNi_XO_Y$ nano-compounds have relatively large surface areas ranging between 75-120 $m^2\ g^{-1}$, whereas Ni/CeO_2-IMP and Ni/CeO_2-IWI catalysts have small surface areas of about 7 $m^2\ g^{-1}$ related to the CeO_2 support used. Moreover, IMP and IWI methods lead to materials with much larger NiO (20-40 nm) and CeO_2 (about 37 nm) particles sizes.

Raman spectra reveal that nano-crystalline CeO_2 and oxygen vacancies, created by the incorporation of the dopant, are observed presenting the solubility of nickel species into ceria, as a proof to the existence of the strong interactions between nickel and cerium species in $CeNi_XO_Y$ nano-compounds.

XRD evidences that Ni-containing Ni_XMg_2Al hydrotalcite-like compounds (precursors of the catalysts) are formed by CP method, and α nickel hydroxide phase emerges for higher Ni proportions when $x \geqslant 3$. After the calcination at 500 °C, the precursor is transformed to $Ni_XMg_2AlO_Y$ mixed oxides. $Ni_XMg_2AlO_Y$ catalysts are assigned to a mixture of nanoparticles of NiO, MgO and/or to the solid solution of Ni-Mg-(Al)-O. Very small and uniform nanoparticles ranging between 3-6 nm are obtained depending on the Ni content. Ternary $Ni_XMg_2AlO_Y$ nano-compounds have large surface areas between 100-200 $m^2\ g^{-1}$.

TPR analysis discloses that $CeNi_XO_Y$ nano-compounds provide the reduction peaks at temperatures between 200 and 400 °C assigned to the reduction of Ni species. When the Ni/Ce molar ratio increases from 0.02 up to 1, a main reduction peak at about 370 °C becomes more

intense, and slightly shifts towards higher temperature of 390 °C, comparable to bulk NiO (prepared in a similar way) which presents a reduction peak at about 390°C,[1] $CeNi_XO_Y$ solids possess high proportions of very active Ni species which present the characteristic of being able to be reduced and reoxidized easily and reversibly, which is due to the existence of strong interactions between nickel and cerium species. This characteristic TPR peak at about 270 °C is not clearly visible on Ni/CeO_2 catalysts prepared by IMP and IWI methods.

$Ni_XMg_2AlO_Y$ mixed oxides show an almost single broad TPR peak at temperatures between 560-850 °C assigned to the reduction of Ni species. Compared to bulk NiO which presents a reduction peak at about 390°C, the Ni species in $Ni_XMg_2AlO_Y$ compounds are reduced at higher temperatures. However, the TPR peak clearly shifts to lower temperature when the Ni content increases. $Ni_XMg_2AlO_Y$ mixed oxides with high Ni content are easier reduced at low temperature. For low Ni content the strong interactions between nickel species and other cations either in Ni-Mg-(Al)-O solid solution and/or at the interfaces between small nanoparticles of NiO, MgO and/or Ni-Mg-(Al)-O make the solid difficult to reduce; while if the Ni content increases, the reducibility of the solid becomes closer to that of bulk NiO. However, there are still strong interactions existing between Ni cations and some other cations, because the required temperature for reduction of Ni species is still much higher than the one necessary to reduce bulk NiO (560 °C for the $Ni_{12}Mg_2AlO_Y$ compound compared to 390 °C for NiO).

Therefore the strong interactions existing in the $CeNi_XO_Y$ and the $Ni_XMg_2AlO_Y$ nano-compounds lead to two different comportments, for the $CeNi_XO_Y$ nano-compounds, the reducibility of Ni species is ameliorated at lower temperature (but there is a redox process with a simultaneous reoxidation of the Ni^0 species and the reduction of Ce^{4+} cations); while for the $Ni_XMg_2AlO_Y$ nano-compounds the reduction of Ni species is delayed and a higher temperature is required for the reduction (compared to bulk NiO, and $CeNi_XO_Y$).

In situ XRD analysis demonstrates that the treatment in H_2 at 450 °C for 10 h leads to small nanoparticles of oxides accompanied with a small amount of nanoparticles of metallic nickel species Ni^0 in the $Ni_3Mg_2AlO_Y$ (dNi^0: 4 nm) and $Ni_{12}Mg_2AlO_Y$ compounds (dN^0: 5 nm), but all the oxidized phases related to NiO, MgO and/or $NiMgO_2$ still maintain. Whereas for $CeNi_XO_Y$ compounds, *in situ* XRD analysis demonstrated that after treatment in H_2 at 250 °C for 10 h no Ni^0 is observed.[2]

XPS analysis proved the presence of Ni^{2+} species on the surface of $CeNi_XO_Y$ compounds even after treatment in H_2 at 250 °C.[3] For $Ni_XMg_2AlO_Y$ compounds, Ni^{2+} species are evidenced on the surface of the solids, which is in agreement with the main formation of Ni-Mg-(Al)-O solid solution.

Previous INS experiments evidenced that $CeNi_XH_ZO_Y$ nano-oxyhydrides are formed when treating the $CeNi_XO_Y$ compounds in H_2 at 250 °C.[4] INS experiments discover here that some hydrogen species already exist in the calcined $Ni_XMg_2AlO_Y$ compounds (before H_2 treatment) which are assigned to the OH^- groups. After the treatment in H_2 at 450 °C for 10 h, new peaks are observed in the solids, proving the insertion of new type of hydrogen species into the solids. Ni content and treatment conditions have influences on the nature and concentration of hydrogen species stored in the solids. The formation of $Ni_XMg_2AlH_ZO_Y$ nano-oxyhydrides during the H_2 treatment at 450 °C is shown by INS spectra. No hydride species is inserted into the $Ni_1Mg_2AlO_Y$ compound after the treatment in H_2 at 450 °C; whereas the $Ni_3Mg_2AlO_Y$ and $Ni_{12}Mg_2AlO_Y$ compounds are able to store hydride species after H_2 treatment at 450 °C.

The two types of Ni-based catalysts, $CeNi_XO_Y$ and $Ni_XMg_2AlO_Y$, are studied for the steam reforming of ethanol (SRE, H_2O/EtOH = 3). Many parameters are carefully analyzed by using high concentration of reactant mixture (EtOH: 14 mol%), including reaction temperature, *in situ* activation in H_2, Ni content, preparation method effect, calcination temperature effect, catalyst dilution effect, water partial pressure effect and ethanol concentration effect. Moreover, the efficiency of $CeNi_XO_Y$ and $Ni_XMg_2AlO_Y$ catalysts towards H_2 production are studied under highly diluted conditions (EtOH: 1 mol% or 3 mol%).

Reaction temperature influences ethanol conversion and products distribution. Conversion increases with reaction temperature and total conversion is obtained at 450 °C when the catalysts (50 mg) are *in situ* treated in H_2, *i.e.*, $CeNi_XO_Y$ at 250 °C, $Ni_XMg_2AlO_Y$ at 450 °C. The gas phase products (dry basis) are H_2 (about 50 mol%), CO_2 and CH_4, without the formation of CO. Solid carbon is formed after SRE at 450 °C. Undesirable products, such as acetaldehyde and acetone that can be produced from dehydrogenation and aldol condensation, are obtained when reaction temperature is lower than 350 °C. As expected, clearly SRE is favored with high temperatures.

The activation in H_2 is evidenced as an important factor to influence the catalytic performance. The treatment temperature optimized for $CeNi_XO_Y$ catalysts with different Ni contents is of about 250 °C which corresponds to the first TPR peak. It is attributed to the

reduction of very active Ni species being able to be reduced and reoxidized easily and reversibly in the $CeNi_XO_Y$ compounds. When treatment temperature is higher than 300 °C, conversion decreases.

The optimum treatment temperature for $Ni_XMg_2AlO_Y$ catalysts can be different which depends on the Ni content as it has been shown that TPR peak shifts to low temperature with higher Ni content. Treatment temperature influence is analyzed between 160 °C and 700 °C, the optimum temperature can be proposed at 450 °C taking into account ethanol conversion, products distribution and carbon formed. A higher amount of solid carbon is produced when $Ni_XMg_2AlO_Y$ compound is treated in H_2 at a temperature higher than 550 °C.

Ni content strongly affects ethanol conversion and products distribution. Conversion globally increases with Ni content, and total conversion is obtained at 450 °C over $CeNi_XO_Y$ catalysts (treated in H_2 at 250 °C) when $Ni/M_T \geqslant 0.5$ ($Ni/M_T = x/(1+x)$), and over $Ni_XMg_2AlO_Y$ catalysts (treated in H_2 at 450 °C) when $Ni/M_T \geqslant 0.8$ ($Ni/M_T = x/(3+x)$). H_2 formation maintains around 50 mol% when $Ni/M_T \geqslant 0.5$, while CO_2 and CH_4 globally increase with Ni content. Acetaldehyde declines to zero when $Ni/M_T \geqslant 0.5$, while CO presents a maximum at $Ni/M_T = 0.5$. Ethylene and acetone are obtained over the catalysts with low Ni content ($Ni/M_T \leqslant 0.24$), whereas solid carbon starts to be formed when $Ni/M_T \geqslant 0.24$ and increases with Ni content. Clearly, the increase of conversion for high Ni content leads to the increase of carbon formation.

The influence of preparation method is studied on Ce-Ni catalysts prepared by different methods, namely, co-precipitation, impregnation and incipient wetness impregnation method. It is shown that Ce-Ni catalysts prepared by different methods but with the similar Ni loading demonstrate relatively similar catalytic activity (even if the $CeNi_XO_Y$ compounds are more active), but exhibit quite different catalytic stability. $CeNi_XO_Y$ mixed oxides show much better stability than the other two types of Ni/CeO_2 catalysts, which is ascribed to the large surface area and small NiO and CeO_2 nanoparticles obtained by the co-precipitation method. Besides, the lower amount of homogeneous graphitic filamentous carbon species formed on $CeNi_XO_Y$ catalysts contribute to the catalytic stability.

The present $CeNi_XO_Y$ and $Ni_XMg_2AlO_Y$ mixed oxides are reported as highly active and efficient catalysts for H_2 production from SRE. The $Ni_{12}Mg_2AlO_Y$ catalyst (treated in H_2 at 450 °C) allows obtaining CO-free H_2 production of 3 mol mol_{EtOH}^{-1} ($EtOH/H_2O/N_2 = 1/3/96$) at

300 °C. The $Ni_3Mg_2AlO_Y$ (treated in H_2 at 450 °C) and $CeNi_1O_Y$ (treated in H_2 at 250 °C) catalysts are able to completely convert ethanol at 450 °C to produce CO-free H_2 of about 3 mol mol_{EtOH}^{-1} even with higher ethanol concentration ($EtOH/H_2O/N_2$ = 3/9/88). A very high H_2 production of about 5 mol mol_{EtOH}^{-1} is reported at 650 °C. It has to be remarked that the formation of CO and CH_4 limits the yield to hydrogen to no more than 90% (corresponding to 5.4 mol mol_{EtOH}^{-1}) in the best conditions. As a matter of fact, working at high temperature water gas shift equilibrium does not allow such a yield to increase, while at lower temperature the yield is also limited by the methane steam reforming equilibrium.

The high activity to ethanol and the high selectivity to hydrogen of the present $CeNi_XO_Y$ and $Ni_XMg_2AlO_Y$ catalysts are closely related to their physicochemical properties. The simple co-precipitation method allows producing $CeNi_XO_Y$ and $Ni_XMg_2AlO_Y$ mixed oxides with large surface areas, and with small nanoparticles of NiO, CeO_2, and/or Ni-Mg-(Al)-O. Once *in situ* treated in H_2 ($CeNi_XO_Y$: 250 °C, $Ni_XMg_2AlO_Y$: 450 °C), the very active Ni species either in the solid solution of Ce-Ni-O and Ni-Mg-(Al)-O and/or at the interface of small nanoparticles of NiO, CeO_2, or Ni-Mg-(Al)-O, can be easily reduced and reoxidized (existing as Ni^0, $Ni^{\delta+}$, Ni^{2+} in the system) due to the strong interactions between Ni species and other cations (Ce^{4+}, Mg^{2+} and Al^{3+}). XRD shows that the $Ni_XMg_2AlO_Y$ catalysts after SRE present the oxidized phases related to NiO, MgO and/or $NiMgO_2$, and the Ni^0 phase. The crystallite sizes of NiO and/or $NiMgO_2$ are very close to the values obtained in the fresh catalyst (calcined at 500 °C), and the average nanoparticle size of Ni^0 species is also very close to the value measured from the compounds treated in H_2 at 450 °C. Clearly the Ni species are the active phase; however, the other cations in presence have also an influence on the catalytic results.

Moreover, a novel catalytic technology is proposed to support a sustainable H_2 production at room temperature from ethanol (and water) with the presence of O_2. The two types of Ni-based catalysts, $CeNi_XO_Y$ and $Ni_XMg_2AlO_Y$ are reported for the oxidative steam reforming of ethanol (OSRE). The present new technology enables to remarkably save energy by smartly taking advantages of the energy released from the strong exothermic chemical reaction between the hydride species (H^-) stored in the $CeNi_XH_ZO_Y$ and $Ni_XMg_2AlH_ZO_Y$ catalysts and O_2, together with the exothermic ethanol partial oxidation (POE). A part of hydride species are consumed by O_2 to provide enough chemical energy to drive the catalytic reaction at room temperature, in the meantime the hydride species are continuously generated from ethanol to make the reaction

sustainable. Hence, a huge variation of temperature between the catalyst bed and the oven can be observed which depends mainly on the hydrogen stored in the solid. Such a unique advantage is able to continuously completely convert ethanol and produce hydrogen with the requirement of only a very small amount of extra power, and allows lowering the oven temperature down to 60 °C. $CeNi_XH_ZO_Y$ and $Ni_XMg_2AlH_ZO_Y$ catalysts show very good catalytic stability even if small amount of carbon is formed which is related to the graphitic filamentous carbon species.

In the applied conditions for OSRE, the Ni content has a significant effect on the products distribution; while the activity is mainly related to the hydrogen storage capacity of the solid (hydrogen species inserted into the solids by H_2 treatment) depended also on the Ni content. Total ethanol conversion can be achieved on all the Ni-based catalysts studied, however, the OSRE reaction has to be activated at higher temperatures on the $CeNi_{0.3}O_Y$ and $Ni_1Mg_2AlO_Y$ catalysts. Moreover, the $Ni_1Mg_2AlO_Y$ catalyst needs more energy (T_{Oven} = 215 °C) to maintain the reaction.

The $CeNi_1H_ZO_Y$and $Ni_3Mg_2AlH_ZO_Y$ nano-oxyhydrides are shown to be the best catalysts in the series analyzed. Total ethanol conversion and 45% H_2 (in mol.) in the gas phase products are reported with the oven temperature at only 60 °C with very good catalytic stability. To our knowledge, this is the best result that has been ever reported for a low-cost catalytic system.

6.1 Proposal of active phase

With the objective to determine the active metal converting ethanol to H_2 production, the distribution of Ni species inside the solids attracts our interests. Thus two series of Ni-based catalysts, $CeNi_XO_Y$ and $Ni_XMg_2AlO_Y$ mixed oxides, as well as the Ni_XMg_2Al HT-like compounds (catalyst precursors without calcination), are studied by XPS. As shown in **Fig. 6-1**, the surface Ni molar ratios determined by XPS are compared to the bulk Ni molar ratio measured by ICP-MS. The 45 ° diagonal line corresponds to an ideal case of completely homogeneous distribution of nickel inside the solid. It is clearly seen that binary $CeNi_XO_Y$ solids show very homogeneous distribution of nickel, while ternary Ni-Mg-Al compounds seem to give also rather good results. The Ni/M_T ratios on surface appear relatively lower than those in bulk, but the values respect very well to the Ni content (**Fig. 6-1**). In other words, all the different series of Ni-based catalysts studied show the same tendency for Ni distribution in the solids, whatever the components of the catalysts. This result suggests a very good incorporation of nickel species into the surrounding metal cations.

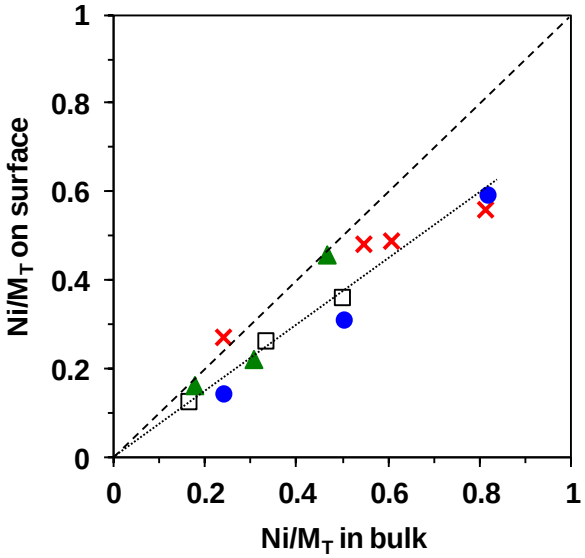

Fig. 6-1 Variation of surface Ni molar ratios (XPS) as a function of bulk Ni molar ratios (ICP-MS) for Ni-based catalysts. $Ni_XMg_2AlO_Y$ catalysts (●), Ni_XMg_2Al HT-like compounds(×), $CeNi_XO_Y$ catalysts (□) from reference [3], $CeNi_XO_Y$ catalysts (▲) from reference [5].

Fig. 6-2 compares the catalytic results of SRE at 450 °C obtained over two types of Ni-based catalysts. As plotted as a function of Ni molar ratio, it is very interesting to find out that both $CeNi_XO_Y$ and $Ni_XMg_2AlO_Y$ catalysts exhibit very good similarity in catalytic behaviors, exhibiting very similar evolution for ethanol conversion and products distribution. This shows the important role that nickel plays in the SRE reaction. Some differences can be seen in the products distribution for low Ni content. It is relatively logical that the influence of the second (or third) cation is easier to see when it is found in higher concentration, when stronger interactions exist due to the higher concentrations of Ce and Mg or Al.

There is a global increase in ethanol conversion *versus* Ni content (**Fig. 6-2**). Total conversion can be nearly achieved when $Ni/M_T \geqslant 0.5$. H_2 formation slightly decreases with Ni content and maintains about 55 mol% among the gas phase products, which is due to the high concentration of gaseous products derived from the relatively high conversion of ethanol in a concentrated feed ($EtOH/H_2O/N_2$ = 14/42/44).

It has to be noted that the Mg_2AlO_Y catalyst in the absence of nickel and the $CeNi_{0.02}O_Y$ catalyst with very low Ni loading (0.3 wt%) demonstrate very low conversion of ethanol accompanied with a high proportion of undesirable by-products. The Mg_2AlO_Y catalyst demonstrates 8% ethanol conversion with about 40% acetaldehyde and 17% ethylene as by-products; while the $CeNi_{0.02}O_Y$ catalyst shows 18% conversion with about 11% acetone

formation. Acetaldehyde is observed in higher quantity over $Ni_XMg_2AlO_Y$ catalyst, while acetone is found in higher quantity over $CeNi_XO_Y$ at very low Ni content.

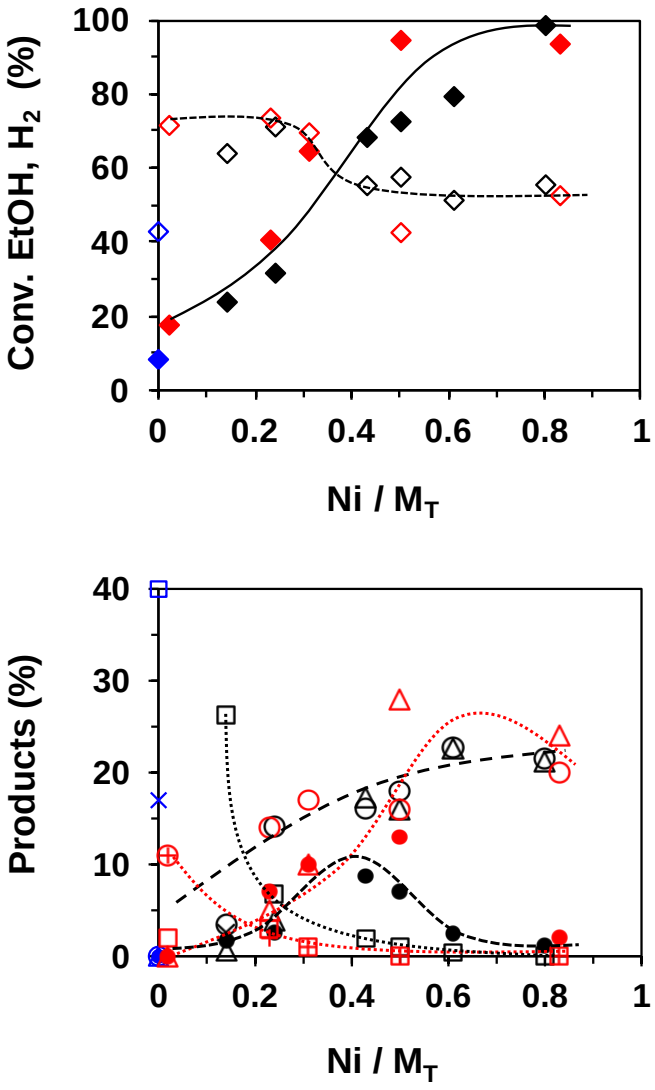

Fig. 6-2 SRE at 450 °C over Ni-based catalysts as a function of Ni molar ratio to all the metals. $CeNi_XO_Y$ (red), $Ni_XMg_2AlO_Y$ (black) and Mg_2AlO_Y (blue). Ethanol conversion (◆), H_2 (◇), CO_2 (○), CH_3CHO (□), CO (●), CH_4 (△), ethylene (×) and acetone (+) formation. Reaction conditions: catalyst: 50 mg; $EtOH/H_2O/N_2$ = 14/42/44; time: 5 h for each reaction.

When the Ni content increases, CO_2 formation undergoes a gradual rise, whereas acetaldehyde and acetone formation significantly declines. The formation of CH_4 and CO present a maximum when $Ni/M_T \approx$ 0.5. Based on the above results, it suggests that $CeNi_XO_Y$ and $Ni_XMg_2AlO_Y$ catalysts have the same Ni species behaving as the active phase even though Ni species can be surrounded by different neighbor atoms which can influence the products

distribution (**Fig. 6-2**). In fact XPS analysis has revealed very similar and homogenous distribution of Ni species inside the two types of Ni-based catalysts (**Fig. 6-1**).

Such a hypothesis is also supported by the catalytic results of OSRE catalyzed by $CeNi_XH_ZO_Y$ and $Ni_XMg_2AlH_ZO_Y$ nano-oxyhydrides (**Fig. 6-3**). The significant variation of temperature is observed in both catalytic systems due to the chemical energy released from the strong exothermic reaction between oxyhydrides and O_2 ($H^- + 0.5\ O_2 \rightarrow OH^-$). Thus the reaction can be performed at only 60 °C (except on the $Ni_1Mg_2AlO_Y$ catalyst which does not form an oxyhydride during pretreatment in H_2 at 450 °C).

Total ethanol conversion is obtained on two types of Ni-based compounds independent on the Ni content. Products distributions follow similar evolutions on both $CeNi_XH_ZO_Y$ and $Ni_XMg_2AlH_ZO_Y$ catalysts (**Fig. 6-3**). H_2 formation exhibit a maximum when $Ni/M_T \approx 0.5$. When Ni content increases, CO_2 formation shows a gradual increase, while CO formation undergoes a gradual decrease. Both products proportions become steady for higher Ni content. Only very low formation of acetaldehyde and methane are obtained on both $CeNi_XH_ZO_Y$ and $Ni_XMg_2AlH_ZO_Y$ catalysts whatever the Ni content.

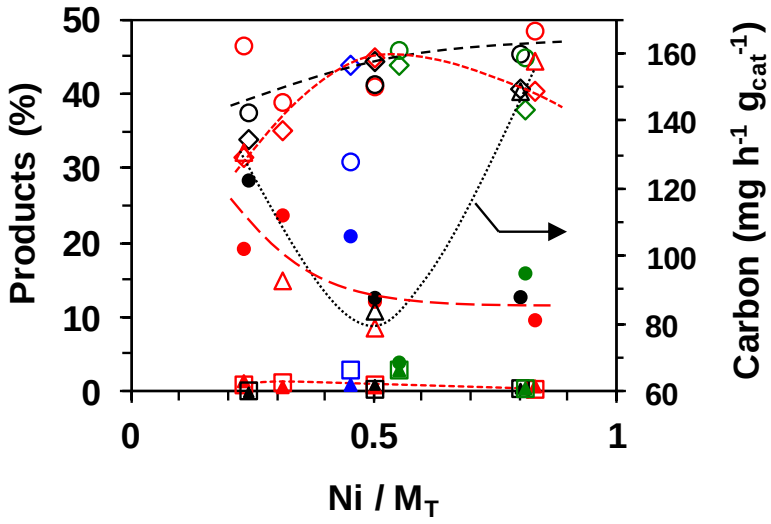

Fig. 6-3 OSRE over Ni-based nano-oxyhydride catalysts as a function of Ni molar ratio to all the metals. $CeNi_XH_ZO_Y$ (red), $Ni_XMg_2AlH_ZO_Y$ (black) and Ni_XMg_2Al HT-like compounds (green). The blue symbols correspond to the results reported in our previous publication.[6] Ethanol conversion (◆), H_2 (◇), CO_2 (○), CO (●), CH_3CHO (□), CH_4(▲) and carbon (△) formation. Ethanol conversion maintains constantly about 100% independent on the Ni content. Reaction conditions: catalyst: 30 mg; $H_2O/EtOH/O_2/N_2$ = 3:1:1.6:1.3; T_{Oven} = 60 °C (except the $Ni_1Mg_2AlO_Y$ catalyst, T_{Oven} = 215°C).

Based on all the above results discussed, it is reasonable to conclude that $CeNi_XO_Y$ and $Ni_XMg_2AlO_Y$ catalysts have the same active phase. That is the Ni species strongly interacting with Ce species in binary $CeNi_XO_Y$ compounds and the Ni species showing strong interactions with Mg and Al species in ternary $Ni_XMg_2AlO_Y$ compounds. Such active Ni species either in the solid solution of Ce-Ni-O and Ni-Mg-(Al)-O and/or at the interface of small nanoparticles of NiO, CeO_2, or Ni-Mg-(Al)-O, can be easily reduced and reoxidized (existing as Ni^0, $Ni^{\delta+}$, Ni^{2+} in the system) due to the strong interactions between Ni^{2+} cations and other cations (Ce^{4+}, Mg^{2+} and Al^{3+}) in the oxide catalyst. Therefore, Ni-based mixed oxides with the same proportion of Ni among the metals (molar ratio) could demonstrate very similar catalytic performances for either SRE or OSRE.

6.2 Proposal of active site and possible mechanism

In order to understand the correlations between the activity and the overall Ni species in the different catalysts, **Fig. 6-4** (A) reports SRE activity (in mol of ethanol converted per gram of catalyst per hour) measured at 450 °C as a function of the Ni proportion in the compounds. The $CeNi_XO_Y$ and $Ni_XMg_2AlO_Y$ catalysts activities are found to obey almost the same linear evolution curve with Ni molar ratio. The activity reported in mol ethanol converted per gram of catalyst per hour exhibits a global rising trend with the increase of Ni content, which is already observed in **Fig. 6-2**. $Ni_XMg_2AlO_Y$ catalysts show a relatively homogeneous linear increase in activity *versus* Ni content and the highest activity is obtained when Ni content is of 0.8 ($Ni_{12}Mg_2AlO_Y$); while the $CeNi_XO_Y$ catalysts present a higher dispersion regarding to the linear evolution for high Ni contents.

Whatever the Ni content is, $CeNi_XO_Y$ catalysts seem to constantly show a higher activity than the value obtained on $Ni_XMg_2AlO_Y$ catalysts. Some slight differences in the activity curves can be seen which indicate that the number of active sites and/or the activity of the sites (Ni species) in $CeNi_XO_Y$ and $Ni_XMg_2AlO_Y$ catalysts is different. However, it is necessary to deeply analyze the activity.

Fig. 6-4 (B) displays the activity reported in mol ethanol converted per mol of nickel per hour, which is obtained by distributing the activity to the Ni molar content in the solids. Reporting activity in this way, it is possible to extract the activity of a mole of Ni species, so the activity of a Ni species in the different environments (in the two series of solids) can be seen. It is

interesting to observe that two different types of activity curves are obtained for $CeNi_XO_Y$ and $Ni_XMg_2AlO_Y$ catalysts, respectively.

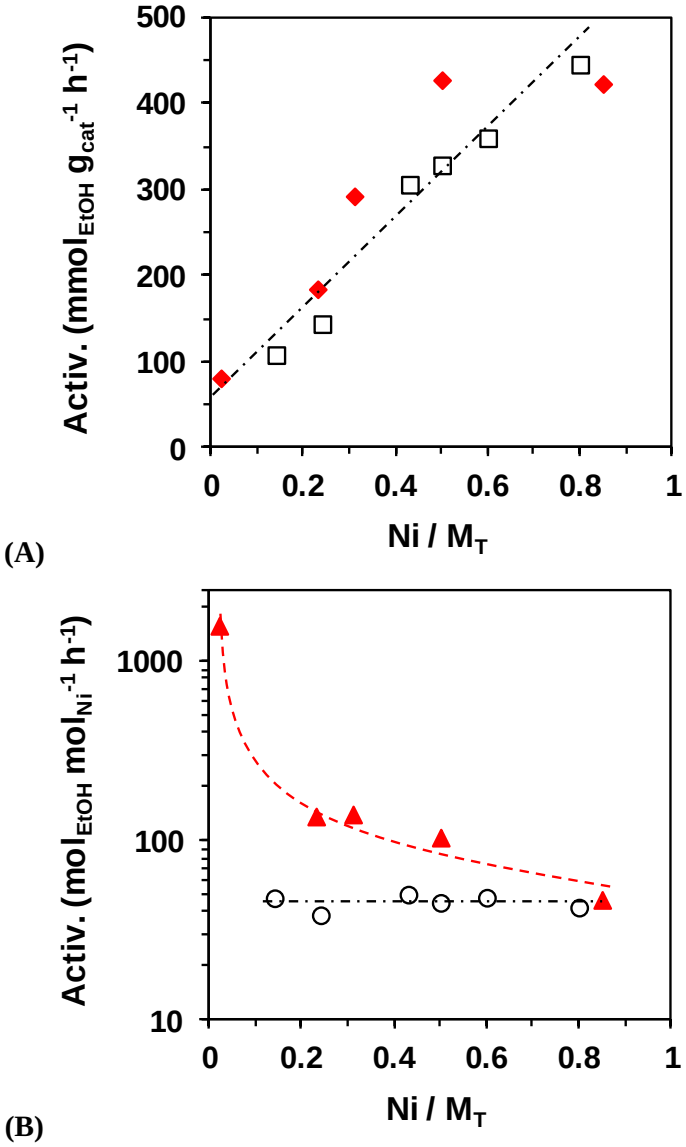

Fig. 6-4 Activity of $CeNi_XO_Y$ (◆,▲) and $Ni_XMg_2AlO_Y$ (□,○) catalysts measured at 450 °C for SRE as a function of Ni molar ratio.

$CeNi_XO_Y$ catalysts show an index fell in activity with increasing Ni loading, which indicates that the number of active sites does not increase with Ni loading (**Fig. 6-4** (B)). The highest activity is reported on $CeNi_{0.02}O_Y$ (0.3 wt% Ni), while the lowest value is obtained on $CeNi_5O_Y$ (53 wt% Ni). It suggests that not all the Ni species in the catalysts can behave as the active sites; the number of active sites is diluted by the growing Ni loading and the globally growing surface area. It appears clearly that the Ni species which are active are obtained in higher proportion at

low Ni content. Then when the Ni content increases, even if active Ni species are added (shown by the increase of activity with Ni content **Fig. 6-4** (A)), inactive Ni species are also added in higher proportion. In other words, if Ni content increases, the proportion of inactive Ni species added is higher compared to the proportion of active Ni species added. Therefore, as metallic Ni^0 increases with the Ni content, there is a low probability that the active Ni species correspond to metallic Ni^0. It has been disclosed by XRD analysis that the $CeNi_XO_Y$ compounds with $x < 0.5$ correspond to a solid solution with the substitution of Ni^{2+} cations in CeO_2 lattice, to a mixture of crystallized NiO coexisting with the solid solution when $0.5 \leqslant x < 1$, and to a mixture of the nanoparticles consisting of NiO and CeO_2 when $x > 1$. Moreover, in a previous work it has been shown by XPS that some very small nanoparticles of NiO are always present whatever the Ni content.[3]

$Ni_XMg_2AlO_Y$ catalysts present a constant activity, which does not vary when the Ni content changes. This result clearly shows that the activity of the Ni species remains the same whatever the Ni content. One Ni species in $Ni_XMg_2AlO_Y$ compounds is able to convert the same amount of ethanol per hour, whatever the $Ni_XMg_2AlO_Y$ compound is. This also suggests that the number of active sites respect very well to the Ni loading. In fact, this is in very good agreement with the XRD and XPS results obtained on $Ni_XMg_2AlO_Y$ compounds. No matter what the Ni content, the compound is ascribed to a mixture of nanoparticles of NiO, MgO and/or to a solid solution of Ni-Mg-(Al)-O. The crystallites sizes of NiO and/or Ni-Mg-(Al)-O maintain in a narrow range of between 3-6 nm when Ni loading increases. And there is a homogeneous distribution of Ni in the $Ni_XMg_2AlO_Y$ compounds.

Hence more active sites (with the same activity) can be generated in the compound with higher Ni loading. When the Ni content increases, the added Ni species present all the same activity, or in the added Ni species there is always the same proportion of active and inactive Ni species.

The activity (in mol g^{-1} h^{-1}) of $CeNi_XO_Y$ and $Ni_XMg_2AlO_Y$ catalysts for OSRE is also compared in **Fig. 6-5**. The same constant activity is measured over both $CeNi_XO_Y$ and $Ni_XMg_2AlO_Y$ catalysts (**Fig. 6-5** (A)), which is independent on the Ni content. It has been shown in **Fig. 6-3** that $CeNi_XH_ZO_Y$ and $Ni_XMg_2AlH_ZO_Y$ nano-oxyhydride catalysts are able to completely convert ethanol to produce hydrogen whatever the Ni content. Hence the same

activity can be obtained when total ethanol conversion is distributed to the same catalyst mass used (30 mg).

Fig. 6-5 (B) shows the activity reported in mol ethanol converted per mol of nickel per hour, which is measured by distributing the activity to the Ni molar content in the catalyst. In that case, two activity curves with the same trend are obtained for $CeNi_XO_Y$ and $Ni_XMg_2AlO_Y$ catalysts, respectively.

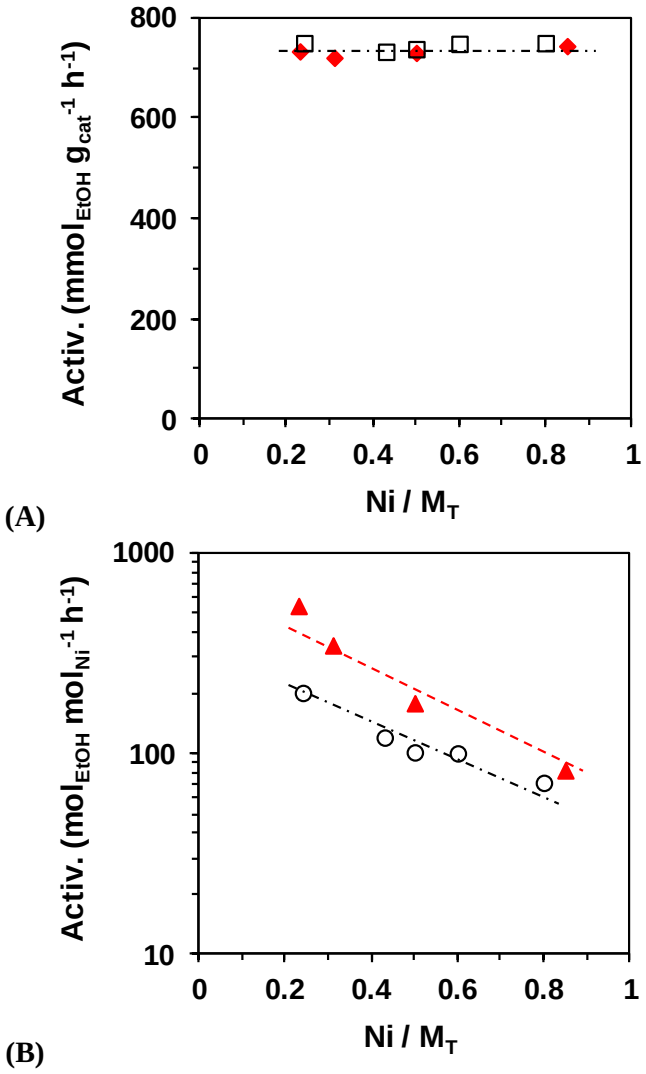

Fig. 6-5 Activity of $CeNi_XO_Y$ (◆,▲) and $Ni_XMg_2AlO_Y$ (□,○) catalysts for OSRE as a function of Ni molar ratio.

It is found that the activity (in mol mol_{Ni}^{-1} h^{-1}) of both Ni-based catalysts for OSRE shows a decreasing tendency *versus* Ni content (**Fig. 6-5** (B)). The activity declines almost linearly when the Ni loading increases. It can be explained by the fact that activity (in mol g_{cat}^{-1} h^{-1}) is divided

by the growing Ni molar ratio when the ethanol conversion is constantly of about 100%. However, it is important to recall that the activity is already very high with the low Ni content, so the active sites are created with the low Ni concentration. Moreover $CeNi_XO_Y$ catalysts always demonstrate higher activity than that measured over $Ni_XMg_2AlO_Y$ catalysts. That is because more nickel is needed in the ternary $Ni_XMg_2AlO_Y$ compounds in order to obtain the same Ni molar ratio of the binary $CeNi_XO_Y$ compounds. The highest activity is reported on the $CeNi_{0.3}O_Y$ catalyst (7.9 wt% Ni, $Ni/M_T = 0.23$), and it is divided by about two on the $Ni_1Mg_2AlO_Y$ catalyst (21.9 wt% Ni, $Ni/M_T = 0.23$). Based on the correlation between activity (both SRE and OSRE) and Ni molar ratio, an active site certainly involving Ni species in close interaction with other cations can be predicted but with further extraction of characterizations.

In TPR experiment, a linear relationship is established between H_2 consumption and the Ni content of Ni-based catalysts. As reported in **Fig. 6-6**, H_2 consumption during TPR exhibits the same trend *versus* the Ni content of all the Ni-based catalysts (Ce-Ni catalysts, $Ni_XMg_2AlO_Y$ catalysts and Ni_XMg_2Al HT-like compounds), showing that H_2 is nearly completely consumed to reduce the nickel species in the compounds. However, there is slight variation in the consumption of hydrogen, which is probably due to that i) for $CeNi_XO_Y$ catalysts, H_2 consumed at temperatures higher than 600 °C is not taken into account, as a matter of fact, a reduction peak at approximately 820 °C is observed attributed to the reduction of bulk Ce^{4+} to Ce^{3+}; ii) some hydrogen can migrate into the compounds when treated in H_2. The reduction process of the present $CeNi_XO_Y$ and $Ni_XMg_2AlO_Y$ catalysts can be generally expressed by the reduction of Ni species and simultaneous creation of anionic vacancy (**Eq. 6-1**). However, the Ni species are not reduced directly to Ni^0 over Ce-Ni compounds at low temperature due to the existence of a redox process in the presence of Ce cations (**Eq. 6-2**). This phenomenon allows still increasing the number of anionic vacancies.

$$Ni^{2+} + O^{2-} + H_2 \rightarrow Ni^0 + H_2O + \square \text{ (}\square\text{: anionic vacancy)} \qquad \textbf{Eq. 6-1}$$

$$2Ce^{4+} + Ni^0 \leftrightarrow 2Ce^{3+} + Ni^{2+} \qquad \textbf{Eq. 6-2}$$

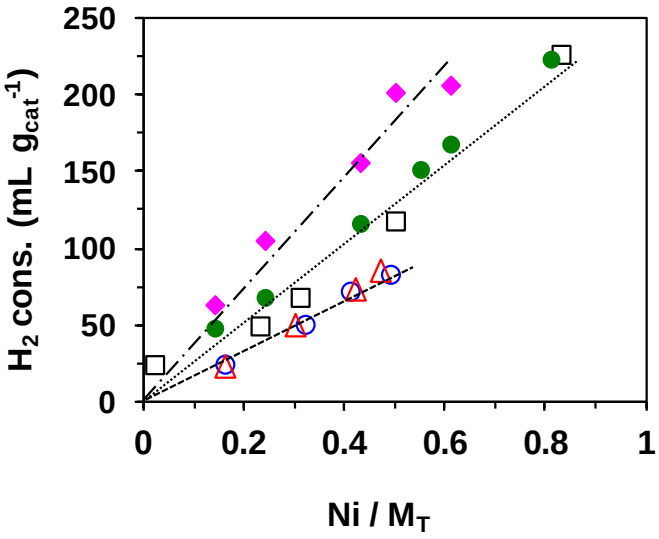

Fig. 6-6 H_2 consumption of Ni-based catalysts during TPR *versus* Ni molar ratio to all the metals. $Ni_XMg_2AlO_Y$ catalysts (◆), Ni_XMg_2Al HT-like compounds (●), $CeNi_XO_Y$ catalysts (□), *x*-Ni/CeO_2-IMP catalysts (○) and *x*-Ni/CeO_2-IWI catalysts (△).

It has been shown by INS experiment that the *in situ* treatment in H_2 leads to the formation of $CeNi_XH_ZO_Y$ oxyhydrides (at 250 °C)[6] and $Ni_XMg_2AlH_ZO_Y$ oxyhydrides (at 450 °C). The hydrogen species are inserted into the $Ni_XMg_2AlO_Y$ and $CeNi_XO_Y$ compounds in the form of hydride species (H^-), which has been well evidenced in **Fig. 6-7** by the presence of new peaks in INS spectra.

As a matter of fact, to be rigorous, the INS spectra of the hydride species generated *via* the activation in H_2 is obtained after subtraction of the spectra of the compounds treated in vacuum at 200 °C. In order to understand how hydrogen is stored in the compound, two pathways can be proposed.

i) Hydrogen can be heterolytically dissociated on an anionic vacancy and an O^{2-} species of the solid (**Eq. 6-3**). This is in agreement with TPR and *in situ* XRD results. Hydrogen is consumed in TPR mainly to reduce Ni species and simultaneously create anionic vacancy. Metallic Ni^0 species were not evidenced in the $CeNi_XO_Y$ compound (20 wt% Ni) by *in situ* XRD after H_2 treatment at 250 °C.[6] For $Ni_XMg_2AlO_Y$ compounds (x = 3 and 12), after *in situ* treatment in H_2 at 450 °C, all the oxidized nickel phases of NiO and/or Ni-Mg-(Al)-O are well maintained even though Ni^0 species emerge.

$$O^{2-}\ M^{n+}\ \square + H_2 \rightarrow OH^-\ M^{n+}\ H^-\ (\square\text{: anionic vacancy; } M^{n+}\text{: metal cation}) \qquad \textbf{Eq. 6-3}$$

ii) Hydrogen can be homolytically dissociated on Ni^0 species. It has been reported that metallic nickel adsorbs hydrogen;[7] therefore, in addition to route i) proposed above, the homolytic dissociation of H_2 on Ni^0 can be also taken into account. This is supported by TPR and *in situ* XRD results. Metallic Ni^0 species are observed in the $Ni_3Mg_2O_Y$ and $Ni_{12}Mg_2O_Y$ compounds after the activation in H_2 at 450 °C.

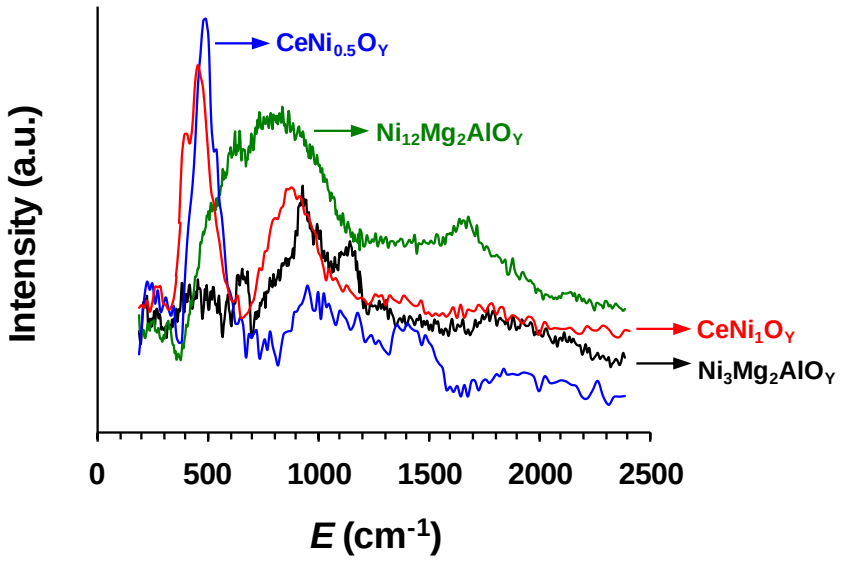

Fig. 6-7 INS spectra of $CeNi_{0.5}O_Y$ (blue) and $CeNi_1O_Y$ (red) treated in H_2 at 250 °C from reference [6], and INS spectra of $Ni_3Mg_2AlO_Y$ (black) and $Ni_{12}Mg_2AlO_Y$ (green) treated in H_2 at 450 °C. All the spectra are obtained after subtraction of the INS spectra of the corresponding calcined compounds.

However, oxidized phases related to NiO, MgO and $NiMgO_2$ are well maintained after the treatment in H_2 at 450 °C, showing the $Ni_3Mg_2O_Y$ and $Ni_{12}Mg_2O_Y$ compounds also undergo the heterolytic dissociation of H_2. It is important to recall that the activity of the Ni species (in mol mol_{Ni}^{-1} h^{-1}) is higher or the same for low Ni content, therefore it is more highly probable that it is related to a partially reduced solid involving Ni cations and anionic vacancies.

In the present thesis, two types of Ni-based catalyst, $CeNi_XO_Y$ and $Ni_XMg_2O_Y$, are studied for H_2 production from ethanol through the steam reforming and oxidative steam reforming reactions. In the SRE reaction, the Mg_2AlO_Y catalyst in the absence of nickel and the $CeNi_{0.02}O_Y$ catalyst with very low Ni loading (0.3 wt%) exhibit very low ethanol conversion accompanied with a high proportion of undesirable by-products, such as ethylene, acetaldehyde and acetone. In the OSRE reaction, the reaction must be activated at high temperature over the $CeNi_{0.3}O_Y$ ($T_{Ini.}$ =

276 °C) and $Ni_1Mg_2AlO_Y$ ($T_{Ini.}$ = 388 °C) catalysts. Moreover, the oven temperature cannot be lowered to 60 °C for the $Ni_1Mg_2AlO_Y$ catalyst but must be maintained at 215 °C.

Therefore, not surprisingly, nickel species constitute the active phase. The characterizations (XRD, XPS, Raman and TPR) prove the existence of strong interactions between Ni species and Ce, Mg and/or Al cations. The *in situ* activation in H_2 is an essential step for $CeNi_XO_Y$ (at 250 °C) and $Ni_XMg_2O_Y$ (at 450 °C) catalysts to demonstrate good activity for SRE and OSRE. In such a condition, the solids are partially reduced (TPR, *in situ* XRD) accompanied with the creation of anionic vacancies (INS). The redox properties of Ce-Ni system, due to the strong interaction between Ni and Ce species, according to **Eq. 6-1** and **Eq. 6-2**, allow increasing the amount of anionic vacancies. Therefore, for the $CeNi_XO_Y$ compounds, an active site involving an anionic vacancy, an O^{2-} species, and cations in close interaction can be envisaged for the heterolytic dissociation of ethanol, according to **Eq. 6-4**.[6] Once *in situ* treated in H_2, the solid is in a partially reduced state, and H_2 can be produced according to **Eq. 6-5** (with ethanol dissociated as in **Eq. 6-4**).

$$O^{2-}\ M^{n+}\ \square + C_2H_5OH \rightarrow OH^-\ M^{n+}\ H^- + CH_3CHO\ (\square\text{: anionic vacancy}) \qquad \textbf{Eq. 6-4}$$

$$OH^-\ M^{n+}\ H^- + C_2H_5OH \rightarrow OH^-\ M^{n+}\ H^- + CH_3CHO + H_2 \qquad \textbf{Eq. 6-5}$$

As shown in **Fig. 6-8**, an active site has been modeled in our laboratory by an ensemble of two cations (nickel and cerium) in strong interaction.[8] Such a site is expressed as ^{X}Ni-^{Y}M generally where *X* and *Y* are the number of coordinative unsaturations, *i.e.*, anionic vacancies on each cation. It appears that different kinds of active sites which differs from each other in terms of the environment of Ni can exist.[9] Each elementary ensemble is associated with a particular reaction. Depending on the unsaturation degree of the active site, conversion of ethanol can lead to different products.

In the latest literature, Ni and CeO_2 centers or Ni and ZrO_2 centers with strong metal-oxide interaction have been discussed for ethanol steam reforming.[10,11] In SRE catalyzed by Ni/CeO_2, the active components included metallic Ni^0 and Ce^{3+} in strong interaction.[10] Ni helps in the adsorption of ethanol and in the cleavage of C-C bond, while Ce^{3+} facilitates the decomposition of water with the subsequent generation of OH groups which are proposed to be essential for reacting with C_xH and C_yO_zH and produce CO_2 and H_2.[10] In another case, a nanocomposite

$Ni@ZrO_2$ catalyst with enhanced metal-support interaction showed good activity and stability for H_2 production through SRE.[11] The introduction of Ni particles into the framework of ZrO_2 support with high oxygen mobility could effectively increase the accessibility of the metal particles. The confinement effect of nickel-zirconia could prevent metal particles from sintering, leading to good stability.[11]

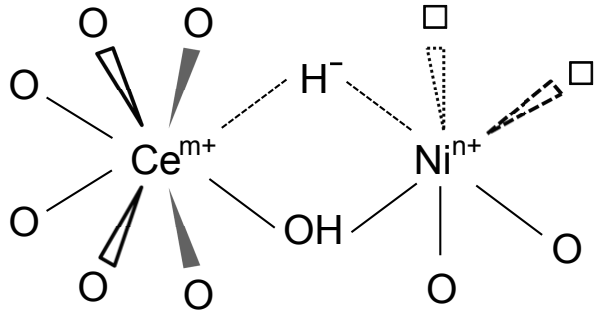

Fig. 6-8 Active site modeling of $CeNi_XO_Y$ catalyst for H_2 production from transformation of bio-ethanol. Ni^{n+}: Ni^{2+} or $Ni^{\delta+}$; Ce^{m+}: Ce^{4+} or Ce^{3+}.^{3}Ni-^{1}Ce site. (The number of anionic vacancies is arbitrary)

Hydrotalcite-like compounds with a general formula of $[M^{2+}_{1-x}M^{3+}_x(OH)_2]^{x+}(A^{n-})_{x/n}\cdot mH_2O$, are the solids that have a structure closely related to that of the mineral hydrotalcite. The structure of HT-like compounds is shown in **Fig. 6-9**. It consists of brucite-like layered double hydroxides where the substitution of M^{2+} with M^{3+} cations leads to a net positive charge, compensated by exchangeable anions in the interlayer space.[12] In brucite ($Mg(OH)_2$), bivalent cation (*e.g.* Mg^{2+}) and trivalent cations (*e.g.* Al^{3+}) are sixfold coordinated to form octahedral that share edges to constitute infinite layer. Anionic clays in a layer-type lattice as a consequence of the presence of relatively small, twofold positively charged cations in proximity with polarisable OH^- ions, as schemed in **Fig. 6-10**.[13]

Recently, Ni-based ex-hydrotalcite mixed oxides have been largely reported as good catalysts for SRE and/or OSRE.[14-18] The good catalytic activity, selectivity and stability are demonstrated by mainly the strong interactions between Ni species and other cations, *e.g.*, Mg, Al, Zn, Cu and Co. No matter in ternary Ni-Mg-Al, Ni-Zn-Al, Co-Mg-Al and Co-Zn-Al systems,[14,15,18] or in Cu-, Zn-promoted Ni-Mg-Al quaternary systems;[16,17] active metals (Ni species and/or Ni-Cu or Ni-Zn bimetals) interact closely with other cations by the incorporation of Ni species into the matrix of other cations, which leads to the small particle sizes, good metal dispersion and high stabilization of the active metal phases with enhanced synergetic effect with other cations.

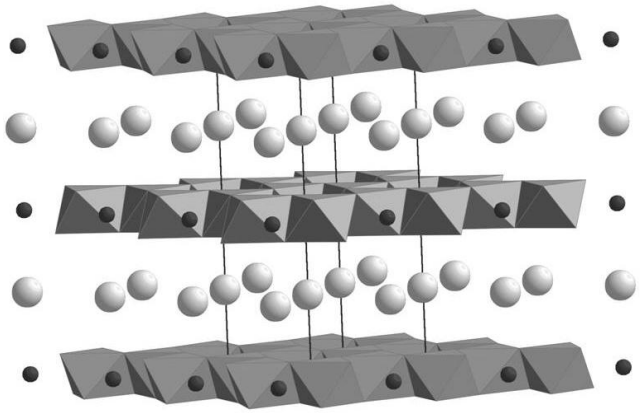

Fig. 6-9 Schematic image of the structure of hydrotalcites.[12] Small spheres represent bivalent and trivalent cations, *e.g.* Mg^{2+} and Al^{3+}; big spheres represent the compensating anions (*e.g.* CO_3^{2-}).

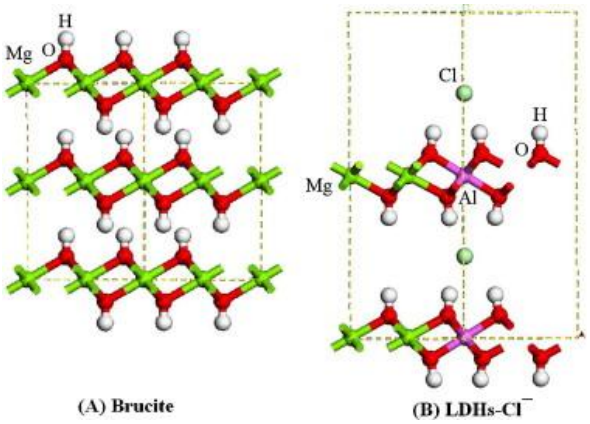

Fig. 6-10 Schematic models of the structures of brucite and hydrotalcites.[13]

$Ni_XMg_2AlO_Y$ ex-hydrotalcite catalysts studied in the present thesis have shown very strong interactions between Ni species and Mg and/or Al cations either in Ni-Mg-(Al)-O solid solution and/or at the interfaces between small nanoparticles of NiO, MgO and/or Ni-Mg-(Al)-O, evidenced by XRD, XPS, TPR. The H_2 treatment at 450 °C leads to partially reduced solids with simultaneous generation of anionic vacancies (shown by INS).

Hence it is reasonable to propose a similar active site involving an anionic vacancy, an O^{2-} species, and cations in close interaction. In fact, it has been reported in the literature that anionic vacancies can be created in Mg/Al mixed oxide by the presence of coordinatively unsaturated Al^{3+} species.[19] If Ni is added into the binary Mg-Al system, of course the number of anionic vacancies increases. The active site for $Ni_XMg_2AlO_Y$ catalysts is modeled in **Fig. 6-11** by an ensemble of two cations (nickel-magnesium or aluminum) in strong interaction, which can be also generally expressed by ^{X}Ni-^{Y}M.

This model also presents the advantage to be in good agreement with the synergetic effect observed when several cations with strong interactions are in presence in a mixed oxide. Metallic Ni^0 can also participate in the reaction when it is presented; however all the results obtained cannot be explained by simply attributing the activity to this species.

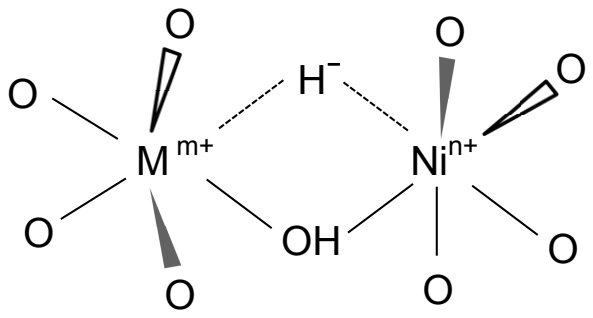

Fig. 6-11 Active site modeling of $Ni_XMg_2AlO_Y$ catalyst for H_2 production from transformation of bio-ethanol. Ni^{n+}: Ni^{2+} or $Ni^{\delta+}$; M^{m+}: Mg^{2+} or Al^{3+}. ^{1}Ni-^{1}M site. (The number of anionic vacancies is arbitrary)

Based on the proposed active sites for $CeNi_XO_Y$ and $Ni_XMg_2AlO_Y$ catalysts, the possible mechanism for ethanol transformation can be envisaged. Taking into account the ^{X}Ni-^{Y}M ensemble, for example, at a lower number of anionic vacancies on the site (^{1}Ni-^{1}M), acetaldehyde and H_2 can be produced by heterolytic abstraction of hydrogen (**Fig. 6-12** (A)). Each elementary ^{X}Ni-^{Y}M ensemble is associated with a particular reaction. Depending on the unsaturation degree of the active site, conversion of ethanol can lead to different products.[6]

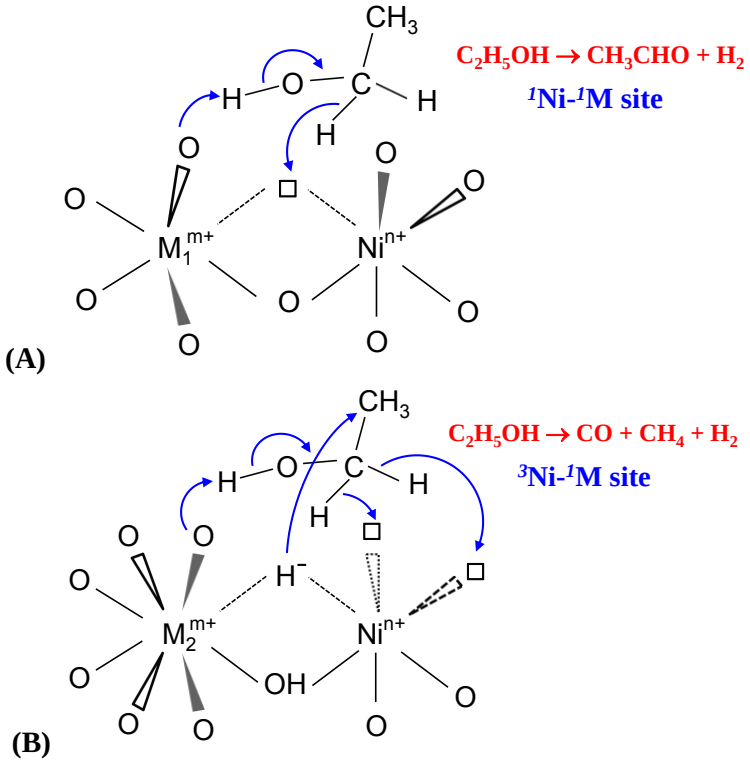

Fig. 6-12 Mechanism and active site modeling for ethanol transformation over $CeNi_XO_Y$ or $Ni_XMg_2AlO_Y$ catalysts. Ni^{n+}: Ni^{2+} or $Ni^{\delta+}$; M_1: Mg^{2+} or Al^{3+}; M_2: Ce^{4+}, Ce^{3+}.

As demonstrated in **Fig. 6-12** (B), the ^{3}Ni-^{1}M site leads to the formation of H_2, CO and CH_4. At a higher number of anionic vacancies on the site (^{3}Ni-^{3}M), ethanol can be converted to H_2, CO and carbon which involves the transformation of CH_4 to H_2 on such a site,[20] according to **Eq. 6-6**.

After *in situ* activation in H_2, hydride species (H^-) formed is localized in an anionic vacancy and H^+ species form a hydroxyl group (OH^-) with O^{2-} species (**Eq. 6-3**). The high reactivity of the hydride species permits consumption of O_2 (strongly exothermic) forming OH^- and then H_2O, and therefore the compound can present an enhancement at the surface of the concentration of hydroxyl groups (**Eq. 6-7**); it also permits the transformation of O_2 into selective oxygen species (O^{2-}) which regenerate the active site (**Eq. 6-8**).

$$2\ O^{2-}\ M^{n+}\ \square + CH_4 \rightarrow 2\ OH^-\ M^{n+}\ H^- + C\ (\square\text{: anionic vacancy})$$ **Eq. 6-6**

$$H^- + 0.5\ O_2 \rightarrow OH^-$$ **Eq. 6-7**

$$2\ OH^- \rightarrow O^{2-} + \square + H_2O$$ **Eq. 6-8**

The proposed active site and mechanism based on all the present experimental results are helpful for us to understand the possible roles that Ni-based mixed oxide catalysts play in the transformation of ethanol to H_2 production. However, deeper characterizations and analysis are still necessary to further study and understand better this catalytic system.

6.3 References

[1] L. Jalowiecki-Duhamel, S. Debeusscher, H. Zarrou, A. D'Huysser, H. Jobic and E. Payen,*Catal. Today*, 2008, **138**, 266.

[2] C. Pirez, *Thèse*, Univ. Lille 1, décembre 2010.

[3] A. Ponchel, A. Huysser, C. Lamonier and L. Jalowiecki-Duhamel, *Phys. Chem. Chem. Phys.*, 2000, **2**, 303.

[4] L. Jalowiecki-Duhamel, S. Debeusscher, H. Jobic and E. Payen, *Int. J. Nuclear Hydrogen Production and Applications*, 2009, **2**, 148.

[5] L. Jalowiecki-Duhamel, H. Zarrou and A. D'Huysser, *Catal.Today*, 2008, **138**, 124.

[6] C. Pirez, M. Capron, H. Jobic, F. Dumeignil and L. Jalowiecki-Duhamel, *Angew.Chem. Int. Ed*,2011, **50**, 10193.

[7] S. Kacimi, D. Duprez and J. A. Dalmon, *J. Chim.Phys.Biol.*, 1997, **94**, 525.

[8] C. Lamonier, A. Ponchel, A. D'Huysser and L. Jalowiecki-Duhamel, *Catal. Today*, 1999, **50**, 247.

[9] L. Jalowiecki-Duhamel, *Int. J. Hydrogen Energy*, 2006, **31**, 191.

[10] S. Li, C. Zhang, Z. Huang, G. Wu and J. Gong, *Chem. Commun.*, 2013, **49**, 4226.

[11] W. Xu, Z. Liu, A. C. Johnston-Peck, S. D. Senanayake, G. Zhou, D. Stacchiola, E. A. Stach and J. A. Rodriguez, *ACS Catal.*, 2013,**3**, 975.

[12] D. P. Debecker, E. M. Gaigneaux and G. Busca, *Chem. Eur. J.*, 2009, **15**, 3920.

[13] Q. Xu, Z.-m. Ni and J.-h. Mao, *Journal of Molecular Structure: THEOCHEM*, 2009, **915**, 122.

[14] C. Resini, T. Montanari, L. Barattini, G. Ramis, G. Busca, S. Presto, P. Riani, R. Marazza, M. Sisani, F. Marmottini and U. Costantino, *Appl. Catal. A*, 2009, **355**, 83.

[15] L.J.I. Coleman, W. Epling, R.R. Hudgins and E. Croiset, *Appl. Catal.A*, 2009,**363**, 52.

[16] X.-P. Yu, W. Chu, N. Wang and F. Ma, *Catal.Lett.*,2011, **141**, 1228.

[17] G. Zeng, Q. Liu, R. Gu, L. Zhang and Y. Li, *Catal. Today*,2011, **78**, 206.

[18] R. Guil-López, R. M. Navarro, M. A. Peña and J. L. G. Fierro, *Int. J. Hydrogen Energy*,2011, **36**, 1512.

[19] M. Bolognini, F. Cavani, D. Scagliarini, C. Flego, C. Perego and M. Saba, *Catal. Today*, 2002, **75**, 103.

[20] L. Jalowiecki-Duhamel, H. Zarrou and A. D'Huysser, *Int. J. Hydrogen Energy*, 2008, **33**, 5527.

7 General conclusion

Hydrogen production by catalytic transformation of bio-ethanol was studied over Ni-based mixed oxide catalysts, $CeNi_XO_Y$ and $Ni_XMg_2AlO_Y$. These catalysts were studied through two routes: steam reforming of ethanol ($H_2O/EtOH = 3$) and oxidative steam reforming of ethanol.

The $CeNi_XO_Y$ and $Ni_XMg_2AlO_Y$ catalysts were prepared by the co-precipitation method and characterized by numerous physicochemical techniques. $CeNi_XO_Y$ binary mixed oxides have relatively large surface areas between 75-120 $m^2\ g^{-1}$, while $Ni_XMg_2AlO_Y$ ternary ex-hydrotalcite mixed oxides have large surface areas between 100-200 $m^2\ g^{-1}$. $Ni_XMg_2AlO_Y$ nano-compounds are composed of small and uniform nanoparticles of NiO, MgO and/or the solid solution of Ni-Mg-(Al)-O with particles sizes between 3-6 nm determined by XRD. $CeNi_XO_Y$ nano-compounds are constituted of nanoparticles of NiO (10 nm) and CeO_2 (5 nm). Ni^{2+} species are evidenced on the surface of $Ni_XMg_2AlO_Y$ compounds mainly assigned to the existence of Ni-Mg-(Al)-O solid solution (XPS). Raman analysis reveals that the solubility of nickel species into nano-crystalline CeO_2 leads to the creation of oxygen vacancies in $CeNi_XO_Y$ compounds. All the results show the existence of strong interactions between Ni species and other cations (Ce, Mg and Al).

$CeNi_XO_Y$ compounds show two TPR peaks of Ni species between 200-400 °C. The first peak between 200-300 °C is attributed to the reduction of Ni species in the solid solution and/or small NiO (about 2 nm) nanoparticles, due to the strong interactions between Ni and Ce species leading to such Ni species being able to be reduced and reoxidized easily and reversibly. The second peak at temperature between 300-400 °C is due to the reduction of large NiO particles (10 nm). $Ni_XMg_2AlO_Y$ compounds present an almost single broad TPR peak visible between 560-850 °C which is assigned to the reduction of Ni species that strongly interact with Mg and/or Al cations. The TPR peak shifts to lower temperatures if the Ni content increases. *In situ* XRD in H_2 shows small nanoparticles of oxides accompanied with a small amount of metallic nickel species (4-5 nm) in $Ni_XMg_2AlO_Y$ ($x \geqslant 3$) compounds treated in H_2 at 450 °C. INS experiment proves the existence of hydroxyl groups (H^+ species) in both the calcined compounds, and H_2 treatment leads to the formation of $CeNi_XH_ZO_Y$ (250 °C) and $Ni_XMg_2AlH_ZO_Y$ (450 °C) nano-oxyhydrides with the presence of hydrogen species in the form of hydride (H^-).

$CeNi_XO_Y$ catalysts have an optimized treatment temperature of about 250 °C corresponding to the first TPR peak. The optimized treatment temperature for $Ni_XMg_2AlO_Y$ catalysts can be

different depending on the Ni content. However, an optimum temperature can be proposed at 450 °C. Once *in situ* treated in H_2, $CeNi_XO_Y$ and $Ni_XMg_2AlO_Y$ catalysts (50 mg) demonstrate very good catalytic performances for the steam reforming of ethanol (EtOH: 14 mol%). Total ethanol conversion and about 50 mol% H_2 formation are obtained at 450 °C. Acetaldehyde and acetone are formed at temperatures lower than 350 °C. When Ni molar ratio is higher or equals to 0.5, total ethanol conversion with 50% H_2 can be obtained at 450 °C. The $Ni_{12}Mg_2AlO_Y$ catalyst allows obtaining a low-temperature high-yield H_2 production of 3 mol mol_{EtOH}^{-1} (with a feed of EtOH at 1 mol%) at 300 °C without the formation of CO. The $Ni_3Mg_2AlO_Y$ and $CeNi_1O_Y$ catalysts are able to produce a very high H_2 production of about 5 mol mol_{EtOH}^{-1} at 650 °C (EtOH: 3 mol%).

The $CeNi_XH_ZO_Y$ and $Ni_XMg_2AlH_ZO_Y$ oxyhydrides (30 mg) obtained by H_2 treatment enable to completely convert ethanol (100%) and produce H_2 (about 45 mol%) at room temperature through the oxidative steam reforming of ethanol ($H_2O/EtOH/O_2$ = 3:1:1.6). The energy released from the strong exothermic reaction between the hydride species stored in the catalysts is used to drive the reaction, which allows lowering the oven temperature down to only 60 °C. A huge variation of temperature between the catalyst bed and the oven therefore can be observed. In the meantime the hydride species are continuously formed from ethanol to make the reaction sustainable. The Ni content strongly affects the products distribution while the activity is mainly related to the hydrogen storage capacity of the solid depending also on the Ni content. Both catalytic systems show very good stability after about 80 h on stream.

$CeNi_XO_Y$ and $Ni_XMg_2AlO_Y$ catalysts show very similar evolution of ethanol conversion and products distribution for SRE and OSRE due to the homogenous distribution of the same active Ni species surrounded by different neighbor atoms. Such active Ni species either in the solid solution of Ce-Ni-O and Ni-Mg-(Al)-O and/or at the interface of small nanoparticles of NiO, CeO_2, or Ni-Mg-(Al)-O, can be easily reduced and reoxidized (existing as Ni^0, $Ni^{\delta+}$, Ni^{2+} in the system) due to the strong interactions between Ni^{2+} cations and other cations (Ce^{4+}, Mg^{2+} and Al^{3+}) in the oxide catalyst. Therefore an active site involving Ni species in close interactions with other cations expressed as ^{X}Ni-^{Y}M can be proposed. It belongs to a partially reduced catalyst (oxyhydride) involving an anionic vacancy, an O^{2-} species, and cations, which is formed during the *in situ* H_2 treatment. Ethanol is heterolytically dissociated on such a site and converted to different products depending on the number of anionic vacancies.